0004888

Report No. FAA-RD-71-86

AN INVESTIGATION OF MICROWAVE LANDING GUIDANCE SYSTEM SIGNAL REQUIREMENTS FOR CONVENTIONALLY EQUIPPED CIVILIAN AIRCRAFT

Maurice H. Lanman III
Transportation Systems Center
55 Broadway Cambridge, Ma. 02142

transpo 72
U.S. International Transportation Exposition
Dulles International Airport
Washington, D.C.
May 27-June 4, 1972

JUNE 1971
TECHNICAL REPORT

Availabiliy is unlimited. Document may be released to the National Technical Information Service, Springfield, Virginia 22151, for sale to the public.

Prepared for

DEPARTMENT OF TRANSPORTATION
FEDERAL AVIATION ADMINISTRATION
Systems Research & Development Service
Washington, D.C. 20591

The contents of this report reflect the views of the Transportation System Center which is responsible for the facts and the accuracy of the data presented herein. The contents do not necessarily reflect the official views or policy of the Department of Transportation. This report does not constitute a standard, specification or regulation.

1. Report No.	2. Government Accession No.	3. Recipient's Catalog No.
FAA-RD-71-86		

4. Title and Subtitle	5. Report Date
An Investigation of Microwave Landing Guidance System Signal Requirements For Conventionally Equipped Civilian Aircraft	June 1971
	6. Performing Organization Code
7. Author(s) Maurice H. Lanman III	8. Performing Organization Report No. DOT-TSC-FAA-71-24
9. Performing Organization Name and Address DOT/Transportation Systems Center 55 Broadway Cambridge, Mass. 02142	10. Work Unit No. FA-08
	11. Contract or Grant No.
12. Sponsoring Agency Name and Address Federal Aviation Administration Washington, D. C.	13. Type of Report and Period Covered Technical Report
	14. Sponsoring Agency Code

15. Supplementary Notes

16. Abstract

This report describes efforts leading to the determination of minimum suitable scan rates for the azimuth and Elevation #1 functions of the microwave Landing Guidance System (LGS) proposed by RTCA SC-117, based on performance requirements of two conventionally equipped civilian aircraft. Two complementary methods are used; one involving a full nonlinear digital simulation, the other involving direct covariance matrix propagation. Wind and turbulence models, aircraft models and LGS models are described in detail. Safety and pilot acceptability criteria for performance evaluation are developed. Results are presented in terms of minimum scan rate maximum beam noise constraints. Limitations of the methods and data are also discussed and required further work outlined.

17. Key Words	18. Distribution Statement
Microwave Landing System Landing Guidance System Scanning Rate Scanning Beam ILS	Availability is unlimited. Document may be released to the National Technical Information Service, Springfield, Virginia 22151, for sale to the public.

19. Security Classif. (of this report)	20. Security Classif. (of this page)	21. No. of Pages	22. Price
Unclassified	Unclassified	171	$3.00 PC .95 MF

TABLE OF CONTENTS

	Page
PREFACE	iv
*1. INTRODUCTION	1
2. PROBLEM DEFINITION AND APPROACH	3
3. ATMOSPHERIC TURBULENCE MODELS	12
3.1 Steady Wind and Wind Shear	12
3.2 Wind Gusts	14
3.3 Simplifications for the Covariance Propagation Equations	20
4. LGS SCANNING BEAM AND CONVENTIONAL ILS MODELS	23
*4.1 LGS Scanning Beam Model	23
*4.1.1 Signal Noise and Sampling Noise	26
4.1.2 Noise and Bias Specifications	29
4.1.3 Scanning Rates	30
4.2 Conventional ILS Model	30
5. AIRCRAFT MODELS	32
5.1 Discussion	32
5.1.1 "Heavy Jet Transport" Vs. "Light Maneuverable"	32
5.1.2 Aircraft Models	32
5.2 The Convair 880 Jet Transport	33
5.2.1 Airframe	33
5.2.2 Autopilot and Flight Controls	33
5.2.3 Modifications for the Covariance Propagation Equations	40
5.3 The PA-30 Twin Comanche	41
5.3.1 Airframe	41
5.3.2 Autopilot	41
5.4 Dynamic Characteristics of the Aircraft	41
5.4.1 Inner Loops	45
5.4.2 Path Following Loops	45
6. PERFORMANCE CRITERIA DURING APPROACH AND LANDING	52
*6.1 Critical Variables for a Safe Landing	53
*6.2 Critical Variables for Safe Landing - PA-30	56
*6.3 Pilot Acceptability Factors	56
6.4 Generation of Critical Variables from Aircraft State Vector	58
6.5 Computation of Variances for Critical Variables	60

*These Sections, taken in order, will provide a fairly complete summary of the important aspects of this report.

TABLE OF CONTENTS (CONT.)

Page

6.5.1 Combining the Effects of Various Disturbances..... 61
6.5.2 Composite Variables..... 62

7. EFFECTS OF SCANNING RATE & BEAM AMONALIES ON PERFORMANCE DURING APPROACH & LANDING..... 66
*7.1 General..... 66
*7.1.1 Deterministic Disturbances..... 66
*7.1.2 Random Disturbances..... 67
*7.1.3 An Example of the Relative Effects of Scan Rate, Beam Noise and Wind Gusts.... 68
7.1.4 CV-880 Touchdown Performance With Conventional ILS..... 68
7.2 Lateral System Results - Azimuth Scanning Rate and Noise..... 69
*7.2.1 CV-880 - Critical Touchdown Variables... 69
*7.2.2 CV-880 Pilot Acceptability Factors..... 70
7.2.3 PA-30 Pilot Acceptability Factors..... 72
7.3 Longitudinal System Results - Elevation #1 Scanning Rate and Noise..... 73
7.3.1 CV-880 Critical Touchdown Variables..... 73
7.3.2 CV-880 Pilot Acceptability Factors..... 73
7.3.3 PA-30 Acceptability Factors..... 74
*7.4 Summary..... 75
7.5 Interpretations..... 75
7.5.1 Implications of a Percentage Increase in 1σ Value to the Probability of Exceeding a Limit - Critical Variables at Touchdown..... 75
7.5.2 Pilot Acceptability Factors - The Effects of a Coupler Filter..... 78

8. CONCLUSIONS..... 115
*8.1 General Conclusions..... 115
*8.2 Conclusions for the Azimuth Signal..... 115
*8.3 Conclusions for the Elevation #1 Signal..... 115

9. SUMMARY OF LIMITATIONS..... 118
9.1 General..... 118
9.2 Covariance Propagation Method..... 118
9.3 Wind Models..... 118
9.4 LGS Model..... 118
9.5 Aircraft Models and Touchdown Criteria..... 119
9.6 Pilot Acceptability Criteria..... 119
9.7 Statistical Procedure - Probability of Safe Landing..... 119

TABLE OF CONTENTS (CONT.)

Page

9.8 Decision Window and Missed Approach..... 120
9.9 Signal Requirements for Terminal Area Guidance..... 120
9.10 The Use of DME and Elevation #2 Information. 121
9.11 LGS Signal Requirements for Advanced Autopilots..... 121

APPENDIX A..... A-1

APPENDIX B..... B-1

APPENDIX C..... C-1

APPENDIX D..... D-1

APPENDIX E..... E-1

LIST OF ILLUSTRATIONS

		Page
2-1.	General Statement of the Problem	4
2-2.	The Approach & Landing Problem	5
2-3(a).	Probability of Exceeding a Limit Vs. Scan Rate - Hypothetical	10
2-3(b).	Scan Rate-Beam Noise Tradeoff For Various Probability Levels	10
3-1.	Wind Shear Profiles: Logarithmic and Piecewise Linear Approximation	13
3-2.	L & σ Vs. Altitude	18
3-3.	Turbulence Bandwidth Vs. Altitude	19
4-1.	Schematic Diagram: Scanning Beam Processing	24
4-2.	Plan View: Typical Layout Azimuth and Elevation Antennas	25
4-3.	Signal and Processing Model for Scanning Beam	27
4-4.	Errors Due to Wind Gusts, Signal Noise, and Sampling, Vs. Gust Intensity	28
5-1.	CV-880 Lateral Position Control System	34
5-2.	CV-880 Autoland Vertical Position Control System	35
5-3.	CV-880 Yaw & Decrab Control System	36
5-4.	CV-880 Altitude Hold	37
5-5.	CV-880 Autothrottle	38
5-6.	CV-880 Servo & Control Surface Dynamics	39
5-7.	PA-30 Lateral Control System	42
5-8.	PA-30 Longitudinal Control System	43
5-9.	PA-30 Autothrottle	44
5-10.	Inner Loop Transient Responses, CV-880, PA-30	46

LIST OF ILLUSTRATIONS (Cont)

Page

5-11. Glideslope Transient Response at 200 ft. Altitude (Vs. Time) 47

5-12. "Localizer" Transient Response at 200 ft. Altitude (Vs. Time) 48

5-13. Glideslope Transient Response at 200 ft. Altitude (Vs. Ground Distance) 49

5-14. "Localizer" Transient Response at 200 ft. Altitude (Vs. Distance) 50

6-1. RMS Error as a Function of Gust Strength 56

6-2. Relations Between Aircraft Velocity Vectors (Horizontal Plane) 59

6-3. Longitudinal Touchdown Position 61

6-4. Longitudinal Position Dispersion Related to Glideslope Deviation 63

6-5. Longitudinal Dispersion At Touchdown 64

7-1. CV-880 Lateral System Response to Wind Shear At 50 and 1 Scans Per Second 79

7-2. Relative Dispersion in Longitudinal Position Vs. Relative Gust Intensity (No Beam Noise) 80

7-3. Relative Dispersion in Longitudinal Position Vs. Relative Gust Intensity With Beam Noise 81

7-4. Relative Effects of Beam Noise and Sample Noise Vs. Wind 82

7-5. Relative Effect of Scan Rate on Lateral Touchdown Variables - Worst Case Wind - No Beam Noise 83

7-6. Relative Effect of Scan Rate on Lateral Touchdown Variables, Worst Case Wind + Beam Noise 84

7-7(a). 1σ Lat. Pos. (3 Sec. After TD) Vs. Scan Rate .. 85

LIST OF ILLUSTRATIONS (Cont)

Page

7-7(b). Lateral Position Dispersion Vs. Scan Rate..... 85

7-7(c). Cross Track Velocity Dispersion Vs. Scan Rate..... 86

7-7(d). Roll Angle Dispersion Vs. Scan Rate..... 86

7-8(a). Scan Rate - Beam Noise Tradeoff For Performance Equivalent to Cat III Conv. ILS... 87

7-8(b). Beam Noise - Scan Rate Tradeoff For Dispersion Increases Half Those With Cat III Conventional ILS or 0.5%, Whichever is Greater..... 87

7-9. 2σ Roll Angle (ϕ) Vs. Beam Noise Final Approach - No Wind..... 88

7-10. 2σ Roll Rate (p) Vs. Beam Noise Final Approach - No Wind..... 88

7-11. 2σ Heading Angle (ψ) Vs. Beam Noise Final Approach - No Wind..... 89

7-12. 2σ Aileron Activity (δ_a) Vs. Beam Noise Final Approach - No Wind..... 89

7-13. 2σ Rudder Activity (δ_a) Vs. Beam Noise Final Approach - No Wind..... 90

7-14. 2σ Lateral Position Deviation Vs. Beam Noise At Flare Altitude - No Wind..... 91

7-15. 2σ Indicated Lateral Pos. Dev. (Y_I) Vs. Beam Noise - Flare Altitude - No Wind..... 91

7-16(a). Beam Noise - Scan Rate Tradeoff Pilot Acceptability Factors CV-880 Lateral System (Coupler Filter Time Constant = .025 Sec.)... 92

7-16(b). Beam Noise - Scan Rate Tradeoff Pilot Acceptability Factors CV-880 Lateral System (Coupler Filter Time Constant = 0.5 Sec.).... 93

7-17. 2σ Roll Angular Activity Vs. Beam Noise Final Approach - No Wind..... 94

LIST OF ILLUSTRATIONS (Cont)

Page

7-18. 2σ Roll Rate Activity Vs. Beam Noise Final Approach - No Wind..... 94

7-19. 2σ Rudder Activity Vs. Beam Noise Final Approach - No Wind..... 94

7-20. 2σ Heading Angular Activity Vs. Beam Noise..... 95

7-21. 2σ Aileron Activity Vs. Beam Noise..... 95

7-22. 2σ Lateral Position Deviation Vs. Beam Noise.... 96

7-23. 2σ Indicated Lat. Pos. Dev. Vs. Beam Noise..... 96

7-24(a). Beam Noise - Scan Rate Tradeoff Pilot Acceptability Factors PA-30 Lateral System (Coupler Filter Time Constant = .025 Sec.)... 97

7-24(b). Beam Noise - Scan Rate Tradeoff Pilot Acceptability Factors PA-30 Lateral System (Coupler Time Constant: 0.5 Sec.)..... 98

7-25. Relative Effects of Scan Rate on Longitudinal Touchdown Variables - Worst Case Wind - No Beam Noise..... 99

7-26. Relative Effects of Scan Rate on Longitudinal Touchdown Variables - Worst Case Wind & Beam Noise..... 100

7-27(a). Longitudinal Position Dispersion Vs. Scan Rate..... 101

7-27(b). Sink Rate Dispersion Vs. Scan Rate..... 102

7-27(c). Pitch Angle Dispersion Vs. Scan Rate..... 102

7-28(a). Scan Rate - Beam Noise Tradeoff For Performance Equivalent To Cat III Conv. ILS.. 103

7-28(b). Scan Rate - Beam Noise Tradeoff For Long Pos. Dispersion Increase Half That With Conv. ILS and Sink Rate Disp. Increase 0.5%.. 103

7-29. 2σ Pitch Angular Activity Vs. Beam Noise Final Approach - No Wind..... 104

LIST OF ILLUSTRATIONS (Cont)

Page

7-30. 2σ Pitch Rate Activity Vs. Beam Noise Final Approach - No Wind..... 104

7-31. 2σ Elevator Activity (δ_a) Vs. Beam Noise Final Approach - No Wind..... 105

7-32. 2σ Pitch Angle Dev. Vs. Beam Noise Flare Altitude - No Wind..... 106

7-33. 2σ Airspeed Deviation Vs. Beam Noise Flare Altitude - No Wind..... 106

7-34. 2σ Glideslope Deviation (Z) Vs. Beam Noise Flare Altitude - No Wind..... 106

7-35(a). Beam Noise - Scan Rate Tradeoff Pilot Acceptability Factors CV-880 Longitudinal System (Coupler Filter Time Constant: 0.025 Sec.)..... 107

7-35(b). Beam Noise - Scan Rate Tradeoff Pilot Acceptability Factors CV-880 Longitudinal System (Coupler Filter Time Constant: 0.5 Sec.)..... 108

7-36. 2σ Pitch Angular Activity Vs. Beam Noise..... 109

7-37. 2σ Elevator Activity Vs. Beam Noise..... 109

7-38. 2σ Pitch Rate Activity Vs. Beam Noise..... 110

7-39. 2σ Pitch Angle Deviation Vs. Beam Noise..... 111

7-40. 2σ Airspeed Deviation Vs. Beam Noise..... 111

7-41. 2σ Glideslope Deviation Vs. Beam Noise..... 112

7-42. 2σ Indicated Glideslope Deviation Vs. Beam Noise..... 112

7-43(a). Beam Noise - Scan Rate Tradeoff Pilot Acceptability Factors PA-30 Longitudinal System (Coupler Time Constant: 0.025 Sec.).. 113

7-43(b). Beam Noise - Scan Rate Tradeoff Pilot Acceptability Factors PA-30 Longitudinal

LIST OF ILLUSTRATIONS (Cont)

Page

System (Coupler Filter Time Constant: 0.5 Sec.) 114

8-1. Scan Rate Beam Noise Tradeoff For Azimuth Signal 116

8-2. Scan Rate-Beam Noise Tradeoff For Elevation #1 Signal 116

LIST OF TABLES

		Page
3-1.	Atmospheric Turbulence Spectra	15
3-2.	Pseudo Rotation Rate Spectra	20
3-3.	Spectra and Parameter Values for Covariance Propagation Programs	21
4-1.	Errors Per Scan for Scanning Beam	29
4-2.	Category III ILS Errors	30
4-3.	Spectral Characteristics of ILS Errors	31
5-1.	Summary of Dynamic Characteristics of Path Following Loops CV-880 and PA-30	51
6-1.	Limits and Nominals for Safety Critical Touchdown Variables	55
7-1.	Errors in Position at Nominal Flare Altitude Due to Beam Bias, 2.5° Glideslope	67
7-2.	Effects of Category III ILS Noise on CV-880 Touchdown Performance - Worst Case Wind	69
7-3.	Effects of Percentage Increase in 1σ Value on Probability of Exceeding a Limit for a Gaussian Random Variable	77

PREFACE

The analytical methods, computer programs, and resulting data used for this study were generated by Messrs. Mukund Desai, Paul Madden, and Dr. Duncan MacKinnon of the M.I.T. Charles Stark Draper Laboratories, under Contract DOT-TSC-91.

Appendices A, B, C, D and E, some of which originally appeared in M.I.T. CSDL Report R-666, June 1970, were written by these gentlemen.

SUMMARY

This report addresses the problem of determining minimum suitable requirements for scan rate as a function of beam noise for the proposed Microwave Landing System for two classes of conventionally equipped civilian aircraft, a typical heavy jet transport and a light maneuverable general aviation aircraft.

A major portion of the effort involved development of analytical methods applicable to the problem, including development of a pertinent set of landing performance criteria, and refinement of aircraft, wind, and guidance beam models.

Two basic analysis methods are used. The first is a full non-linear simulation of an aircraft on final approach, including all known effects. This simulation generates deterministic results corresponding to a single set of conditions. To obtain statistically valid results for random disturbances, it would be necessary to generate a vast number of simulation runs for each set of conditions of interest. A second method, that of directly propagating mean square error about a nominal trajectory, (covariance propagation) is preferred for evaluating the effects of random disturbances such as beam noise and wind gusts. Use of this method requires, however, that linear approximations to the models be developed. Once this is done, mean square deviations from nominal approach trajectories are available as outputs directly and are used for statistical comparison against limits defined to be critical to safety and pilot acceptability.

Two sets of critical variables and limits are defined as performace criteria. The first sets absolute limits on touchdown position, attitude, and velocity variables such that exceeding the limits would lead to an accident. The second sets 2 sigma limits on variables deemed important for pilot acceptability during approach, such as control activity, attitude activity, and deviations from glideslope.

Problems were encountered in generating absolutely valid results at touchdown with the covariance propagation method as a result of the extreme nonlinearity in performance at low altitudes (under 50 feet) due to ground effect and to the effects of time dispersion in touchdown point. Neither effect can be implicitly included in the covariance propagation equations. To circumvent this problem, a comparative approach was taken such that the mean square value at touchdown under various noise and scan rate values are related on a percen-

tage increase basis to those with a perfect, continuous landing guidance signal. Results are also generated for a "best case" category III conventional ILS and used as another point of reference in evaluating critical touchdown variables.

Results applicable to conventionally equipped civilian aircraft can be summarized as follows:

1. Safety factors tend to be relatively insensitive to beam noise and control the minimum scan rate. Position variables are an order of magnitude more sensitive to scan rate than are velocity or attitude variables.

2. Pilot acceptability factors tend to be relatively insensitive to scan rate and control maximum acceptable beam noise.

3. For the azimuth signal, constraints imposed by performance criteria are such that 2 scans per second will provide acceptable performance at beam noise equivalent to RTCA SC-117 specification values. (RTCA recommended 5 scans per second).

4. For the Elevation #1 function, signal constraints imposed by safety criteria indicate that 1 or 2 scans is acceptable. However, the sensitivity of pilot acceptability factors to beam noise requires a minimum of 5 scans at beam noise levels equivalent to RTCA SC-117 specification values. (RTCA recommended 5 scans per second).

1. INTRODUCTION

A microwave Landing Guidance System (LGS) using scanning beams has been proposed by the Radio Technical Commission for Aeronautics (RTCA), Special Committee 117 (SC-117) to upgrade instrument landing capabilities and to eventually replace today's VHF-ILS (Ref. 1). The major advantage of the proposed scanning beam system is its relative freedom from multipath and siting problems. Since only a small segment of space is illuminated at any given instant, the likelihood of signal degradation from terrain reflections and overflight is minimized.

The proposed maximum system (SC-117 configuration K) also includes greatly expanded guidance capabilities, (wide angle coverage to 20NM, elevation guidance for flare, DME and azimuth guidance for rollout, considerably upgraded accuracy and reliability of all functions) directed towards permitting safe instrument landings under FAA Category III conditions and providing some relief to the terminal area traffic problem by allowing curved approaches, precise interleaving of arriving flights, and multiple final approach paths.

One of the major areas of concern in the implementation of such a system is the question of scanning rate. High scan rates present significant problems to the antenna and receiver designers. The antenna angular velocity (for mechanical antennas) directly affects the complexity of the platform through accuracy and repeatibility requirements on the direction of radiation. The dwell time of the beam at the aircraft receiver, which is critical to the ability to decode the signal on the beam, is also inversely proportional to scan rate for a given beam width and area of coverage.

The scan rate, however, must be high enough to insure that information available to an aircraft on approach is sufficient to allow it to follow a path in space and to touch down within some safe limits.

This report will address the problem from the flight performance point of view and will develop, present and demonstrate a set of analytical tools which, for any particular aircraft-autopilot combination, are capable of pinpointing critical factors in the selection of scan rate and the sensitivity of these factors to scan rate. Performance is judged solely on observable flight variables (e.g., control activity, position, velocity, attitude) during the approach and touchdown phase of flight. Only fully automatic landings are considered

for final straight-in approach. The method is demonstrated on two extremes of aircraft representative of conventional civilian aviation today: a heavy jet transport, the Convair 880, and a "light maneuverable" craft - the Piper PA-30 (Twin Comanche).

It should be understood that these aircraft are by no means representative of the full spectrum of all available and future aircraft. In fact, with autopilot-couplers designed for use with conventional ILS, they do not make very good use at all of the greatly increased information available from the LGS. Nor is it necessarily true that they are, or will be qualified for Category III landings as currently configured. The results do serve to demonstrate the level susceptibility of conventionally equipped civilian aircraft to LGS scanning rate and beam noise. It is not intended, however, that results for the CV-880 and PA-30 define a universal minimum suitable scan rate, since the ultimate scan rate selection (from a flight performance point of view) will probably depend on the characteristics of advanced autopilots which will more fully utilize LGS capabilities.

The remainder of the report is organized as follows: Section 2 describes the general problem and the approach used. Sections 3, 4 and 5 discuss the wind model, LGS model, and aircraft models, respectively. Section 6 defines safety and pilot acceptability criteria against which aircraft and landing system performance are to be compared and discusses statistical techniques, difficulties, and approximations in applying the criteria. Section 7 presents the data assembled from simulation and covariance propagation programs in terms of safe and acceptable landing criteria with wind, beam noise and scan rate as parameters. Section 8 presents conclusions, and suggests various tradeoffs in choosing minimum suitable scan rate. Section 9 concludes by discussing the limitations or applicability of the results and summarizes plans for future extension of the study.

Pertinent references are listed following each section. A series of appendices containing technical details are also included.

References

1. RTCA SC-117, *A New Guidance System for Approach and Landing*, DO-148, December 18, 1970.

2. PROBLEM DEFINITION AND APPROACH

Figure 2-1 illustrates the nature of the problem in its most basic form. It is desired to evaluate the performance of the controlled system based on some specific criteria, in the presence of various kinds and levels of disturbance inputs, with control being generated through feedback of critical variables which are subject to measurement errors. The evaluation procedure should provide information on the relative success in meeting performance criteria as input, feedback, and system parameters are varied.

For the case at hand, the controlled system is an aircraft with autopilot, in the final approach phase of flight; performance criteria are expressed in terms of deviations from nominal trajectory and are limited by safety and pilot acceptability consideration; disturbance inputs include steady winds, wind shear and wind gusts; information fed back to control the aircraft includes position errors via LGS and the attitude and rate variables available from on board sensors. Measurement errors may take the form of bias and random noise. Figure 2-2 illustrates in more detail some of these considerations.

The parameter of primary importance in this study is the sampling rate of the LGS.

The fundamental question with regard to the sampled LGS information is: How does the sampling rate affect the ability of a particular aircraft to meet its performance criteria and accomplish a safe and acceptable automatic approach and landing?

To answer this question one must explore in depth the effects of sampling rate on the ability to (1) fly an undisturbed trajectory, (2) tolerate the aerodynamic environment, and (3) tolerate errors in the sampled LGS signal.

Validity in an analytical solution requires that accurate models for the blocks of Figure 2-2 be developed and that appropriate methods of analysis using these models be selected. Once detailed models are developed, based on best available data, it is easy to see that a paper analysis is out of the question. The complexity and the vast number of variables involved in flight and control dynamics, wind response, and performance evaluation dictate a requirement for more sophisticated computer analysis techniques.

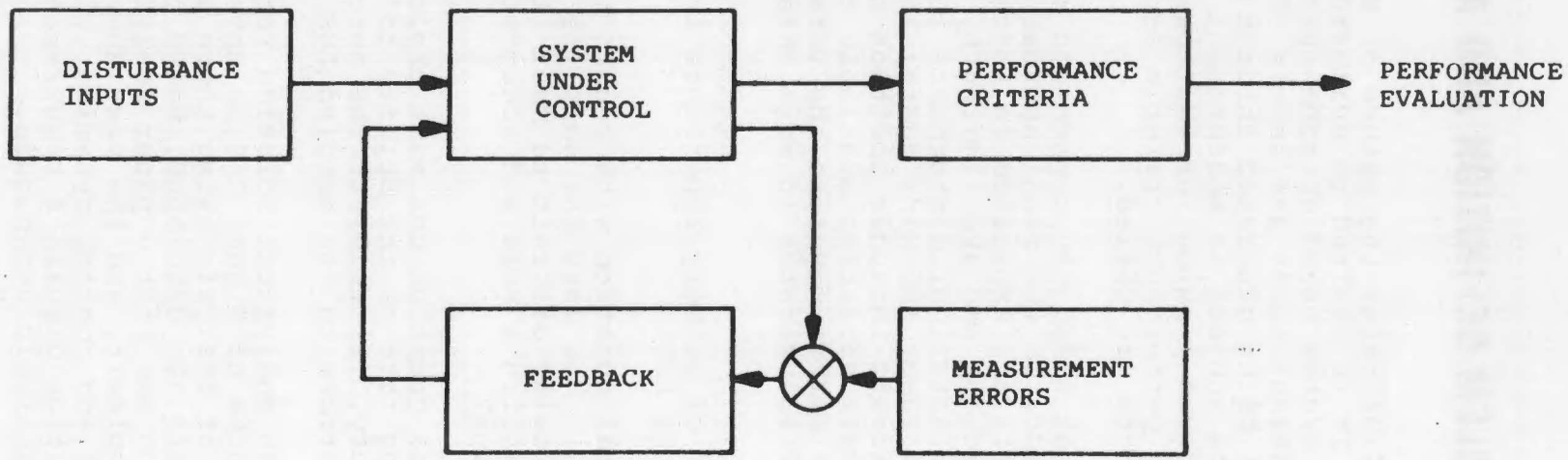

Figure 2-1. General Statement of the Problem

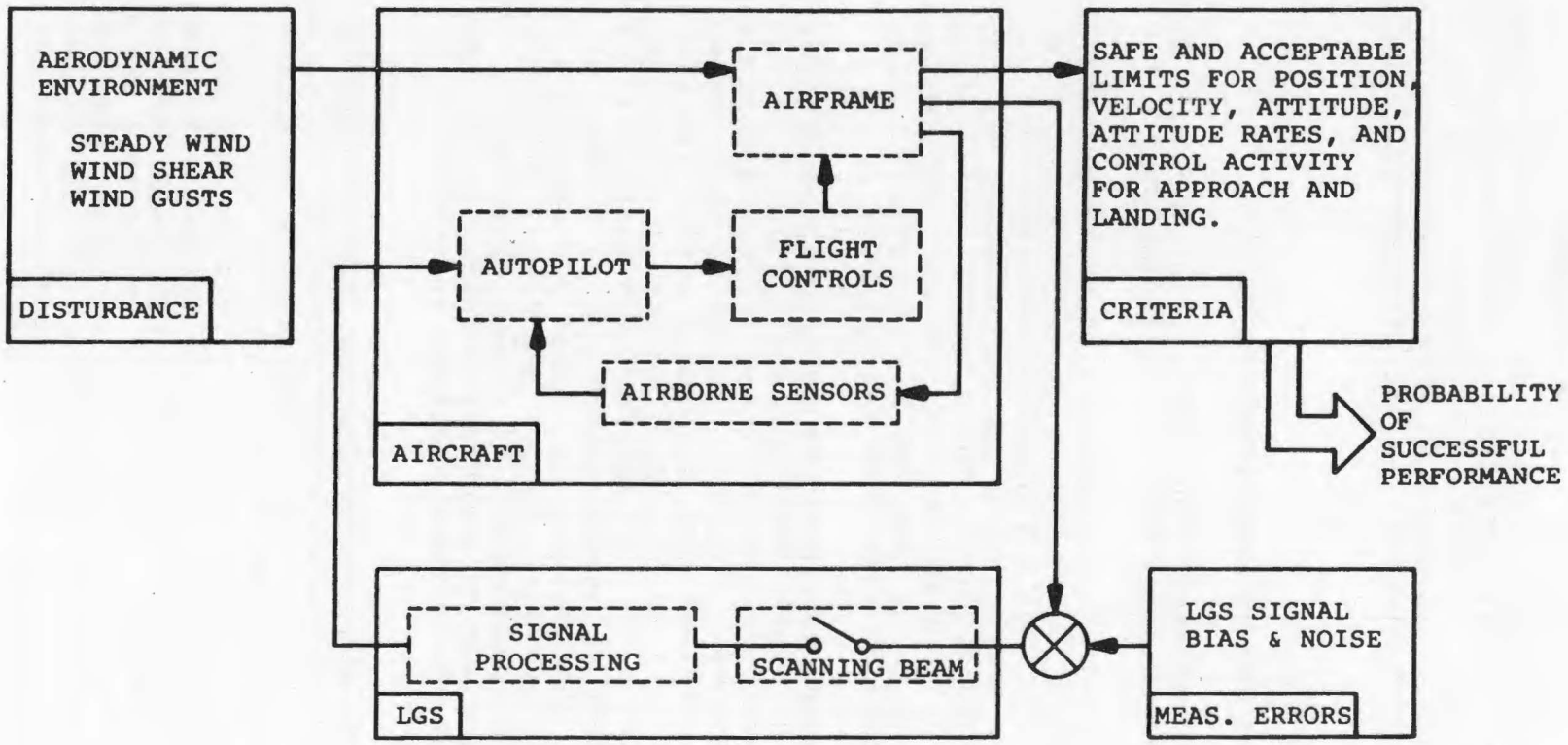

Figure 2-2. The Approach & Landing Problem

Two complementary methods are used in this study. The first is an all digital simulation which includes the airframe, autopilot, flight controls, disturbance inputs and all non-linearities and cross coupling terms involved in such a system. It operates directly on the aircraft state vector through Equation 2-1:

$$\dot{\underline{x}} = F\underline{x} + G\underline{u} \qquad (2\text{-}1)$$

where $\underline{x}$ is the vector describing the system

F, G are matrices representing the aircraft dynamics
$\underline{u}$ is the forcing function or disturbance

Through suitable integration of this equation from initial condition through touchdown (digitally, second or third order Runge-Kutte numerical integration techniques are used) a time history of the state vector may be generated for any particular disturbance inputs, u(t). There are no restrictions on the matrices F & G; they may be time varying, may contain state-dependent terms (i.e. they may be non-linear) . For the actual formulation used in this case see Appendix A.

The aerodynamic equations used do involve linearization about a stable flight condition and stability derivatives as normally understood form the basis for aerodynamic terms of the F & G matrices. They are allowed to vary, however, when non-linear conditions such as ground effect are encountered. Stability derivatives and the $\underline{x}$ vector, for the purposes of solveing equation 2-1 are defined with respect to stability axes (as opposed to instantaneous aircraft axes, or space fixed axes). This simulation method has been used extensively by the MIT Charles Stark Draper Laboratory in previous studies (Ref. 1) on various aspects of flight performance. The development and use of stability derivatives as a method of solving flight performance problems is treated by Blakelock in Reference 2.

In dealing with random forcing function such as wind gusts and beam noise, the direct simulation leaves much to be desired. With the direct simulation a subroutine is used to generate random numbers which are then conditioned to enter the simulation as the proper forcing function. In order to estimate the statistical relationship between input and performance factors, many different runs would be required with different random number sequences. To obtain the variance of a particular state variable, the results must be root mean squared for each particular time of interest. A vast number of runs would be required for each condition of interest if this method were attempted.

A second method, preferred for statistical evaluation, involves propagating the mean square value of the state vector directly. If the system behaves according to Equation (2-1), then the covariance matrix for the state variables behave according to Equation (2-2) (Ref. 3).

$$\dot{X} = FX + XF^T + GQG^T \tag{2-2}$$

$$X(t) = E[(\underline{x}(t) - \bar{x}(t))\ (x(t) - \bar{x}(t))] \tag{2-3}$$

$$Q(t) = E[(u(t) - \bar{u}(t))\ (u(t) - \bar{u}(t))] \tag{2-4}$$

where $X(t)$ is the covariance matrix at time t
E is the expected value operator
$Q(t)$ is the disturbance covariance matrix at time t
$\bar{x}(t)$, $\bar{u}(t)$ are mean values of $x(t)$ and $u(t)$
F, G, as defined in (2-1)

The following conditions must hold however:

(1) The system must be linear.
(2) $u(t)$ must be uncorrelated (white) noise.

Condition (1) is required since, for statistical validity, F or G may not depend on X or Q [For Equation (2-1) this is not necessary since each solution is a deterministic function of u and initial condition on x). Condition (2) imposes no real constraint since with proper filtering most random processes of interest can be generated from white noise; in practice this is done by expanding the $\underline{x}$ vector as required and adding the filtering to the F matrix (Ref. 3). Although they must be linear, the F and G matrices may still be time varying.

Linearization of the F & G matrices for the flight performance case involves dropping any signal limits imposed in the autopilot and ignoring all cross coupling terms (products of perturbations). Other simplifications in the interests of computational efficiency are also made; these are discussed in later sections.

There are also some mechanization problems in dealing with the effects of a sampled input (scanning beam) on a continuous system. A more complete description of the mechanization of both the simulation and the covariance propagation method appear in Appendix A.

The fact that the covariance propagation equation must be linear brings with it one significant advantage; linearity implies that superposition holds. It is therefore possible

to generate a single covariance matrix in response to a unit gust strength and one in response to unit beam noise and linearly combine the results to generate the covariance matrix for any other particular set of wind and noise conditions. [Provided that the system and disturbance dynamics remain constant]. The F & G matrices are, however, dependent upon scan rate, so it is necessary to generate a set of these unit covariance matrices for each scan rate of interest.

The unit covariance matrix will generally be referred to as the covariance sensitivity matrix and be represented by $Z(w_o)$ or $Z(n_o)$, where w_o and n_o are unit gust strength and beam noise variance, respectively.

In order to assure that simplifications and assumptions required to use the covariance propagation method do not significantly distort the system model, the linearized system matrices, F and G, are used to generate simulation results for particular wind and noise conditons which are then compared with results using the original, nonlinear, F and G matrices with the same input conditions.

In addition to providing a check on the covariance propagation program, the simulation will be used to generate nominal trajectories for all deterministic inputs under consideration (wind shear, beam bias, etc.), to provide a basis for specifying the dynamic characteristics of the aircraft being simulated, and to generate representative trajectories with wind gusts and beam noise for various scan rates.

The results of the covariance propagation programs will be used to statistically compare performance under various conditions against criteria established for safety and pilot acceptability.

The ideal method for statistical comparison is, of course, in a probabilistic sense; that is, comparing the probability of exceeding a limit under one set of conditions against that of exceeding it under another set of conditions. If the variable involved is (or can be assumed) gaussian, then knowledge of the variance or standard deviation is sufficient to compute these probabilities.

For example, suppose the limit for safety on an hypothetical variable x is $\pm$ 5, and that under worst case wind and noise conditions the variances (σ^2) of x generated by the covariance propagation programs for 10 and 1 samples per second were 1.10 and 1.30, respectively. The one sigma (1σ) values are then 1.05 and 1.14 respectively. The limit at 10 scans per second represents a 4.76σ value while at 1 scan

it represents a 4.38σ value. From standard tables for the gaussian distribution function, we find the probability of exceeding the limit at 10 scans per second is approximately $2x10^{-6}$ while that at 1 per second is $1.2x10^{-5}$. For a family of scan rates and beam noise rates a family of curves such as those of Figure 2-3(a) would result. It is then possible to choose an acceptable probability level and generate beam noise scan rate trade off curves such as those of Figure 2-3(b). All combinations of beam noise values and scan rates to the right and below a constraint curve are then acceptable for that particular constraint.

Unfortunately, limits on variables critical to safety of the landing are defined at touchdown, and the covariance propagation method as now mechanized for this problem encounters significant difficulties in generating absolutely valid results at touchdown. The presence of ground effect during the last 30 feet of descent for a large aircraft such as the CV-880 is one source of these difficulties. The other major significant source is in the formulation of the equations. The covariance matrix is propagated for deviations about a nominal trajectory with nominal time as the index. Since critical points in the trajectory, (flare initiation, decrab initiation, and touchdown) are functions of altitude rather than time, they do not necessarily occur at nominal time. Variations in time affect those variables with significant rates of change during the period of interest, such as longitudinal touchdown position, whose rate of change is equal to forward groundspeed. (Most of the lateral variables of interest also have significant nominal time dependence during the decrab maneuver). Under high wind conditions variations in time from flare altitude to touchdown and time from decrab altitude to touchdown can be large, due to the low nominal sink rate and large sink rate dispersions. (Sink rate statistics are also heavily dependent on ground effect). Attempts to form even partially valid approximations to account for time dispersion have been unsuccessful to date except for limited applications.

Therefore, although absolute safety limits for critical touchdown variables are set (see Section 6), it will not be possible to state with any confidence the probability of meeting those limits.

It is possible, however, to evaluate the effects of scan rate and beam noise on these variables in a comparative manner. Using the partial results generated by the covariance propagation equations, one can show percentage variation in RMS deviation of critical variables at touchdown as scan rate, beam noise or other disturbances are varied. It is unlikely

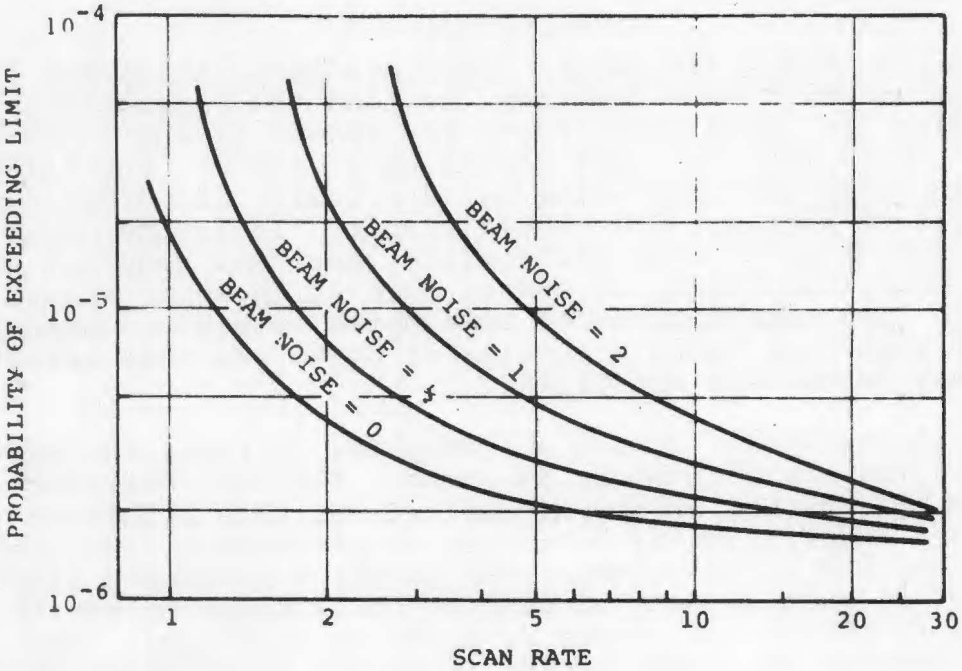

Figure 2-3(a). Probability of Exceeding a Limit Vs. Scan Rate - Hypothetical

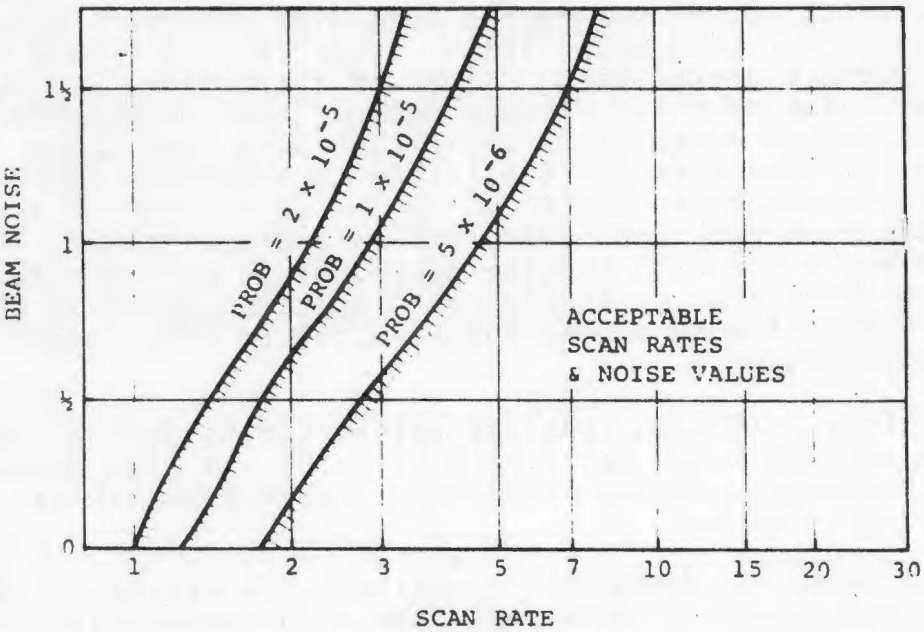

Figure 2-3(b). Scan Rate-Beam Noise Tradeoff For Various Probability Levels

that the effects not accounted for would cause significantly different percentage deviation under similar conditions.

It is then possible to identify:

(1) Those of the critical variables which are most sensitive to scan rate and/or beam noise.
(2) Scan rates and noise levels which cause significant increases in critical variable deviations from the ideal condition of a perfect continuous information system.
(3) Scan rates and noise levels which cause increases in deviations corresponding to those of a Category III conventional ILS with a "best case" noise model.

In areas other than near touchdown (final approach, decision height, flare initiation) the assumptions required to linearize the flight and control equations do not have serious effects on the results. It is therefore expected that the covariance propagation results in these areas are close to absolutely valid. A direct comparison can be made between these results and limits set for pilot acceptability in Section 6.

References

1. Desai, M., MacKinnon, D., Madden, P., *Optimal and Suboptimal Flight Path Control in the Terminal Area Using Radio-Inertial Measurements*, MIT Draper Lab Report R-666, July 1970.

2. Blakelock, J. H.; *Automatic Control of Aircraft and Missiles*, John Wiley & Sons, 1965 - Chapters 1 & 3.

3. Bryson, A. E., and Ho, Yu-Chi, *Applied Optimal Control*, Blaisdell Co., 1969 - Chapter 11.

3. ATMOSPHERIC TURBULENCE MODELS

The most critical factor affecting an aircraft's ability to land is the atmospheric environment or wind with which it must contend during final approach. Wind may be divided, for modelling purposes, into three categories: (1) Steady Winds (headwind, or tailwind, crosswind); (2) Wind Shear (steady wind gradient with altitude); and (3) Wind Gusts (random turbulence).

In order to realistically evaluate landing performance of simulated aircraft, it is necessary to define as accurately as possible the charactecistics of the environment that these aircraft are subjected to in the real world. A thorough literature search has therefore been undertaken to define a worst case (99% probable) set of conditions and to determine the characteristics of importance in and the interrelation between the three wind categories.

3.1 STEADY WIND AND WIND SHEAR

These parameters are relatively easy to deal with since they are "deterministic" functions and can be easily measured in the real world. Steady wind is normally defined at a "reference altitude" of 50 feet. For our purposes, this steady wind at 50 feet will be called "mean reference wind". The mean wind at any other altitude (up to approximately 400 feet) is a function of the wind shear profile and is generally taken to vary logarithmically with altitude (Ref. 3; Ref. 7; p. 17) according to Equation (3-1):

$$U_w(h) = U_{wo}[1 + K_s \text{ Log } (h/ho)] \qquad (3\text{-}1)$$

where: $U_w(h)$ = mean wind at altitude h
U_{wo} = mean reference wind
h_o = reference altitude
K_s = empirically determined constant

Equation (3-1) has been rearranged and slightly simplified in comparison to those appearing in the references to better reflect its meaning in terms of our variables. The constant of proportionality K_s, is a function of ground surface roughness; the more wind impedance offered by the ground surface, the higher Ks will be. For comparison K_s for ice or mud flats is 0.2, for tall thick grass, 6-20 inches high, K_s=.45 (after Ref. 7). With a 25 kt headwind at 50 ft., the corresponding winds at 100 and 200 ft. would be 27.8 and 31.8 kts respectively. Figure 3-1 plots $U_w(h)$ with K_s=0.5, a condition which we shall use as "worst case". Figure 1 also shows a further simplifi-

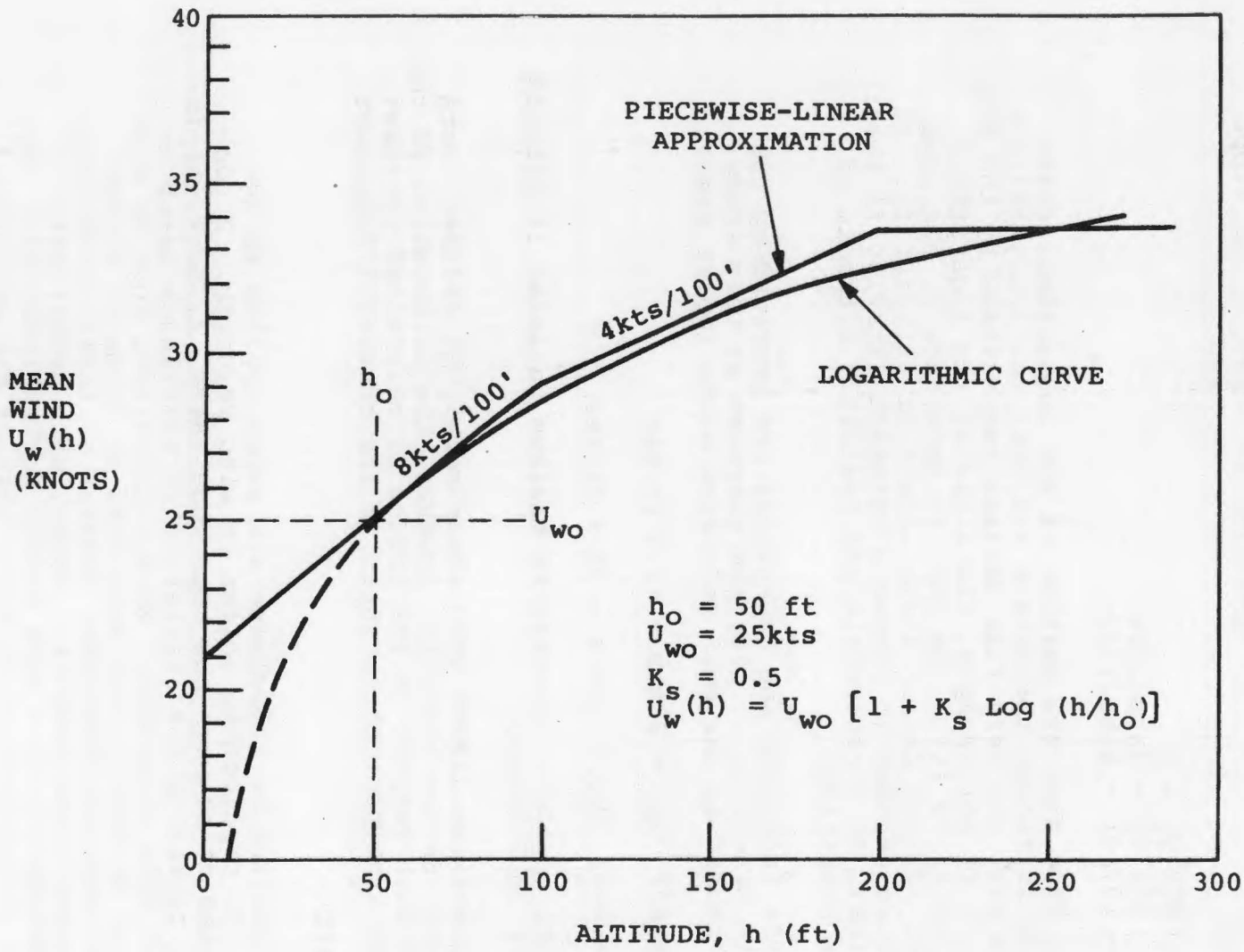

Figure 3-1. Wind Shear Profiles: Logarithmic and Piecewise Linear Approximation

cation. A piecewise linear approximation will be used in lieu of the actual logarithmic profile to reduce computation time. The approximation chosen agrees quite well with the logarithmic curve above 50 ft., and is specified in terms of its slope as follows:

Above 200 ft - 0
100 - 200 ft - 4kts/100ft
0 - 100 ft - 8kts/100ft

It is felt that the portion of the logarithmic curve below 50 ft is rather too severe and does not truly reflect conditions over the very flat surface represented by the runway. (At 25 ft for example, the slope of the logarithmic curve is 30kts/100 ft). The FAA, in Reference 1, has also recommended maximum design shear levels of 8kts/100 ft. It was therefore decided to choose a constant 8kts/100 ft shear below 50 feet, as a reasonable and realistic estimate of worst case condition.

The 99% headwinds and crosswinds are provided by the appendix to Reference 1. For the purposes of this study, these are chosen as the mean reference winds (worst case):

Headwind: U_{WO} = 25kts = 42.3 ft/sec

Crosswind: V_{WO} = 15kts - 25.4 ft/sec

In addition, a generally accepted maximum tailwind is defined at 10kts or 16.9 ft/sec.

The piecewise linear wind shear model, as defined, acts directly only on the headwind; however, the orientation of the total wind with respect to the ground is maintained constant, introducing a proportionate shear in the crosswind component.

3.2 WIND GUSTS

Wind gusting or turbulence are names applied to non constant, non predictable shifts in wind velocity. A considerable amount of work has been done (Refs. 2, 3, 4, 5) in attempting to define the statistics of turbulence based on the limited data available. Random processes, such as turbulence, are generally best specified in terms of either their power spectra (frequency domain) or their autocorrelation functions (time domain). Since, with actual data, spectral estimation is a more easily accomplished task than estimation of correlation in time, most of the work done appears in the form of power spectra. Table 3-1 lists a number of empirically determined or generally accepted analytic

TABLE 3-1
ATMOSPHERIC TURBULENCE SPECTRA

Von Karman (after ref 2)

$$\Phi_u(\omega) = \sigma_u^2(2L_u/\pi U_o)\cdot\frac{1}{[1+1.79(L_u\omega/U_o)^2]^{5/6}}$$

$$\Phi_v(\omega) = \sigma_v^2(L_v/\pi U_o)\cdot\frac{[1+4.78(L_v\omega/U_o)^2]}{[1+1.79(L_v\omega/U_o)^2]^{11/6}}$$

$$\Phi_w(\omega) = \sigma_w^2(L_w/\pi U_o)\cdot\frac{[1+4.78(L_w\omega/U_o)^2]}{[1+1.79(L_w\omega/U_o)^2]^{11/6}}$$

Dryden (ref 2)

$$\Phi_u(\omega) = \sigma_u^2(2L_u/\pi U_o)\cdot\frac{1}{[1+(L_u\omega/U_o)^2]}$$

$$\Phi_v(\omega) = \sigma_v^2(L_v/\pi U_o)\cdot\frac{[1+3(L_v\omega/U_o)^2]}{[1+(L_v\omega/U_o)^2]^2}$$

$$\Phi_w(\omega) = \sigma_w^2(L_w/\pi U_o)\cdot\frac{[1+3(L_w\omega/U_o)^2]}{[1+(L_w\omega/U_o)^2]^2}$$

Lappe (ref 2)

$$\Phi_{u,v,w}(\omega) = \sigma^2(L/U_o)\cdot\frac{1}{[1+L\omega/U_o]^2}$$

FAA (ref 1)

$$\Phi_{u,v,w}(\omega) = \sigma^2(2L/U_o)\cdot\frac{1}{1+(L/U_o)^2\omega^2}$$

where:

subscripts u,v,w refer to longitudinal, lateral, and vertical axes respectively

$\Phi(\omega)$ = turbulence power spectrum; $(ft/sec)^2/rad/sec$
ω = temporal frequency (rad/sec)
σ = root mean square gust intensity (ft/sec)
L = scale length (ft)
U_o = aircraft nominal airspeed (ft/sec)

expressions for turbulence spectra in all three axes (lateral, longitudinal, vertical). (The FAA model for all three axes is identical to the Dryden longitudinal spectrum). Gault and Gunter, in Reference 2, have compared these expressions against actual data and find the Von Karman spectra to be most representative of true conditions. The main point of difference between Von Karman and the others are the denomina- to exponents, 5/6 or 11/6 as opposed to 1 or 2. This affects the slope of the rolloff at higher frequencies, so that below the half power frequency the spectra tend to agree very well. The Von Karman contains relatively more energy at high frequencies, but less around the break frequency. It is felt that since the differences are minor and since an aircraft tends to filter high frequency gusts, that the added complexity involved in using the Von Karman spectra is not warranted for our problem. The FAA and Lappe spectra are further simplifications, using but one form for all three axes. It is not necessary, for simulation purposes, to take advantage of these simplifications, consequently the Dryden Spectra were used in their study.

The choice of rms gust intensity, σ, and scale length, L, is another point on which there is considerable disagreement, again, due primarily to the fact that adequate data does not exist over the wide range of possible atmospheric conditions and geographic location. References 3 and 4, however, do contain a set of empirically generated equations for computing these parameters as a function of mean wind and altitude. Statistically, the confidence level in assigning the actual numbers in Equations (3-2), (3-3), and (3-4) is not very high, but as the best information currently available, they should serve as representative conditions.

$$\sigma_w = 1.67 + 0.08U_{wt}(h) \text{ (ft/sec)} \tag{3-2}$$

$$L_w = h \tag{3-3}$$

$$L_u = L_v = 145(h)^{-1/3} \tag{3-4}$$

where: $U_{wt}(h)$ is the total mean wind speed at altitude h

It is assumed that the aircraft under consideration is moving through a horizontally homogeneous turbulence field, and the values for σ_u and σ_v are determined from Equation (3-5):

$$\frac{\sigma_u^2}{L_u} = \frac{\sigma_v^2}{L_v} = \frac{\sigma_w^2}{L_w} \tag{3-5}$$

$$\text{Hence: } \sigma_u^2 = \sigma_v^2 = \frac{L_u}{L_w}\sigma_w^2 \tag{3-6}$$

Suitable combination of Equations (3-2), (3-3), (3-4), and (3-5) with the linear approximation for $U_w(h)$ will then yield all σ and L parameters.

The remaining term in the spectra equation U_o, nominal airspeed is determined on approach by pilot setting. Equation (3-7) defines this nominal (one method currently used by pilots to set airspeed) in terms of aircraft stall speed and estimated wind parameters.

$$U_o = 1.3U_{STALL}+0.5U_{wo}+2\sigma_u \qquad (3\text{-}7)$$

Equations (3-5) and (3-6) appear to break down, however, below 50 ft; according to (3-3) and (3-4) scale lengths would tend to zero with decreasing altitude, and the use of (3-5) to compute σ_u, σ_v would result in excessively large gust intensities at altitudes below 50 ft. The following constraints are therefore imposed:

$$L_u \text{ min} = L_v \text{ min} = 600 \text{ ft} \qquad (3\text{-}8)$$

$$L_w \text{ min} = 30 \text{ ft} \qquad (3\text{-}9)$$

$$\sigma_u \text{ max } (h) = \sigma_v \text{ max } (h) = 2\sigma_w(h) \qquad (3\text{-}10)$$

Figure 3-2 shows the variation of L and σ with altitude with constraints as imposed by (3-8), (3-9) and (3-10)

Figure 3-3 plots the bandwidth of the aerodynamic turbulence vs. altitude for two aircraft (bandwidth is related to approach speed, U_o), the CV-880 and PA-30 currently being used in the simulation. The Dryden spectra are assumed.

The fact that the aircraft has finite dimension sometimes comparable to gust scale length requires that gust gradients also be considered as atmospheric noise inputs to the aircraft. These take the form of pseudo rotational rates and have spectra and variances related to the longitudinal, lateral, and vertical gust components. The spectra computed based on the Dryden model are shown in Table 3-2.

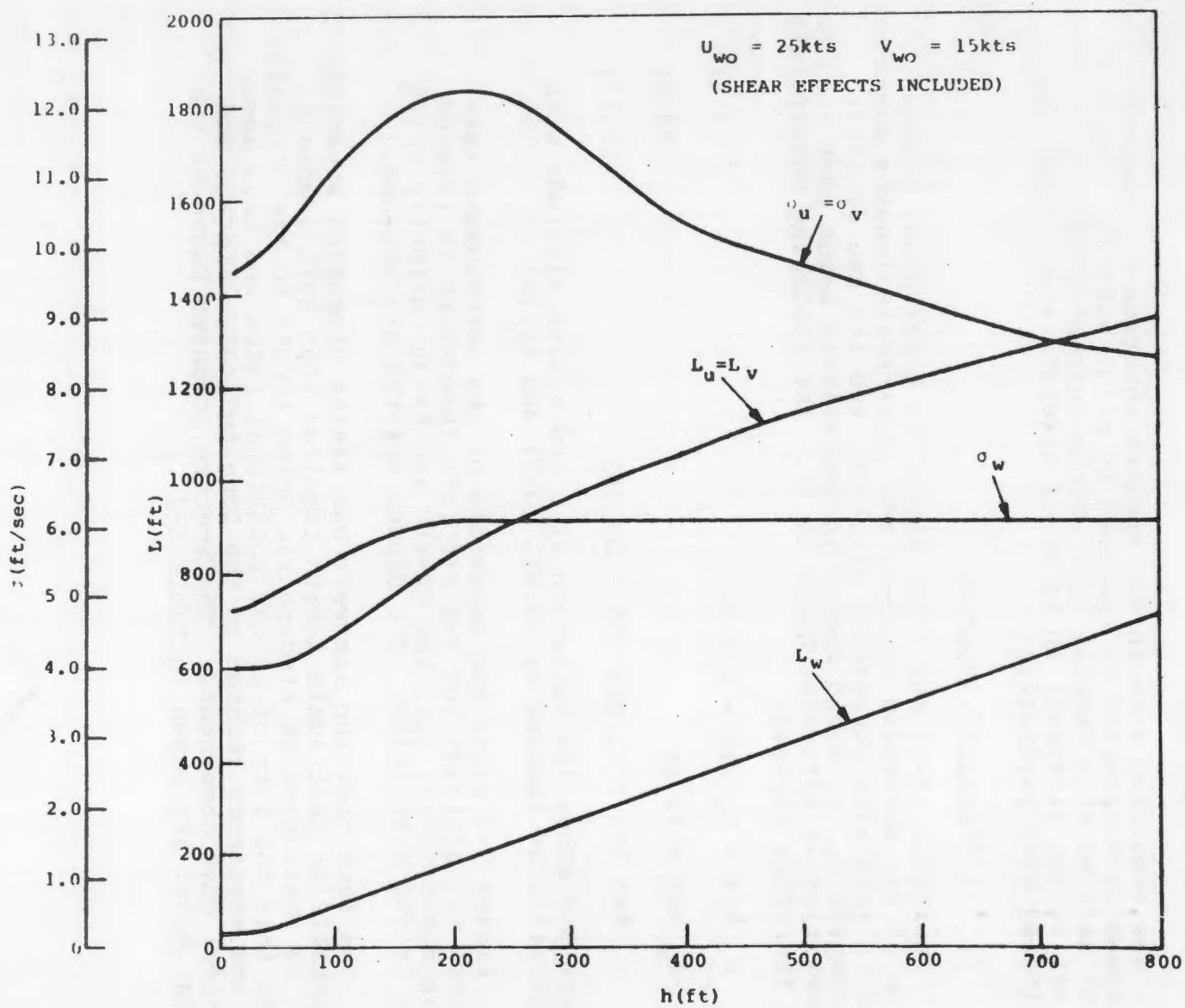

Figure 3-2. L & σ vs. Altitude

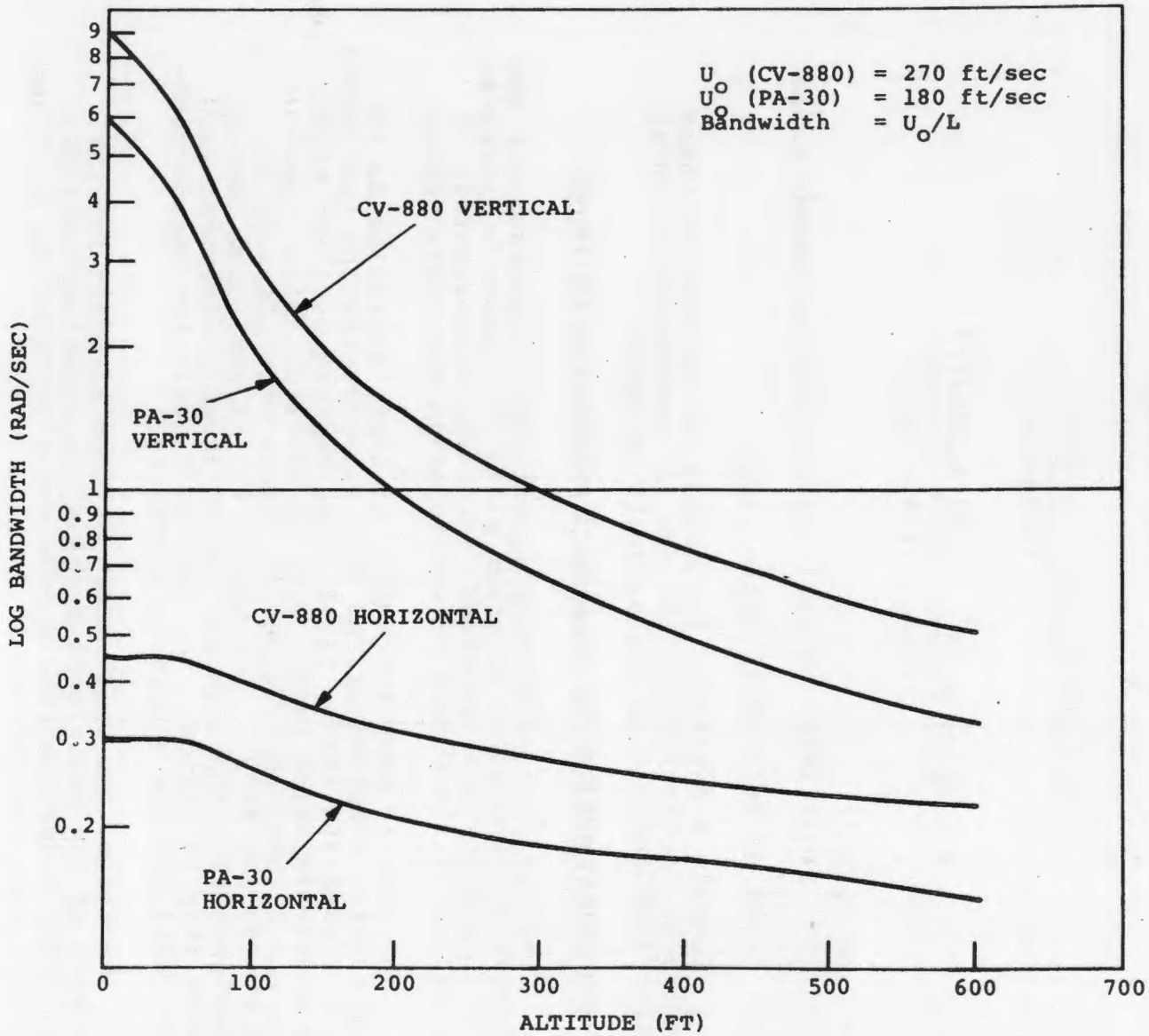

Figure 3-3. Turbulence Bandwidth vs. Altitude

TABLE 3-2
PSEUDO ROTATION RATE SPECTRA

$$\Phi_q(\omega) = \Phi_w(\omega) \frac{(\omega/U_o)^2}{1+(4b\omega/\pi U_o)^2}$$

$$\Phi_r(\omega) = \Phi_v(\omega) \frac{(\omega/U_o)^2}{1+(3b\omega/\pi U_o)^2}$$

$$\Phi_p(\omega) = \frac{\sigma_w^2}{U_o L_w} \frac{0.8(\pi L_w/4b)^{1/2}}{1+(4b\omega/\pi U_o)^2}$$

b = wing span
subscripts p,q,r refer to roll, pitch, and yaw pseudo rates, respectively
other terms as defined in Table (3-1)

Appendix B describes the method for generating these spectra by digital simulation and the mechanism for introduring turbulence into the aircraft dynamics.

3.3 SIMPLIFICATIONS FOR THE COVARIANCE PROPAGATION EQUATIONS

Computational efficiency is extremely important for the covariance propagation programs since the number of integration (hence the time required) increases approximately as the square of the number of variables in the state vector.

In order to keep the number of state variables as low as possible, simplifications such as approximating the second order Dryden spectra by first order expressions, and eliminating the pseudo rotation rates, were considered. Simulation runs with and without these simplifications were compared for both the CV-880 and PA-30. For the CV-880 it was found that performance during approach was not noticeably different with either simplification. For the PA-30, only the pseudo rotation rates produce significant effects.

Therefore, the wind model for both aircraft for the purposes of the covariance propagation equations includes only first order spectra; pseudo rotation rates are included only for runs with the PA-30.

In constructing the propagation programs for a continuous system with sampled input, it was further found that maintain-

ing constant parameters (σ, L) for the gust model also greatly reduces the complexity of computation. (see Appendix A). As can be seen from Figure 3-2, the effects of maintaining constant σ are small since they vary by no more than 10% over the last 600 ft. approach. The scale length, L, affects the bandwidth of the aerodynamic turbulence. Figure 3-3 shows that there is little change in bandwidth of the lateral and longitudinal components during final approach; there is, however, significant variation in vertical component bandwidth. It was decided to choose values near touchdown in order to most accurately reflect performance in this area.

Table 3-3 summarizes the spectra and spectral parameters for use with covariance propagation programs.

TABLE 3-3
SPECTRA AND PARAMETER VALUES
FOR COVARIANCE PROPAGATION PROGRAMS

$$\Phi_u(\omega) = \sigma_u^2 (2L_u/\pi U_o) \cdot \frac{1}{[1+(L_u\omega/U_o)^2]}$$

$$\Phi_v(\omega) = \sigma_v^2 (2L_v/\sqrt{3}\pi U_o) \cdot \frac{1}{[1+(L_v\omega/\sqrt{3}U_o)^2]}$$

$$\Phi_w(\omega) = \sigma_w^2 (2L_w/\sqrt{3}\pi U_o) \cdot \frac{1}{[1+(L_w\omega/\sqrt{3}U_o)^2]}$$

pseudo-rotational rates for PA-30 only:

$$\Phi_q(\omega) = \Phi_w(\omega) \cdot (\omega/U_o)^2$$

$$\Phi_r(\omega) = \Phi_v(\omega) \cdot (\omega/U_o)^2$$

$$\Phi_p(\omega) = (\sigma_w^2/U_o L_o) \cdot \frac{(0.8)(\pi L_w/4b)^{1/3}}{[1+(4b\omega/\pi U_o)^2]}$$

$\sigma_u = \sigma_v = 2\sigma_w$
$L_u = L_v = 600$ ft
$L_w = 30$ ft
b = wing span
other variables as defined in Table 3-1

References

1. FAA Advisory Circular 20-57A, *Automatic Landing Systems*, 12 Jan 1971.

2. Gault, J. D. and Gunter, D. E., Jr.; *Atmospheric Turbulence Considerations for Future Aircraft Designed to Operate at Low Altitude*, J. Aircraft, Vol. 5, No. 6, Nov - Dec 1968.

3. Lappe, U. Oscar, *Low Altitude Turbulence Model for Estimating Gusts Loads on Aircraft*, J. Aircraft, Vol. 3, No. 1, Jan - Feb 1966.

4. Chalk, O. R., Neal, T. P., Harris, T. M., Pritchard, F. E., and Wookcock, R. J., Background Information and User Guide for MIL-F-8785B (ASG), *Military Specification--Flying Qualities of Piloted Airplanes*, AFFDL-TR-69-72, Aug. 1969.

5. Neuman, F. and Foster, J. D., *Investigation of a Digital Automatic Aircraft Landing System in Turbulence*, NASA/Ames Research Center, June 1970.

6. Signal Format Development Team Report to RTCA SC-117. *Microwave Scanning Landing Guidance System (LGS)*, Sept. 5, 1970. Radio Technical Commission for Aeronautics, Washington, D.C.

7. Cafarelli, N. J., and Meyer, M. A., Tacland Studies, AFFDL-TR-68-42, AFFDL/AFSC Wright-Patterson Air Force Base, April 1968.

4. LGS SCANNING BEAM AND CONVENTIONAL ILS MODELS

4.1 LGS SCANNING BEAM MODEL

The RTCA recommended scanning beam system generates four basic functions: DME, azimuth, glideslope elevation, and flare elevation. Azimuth and elevation information is in angular form referenced to the runway centerline. Actual position in x, y, z coordinates with respect to touchdown point requires a knowledge of the geometry of the transmitting antennas with respect to the runway. Figure 4-2 shows in plan view one such configuration which will be used for the purposes of this study. (Figure 4-2 also shows 50 ft. altitude point for a 2.5 degree glideslope).

Since the aircraft currently under consideration are equipped only with autopilots for conventional ILS, they do not make use of either DME or flare elevation information; the rest of this discussion, therefore, will be limited to the azimuth and glideslope elevation functions.

In order to avoid the complexities of examining actual beam and receiver configuration it will be assumed that the autopilot is presented with a discrete angular position indication at each sampling instant. This data is then processed through some form of hold circuit and then goes directly to the localizer and/or glideslope signal inputs of the autopilot as illustrated in Figure 4-1.

The position sample may be corrupted by noise and bias; the hold circuit may be as simple as a zero order hold or in a more complex manner perform partial sample processing. The filter may range from simple first order to complicated noise and notch filters.

Since little of a definitive nature is currently known about the dynamics, errors, and error souress of the scanning beam configuration, only the simplest assumptions will be made here.

The position sample model will include true angular position, bias, and a gaussian noise component which is uncorrelated from sample to sample.

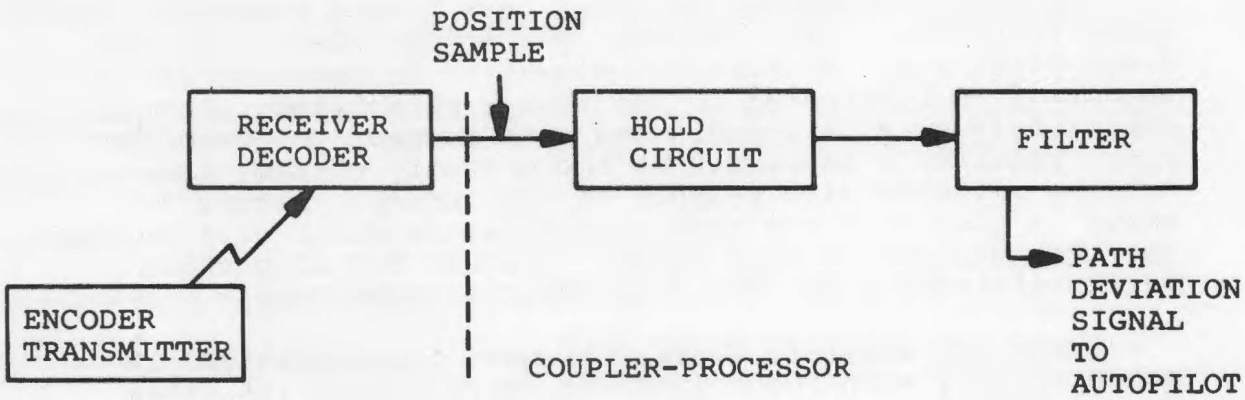

Figure 4-1. Schematic Diagram: Scanning Beam Processing

Possible error inducing effects which are not considered include:

1. Signal Granularity. Based on reasonable assumptions about the receiving-decoding process, granularity in the processed signal is likely to be two orders of magnitude less than the RTCA selected allowable error. See Appendix C.

2. Anomalies and delays due to beam reflections.

3. Possible correlation between every other sample if a two antenna mechanical configuration is used.

4. Receiver processing delays.

5. Other unknown possible sources of error.

It is felt that data does not currently exist to adequately characterize these effects with any confidence.

Results in this report are based on the use of a zero order hold and first order filter with a small time constant.

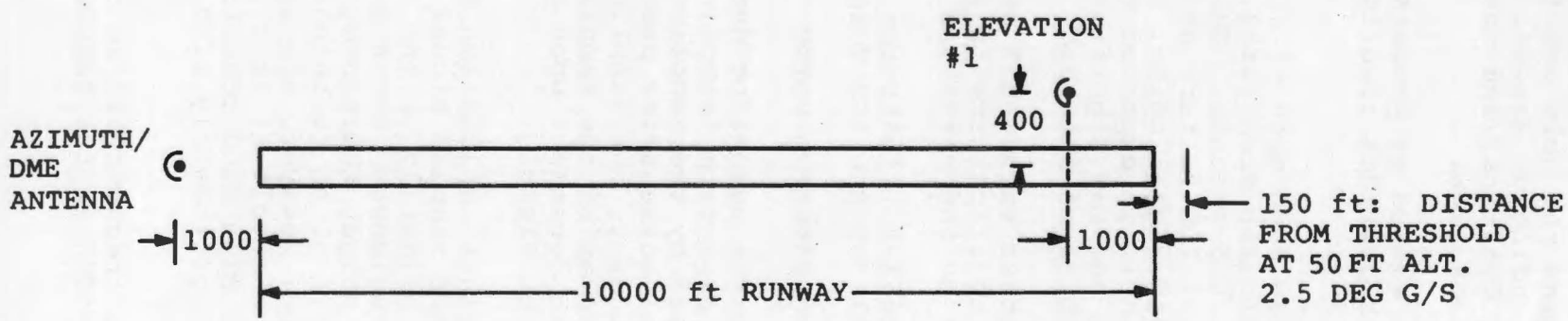

Figure 4-2. Plan View: Typical Layout Azimuth and Elevation Antennas

The problem of optimizing the hold and filter combination is extremely complex, depending on assumed noise characteristics and aircraft/autopilot dynamics, and must be examined from the total system point of view.

As the most simple method of processing, the zero order hold first order filter provides results which will reflect worst case conditions.

Since no attempt has been made at optimizing the filter time constant for particular scan rates, it was chosen rather arbitrarily at .025 seconds. This is extremely low compared to conventional ILS filters and should transmit most of the sampling and signal noise, effectively unfiltered, to the autopilot; again it is expected that this represents worst case processing, and may significantly affect the higher frequency variables of interest.

A second time constant value, 0.5 seconds, is used for a limited set of runs to illustrate in some sense the effects of a normal ILS filter on the variables of interest.

In summary, Figure 4-3 illustrates schematically the signal processing model for the LGS Scanning Beam.

4.1.1 SIGNAL NOISE AND SAMPLING NOISE

The noise entering the autopilot derives not only from the signal noise, but also from "sampling noise", that is, from the aliasing caused by the sampling process. While the bandwidth of the signal noise after processing is roughly half the sampling frequency, the sampling noise occurs at frequencies near multiples of the sampling frequency, its magnitude and bandwidth dependent upon the magnitude and bandwidth of the sampled signal.

There is one important implication for this study. Since the content of the sampled signal is position deviation, its properties depend primarily on the aerodynamic response of the aircraft to turbulence. For a given scan rate in the absence of signal noise, therefore, sampling induced errors will be proportional to turbulence intensity. Errors induced by signal noise, however, are independent of turbulence intensity. The result is that signal noise effects tend to "wash out" for high wind conditions, while sampling noise effects grow proportionately with wind. Figure 4-4 illustrates this effect.

Where the sampling frequency is an order of magnitude or greater than the bandwidth of the sampled signal, sampling

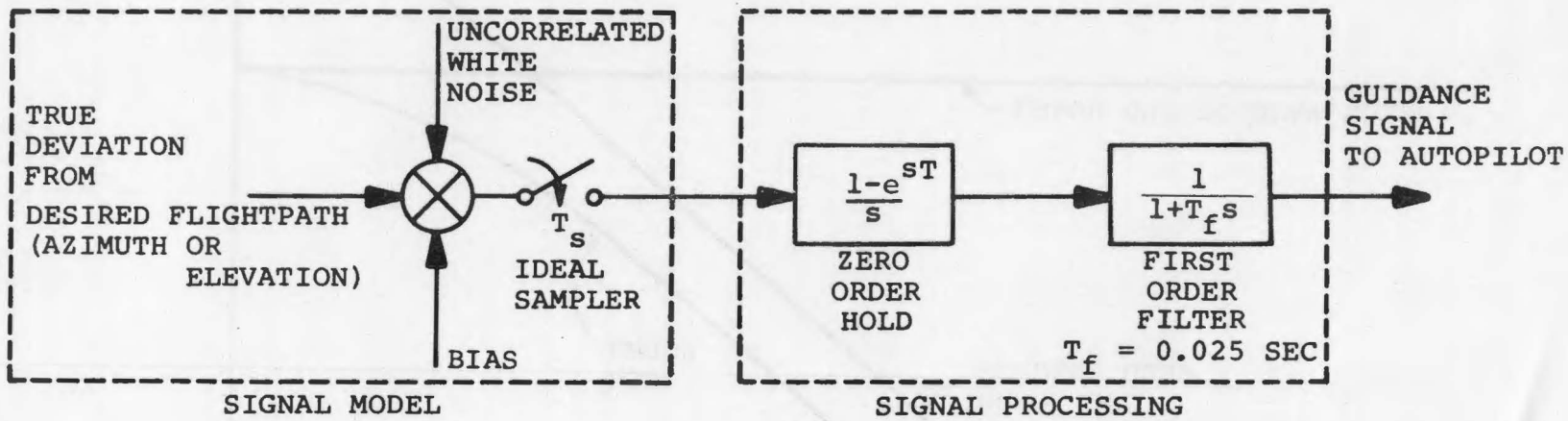

Figure 4-3. Signal and Processing Model for Scanning Beam

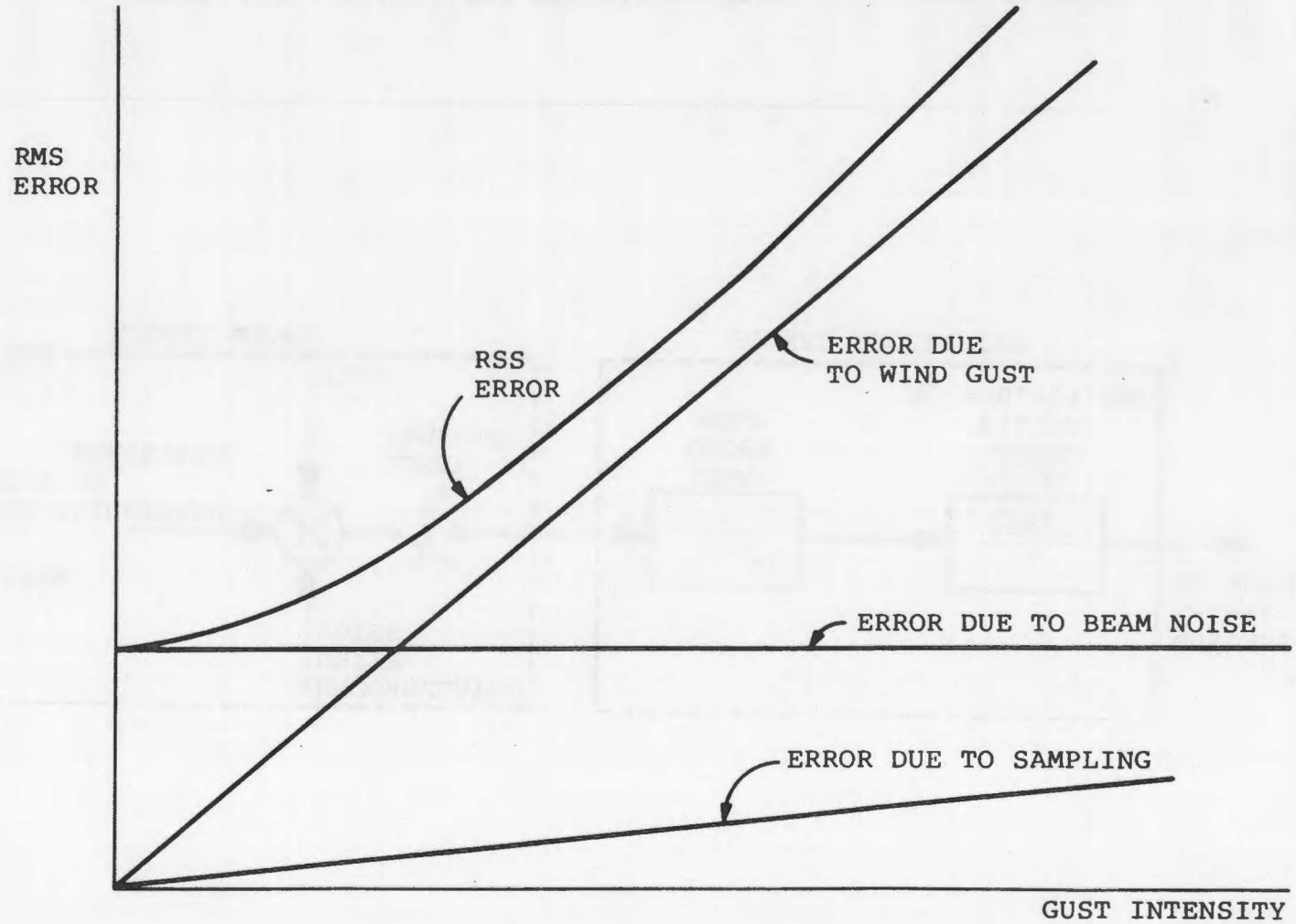

Figure 4-4. Errors Due to Wind Gusts, Signal Noise, and Sampling, vs. Gust Intensity

induced errors tend to become second order (although not unimportant) effects and their proportional contribution to total system errors can probably be expressed in single number percentages.

4.1.2 NOISE AND BIAS SPECIFICATIONS

In quantitatively specifying the noise and bias on the beam, the RTCA guidelines, as published in Reference 1 are used. Since these are given in terms of feet at minimum guidance altitude, some interpretation is required. [Such a specification requires elevation data to be more accurate in terms of angular specification for small angle glideslopes (2.5 degrees) than for large angle glideslopes (10-20 degrees).]

In this study the following assumptions are made:

(1) Angular errors are constant throughout approach.
(2) Angular error is determined from the RTCA linear specifications for configuration K, taken at flare altitude on a 2.5 degree glideslope.
(3) The variance of the random angular error so computed is the variance on the sample prior to processing.
(4) The horizontal beam width of the glideslope elevation signal is wide enough to permit signal detection at flare altitude.

Table 4-1 lists the results of computation based on the above and on numbers from Reference 1 (configuration I and K).

TABLE 4-1
ERRORS PER SCAN FOR SCANNING BEAM

		AZIMUTH	ELEVATION
BIAS	RTCA SPEC	10 ft.	1.2 ft.
	EQUIV ANGLE 50 ft. alt. 2.5 Deg. G/S	.05 deg.	.06 deg.
NOISE	RTCA SPEC	4.5 ft.	0.7 ft.
	EQUIV ANGLE 50 ft. alt. 2.5 Deg. G/S	.023 deg.	.035 deg.

The above numbers will be used as baseline or unit values in generating the covariance sensitivities to beam noise.

4.1.3 SCANNING RATES

Since it is impossible to generate results for all scan rates in the range of interest (1-40 per second), a limited number have been chosen for this study. These are; 40, 10, 5, 2.5 or 2, and 1 scans per second. It is felt that these should provide sufficient data, especially in the lower range, to adequately gauge scanning rate effects on performance of the aircraft under study.

4.2 CONVENTIONAL ILS MODEL

The conventional ILS is modeled as the perfect continuous version of the scanning beam system with added noise.

The noise model is based on ICAO Specifications (Ref. 2) for Category III operations. In order to generate a "best case" for conventional ILS for comparison purposes, the normal shaping of the beam errors from outer marker to middle marker is deleted and a constant 1σ error over the entire approach is assumed. The ICAO 2σ specifications in microamps (μA) are converted to errors in degrees according to Table 4-2.

TABLE 4-2
CATEGORY III ILS ERRORS

	ICAO 2σ Limits (microamps)	Conversion Factor (deg/microamp)	1σ Angular Error (deg)
Localizer	5	.0133	.03325
Glideslope	20	.0046	.046

The most important consideration in specifying ILS errors is the spectral distribution. As opposed to the assumptions made concerning the LGS model, the ILS errors do have significant correlation times (low frequency components; beam bends). Although in any rigorous sense, the spectrum of ILS errors defies general description, a first order spectrum has been postulated as a best available approximation to a general description. Table 4-3 lists the noise bandwidth and correlation time so postulated.

TABLE 4-3
SPECTRAL CHARACTERISTICS OF ILS ERRORS

	Bandwidth	Autocorrelation Time
Localizer	.33 rad/sec	3 sec
Glideslope	.33 rad/sec	3 sec

The coupler processor for conventional ILS becomes simply a first order filter with a time constant of 0.5 seconds.

References

1. RTCA SC-117 Final Report., *A New Guidance System for Approach and Landing*, DO-148, December 1970. Appendix A.

2. ICAO Annex 10: Aeronautical Telecomuunications, April 1968.

5. AIRCRAFT MODELS

5.1 DISCUSSION

5.1.1 "HEAVY JET TRANSPORT" VS. "LIGHT MANEUVERABLE"

At first glance, these titles, as applied to the CV-880 and PA-30, respectively, seem to have very definite implications in terms of flight performance. One thinks of a heavy jet transport as slow to respond, almost "lumbering" through the air, and of the light maneuverable craft as being able to perform maneuvers much more rapidly in time. However, for conventional aircraft, desirable riding and handling qualities for both types are basically the same and, in actuality, autopilots, controls and control surfaces are designed to satisfy goals based on these qualities. The net result is that, within certain bounds, attitude control dynamics for conventional aircraft of any type will be extremely similar. ILS coupler designs being basically limited by the ILS characteristics rather than by aircraft dynamics, should also tend to produce similar path following characteristics (in the time domain).

There are two significant fundamental differences, however: airspeed and weight. Because the PA-30 type craft flies at lower airspeed, it would indeed be more maneuverable in space than the CV-880 type, even though their time responses were identical. The aircraft wing loading, which is directly related to weight, has a significant effect on its performance in wind. One would expect the PA-30 to be blown around by turbulence much more readily than the CV-880.

Therefore, the terms "heavy" and "light" reflect in some sense a sensitivity to wind turbulence, and the terms "jet" and "maneuverable" imply differences in airspeed and maneuverability in space. None of these terms necessarily has any implications for the dynamic characteristics of the aircraft in controlled flight.

5.1.2 AIRCRAFT MODELS

The models include the airframe trimmed to desired flight configuration, the appropriate autopilot functions, control and control surface dynamics. There are minor differences between the nonlinear models used for simulation purposes and the linear ones for the covariance propagation equations.

5.2 THE CONVAIR 880 JET TRANSPORT

5.2.1 AIRFRAME

For approach and landing, the aircraft is assumed to be in a flight condition with full flaps and landing gear down. Appendix E lists the stability derivatives, physical and dynamic characteristics, and other constants of interest for the aircraft in this configuration. Appendix F describes the nonlinear equation of motion including ground effect, flexible body considerations, and hinge moment equations and further discusses assumptions and techniques involved in the simulation.

5.2.2 AUTOPILOT AND FLIGHT CONTROLS

The autopilot modelled for the purposes of this study is the basic Lear Siegler Autoland System designed for use with conventional ILS. Only minor changes have been made in accommodating the scanning beam LGS.

In approach and landing the autopilot provides the following functions: Localizer capture and initial track, Localizer final track, altitude hold, glideslope capture and track, automatic flare and automatic decrab. In addition, airspeed is controlled with an autothrottle loop. Figures 5-1 and 5-2 show the basic lateral and longitudinal position control loops in block diagram form; gains and time constants are also listed on these figures. Figures 5-3, 5-4, and 5-5 depict auxiliary control loops: yaw and decrab, altitude hold, and autothrottle respectively. Control surface dynamics appear in Figure 5-6.

Although no detailed analysis of the various loops and gains are undertaken here, it is possible to point out various important features of the coupler sections of the position control systems. The discussion will be limited to the final track mode, below 600 ft. altitude, since performance in this range is most critical to landing success.

The localizer coupler (Fig. 5-1) operates to command roll angle; it processes the localizer angular deviation (αy) through a constant gain (K_{YT_1}), washed out localizer rate (K_{YT_2}), with some small integral compensation (K_{IYT}); lagged roll ($K_{\phi L}$) is also used for rate compensation. There is no distance sensitive multiplier, which results in linearly increasing loop gain as the aircraft progresses towards the runway.

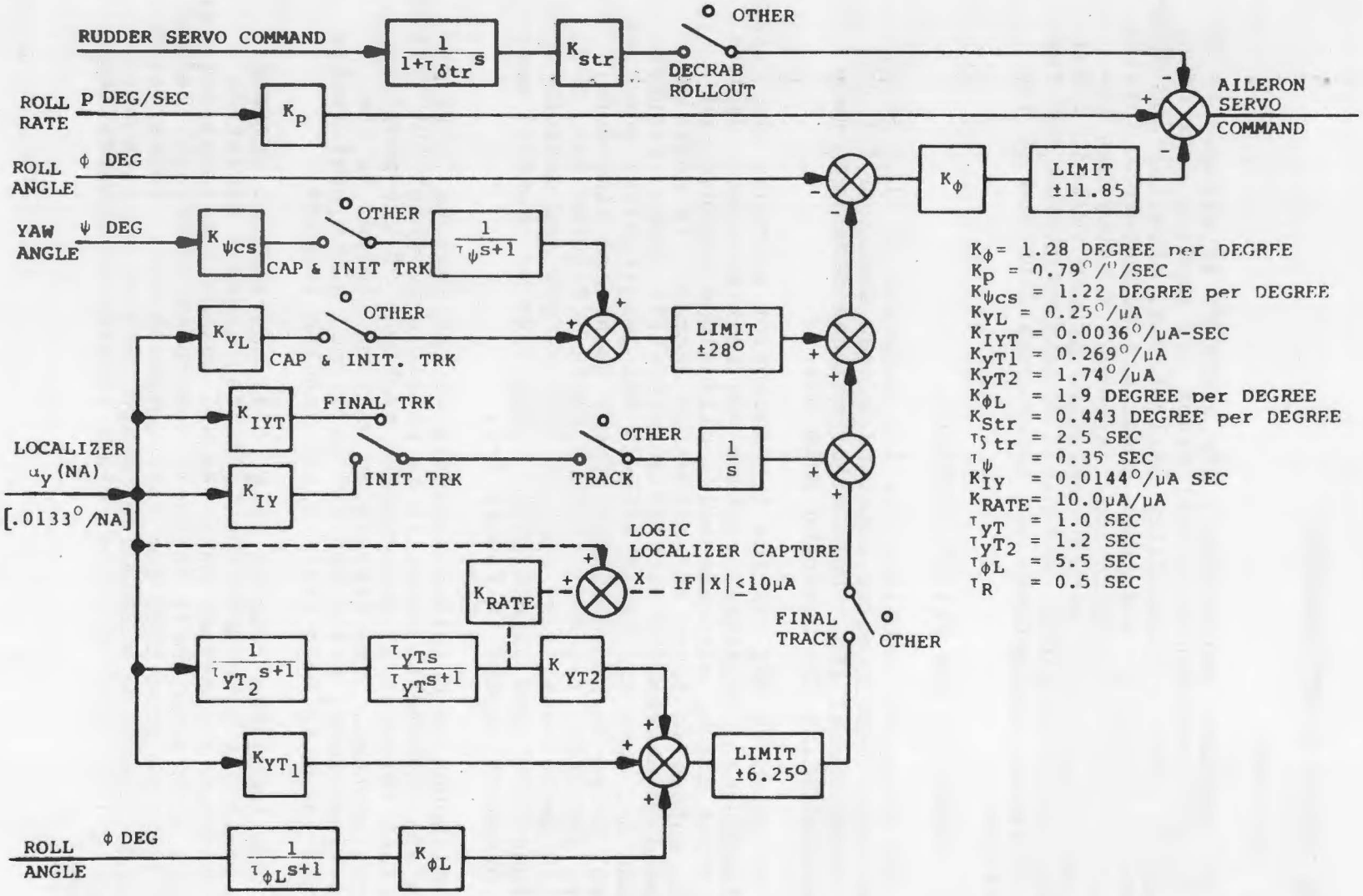

Figure 5-1. CV-880 Lateral Position Control System

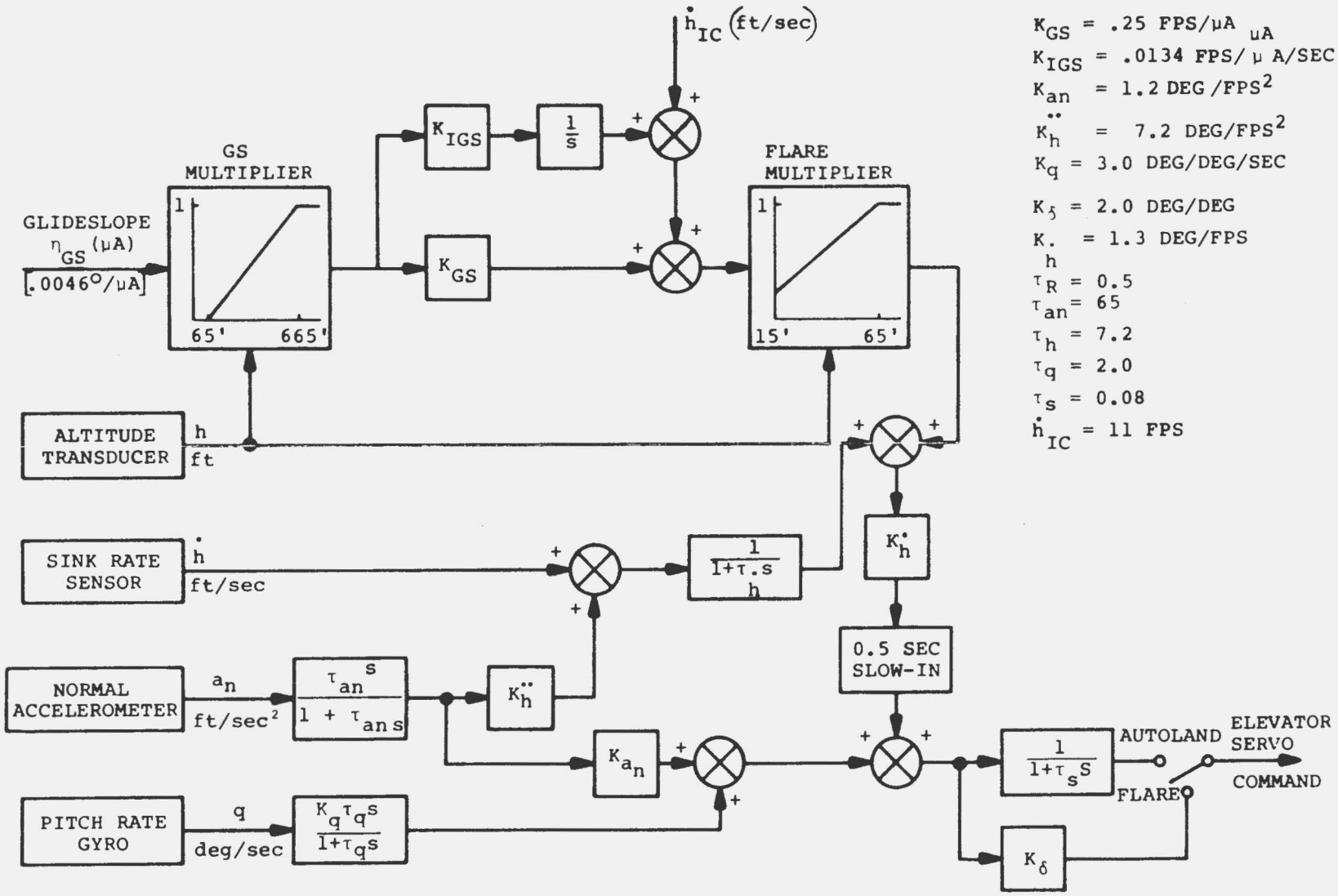

Figure 5-2. CV-880 Autoland Vertical Position Control System

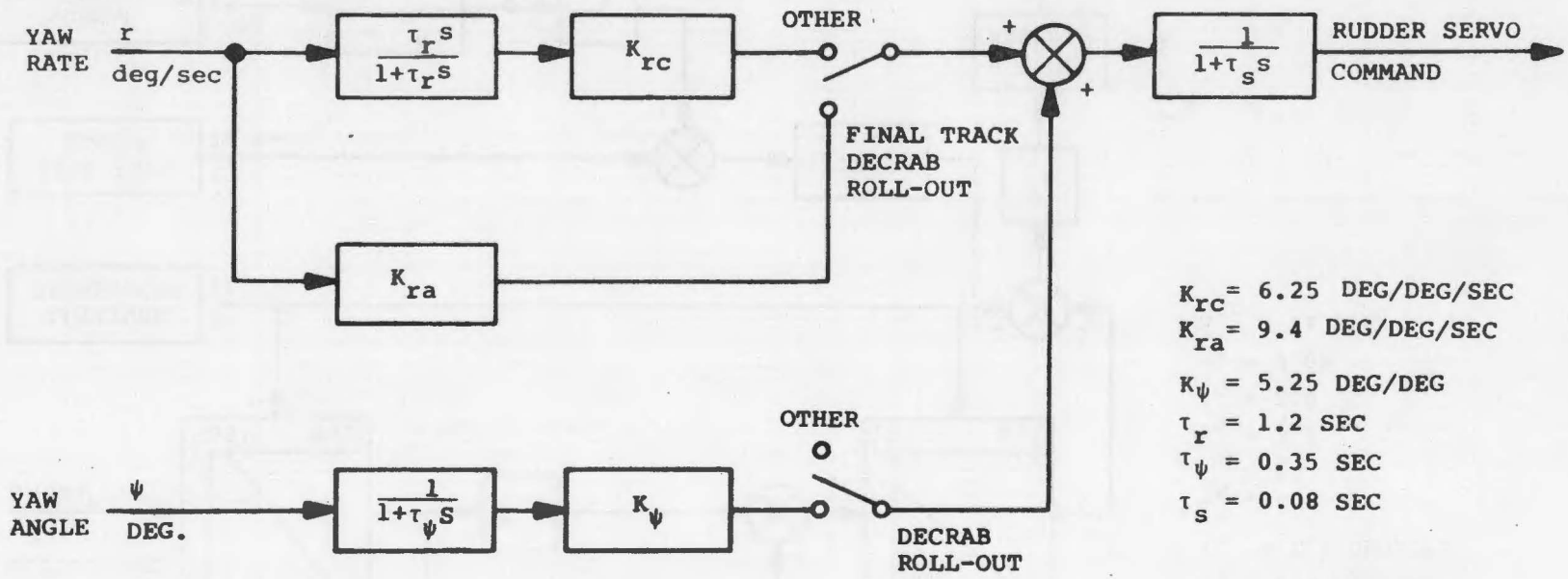

Figure 5-3. CV-880 Yaw & Decrab Control System

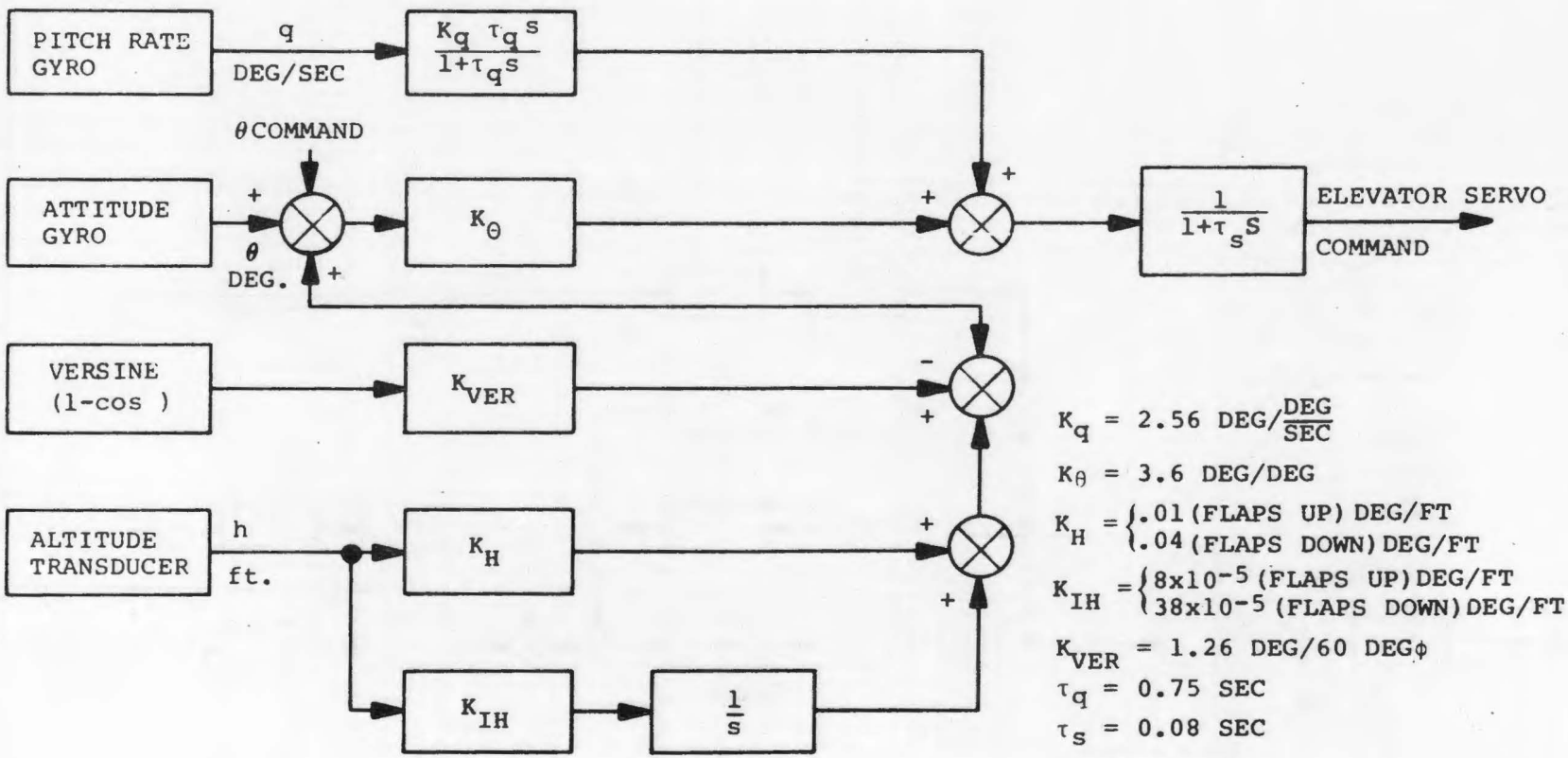

Figure 5-4. CV-880 Altitude Hold

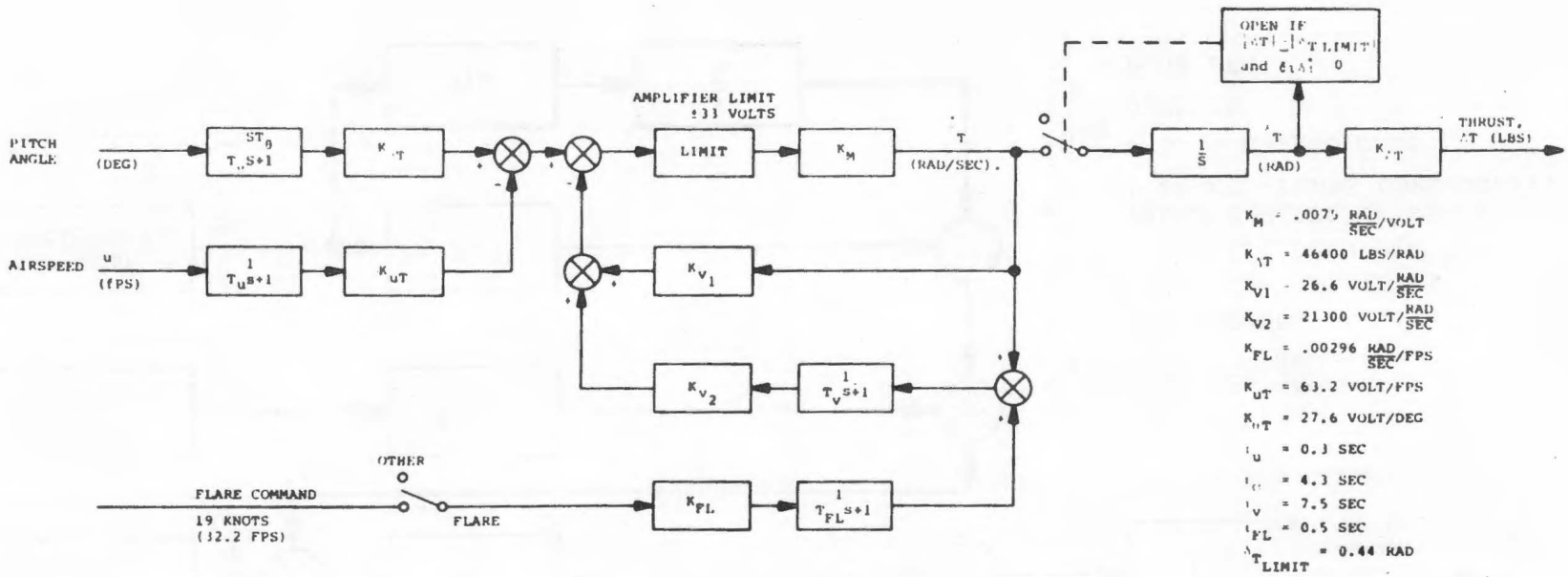

Figure 5-5. CV-880 Autothrottle

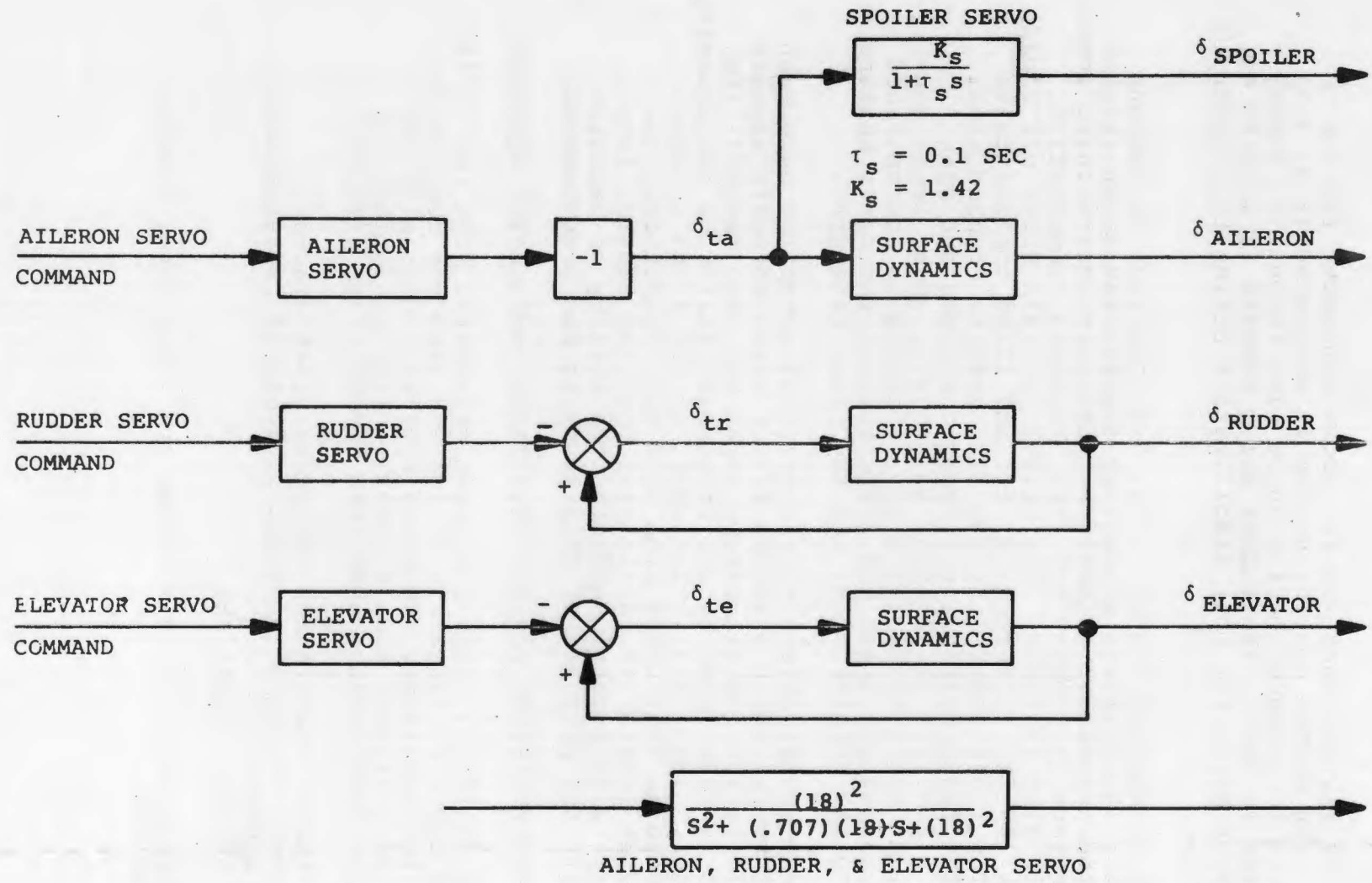

Figure 5-6. CV-880 Servo & Control Surface Dynamics

At 28 ft. altitude (13 ft. above touchdown for the CV-880), the Decrab control system is activated (Fig. 5-3) which acts to command heading angle with respect to runway centerline to zero. The rudder servo command is coupled to the aileron servo for roll stabilization during this maneuver. (Fig. 5-1).

The glideslope coupler (Fig. 5-2) operates to command sink rate; it processes glideslope angular deviation through an altitude sensitive glideslope multiplier (maintaining somewhat constant gain below 665 ft). Integral compensation (K_{IGS}) is also included. The glideslope gain drops off rapidly below 100 ft. to zero at 65 ft. and flare control takes over. The flare control system also acts to command sink rate. The flare multiplier reduces the commanded sink rate as a function of altitude to produce, under ideal conditions, an exponential flare law. Damping is accomplished in both glideslope track and flare through the contributions of the normal accelerometer and the pitch rate gyro.

Minor modifications to the original autopilot have been made. Firstly, the 0.5 second filter which normally appears at the localizer and glideslope input has been removed; its function is taken over by the processing filter of the scanning beam model. (Fig. 4-3). Secondly, it was found in simulation results that under high wind gust conditions, the 6.25 degree limiter in the lateral position control loop (Fig. 5-1) significantly affected the ability to maintain track; for the purposes of this study it has been removed.

5.2.3 MODIFICATIONS FOR THE COVARIANCE PROPAGATION EQUATIONS

The following items have been eliminated from the CV-880 model in order to linearize it for use with the covariance propagation equations. Comparison of runs made with the linear and nonlinear models under similar conditions has shown that none produce more than second order effects:

1) All limits shown in the autopilot block diagrams.
2) All cross coupling terms and products of perturbations. (see Appendix E)
3) Flexible body equations.

Time varying gains for glideslope and flare have, however, been retained.

5.3 THE PA-30 TWIN COMANCHE

5.3.1 AIRFRAME

The simulation and modelling methods are the same for this aircraft with the exceptions that there are no flexible body or hinge moment equations included. Appendix D lists stability derivatives and other physical constants associated with the model.

5.3.2 AUTOPILOT

The autopilot modelled is a version of the Cessna Navomatic 800A, modified for simulation purposes to provide response similar to Cessna 310 performance. For LGS functions it provides localizer and glideslope control only to 50 ft. altitude; there is no flare or decrab control system. A simple autothrottle loop (Fig. 5-9) was also added in order to provide some measure of control over airspeed (which would normally be accomplished by the pilot). Figure 5-7 is a block diagram of the localizer coupler and lateral control system; Figure 5-8 shows the longitudinal system.

Again, the normal glideslope and localizer filters have been removed and included as part of the scanning beam processing model.

Some of the inner loop gains have been increased to provide faster attitude response, and in the longitudinal system, gain scheduling for glideslope error has been added from 1500 ft. down. The constant glideslope gain attained through gain scheduling is roughly equivalent to that of the original autopilot at 200 ft. altitude. With conventional ILS, the pilot would take over control at 200 ft. and perform the remainder of the approach manually. For the purposes of this study, however, automatic control will be maintained to flare altitude, 50 ft. Without gain scheduling, the gain at 50 ft. is four times that at 200 ft. and stability problems may become significant. It is felt, therefore, that most valid results will be obtained with the constant gain system. (Gain scheduling, in reality, is not difficult to accomplish, especially if the autopilot already makes use of altitude information for other purposes, as in Figure 5-8).

5.4 DYNAMIC CHARACTERISTICS OF THE AIRCRAFT

Presented here are selected results from the simulation which show basic response for the path following and attitude loops of the two aircraft. They include transient response runs for position offsets and for attitude commands. The

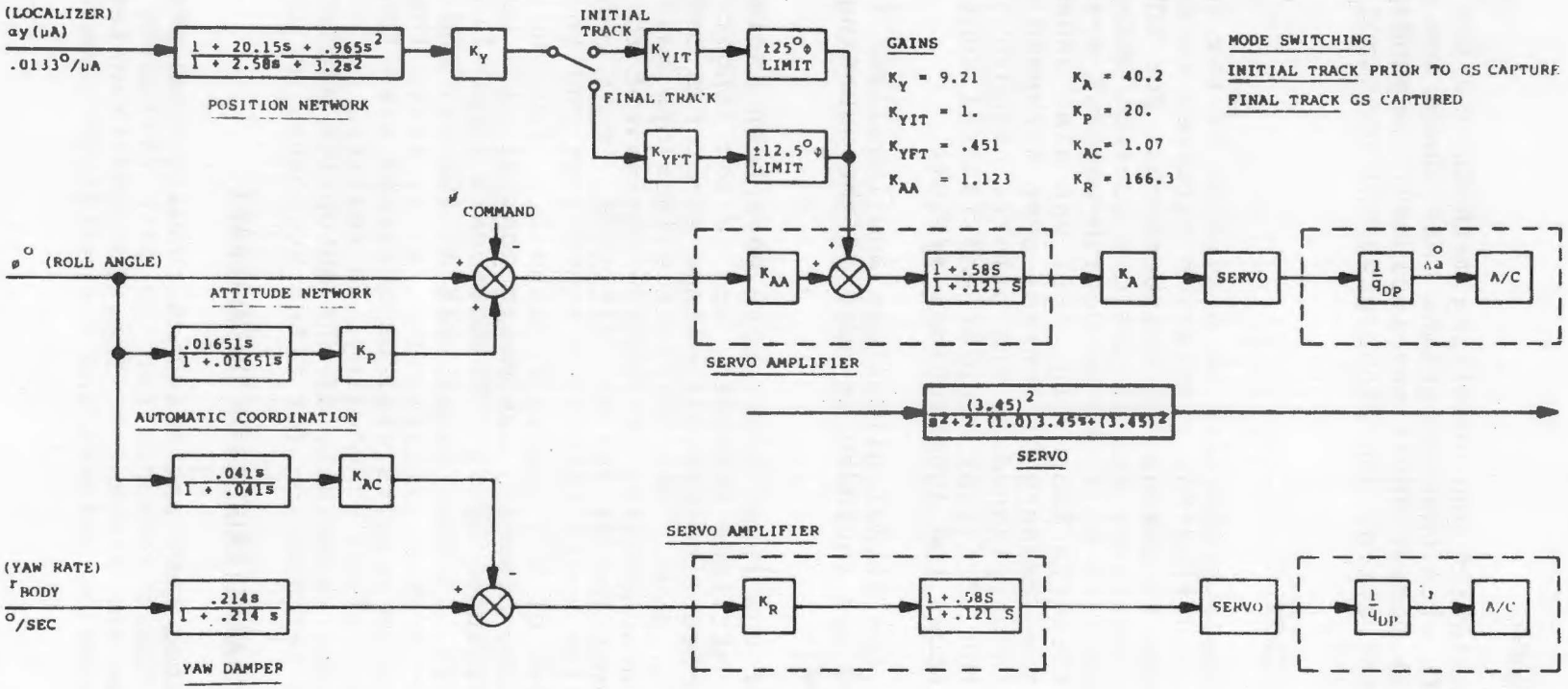

Figure 5-7. PA-30 Lateral Control System

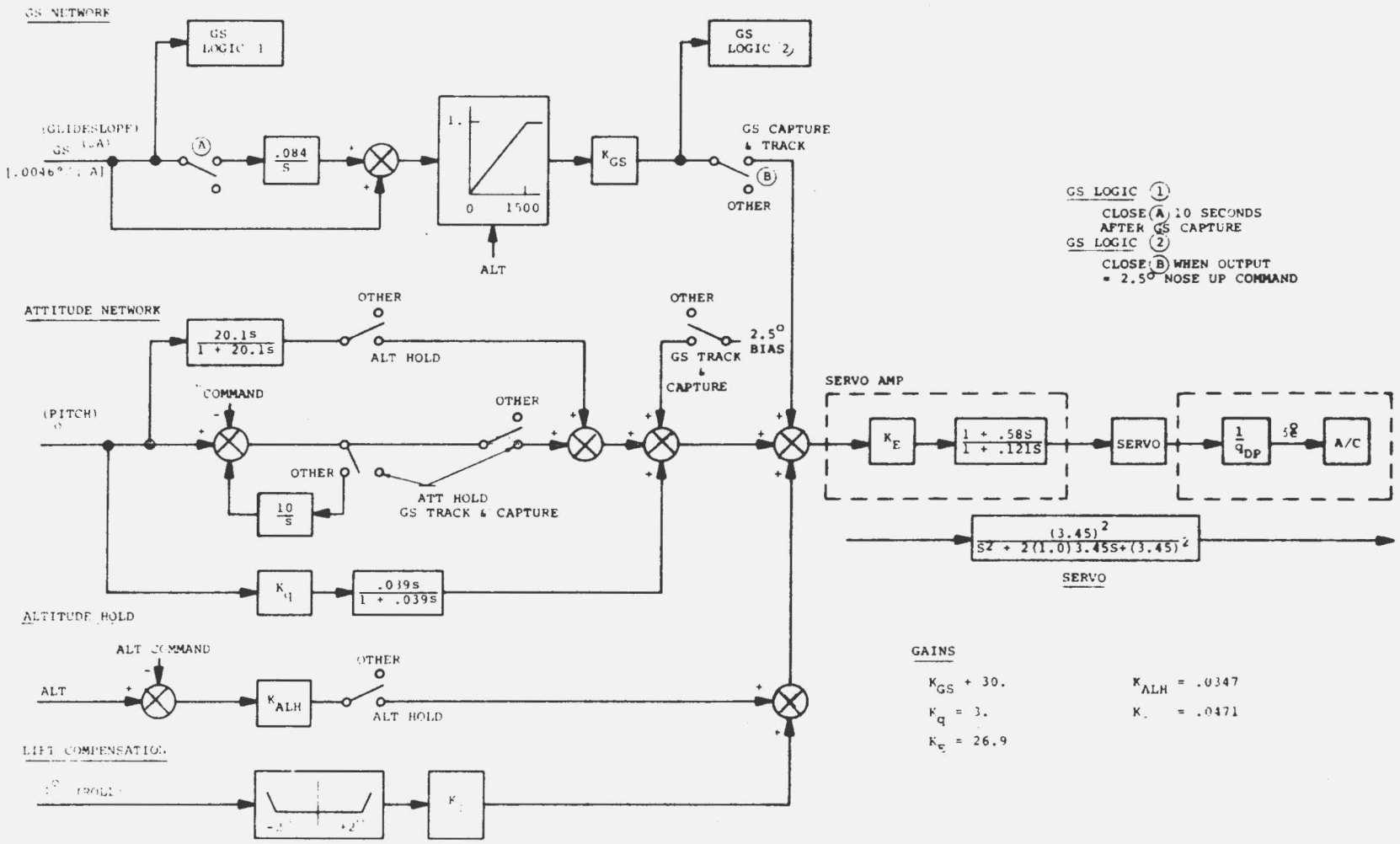

Figure 5-8. PA-30 Longitudinal Control System

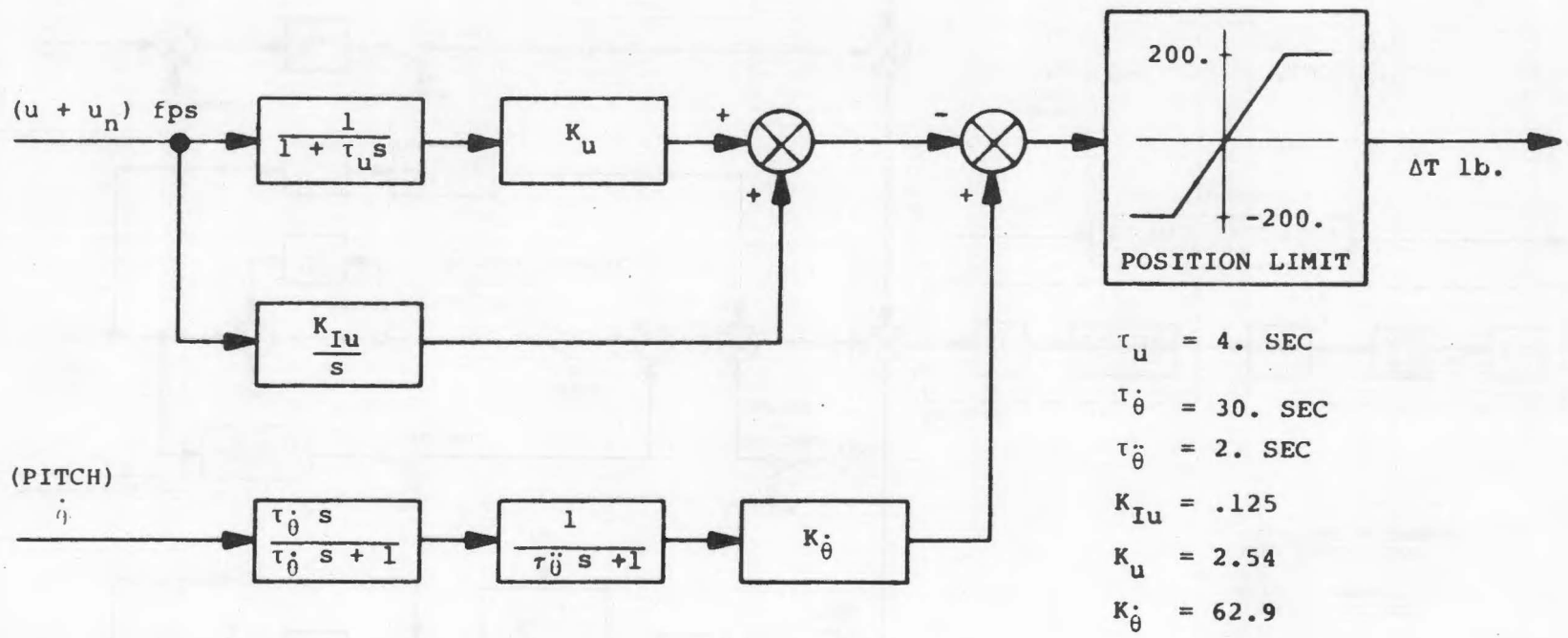

Figure 5-9. PA-30 Autothrottle

localizer responses are taken for constant distance from the antennas (constant gain) and do not necessarily represent the true response of the aircraft to position offsets in an actual approach, but do specify the dynamic properties of the system at the initial point (approximately 15,000 ft. from localizer antenna).

5.4.1 INNER LOOPS

Figure 5-10 shows response of both aircraft to step commands in pitch angle and roll angle. Although not identical, it can be seen that the basic time response envelopes for both aircraft are very similar.

5.4.2 PATH FOLLOWING LOOPS

Figures 5-11 and 5-12 illustrate the transient responses of both aircraft to step offsets in glideslope and azimuth at 200 ft. altitude (15,000 ft. from azimuth antenna). In the longitudinal channel (Fig. 5-11), time responses are almost identical. In the lateral channel (Fig. 5-12), initial crossover points are the same, but the CV-880 is about 30% slower in settling within 10% of final value.

Figures 5-13 and 5-14 plot the same responses vs. forward ground distance, illustrating differences in maneuverability in space of the two vehicles.

Table 5-1 summarizes important features of path following loop transient response and presents estimates of the dominant second order natural frequency and damping ratio.

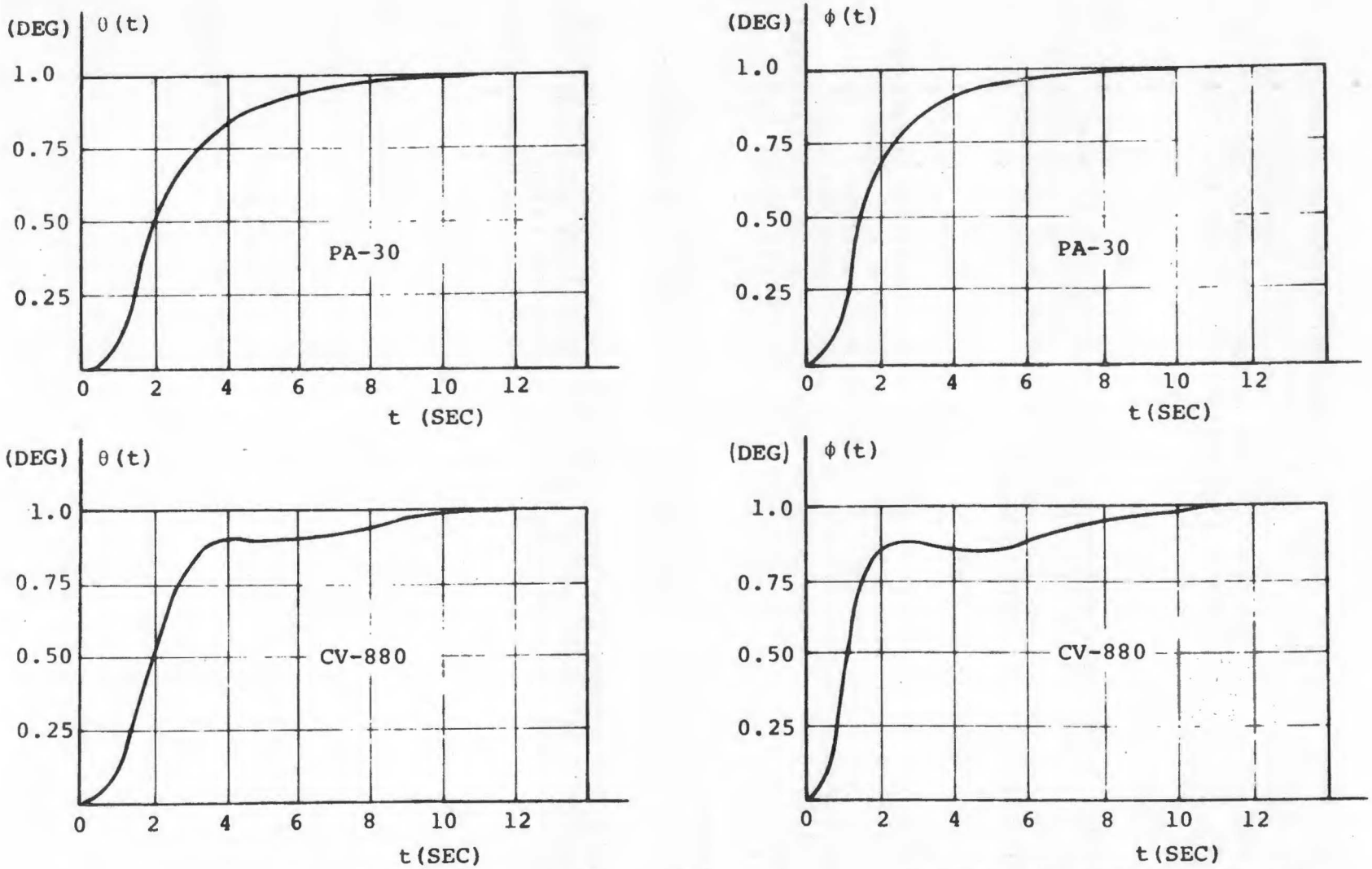

RESPONSE TO STEP COMMAND IN PITCH ANGLE, θ

RESPONSE TO STEP COMMAND IN ROLL ANGLE, ϕ

Figure 5-10. Inner Loop Transient Responses, CV-880, PA-30

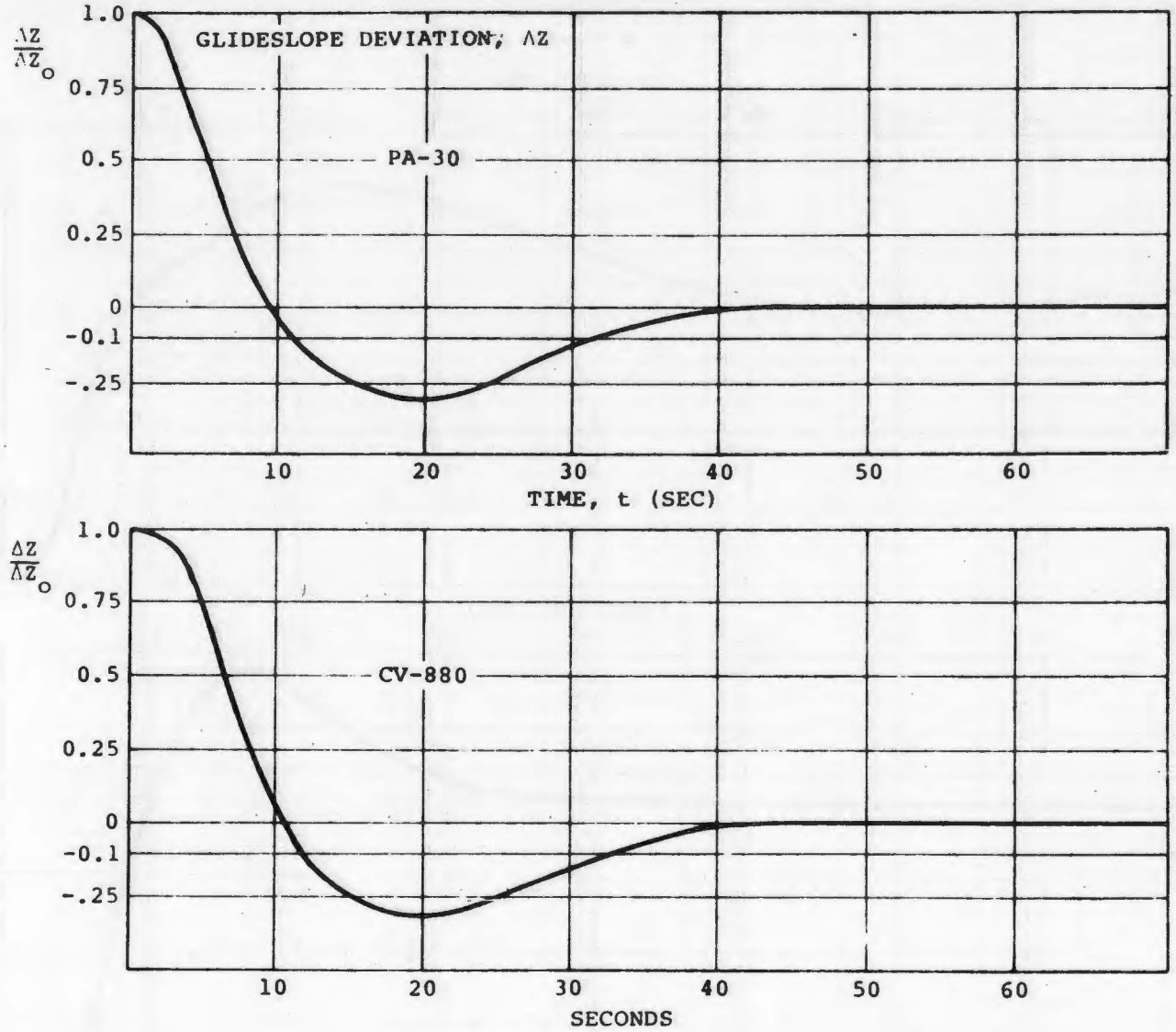

Figure 5-11. Glideslope Transient Response at 200 ft. Altitude (Vs. Time)

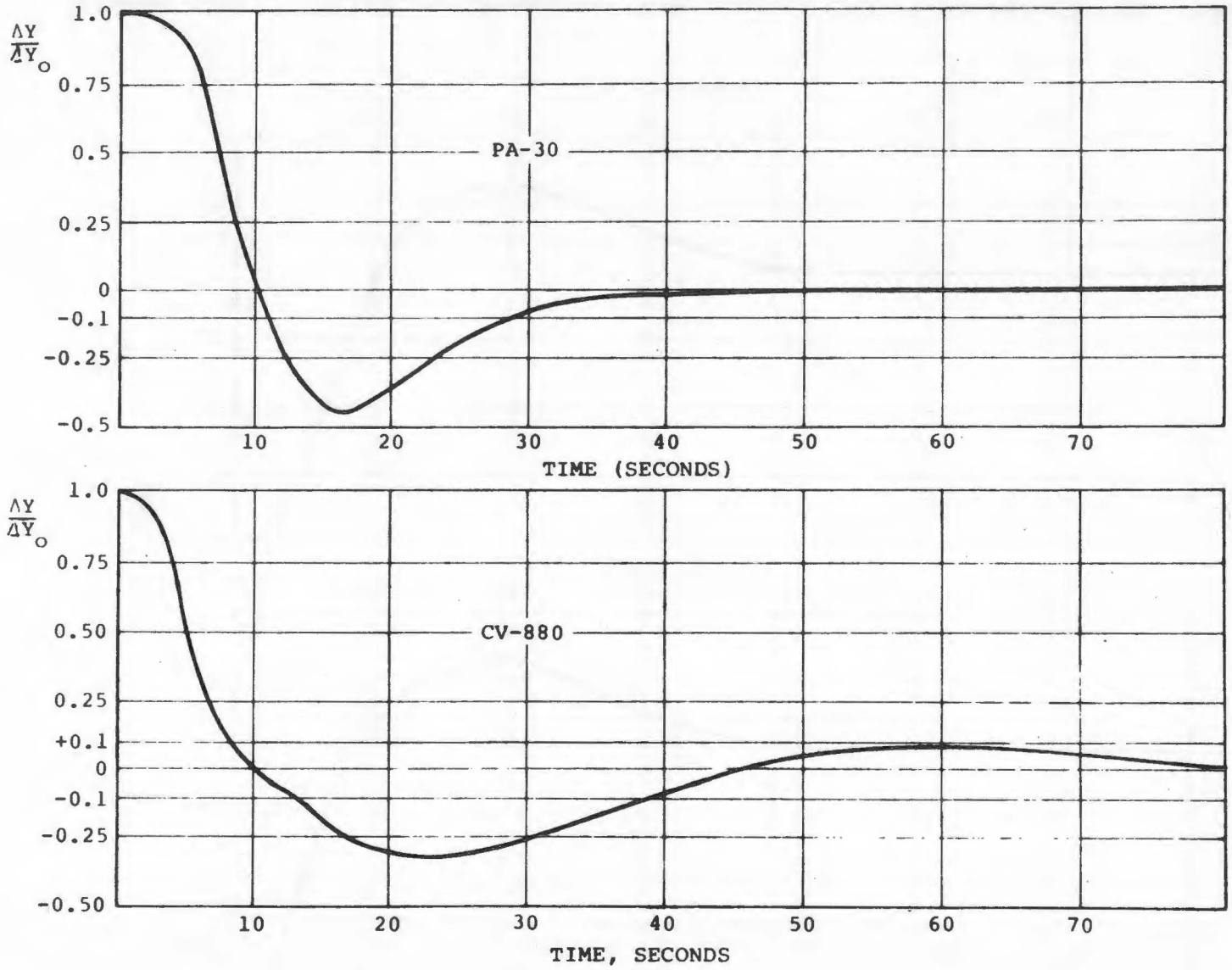

Figure 5-12. "Localizer" Transient Response at 200 ft. Altitude (Vs. Time)

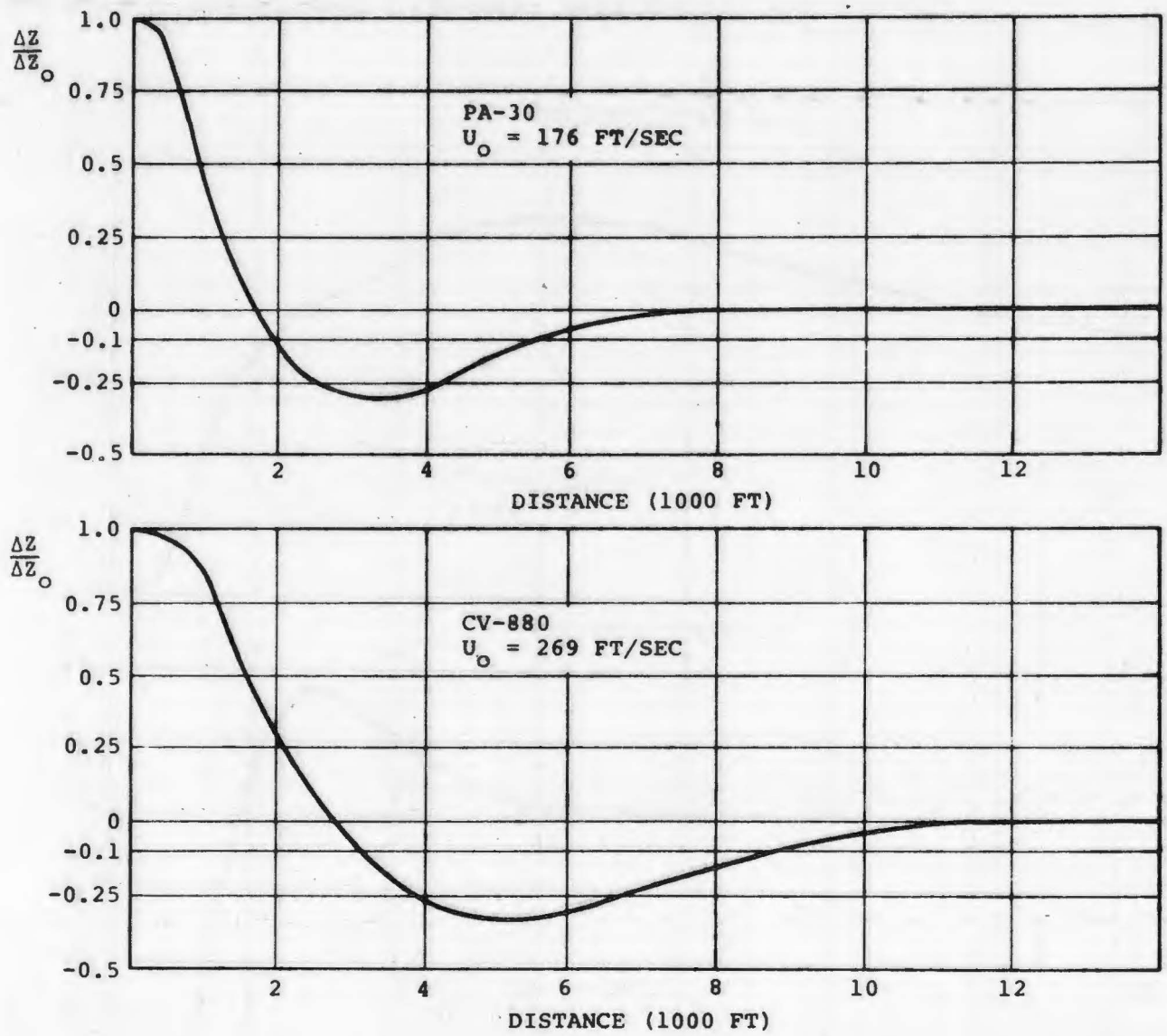

Figure 5-13. Glideslope Transient Response at 200 ft. Altitude (Vs. Ground Distance)

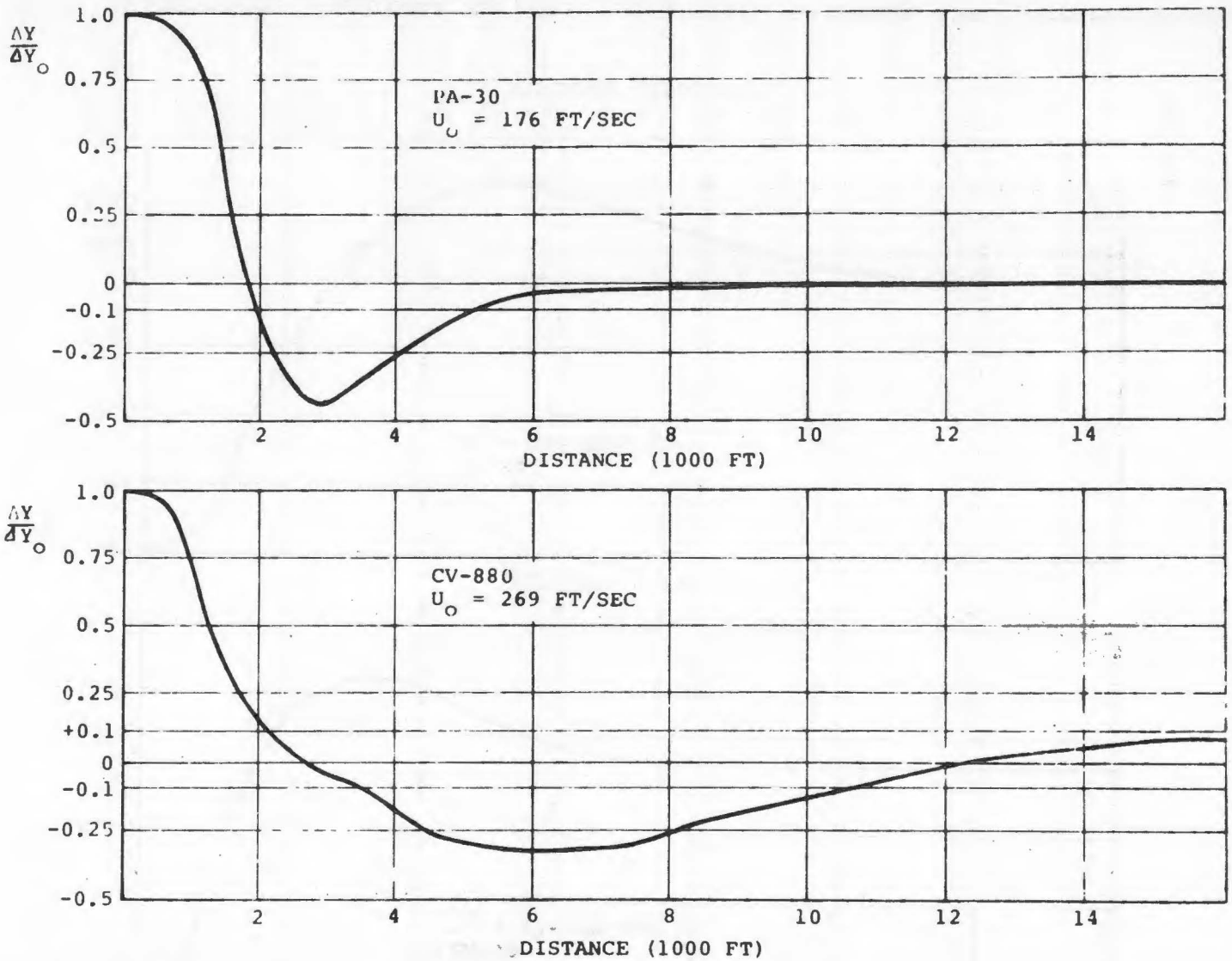

Figure 5-14. "Localizer" Transient Response at 200 ft. Altitude (Vs. Distance)

TABLE 5-1
SUMMARY OF DYNAMIC CHARACTERISTICS OF
PATH FOLLOWING LOOPS CV-880 AND PA-30

U_o(CV-880) = 269 FPS U_o(PA-30) = 176 FPS DISTANCES SPECIFIED FOR NO HEAD OR TAIL WIND		LONGITUDINAL PATH FOLLOWING LOOP		LATERAL PATH FOLLOWING LOOP	
		CV-880	PA-30	CV-880	PA-30
TRANSIENT RESPONSE FIRST CROSSOVER	TIME (SEC)	10.5	10.0	10.0	10.5
	DISTANCE (FT)	2,800	1,700	2,600	1,800
TRANSIENT RESPONSE WITHIN 10% OF FINAL VALUE	TIME (SEC)	33.5	32.0	39.0	29.0
	DISTANCE (FT)	8,700	5,500	10,400	5,200
TRANSIENT RESPONSE MAX OVERSHOOT		32%	31%	33%	44%
ESTIMATED 2ND ORDER UNDAMPED NATURAL FREQUENCY	RAD/SEC	~0.2	~0.2	~0.15	~0.28
	Hz	~.03	~.03	~.024	~.045
ESTIMATED DAMPING RATIO		~0.4	~0.4	~0.45	~0.35
ESTIMATED 2ND ORDER UNDAMPED NATURAL WAVELENGTH	(FT)	~9,000	~5,900	~11,200	~3,900

6. PERFORMANCE CRITERIA DURING APPROACH AND LANDING

In order to interpret the results of the covariance propagation equations in terms of safe landing and pilot acceptability, critical variables and appropriate limits must be defined at touchdown and during approach. Of primary importance is safety, and a fairly definite set of variables and limits can be chosen at touchdown such that if limits are exceeded, the probability of an accident is high. A much more nebulous area involves selecting performance constraints based on passenger comfort and pilot acceptability. They will generally not correspond to safety limits and will depend to a great extent on what aerodynamic environment the pilot expects to encounter. In light wind a pilot's level of tolerance for control activity and attitude variation is certainly less than if he were flying with a 25 knot headwind gusting to 30, and any such activity with light wind will adversely affect his confidence in the landing system.

Given a particular aircraft and autopilot, a pilot's awareness of its performance in wind, the base line for pilot acceptability must be the activity caused by the wind. (In designing an autopilot, of course, the "absolute" limits for pilot acceptability must be taken into account, but for landing system investigation with a fixed autopilot, the best possible performance depends directly on the level of aerodynamic noise for any particular approach; a pilot's decision to attempt the approach with this gust level implies that such performance is "acceptable").

If, as is generally the case, spurious activity due to worst case gust conditions is significantly greater than that due to ILS noise or scan rate, variations in this activity as a function of noise and scan rate under heavy wind conditions will be sufficiently masked by wind response so as to be almost undetectable to the pilot. The net result is that the pilot will respond more adversely to effects of ILS perturbations with no wind than under any other wind condition.

In the safety area, however, it is still necessary to assure that scanning rate and beam noise do not significantly affect the probability of a safe landing even under worst case wind condition.

The preceding paragraphs suggest the requirement for two independent sets of performance criteria and different methods of comparing the data to the criteria.

Assuming the aircraft is fully flight worthy, barring peculiar combinations of conditions and pilot error, limits can be set at the instant of touchdown on position, velocity and attitude such that a safe landing is highly probable. In the absence of detailed rollout performance models, however, some of these are tentative, but should be close to absolute maximums. Although it is not presently possible to compute absolutely the variation in probability of safe landing with current methods, (Section 2) one can examine the variances of the critical variables as generated by the covariance propagation equations and show variations in these variances as scan rate, beam noise, and wind conditions are varied, identifying those scan rates and noise values which begin to significantly affect performance under any wind condition.

Limits on pilot acceptability factors are set based on best information available from FAA, ICAO, and RTCA. Two distinct sets of factors are examined: one at 65 foot altitude, and one set which applies over the entire final approach phase. Once defined, limits can then be compared with 2σ data from the error propagation equations for any set of conditions and tradeoff curves similar to those for safety can be generated. Minimum acceptable sets of conditions are taken where the 2σ data equals the limit.

6.1 CRITICAL VARIABLES FOR A SAFE LANDING – CV-880

Limits quoted in the following paragraphs should not be exceeded more than once in 10^7 landings.

Lateral System

There are four variables chosen as critical to safety at touchdown for the lateral system:

1. Φ, Roll Angle: The primary consideration here is avoiding the possibility of a wing tip or engine pod contacting the ground. With full gear displacement on the CV-880, the inboard engine may touch the runway for roll angles greater than 5 degrees.
2. Y, Lateral Displacement: Obviously it is necessary to touchdown with both wheels of the main landing gear on the runway. For a 150 foot wide runway, this would dictate a constraint of $\pm$ 65 feet from centerline for the CV-880.
3. J, A composite variable indicating the lateral position of the aircraft at sometime after touchdown, assuming no corrective action is taken: In the absence of detailed information on the dynamics of touchdown and rollout, it was decided to require the aircraft to remain on the

runway for 3 seconds with no pilot corrections, assuming that it maintained heading and velocity values present at touchdown. This is a function of lateral touchdown position, heading with respect to runway centerline and forward groundspeed. The constraint, again, is $\pm$ 65 feet from centerline.

4. $\dot{Y}_A$, Cross Track Velocity, (ground velocity component perpendicular to landing gear) This variable is constrained by the capability of the landing gear to sustain a side force. The design limit for gear damage has been estimated from Convair data at $\pm$ 47 ft/sec. (This variable is the true cross track velocity, not simply lateral velocity with respect tothe runway centerline).

Longitudinal System

Critical longitudinal variables for a safe landing are the following:

1. θ, Pitch Angle: The main landing gear must touchdown before the nose gear, setting the lower limit at 0 degrees. The upper limit is set at 10 degrees, such that the tail does not strike the ground on touchdown. Nominal value, no wind, is 3.5 degrees.
2. $\dot{Z}$, Sink Rate: Nominal sink rate is 2.5 ft/sec. Structural damage to the aircraft is likely above 12.5 ft/sec. Therefore, this is taken as an upper limit. It is physically impossible to land with negative sink rate and it appears that any positive sink rate is sufficient to assure a successful landing, therefore, no lower limit is set on this variable.
3. X, Longitudinal Position: The aircraft must not touchdown prior to crossing the threshold. If it is assumed that the elevation #1 antenna is 1,000 feet from the threshold, then nominal touchdown (no wind) occurs at 1,350 feet (approach speed 160 kts). A maximum depends on runway length and rollout characteristics of the aircraft and will not be set here.

Table I summarizes safety criteria for the CV-880. It also lists the nominals and maximum allowable deviations from nominal for four deterministic conditions:

(1) no wind, no beam bias
(2) maximum wind and wind shear
(3) maximum beam bias
(4) worst case combination of (2) and (3).

(The signs attached to nominal values, of course, will reverse

TABLE 6-1
LIMITS AND NOMINALS FOR
SAFETY CRITICAL TOUCHDOWN VARIABLES

			NO WIND		MAX WIND & WIND SHEAR		MAX BEAM BIAS		WIND & BEAM BIAS	
VARIABLE	MINIMUM	MAXIMUM	NOM*	MAX DEV	NOM*	MAX DEV	NOM*	MAX DEV	NOM*	MAX DEV
ϕ (deg)	-5.0	+5.0	0	5.0	-1.5	3.5	0	5.0	-1.5	3.5
Y (ft)	-65.0	+65.0	0	65.0	1.5	63.5	+8.7	56.3	+10.2	54.8
$\dot{Y}_A$(ft/sec)	-47.0	+47.0	0	47.0	-13.9	33.1	0	47.0	-13.9	33.1
J (ft)	-65.0	+65.0	0	65.0	21.2	43.8	0	65.0	21.2	43.8
θ (deg)	0.0	10.0	3.6	3.6	+3.5	3.5	3.6	3.6	3.5	3.5
X (ft)	0.0	----	1350	1350	1440	1325	1325	1325	1415	1415
$\dot{Z}$ (ft/sec)	----	12.5	2.0	10.5	2.5	10.0	2.0	10.5	2.5	10.0

*Data from CV-880 Simulation #56 & 57

for lateral channel variables for reverse crosswind or beam bias). Nominal values are taken from simulation results with the appropriate conditions.

6.2 CRITICAL VARIABLES FOR SAFE LANDING –PA–30

Since at present, aircraft of the PA-30 type do not have automatic flare and decrab modes, safe landing criteria were not developed for this aircraft. However, performance evaluation based on pilot acceptability factors should prove sufficient to estimate minimum suitable scan rates.

6.3 PILOT ACCEPTABILITY FACTORS

It is difficult to tell a priori exactly which phase of approach is critical in terms of pilot acceptability. Therefore, two sets of criteria have been defined for various stages of approach. They are defined as deviations from nominal for a no wind gust condition and are in actuality maximum tolerable perturbations due solely to beam noise and sampling. The justification for approaching pilot acceptability from this point of view is illustrated in Figure 6-1 (Section 4.1.1)

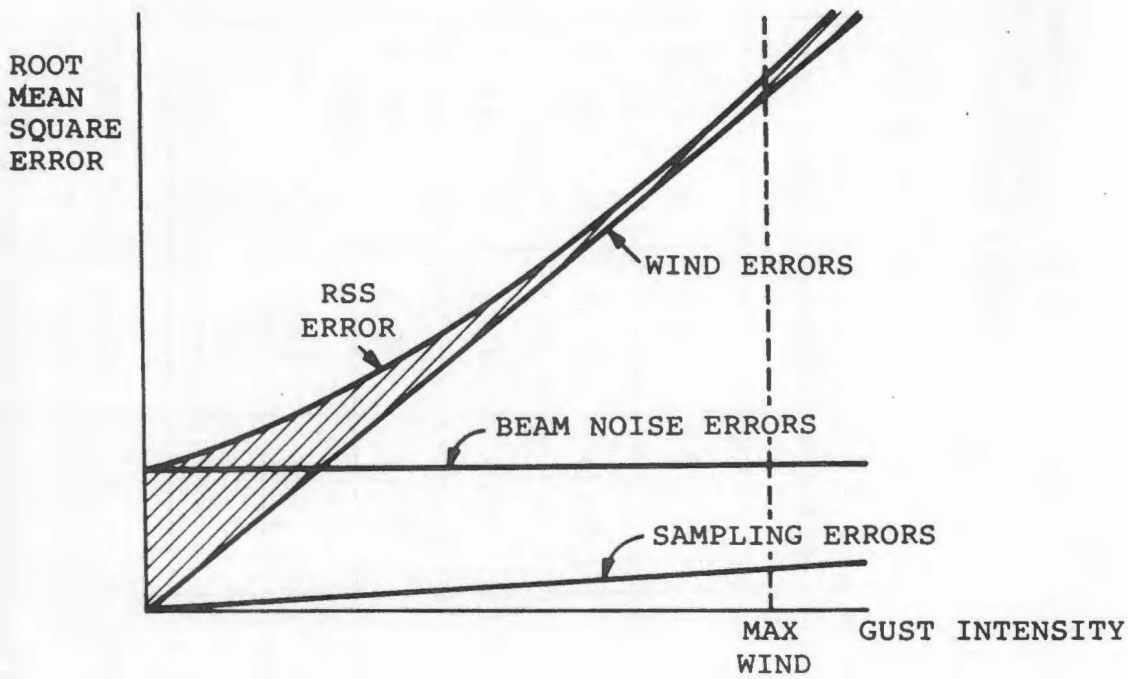

Figure 6-1. RMS Error as a Function of Gust Strength

The shaded area of Figure 1 represents the contribution of scanning errors to the total errors. If errors due to sampling are small, this contribution decreases significantly as wind gust strength is increased, and it has no noticeable effect relative to wind induced errors in the range of maximum wind.

It is impossible to set universally valid limits on pilot acceptability due to its basic dependence on the human factor. In selecting the limits quoted in the following paragraphs, an attempt was made to have them correspond to some threshold of perceptibility.

<u>Acceptable Activity During Final Approach</u> (600 ft. to 65 ft. alt.) (2σ) (No wind)

1.	Roll angle, Φ	$\pm$ 2 degrees
2.	Roll rate, p	$\pm$ 5 degrees/sec
3.	Heading angle, Ψ	$\pm$ 2 degrees
4.	Aileron deflection, δ_a	$\pm$ 1 degrees
5.	Rudder deflection, δ_r	$\pm$ 1 degrees
6.	Pitch angle, θ	$\pm$ 2 degrees
7.	Pitch rate, q	$\pm$ 2 degrees/sec
8.	Normal acceleration, α_n	$\pm$ 0.1 g
9.	Elevator deflection, δ_e	$\pm$ 1 degrees

<u>Acceptable Deviations from Nominal at Flare Initiation</u> (65 ft.) (2σ) (No wind)

1.	Roll angle, Φ	$\pm$ 2 degrees
2.	Heading angle, Ψ	$\pm$ 2 degrees
3.	True localizer deviation, Y	$\pm$ 15 ft.
4.	Indicated lozalizer deviation, Y_I	$\pm$ 15 ft.
5.	Pitch angle, θ	$\pm$ 2 degrees
6.	True glideslope deviation, Z	$\pm$ 4 ft.

7. Indicated glideslope deviation, Z_I — $\pm$ 4 ft.

8. Airspeed, U_A — $\pm$ 5 ft/sec

True localizer and glideslope deviations are not really observable during approach, however, in terms of overall system acceptability they are important criteria.

6.4 GENERATION OF CRITICAL VARIABLES FROM AIRCRAFT STATE VECTOR

All of the critical variables mentioned in Section 6.1 and 6.2 appear explicitly in the aircraft state vector as used in the simulation except J, $\dot{Y}_A$, and X.

The diagram of Figure 2 shows the relative orientation of velocity vectors for the lateral system just prior to touchdown where:

X_E, Y_E = runway coordinate system

X_A, Y_A = aircraft coordinate system

U_{WE}, V_{WE} = wind components in runway coordinates

U_w, V_w = wind components in aircraft coordinates

U_A, V_A = aircraft velocity w.r.t. atmosphere in aircraft coordinate system

$\dot{X}_E$, $\dot{Y}_E$ = aircraft velocity w.r.t. ground in runway coordinate system

$\dot{X}_A$, $\dot{Y}_A$ = aircraft velocity w.r.t. ground in aircraft coordinates

$\bar{U}_{WT}$ = total wind velocity w.r.t. ground

$\bar{V}_T$ = total velocity of aircraft w.r.t. atmospeere

$\bar{V}_g$ = total velocity of aircraft w.r.t. ground

β = sideslip angle; from relative wind to aircraft nose

Ψ = angle from aircraft nose to runway centerline

Ψ_T = true heading angle; angle from aircraft nose to true ground track

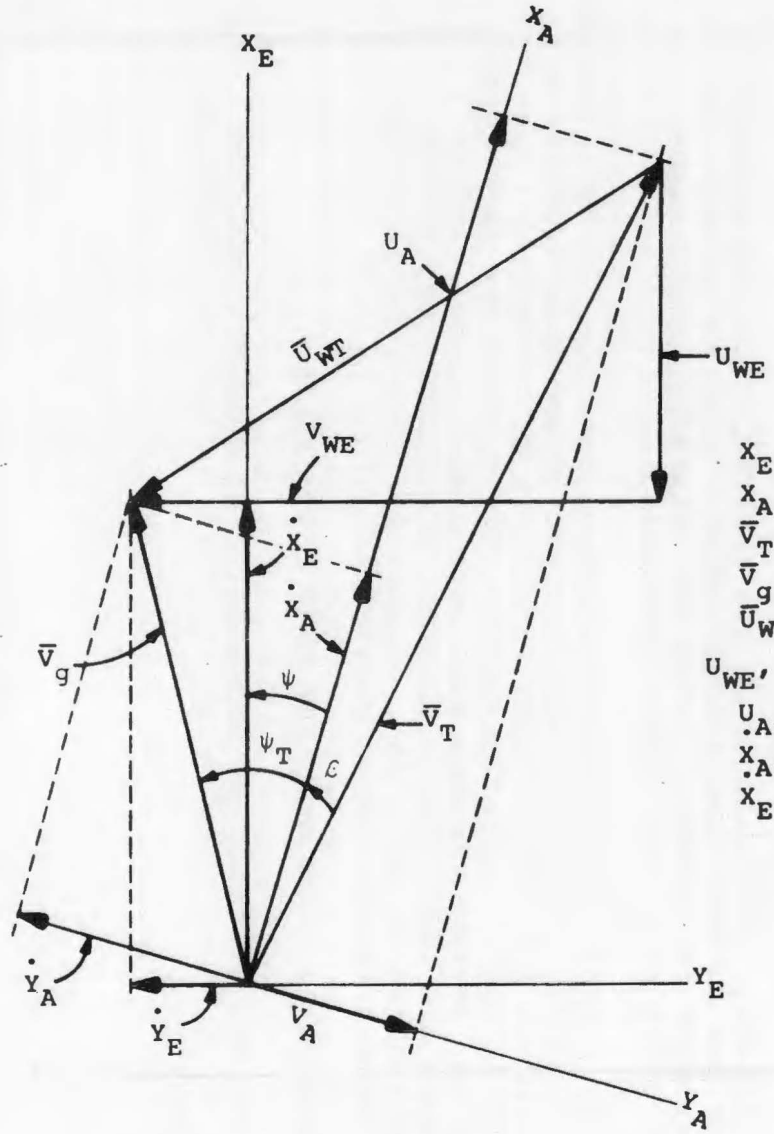

X_E, Y_E = RUNWAY COORDINATES
X_A, Y_A = AIRCRAFT COORDINATES
$\bar{V}_T$ = AIRCRAFT VELOCITY VECTOR w.r.t AIR
$\bar{V}_g$ = " " " w.r.t GROUND
$\bar{U}_{WT}$ = WIND VELOCITY VECTOR w.r.t GROUND
U_{WE}, V_{WE} = WIND COMPONENTS IN RUNWAY COORDS.
U_A, V_A = A/C VELOCITY w.r.t AIR IN A/C COORDS.
$\dot{X}_A$, $\dot{Y}_A$ = A/C VELOCITY w.r.t GROUND IN A/C COORDS.
$\dot{X}_E$, $\dot{Y}_E$ = A/C VELOCITY w.r.t GROUND IN RUNWAY COORDS.
β = SIDESLIP ANGLE
ψ_T = TRUE YAW ANGLE
ψ = HEADING w.r.t. RUNWAY CENTERLINE

Figure 6-2. Relations Between Aircraft Velocity Vectors (Horizontal Plane)

From Figure 6-1, using small angle approximations, the following expressions are developed for the ground velocity components in terms of the state variables Ψ, βU_A, U_W, V_W. (Equations are expressed vectorially; positive angles are clockwise).

$$U_W \approx U_{WE} \tag{6-1a}$$

$$V_W \approx V_{WE} \tag{6-1b}$$

$$\mathring{X}_E \approx \mathring{X}_A \approx U_A + U_W \tag{6-2a}$$

$$\mathring{Y}_E \approx -U_A(\Psi + \beta) + V_W \tag{6-2b}$$

$$\mathring{Y}_A \approx V_A - U_W\Psi + V_W \tag{6-3a}$$

$$\approx -U_A\beta - U_W\Psi + V_W \tag{6-3b}$$

$$\approx \mathring{Y}_E - \mathring{X}_E\Psi \tag{6-3c}$$

If it is assmed that on touchdown, the landing gear impulsively removes the velocity component $\mathring{Y}_A$ without significantly disturbing the attitude or other velocity components, then the heading angle Ψ determines the value of J according to equation (6-4):

$$J = 3\mathring{X}_A\Psi + Y \tag{6-4}$$

In words, the distance of the aircraft from the centerline of the runway three seconds after touchdown is equal to the error at touchdown, Y, plus the lateral velocity along the aircraft nose, $X_A\psi$, times 3 seconds.

The nominal longitudinal touchdown position, X, is a function of glideslope, flare altitude, average groundspeed from flare to touchdown and nominal time from flare to touchdown. For the CV-880 flare initiation occurs 490 ft. from the threshold. Values for average nominal groundspeed and nominal time to touchdown are taken from simulation results to compute the nominals shown in Table 6-1. Figure 6-3 shows the relationship between these various parameters.

6.5 COMPUTATION OF VARIANCES FOR CRITICAL VARIABLES

For the general case computation of variance from the error propagation program results must include the following considerations:

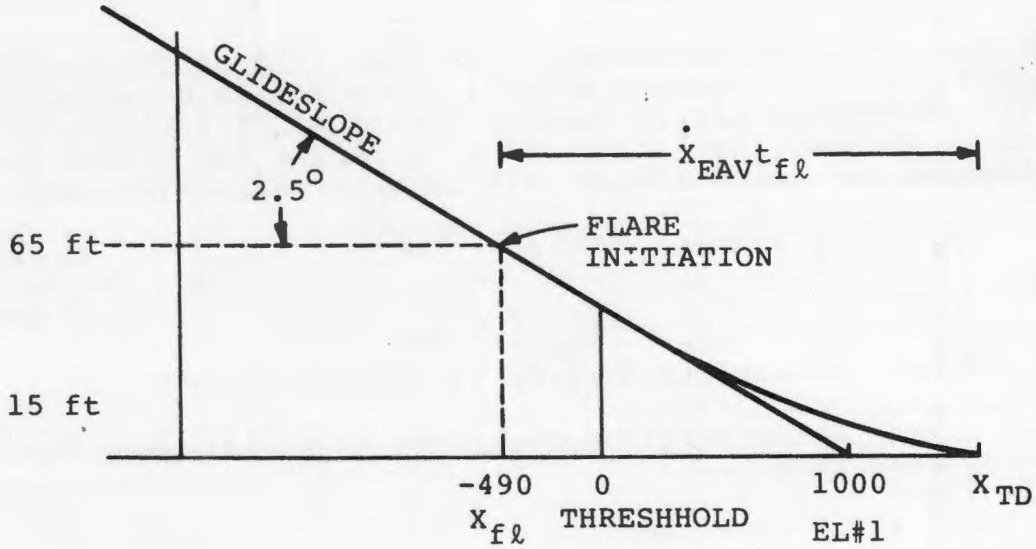

Figure 6-3. Longitudinal Touchdown Position

6.5.1 COMBINING THE EFFECTS OF VARIOUS DISTURBANCES

The error propagation equations operate on a linear system and when used for a single disturbing input generate, in effect, the system sensitivity to that input. Thus the covariance matrix outputs are effectively covariance sensitivities and they may be combined linearly to determine the effects of any particular set of disturbance inputs.

That is

$$\underline{X}(n,w) = \left(\frac{w}{w_o}\right)\underline{Z}(w_o) + \left(\frac{n}{n_o}\right)\underline{Z}(n_o) \qquad (6\text{-}5)$$

where $\underline{X}$ is the covariance matrix for wind gust w and beam noise n, $\underline{Z}(w_o)$ is the output of the error propagation program for reference wind gust w_o, and $\underline{Z}(n_o)$ is the output for reference beam noise; w and n are in terms of mean square intensities. The diagonal elements of $\underline{X}$ are the variances of the aircraft state variables. The operation may also be performed on individual variables; for example

$$\sigma_\theta^2(n,w) = \left(\frac{w}{w_o}\right)\sigma_\theta^2(0,w_o) + \left(\frac{n}{n_o}\right)\sigma_\theta^2(n_o,0) \qquad (6\text{-}6)$$

6.5.2 COMPOSITE VARIABLES

The variances at nominal touchdown time of the variables, J, and $\overset{o}{Y}_A$ may be computed directly from variables appearing in the covariance matrix through Equations (6-3c) and (6-4). If it is assumed that longitudinal airspeed and ground speed deviations are uncorrelated with lateral variables, then:

$$\sigma^2_{\overset{o}{Y}_A} = \sigma^2_{YE} + \psi^2_N \sigma^2_u + \overset{o}{X}{}^2_{EN} \sigma^2_\psi - 2\overset{o}{X}_{EN} \overline{\overset{o}{Y}\psi} \tag{6-7}$$

$$\sigma^2_J = \sigma^2_Y + 9\psi^2_N \sigma^2_u + 9\overset{o}{X}{}^2_{EN} \sigma^2_\psi + 6\overset{o}{X}_{EN} \overline{Y\psi} \tag{6-8}$$

where: subscripts N refer to nominal values

: all quantities evaluated at nominal touchdown time

: σ^2 = variance

$\overline{ab}$ = covariance of variables a and b

ψ_N = 1.8° = .0314 rad. for max. wind.

$\overset{o}{X}_{EN}$ = 213 fps for max. wind.

A rigorous estimate of longitudinal position dispersion at touchdown is not possible with present methods due to its fundamental dependence on time dispersion. One attempted method of estimation involves examining vertical glideslope deviation, δz, at some time, t_n; the slope of the nominal trajectory is given by $\overset{o}{Z}_N/\overset{o}{X}_{EN}$, where Z_N is nominal sink rate and X_{EN} is nominal forward ground speed; and $\delta x(t_n)$ can be computed according to equation (6-9) (small angle approximations in effect)

$$\delta x(t_n) = (\overset{o}{X}_{EN}/\overset{o}{Z}_N)\ \delta z(t_n) \tag{6-9}$$

However, primary interest in δx is not at t_N but at some altitude, Z_N. Figure 6-4 points out the relationship and differences between the two quantities. If it can be assumed that the average slope of the trajectory remains close to nominal between $Z_N+\delta z$ and Z_N, then $\delta x(t_N)$ is a fairly good estimator for $\delta x(Z_N)$. Below flare altitude, however, the slope is neither well defined nor constant as nominal sink rate is decreased, especially in turbulence. When sink rate dispersion is of the same order of magnitude as nominal sink rate, Equation (6-9) as an estimator for $\delta x(Z_N)$ is no longer even remotely correct. (Fig. 6-5).

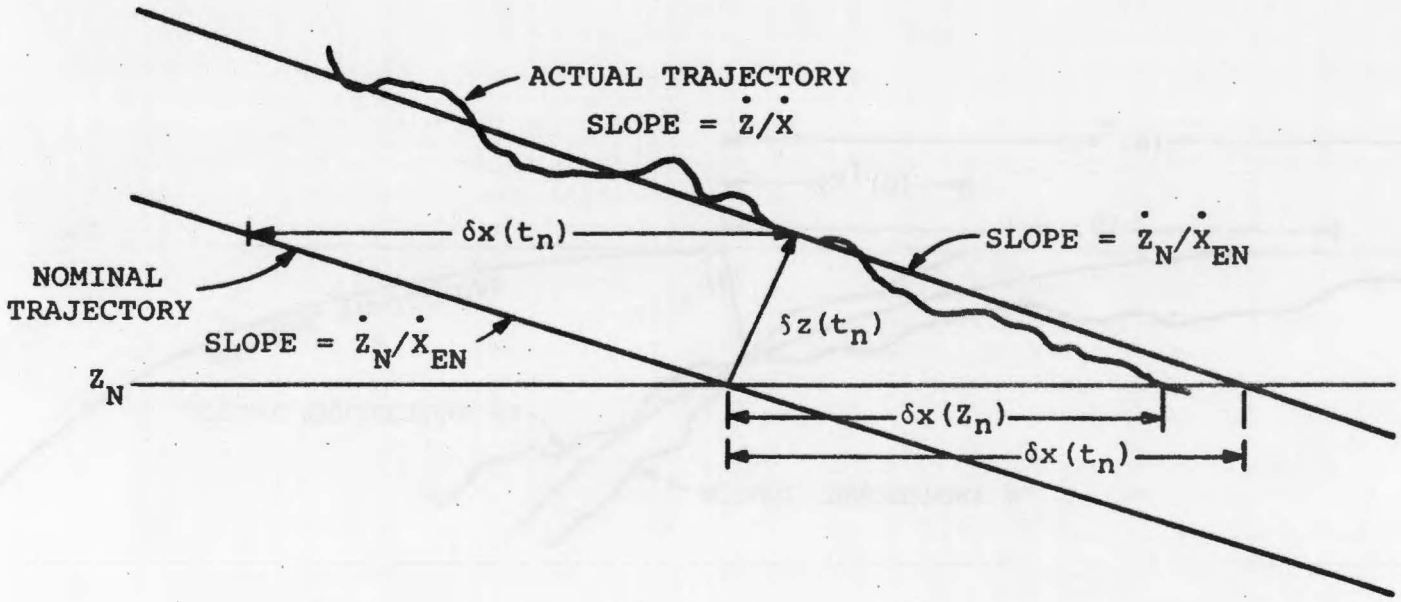

Figure 6-4. Longitudinal Position Dispersion Related to Glideslope Deviation

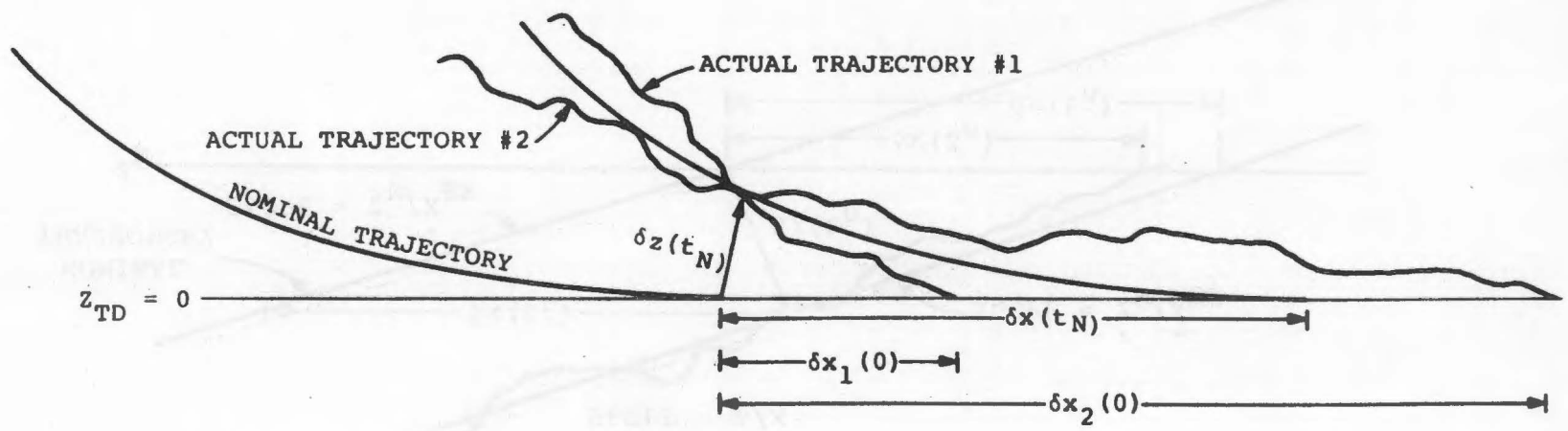

Figure 6-5. Longitudinal Dispersion At Touchdown

Since, above flare altitude, the slope of the trajectory is fairly constant in the average and large compared to deviations, it is possible to examine longitudinal dispersion in a comparative sense by using (6-9) to estimate δx at flare initiation and examining variations in $\sigma_x^2(t_{fl})$ as a function of scan rate, beam noise and wind. This should provide some gauge of this variable's sensitivity to these parameters. Equation (6-10) give this method for calculating the variance.

$$\sigma_x^2(t_{fl}) = \left[\frac{\mathring{X}_{EN}(t_{fl})}{\mathring{Z}_N(t_{fl})}\right]^2 \sigma_z^2(t_{fl}) \qquad (6\text{-}10)$$

$\mathring{X}_{EN}/\mathring{Z}_N$ is of course just the inverse of the glideslope angle expressed in radians and for a 2.5° glideslope $\mathring{X}_{EN}/\mathring{Z}_N=22.9$.

As currently configured scanning beam information is not used in the longitudinal channel below flare, therefore results after flare initiation for longitudinal channel variables will depend on LGS parameters only in so far as they (LGS parameters) determine initial conditions at flare initiation.

7. EFFECTS OF SCANNING RATE & AND BEAM ANOMALIES ON PERFORMANCE DURING APPROACH & LANDING

7.1 GENERAL

Data and results presented in this chapter are based on simulation and covariance propagation runs at scan rates of 40, 10, 5, 2 and 1 per second under various wind and beam anomaly conditions.

In the absence of wind and beam disturbances, simulation results have shown that scanning rate has no effect on performance of either aircraft during approach and landing.

7.1.1 DETERMINISTIC DISTURBANCES

Deterministic disturbances considered in this study include steady winds, wind shear, and beam bias.

Steady winds (by definition) are invariant with time and position and their effects on performance are insensitive to scan rate.

Wind shear is the wind velocity gradient with altitude and requires the aircraft to continually correct under its influence in order to maintain a desired ground track and glideslope. How well the aircraft does this is a function of its dynamic characteristics, and performance may therefore be affected by scanning rate.

For the CV-880 and PA-30 it was found from simulation results that scan rates as low as one per second have no effect on path following ability under worst case shear conditions. However, at the very low scan rates, (1,2) some extraneous inner loop activity is generated at frequencies near the scan rate. The activity was relatively low in magnitude and affected only the higher order variables such as control activity and attitude rates. Figure 7-1 (Figures in this chapter appear following the text, p. 79-114 et seq) shows the CV-880 lateral system response to shear from 200 ft. to 28 ft. (decrab initiation) for 50 scans and 1 scan. At 1 scan, the peak ripple on aileron deflection (δ_a) is less than 0.1 degrees and that on roll rate (p) less than 0.1 degrees/second. As can be seen, roll angle and lateral position are apparently unaffected.

Similar magnitudes were found for the PA-30 in elevator and pitch rate activity at 1 scan per second. However,

these levels for both aircraft are at least an order of magnitude less than limits set for pilot acceptability and should not contribute significantly to minimum scan rate determination.

Beam bias (in the strict sense) produces a time and position invariant error in the trajectory. The only significant errors produced are in position and their magnitude is dependent only on the bias angle and the geometry of the nominal trajectory with respect to the transmitting antennas. For a given glideslope these errors are independent of the aircraft characteristics up to the point of flare initiation. If RTCA 2σ bias levels are assumed (configuration K) then Table 7-1 lists deviations from nominal position at flare altitude (50 ft.) due to beam bias.

TABLE 7-1
ERRORS IN POSITION AT NOMINAL FLARE ALTITUDE
DUE TO BEAM BIAS, 2.5° GLIDESLOPE

Lateral Position Deviation, ΔY	Vertical Position Deviation, ΔZ	Resultant Longitudinal Pos. Dev. at Flare,* ΔX
10.0 Ft.	1.2 Ft.	27.5 Ft.

*computed from ΔZ

Performance with beam bias is not directly affected by scanning rate; however, errors introduced by bias will reduce allowable dispersion levels due to random disturbances, which are affected by scanning rate.

7.1.2 RANDOM DISTURBANCES

Random disturbances considered include wind gusts and beam noise. The two sets of criteria developed in Chapter 6 require the evaluation of the effects of beam noise and scan rate on performance in a gust environment (safety factors) and with no wind (pilot acceptability factors).

As previously discussed it will not be possible to examine absolute variation in touchdown variables as scan rate and beam noise are varied, but comparative evaluation is practibable. Since safety is most critical under worst case wind conditions, performance under these conditions

with a perfect continuous LGS signal will be taken as a baseline for the comparative evaluation. It is then possible to show performance deterioration with scan rate and beam noise as a percentage increase in the rms (1σ) values of the touchdown variables. Those with the most significant increases over the noise and scan rate range of interest are then isolated and investigated in more detail, as the ones most likely to constrain the selection of minimum scan rate.

Performance with respect to pilot acceptability criteria can be examined in an absolute sense using the results of the covariance propagation programs. Data on 2σ values from these programs will be compared directly against the limits set in Section 6, for noise levels and scan rates of interest.

7.1.3 AN EXAMPLE OF THE RELATIVE EFFECTS OF SCAN RATE, BEAM NOISE AND WIND GUSTS

Figure 7-2 illustrates the effects of various scan rates on longitudinal position dispersion for the CV-880 as wind (gust intensity) is increased from zero to maximum. (The effects at 40, 10,and 5 scans are too small to show). The results are expressed as a percentage computed from the ratio of the 1σ value at any point to that at 100% wind with a continuous LGS signal. The same set of curves is replotted in Figure 7-3 with a beam noise of .035 degrees (1σ). A comparison of the two Figures illustrates the separate effects of beam noise and "sampling noise". This is further elucidated by isolating the data for 1 scan and plotting variation from baseline as is done in Figure 7-4. As can be seen, the contribution of sampling noise increased linearly with wind gust strength while the effects of beam noise decrease rapidly as wind is increased.

7.1.4 CV-880 TOUCHDOWN PERFORMANCE WITH CONVENTIONAL ILS

Since absolutely valid results are not available at touchdown and a comparative analysis of scanning rate and beam noise effects on critical variables at touchdown is required, one useful point of reference is performance under similar conditions with a conventional ILS.

A set of covariance propagation runs was made for the CV-880 with the conventional ILS model (see Section 4) the results of which were compared with baseline data from the perfect continuous LGS. For the critical variables at touchdown, Table 7-2 lists these results in terms of percent increase in 1σ value (due to conventional ILS noise) with worst case turbulence.

TABLE 7-2
EFFECTS OF CATEGORY III ILS NOISE ON
CV-880 TOUCHDOWN PERFORMANCE -
WORST CASE WIND

ILS Noise	Increase in 1σ value w.r.t. perfect continuous LGS in worst case wind ICAO Spec: 2.5 μA(1σ) AZ 10 μA(1σ) Elev.
Lateral Position, Y	11.0%
Lateral Position (3 sec. after TD), J	15.2%
Cross Track Velocity, $\dot{Y}_A$	0.33%
Roll Angle, Φ	0.089%
Longitudinal Position, X	14.2%
Sink Rate, $\dot{Z}$	0.16%
Pitch Angle, θ	0.019%

All the data on touchdown variables for the LGS scanning beams to be presented in following sections are expressed with respect to the same baseline (1σ value under worst case wind with perfect continuous LGS) thereby permitting direct comparison.

7.2 LATERAL SYSTEM RESULTS – AZIMUTH SCANNING RATE AND NOISE

7.2.1 CV-880 - CRITICAL TOUCHDOWN VARIABLES

Figures 7-5 and 7-6 summarize the relative effect of scan rate on the lateral system critical variables under worst case wind with and without beam noise. A glance at these Figures plotted on a logarithmic scale shows that scan rate effects on roll angle (Φ) and cross track velocity ($\dot{Y}_A$) under both conditions are at least an order of magnitude less than the effect on lateral position (Y) and lateral position three seconds after touchdown (J). These four variables are plotted individually in Figures 7-7(a), (b), (c), (d) against scan

rate with various levels of beam noise. (Percentage increase in 1σ value for these figures is on a linear scale; note also that the scales are different for each variable). The horizontal lines also shown represent increase in 1σ value with conventional ILS (from Table 7-2) and an increase of half that due to conventional ILS. It is now possible to generate Figure 7-8(a) scan rate-beam noise tradeoffs for dispersion increases equivalent to conventional ILS.

The curves shown represent maximum beam noise-minimum scan rate conditions to just meet the criteria. Any point to the right or below the constraining curve is then an acceptable combination of beam noise and scan rate for the condition stated.

Roll angle, Φ, is not shown because it is felt that its total range of variation (less than .075%) is too small to be of any significance in constraining either scan rate or beam noise. The implications of percentage increase to safe landing probability is discussed more fully in Section 7.5

It is also noted that although cross track velocity $\dot{Y}_A$ has a relatively small range of variation compared with Y, and J, it is equally significant in constraining scan rate and beam noise when related to performance with conventional ILS.

Figure 7-8(b) shows the scan rate-beam noise tradeoff for a hybrid condition: dispersion increases must be either half that of conventional ILS or 0.5%, whichever is greater. (This effectively eliminates Y_A as a constraint). Justification for this approach is discussed in Section 7.5 .

Figures 7-8 and similar ones to follow represent the most significant outputs of this study, and will provide the basis for conclusions developed in Section 8. In interpreting these figures, it is interesting to note that a curve tending toward the vertical implies a predominant sensitivity of that variable to scan rate (sampling noise) while one tending toward horizontal implies a predominant sensitivity to beam noise .

7.2.2 CV-880 PILOT ACCEPTABILITY FACTORS

Lateral channel variables critical to pilot acceptability (Section 6) are listed below. Figure numbers refer to parametric plots of 2σ activity or dispersion in these variables versus beam noise (no wind) with scan rate as the parameter, Limit lines shown on the figures are those set in Section 6.

During Approach

Roll angular activity (Φ) : Fig. 7-9

Roll rate activity (p) : Fig. 7-10

Heading activity (Ψ) : Fig. 7-11

Aileron activity (δ_a) : Fig. 7-12

Rudder activity (δ_r) : Fig. 7-13

At Flare Altitude

Roll angle dispersion (Φ) : Fig. 7-9*

Heading angle dispersion (Ψ) : Fig. 7-11*

Lateral position offset (Y) : Fig. 7-14

Indicated lateral position offset (Y_I) : Fig. 7-15

Control and attitude activity during approach is not generally constant and a worst case point is chosen for these variables based on the time history of their variances during final track generated by the covariance propagation programs. For the CV-880 Lateral System, worst case activity occurs in the vicinity of flare altitude.

The following comments apply to the data presented in this section:

1) The beam noise range over which Figures 7-9 through 7-15 are plotted is roughly five times the RTCA Specification (1σ).
2) All the variables except heading angle (Ψ) exceed their limits for one or more sets of conditions.
3) Aileron activity (Fig. 7-12) decreases below two scans per second. This is related to the coupler filter, inner loop, and aileron dynamics; apparently under these conditions below two per second, the aileron tends to settle to trim value between samples.
4) Indicated lateral position deviation (Fig. 7-15) is the raw signal to the autopilot. Because of the low time constant in the coupler filter most of the noise is directly transmitted to the autopilot.

*Dispersion at flare altitude and activity during final approach for Φ and Ψ are identical, as are the limits. They are therefore not plotted twice.

It is unlikely, however, that the pilot would see such levels on his instruments at the higher scan rates.

5) Lateral position (Fig. 7-14) shows two limits, one assumes no bias, the other assumes a bias level of 10 ft. The limit with bias is considered as worst case and further use of data from this plot will be based on the limit with bias.

Figure 7-16(a) is a composite plot of all lateral channel variables affecting pilot acceptability. Again, it shows beam noise versus scan rate and the curves represent conditions required to just meet the limits. As can be seen, the higher frequency variables, Y_I, δ_a tend to dominate in limiting acceptable beam noise-scan rate values, and are horizontally oriented, indicating an insensitivity to scan rate. This is primarily a consequence of the lack of any substantial filter in the coupler processer, and the resultant transmission of most of the beam and sampling noise into the autopilot.

In order to show the effects of filtering on pilot acceptability factors, a second limited set of runs was made with a 0.5 second time constant in place of the 0.025 second time constant of the coupler-processor. These results are summarized in 7-16(b). It should be noticed that the region of acceptability is considerably enlarged and constraints on Φ, Y, and δ_a now tend to predominate.

7.2.3 PA-30 PILOT ACCEPTABILITY FACTORS

Figures 7-17 through 7-23 present the 2σ data for PA-30 lateral channel pilot acceptability factors. Again, the point of maximum activity during approach is in the vicinity of flare altitude and these are the values used for Figures 7-17 through 7-21.

All the variables except roll rate, p, and rudder activity, δ_r, exceed their limits for one or more sets of conditions.

Figure 7-24(a) is the composite plot for the PA-30, showing the acceptable beam noise and scan rate values for this aircraft in the lateral channel. It can be noted from this Figure that control and attitude activity are relatively less affected by the scanning beam than with the CV-880, and a low frequency term, lateral deviation at flare (Y) tends to dominate for the lower scan rates.

Figure 7-24(b) shows the same curves with the 0.5 second coupler time constant. Y now dominates the acceptable region

by at least a factor of two.

7.3 LONGITUDINAL SYSTEM RESULTS – ELEVATION #1 SCANNING RATE AND NOISE

(Presentation of data in this section is parallel to that of Section 7.1. For general notes on interpretation, refer to Section 7.1)

7.3.1 CV-880 CRITICAL TOUCHDOWN VARIABLES

Figures 7-25 and 7-26 summarize the relative effect of scan rate on the longitudinal system critical variables under worst case turbulence both with and without beam noise. As with the lateral channel, the position variable (X) dominated by at least an order of magnitude over sink rate ($\dot{Z}$) and pitch angle (θ) (Pitch angle at touchdown, not shown on Figure 7-25, is insensitive to scan rate in the absence of beam noise within the limits of computational accuracy).

Figures 7-27(a), (b), and (c) detail percentage increase in these variables with scan rate for various beam noise values. Performance equivalent to that with conventional ILS is also noted.

Figure 7-28(a) presents the scan rate-beam noise trade-off curves for the longitudinal variables corresponding to performance equivalent to that with a conventional ILS. [Pitch angle is not shown since it is felt its total range of variation (less than 0.15%) is too small to be of any significance in constraining scan rate or beam noise]. Sink rate, $\dot{Z}$, although significantly lower in range of variation than longitudinal position, X, dominates the acceptable region when the limitation is imposed with respect to performance with conventional ILS.

Figure 7-28(b) shows beam noise vs. scan rate for a hybrid limitation: increase in dispersion either half that of conventional ILS or 0.5%, whever is greater. Justification for this type of approach is discussed in Section 7.5.

7.3.2 CV-880 PILOT ACCEPTABILITY FACTORS

Longitudinal system variables critical to pilot acceptability (Section 6) are listed below.

During Approach:

Pitch Angular Activity (θ) : Fig. 7-29

Pitch Rate Activity (q) : Fig. 7-30

Elevator Activity (δ_e) : Fig. 7-31

At Flare Altitude

Pitch Angle Dispersion (θ) : Fig. 7-32

Airspeed Dispersion (U_A) : Fig. 7-33

Glideslope Deviation (Z) : Fig. 7-34

Normal acceleration during approach is not available as an output from the covariance propagation equations, however, simulation results for scan rates of interest indicate that it is not a major factor for scan rate-beam noise tradeoff.

Indicated glideslope deviation (Z_I) for the CV-880 is zero at flare altitude as a result of autopilot gain scheduling.

During final approach, control activity is greatest in the initial stages, prior to gain scheduling activation. These values have been used for the curves of Figure 7-29 through 7-31.

All the variables exceed their limits for one or more conditions shown except pitch angle at flare altitude and airspeed at flare altitude.

Figure 7-35(a) presents the scan rate-beam noise tradeoff for this system. Again, the region of permissible combinations is limited by a high frequency variable, elevator activity (δ_e), which is extremely sensitive to noise but insensitive to scan rate (horizontally oriented). Again, this is primarily due to the lack of substantial filtering in the coupler processor.

Results with a 0.5 second filter time constant, plotted in Figure 7-35(b), again show a substantial increase in the region of acceptable values with elevator activity and glideslope deviation (Z) now equally significant in limiting the region.

7.3.3 PA-30 ACCEPTABILITY FACTORS

Figures 7-36, through 7-42, present the 2σ data for PA-30 longitudinal channel pilot acceptability factors. Approach activity for this case decreases monotonically from acquisition. The values for Figures 7-36, -37, and -38 were

taken at approximately 700 ft. altitude and represent roughly the average over the entire approach. All the variables except pitch angle deviation and airspeed deviation at flare altitude exceed their limits for one or more of the conditions shown.

There is a dramatic decrease in elevator activity (Fig. 7-37) and pitch rate activity (Fig. 7-38) at 1 scan per second, indicating the tendency of high frequency variables to settle between scans at low scan rates, but the pitch angle deviation, produced by the pitch rate activity prior to settling remains constant between scans, accounting for the subsequent increase in rms pitch angle (Fig. 7-36) at 1 scan per second.

Figure 7-43(a) is the composite plot for the PA-30 showing acceptable beam noise-scan rate values for the longitudinal channel. As with the CV-880, the region of acceptable values is severely limited by noise sensitive variables, in this case indicated glideslope deviation, Z_I, and pitch rate, q. Figure 7-43(b) shows the improvement with a 0.5 second coupler filter.

7.4 SUMMARY

By way of summary, the reader is referred to the important figures of this section, the various beam noise-scan rate tradeoffs:

Azimuth:

CV-880 Safety Factors	Fig. 7-8(a) Fig. 7-8(b)
Pilot Acceptability Factors	Figs. 7-16(a) & (b) Figs. 7-24(a) & (b)

Elevation #1

CV-880 Safety Factors	Figs. 7-28(a) & (b)
Pilot Acceptability Factors	Figs. 7-35(a) & (b) Figs. 7-43(a) & (b)

7.5 INTERPRETATIONS

7.5.1 IMPLICATIONS OF A PERCENTAGE INCREASE IN 1σ VALUE TO THE PROBABILITY OF EXCEEDING A LIMIT - CRITICAL VARIABLES AT TOUCHDOWN

All of the results of Section 7 related to safety criteria

at touchdown are expressed in terms of percentage increase in 1σ value as beam noise and scan rate are varied from the perfect continuous case with worst case wind.

Without knowledge of the absolute dispersion for the baseline case, this percentage increase has no direct implicataion for the probability of exceeding a specific limit.

It is illuminating, however, to postulate hypothetical relationships between the limit and the 1σ value and, over a range of interest to at least bound probability variation as a function of percentage variation.

If the variables of interest are gaussian, then this is easily done with the aid of tables for the gaussian cumulative distribution function. Table 7-3 shows probability of exeeeding a limit for various percentage increases and various baseline probabilities. As an example, let the limit, L, on a variable, X, be 10 and its 1σ value under baseline conditions be 2.35; then the limit represents a 4.26σ value of that variable and will be exceeded once in 10^5. For an increase of 0.5% in the 1σ value, the limit now represents a 4.24σ value and will be exceeded 1.12 times in 10^5 events, an increase of 12%.

It is felt that a probability budget of 12% for LGS imperfections is certainly reasonable (but probably unachievable) and that it would be unrealistic to limit possible acceptable scan rates and beam noise by variables whose increase in 1σ values are less than 0.5%.

What the preceding paragraphs suggest with respect to the results on safety factors is that there is room for deterioration in some of the critical variables when compared with conventional ILS performance while picking up significant improvements in others at moderate scan rates and beam noise. In particular, rather than constrain performance in $\dot{Y}_A$ and $\dot{Z}$ (Figs. 7-8(a) and 7-28(a) respectively), by conventional ILS performance, it would be more realistic to use a flat 1% or 0.5% constraint. (1% increase in corresponds to a 25-30% probability budget for LGS).

It should be noted further that, in an absolute sense, these increases in probability are significant only if $\dot{Y}_A$ or $\dot{Z}$ is truly a limiting factor in determining the probability of a successful landing. For instance, if the probability of landing off the runway is 1 in 10^6 and that of exceeding the cross track velocity limit ($\dot{Y}_A$) is 1 in 10^8, then an increase to 1.15 in 10^8 for exceeding cross track velocity limit is insignificant in comparison with the limiting factor, 1 in 10^6.

TABLE 7-3
EFFECTS OF PERCENTAGE INCREASE IN 1σ VALUE ON
PROBABILITY OF EXCEEDING A LIMIT FOR A GAUSSIAN RANDOM VARIABLE

Ratio of Limit to 1σ Value for 0% (Baseline)	Probability of Exceeding Limit for Percentage Increase in Value Shown				
	0.0%	0.1%	0.5%	1.0%	5.0
5.99	1 in 10^9	1.03 in 10^9	1.18 in 10^9	1.37 in 10^9	5.2 in 10^9
5.61	1 in 10^8	1.03 in 10^8	1.15 in 10^8	1.35 in 10^8	4.8 in 10^8
5.20	1 in 10^7	1.03 in 10^7	1.13 in 10^7	1.35 in 10^7	4.7 in 10^7
4.75	1 in 10^6	1.02 in 10^6	1.12 in 10^6	1.3 in 10^6	3.3 in 10^6
4.26	1 in 10^5	1.02 in 10^5	1.12 in 10^5	1.25 in 10^5	2.4 in 10^5
3.72	1 in 10^4	1.02 in 10^4	1.1 in 10^4	1.18 in 10^4	1.9 in 10^4
3.09	1 in 10^3	1.02 in 10^3	1.08 in 10^3	1.14 in 10^3	1.7 in 10^3
2.33	1 in 10^2	1.01 in 10^2	1.05 in 10^2	1.1 in 10^2	1.35 in 10^2

Therefore, in interpreting scan rate beam noise trade-offs for safety factors for the CV-880, it is felt that Figures 7-8(b) and 7-28(b) which use the hybrid constraint on critical variables (dispersion increases half that with conventional ILS or 0.5%, whichever is greater) are still conservative but more realistic than ones generated based solely on either a flat percentage or a specific improvement over conventional ILS.

7.5.2 PILOT ACCEPTABILITY FACTORS - THE EFFECTS OF A COUPLER FILTER

As was seen in Section 7 [Figs. 7-16(b), 24(b), 35(b) and 43(b)] a coupler filter significantly reduces activity in higher frequency variables, thereby enlarging the region of acceptable noise and scan rate values for pilot acceptability factors. It is more critical in the longitudinal system, to an extent that, with effectively no filter, neither aircraft satisfies all pilot acceptability constraints for reasonable values of noise and scan rate.

It is certainly reasonable to assume that a significant amount of work will go into designing a coupler filter for each aircraft that intends to fly the LGS and that the filter design will be based on both the scanning rate and the aircraft dynamics. No attempt has been made during this study to accomplish such a design for the aircraft under consideration.

The results, however, do reflect the sensitivity of pilot acceptability factors to filtering and do point out the need for considering filter configurations in further performance studies concerning scanning rate and beam noise. It is felt that results based on a rational filter design would more closely approximate those with a 0.5 second filter than those with the 0.025 second filter.

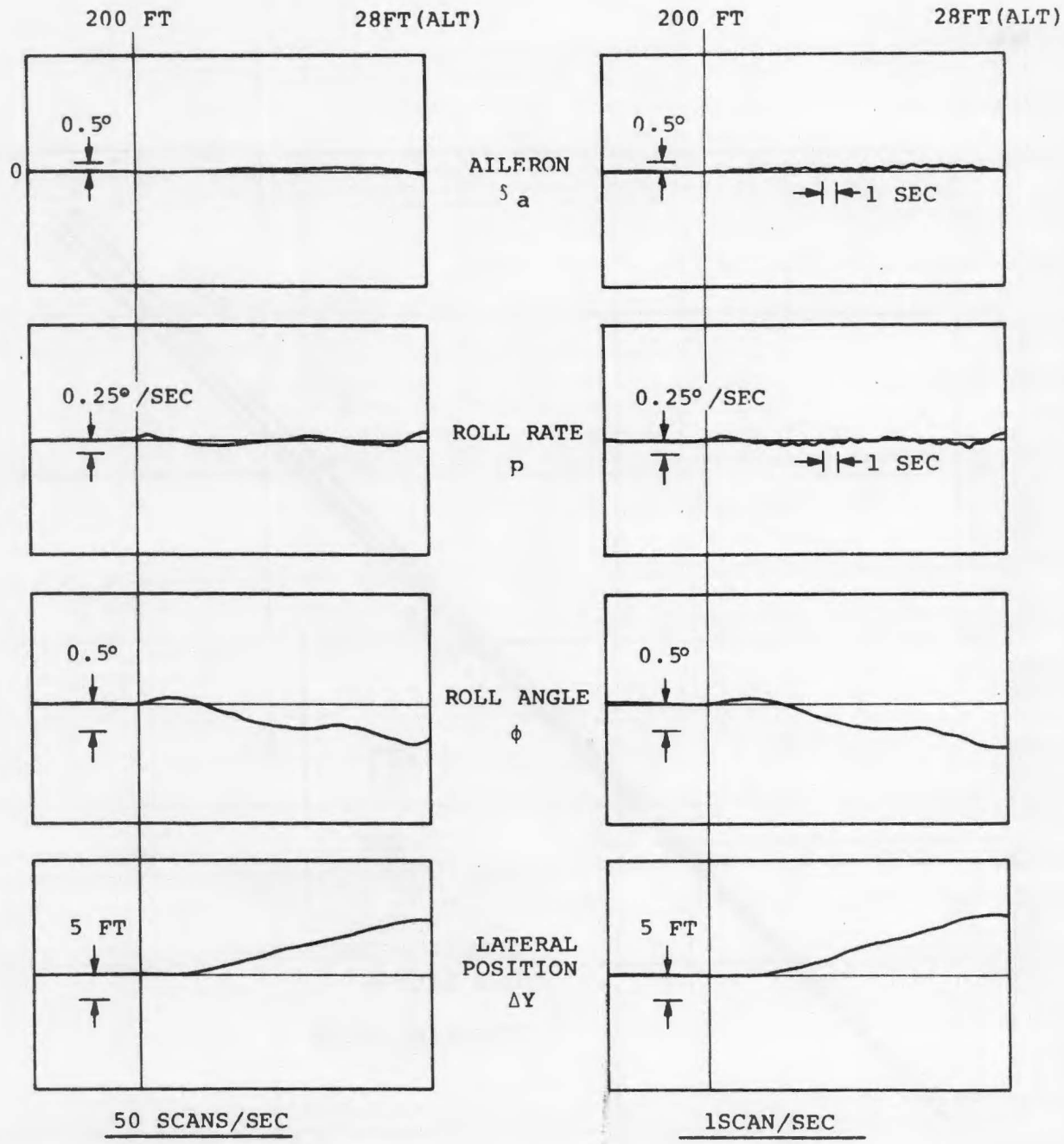

Figure 7-1. CV-880 Lateral System Response to Wind Shear At 50 and 1 Scans Per Second

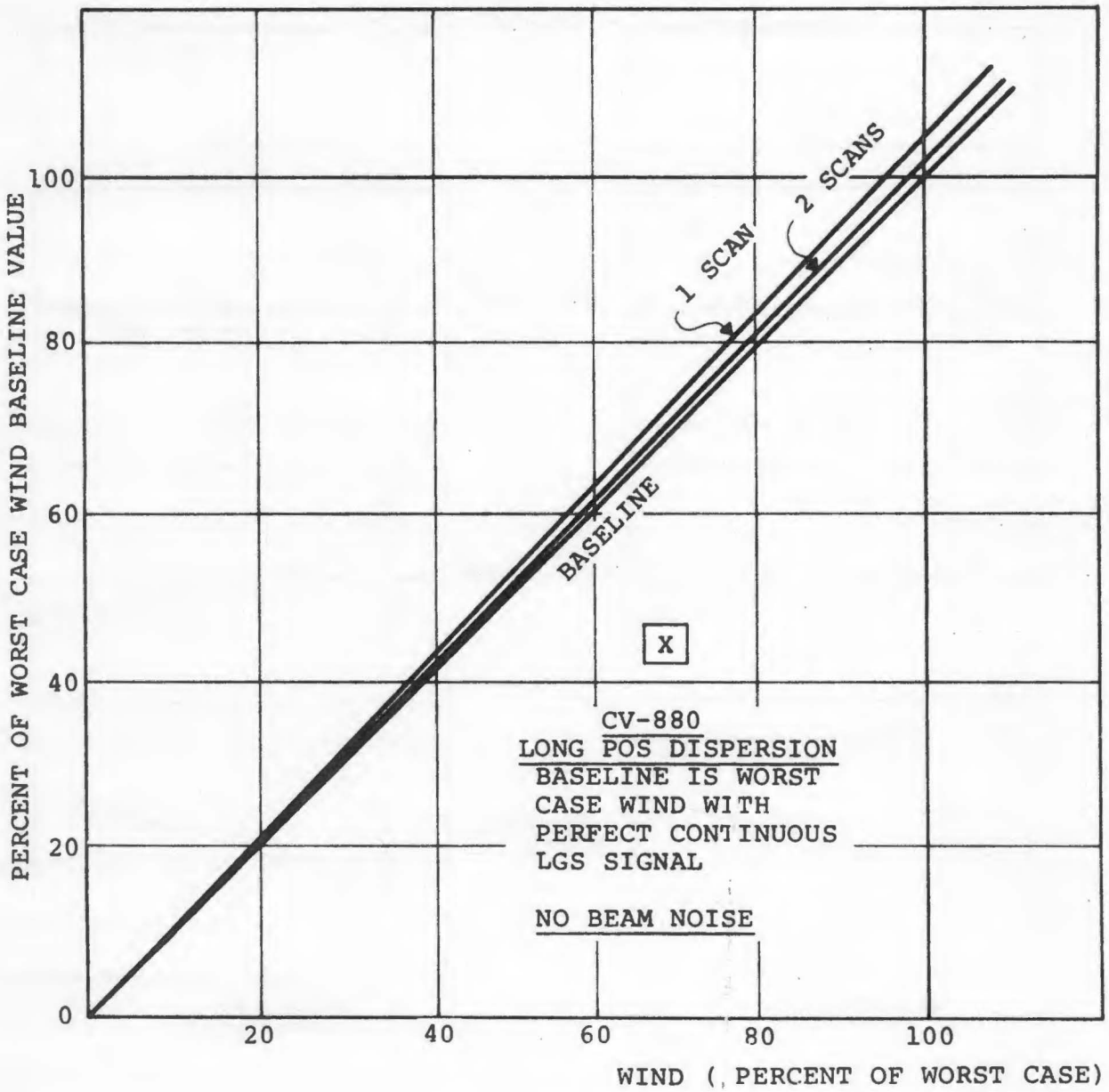

Figure 7-2. Relative Dispersion in Longitudinal Position Vs. Relative Gust Intensity (No Beam Noise)

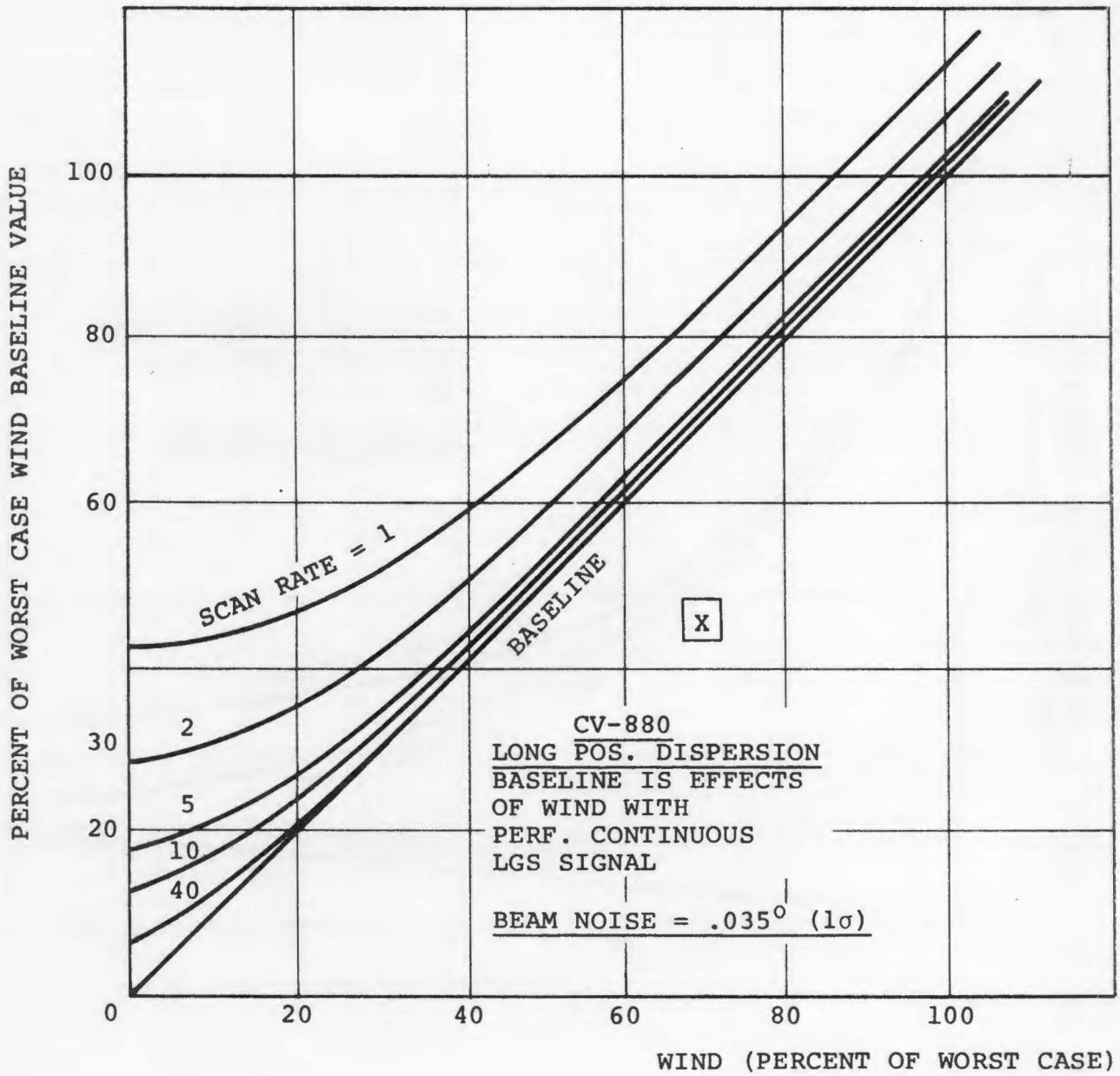

Figure 7-3. Relative Dispersion in Longitudinal Position Vs. Relative Gust Intensity With Beam Noise

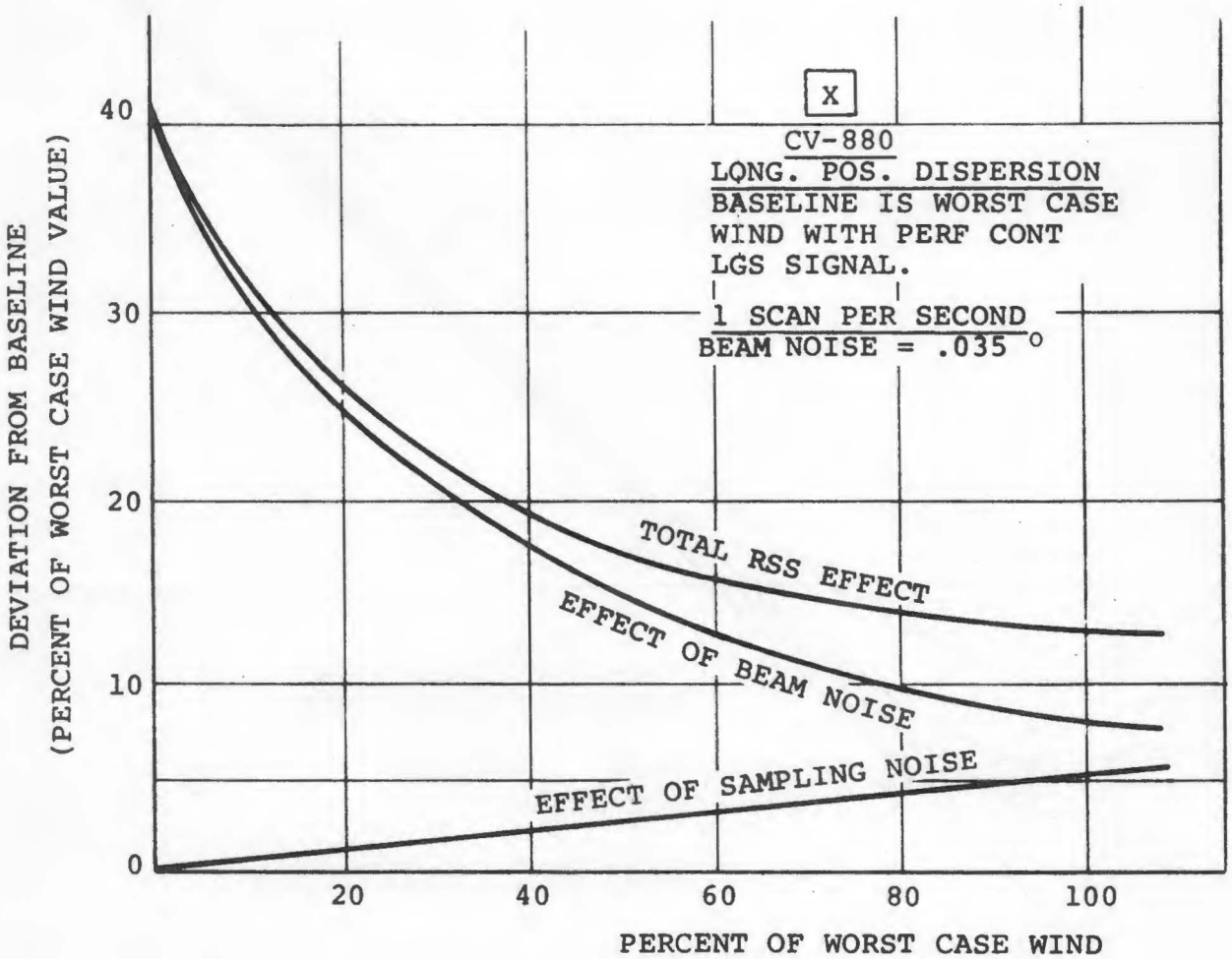

Figure 7-4. Relative Effects of Beam Noise and Sample Noise Vs. Wind

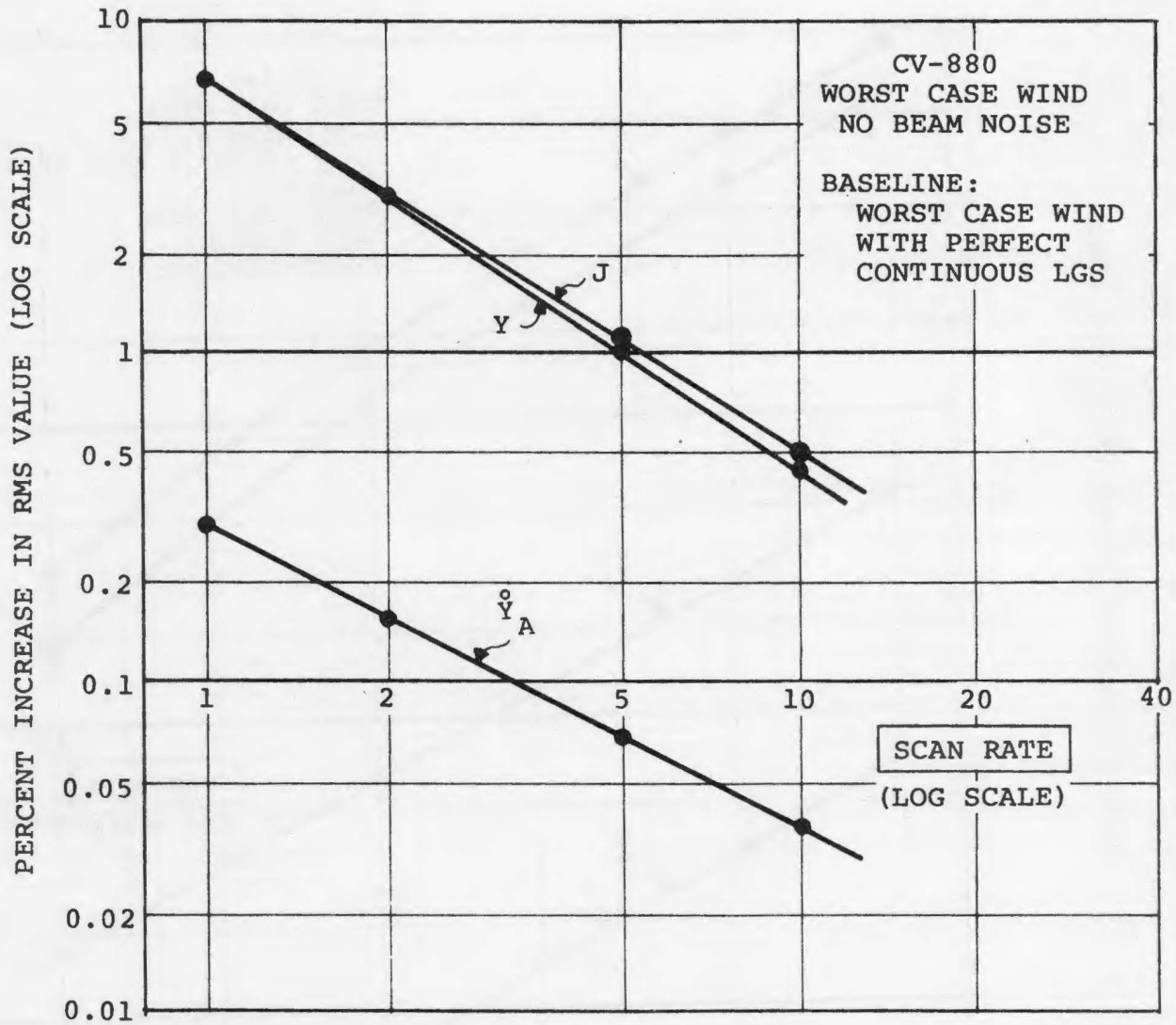

Figure 7-5. Relative Effect of Scan Rate on Lateral Touchdown Variables - Worst Case Wind - No Beam Noise

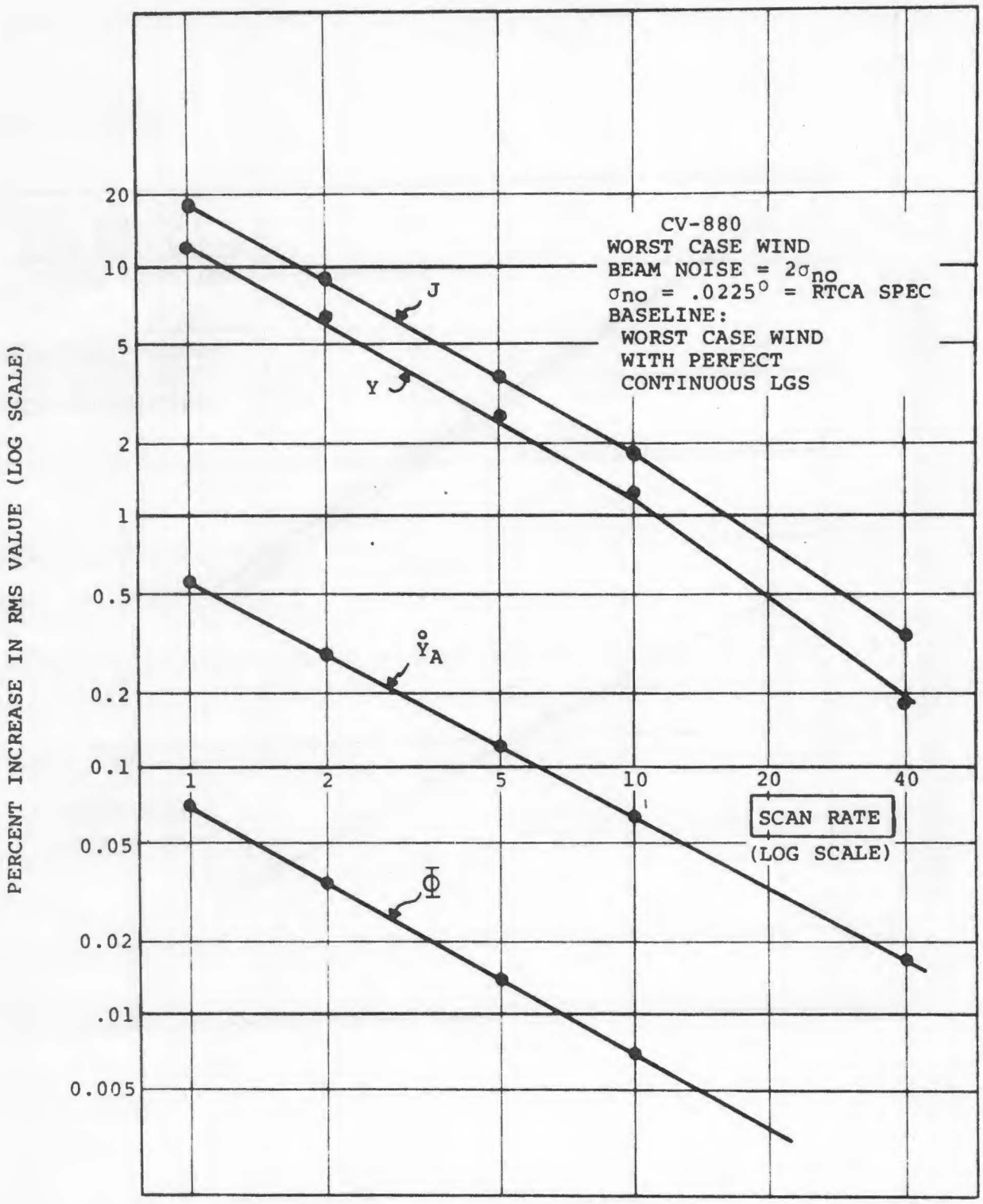

Figure 7-6. Relative Effect of Scan Rate on Lateral Touchdown Variables, Worst Case Wind + Beam Noise

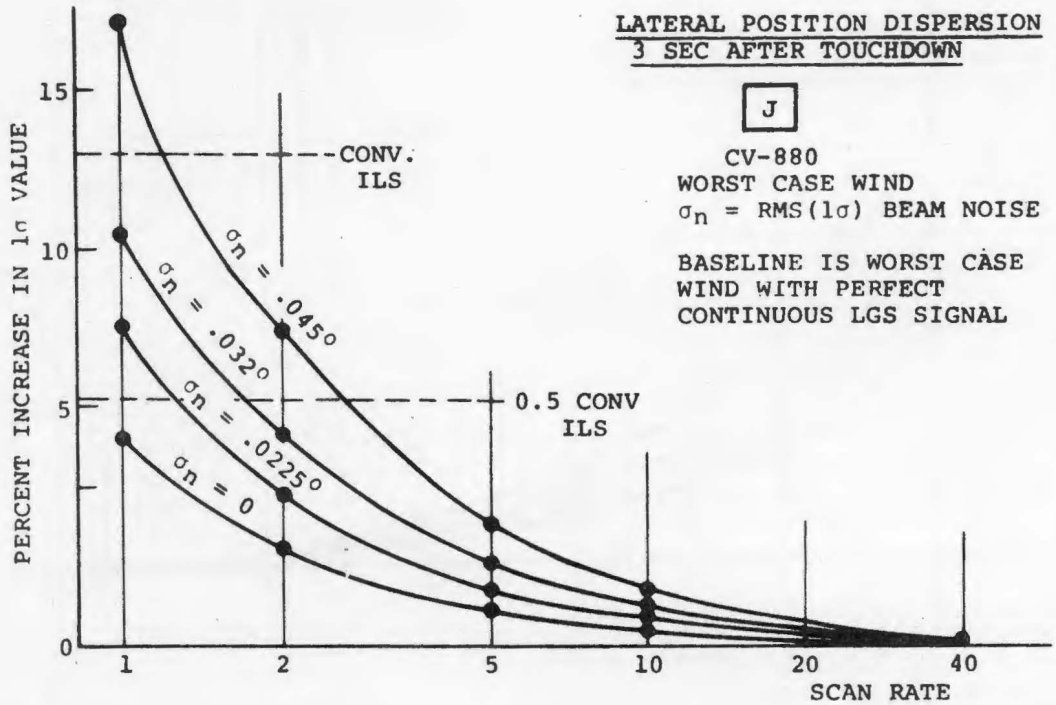

Figure 7-7(a). 1σ Lat. Pos. (3 Sec. After TD) Vs. Scan Rate

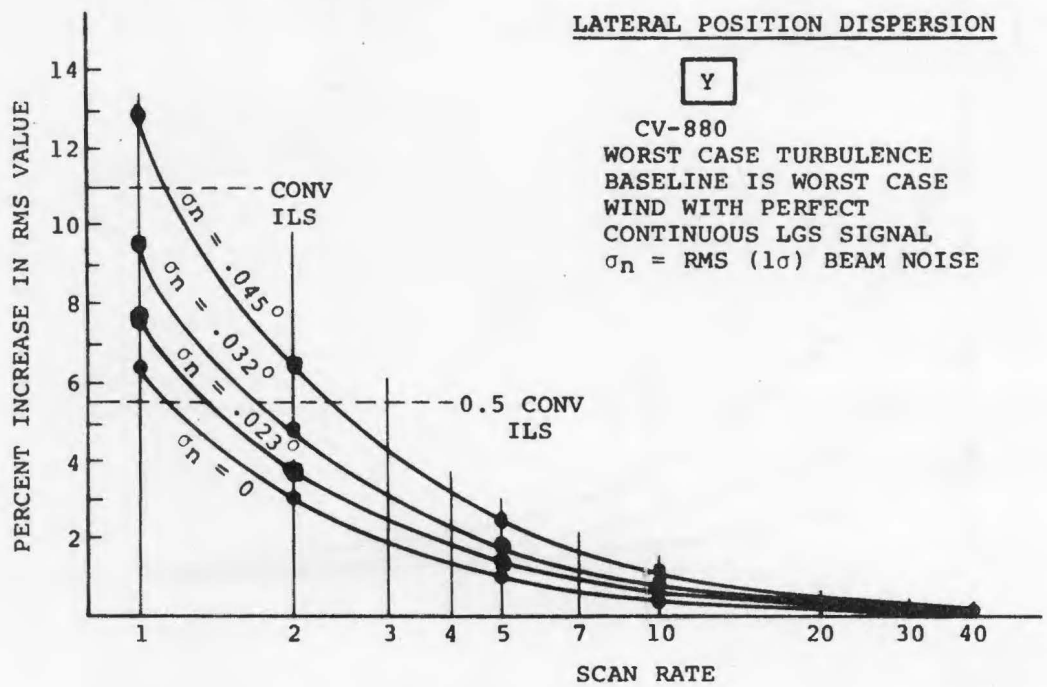

Figure 7-7(b). Lateral Position Dispersion Vs. Scan Rate

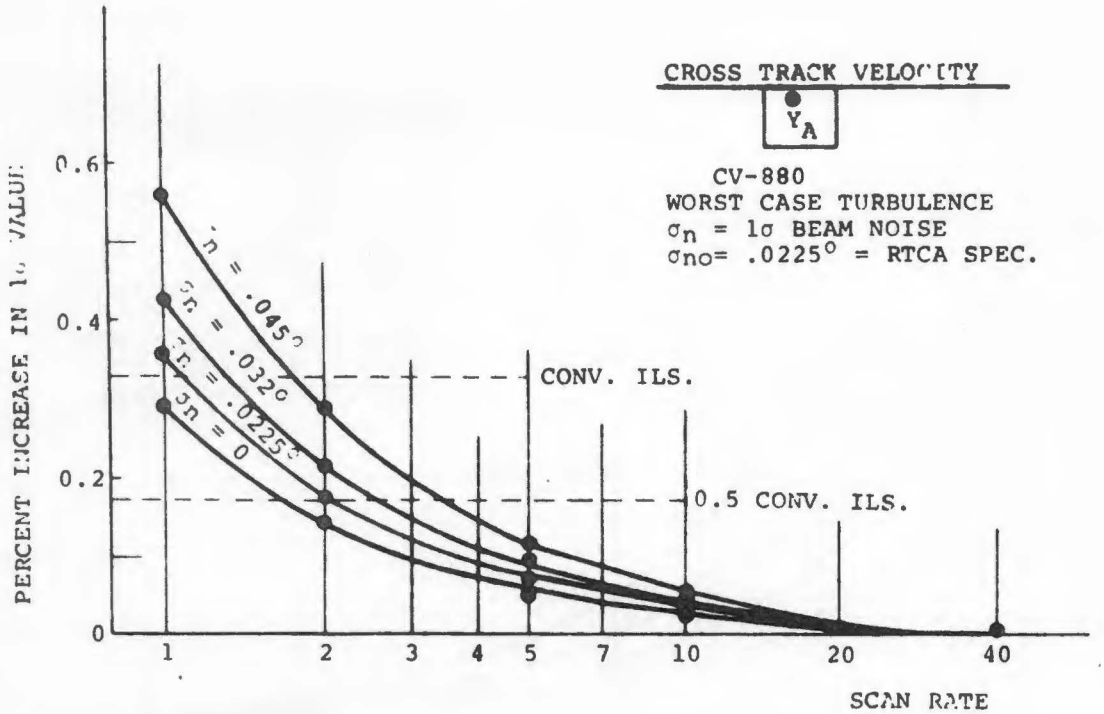

Figure 7-7(c). Cross Track Velocity Dispersion Vs. Scan Rate

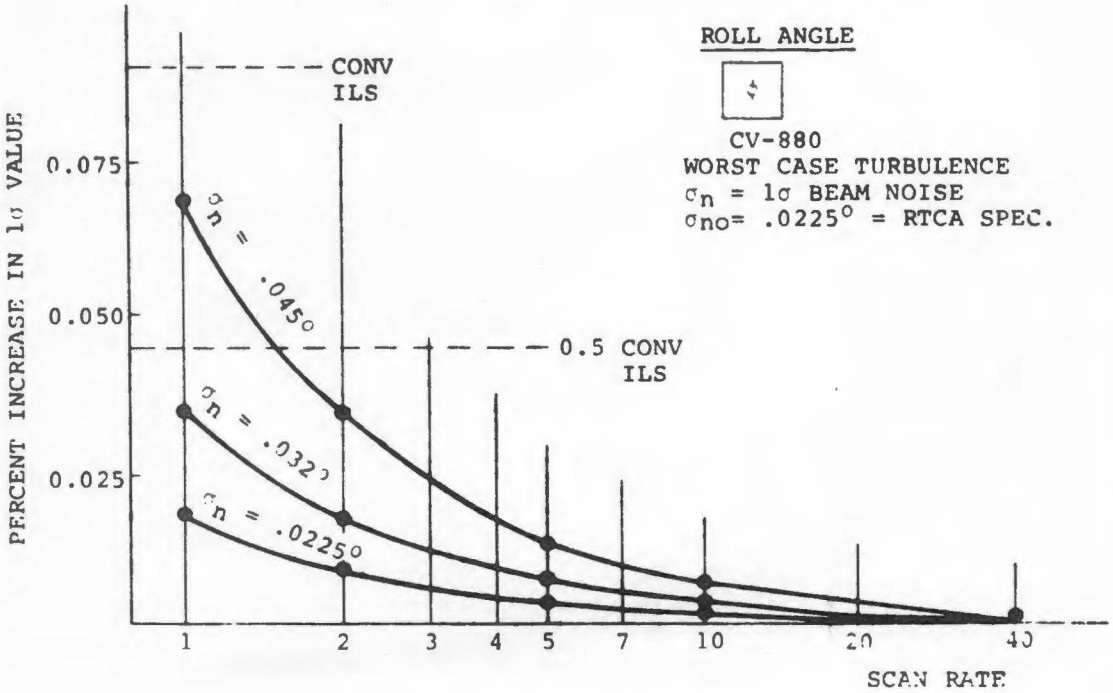

Figure 7-7(d). Roll Angle Dispersion Vs. Scan Rate

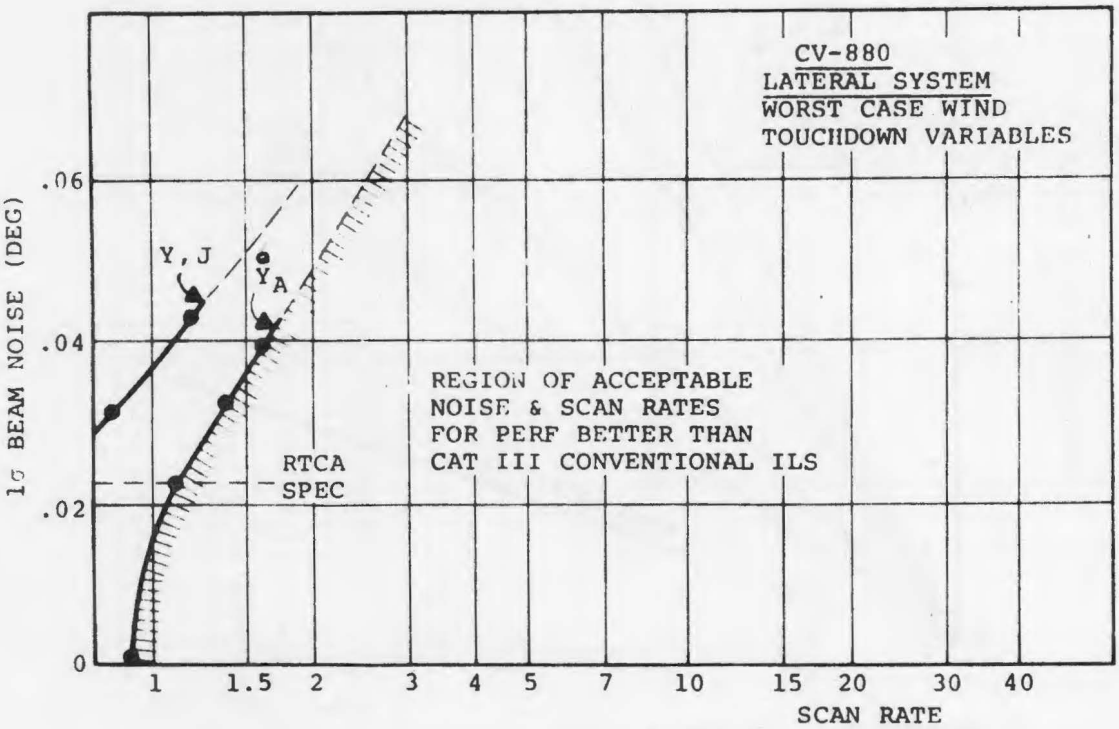

Figure 7-8(a). Scan Rate - Beam Noise Tradeoff For Performance Equivalent to Cat III Conv. ILS

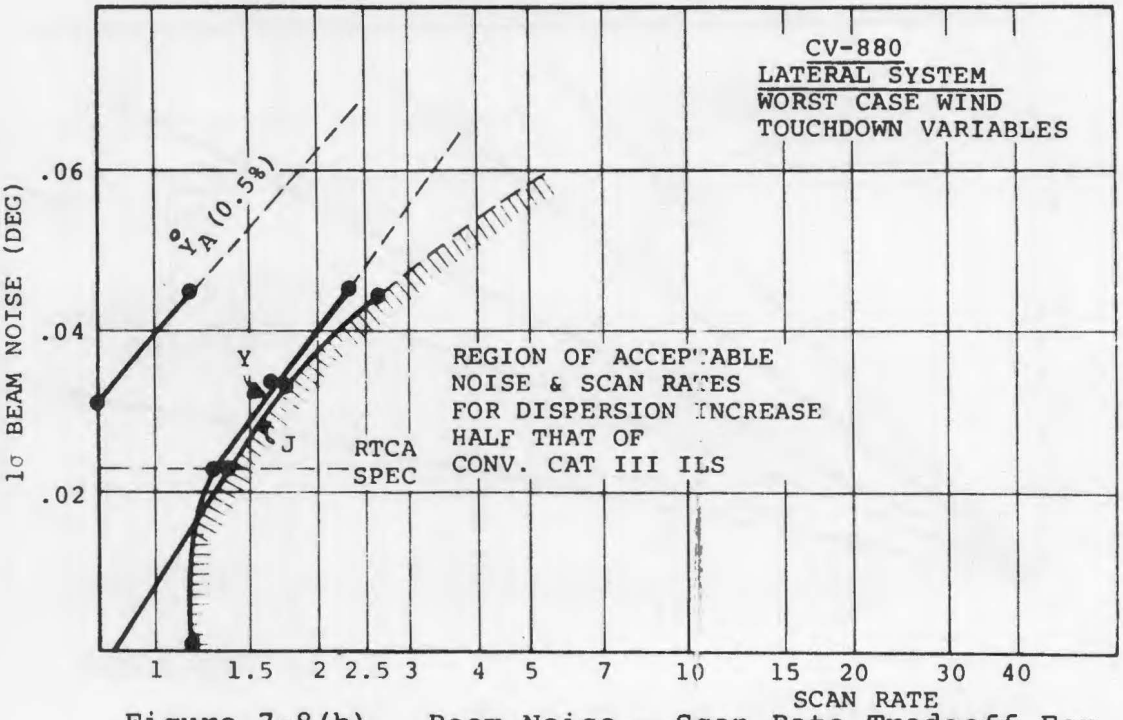

Figure 7-8(b). Beam Noise - Scan Rate Tradeoff For Dispersion Increases Half Those With Cat III Conventional ILS or 0.5%, Whichever is Greater

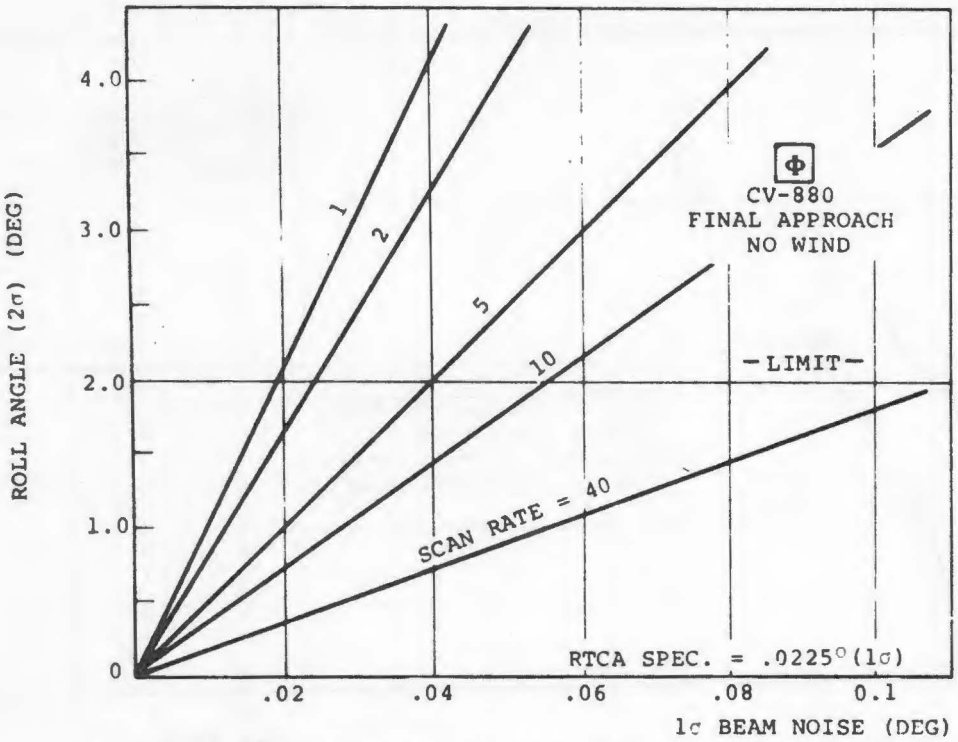

Figure 7-9. 2σ Roll Angle (ϕ) Vs. Beam Noise
Final Approach - No Wind

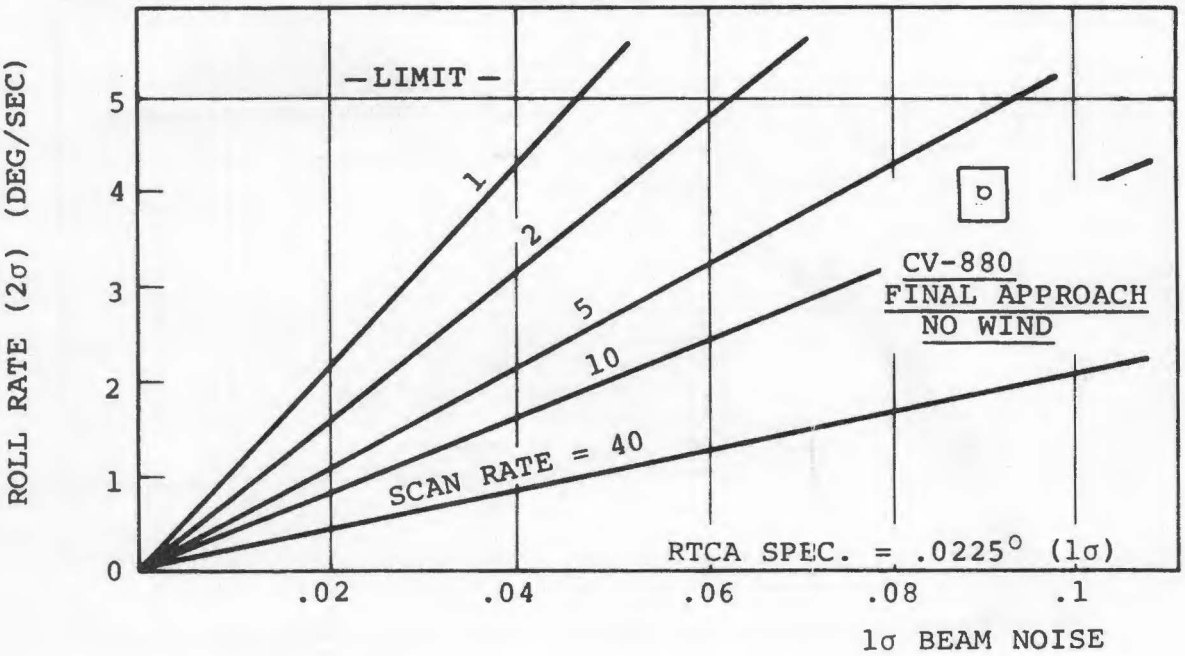

Figure 7-10. 2σ Roll Rate (p) Vs. Beam Noise
Final Approach - No Wind

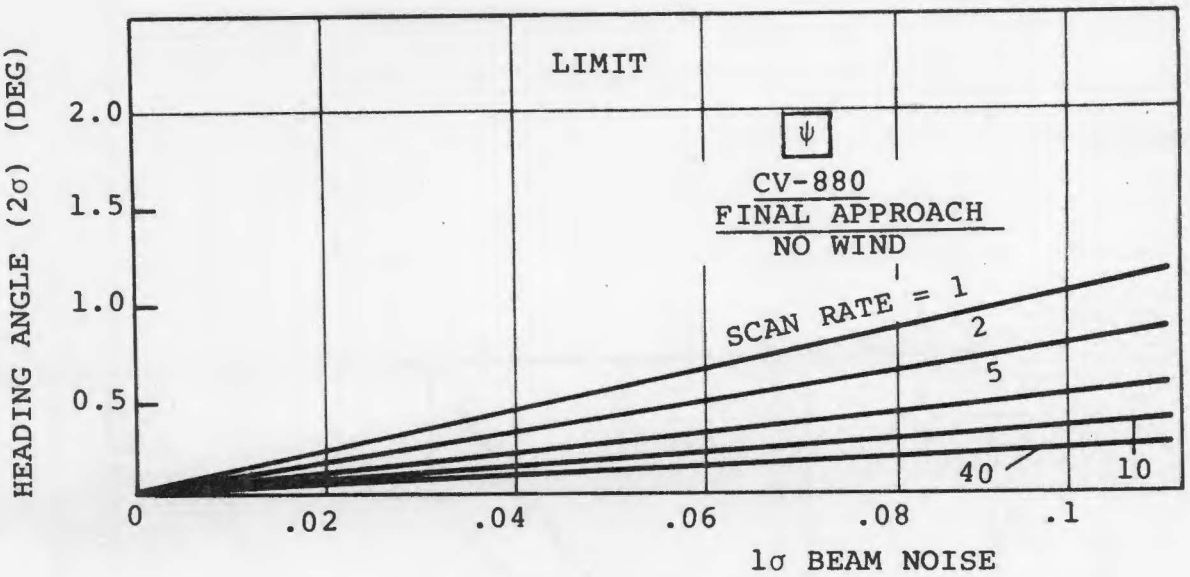

Figure 7-11. 2σ Heading Angle (ψ) Vs. Beam Noise
Final Approach - No Wind

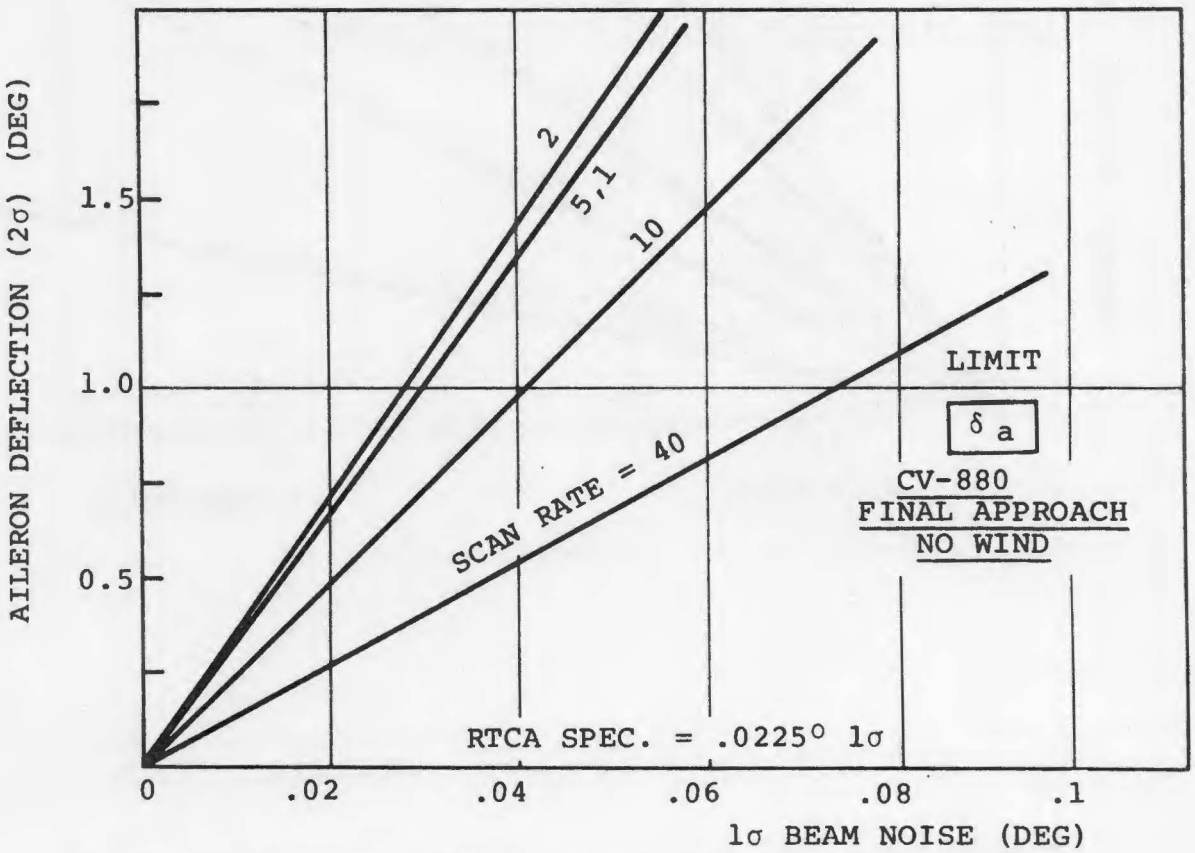

Figure 7-12. 2σ Aileron Activity (δ_a) Vs. Beam Noise
Final Approach - No Wind

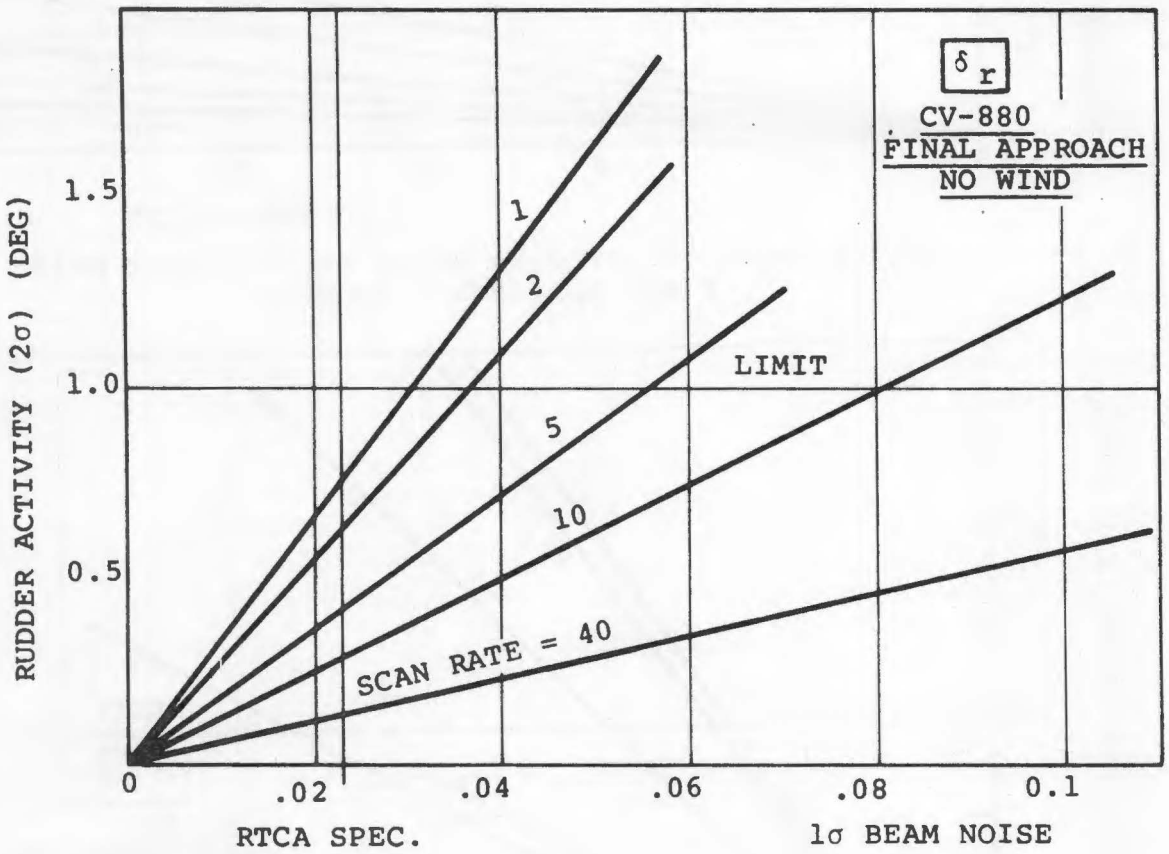

Figure 7-13. 2σ Rudder Activity (δ_a) Vs. Beam Noise
Final Approach - No Wind

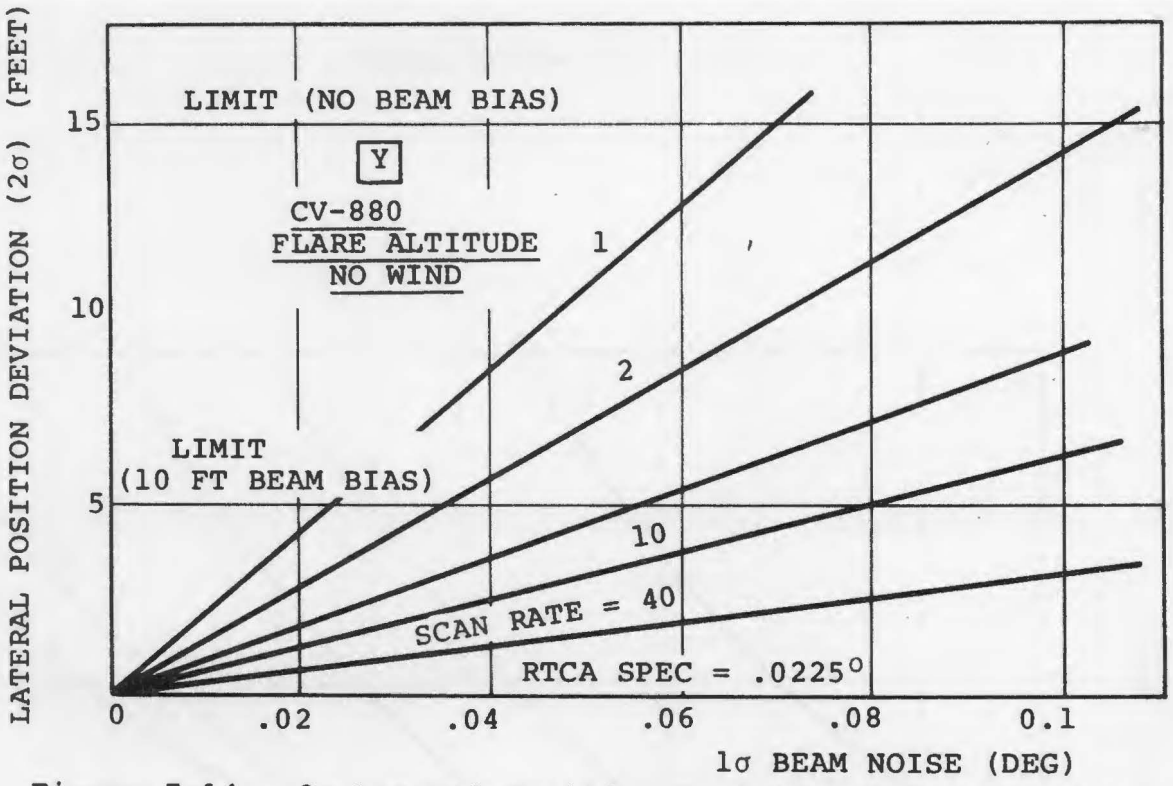

Figure 7-14. 2σ Lateral Position Deviation Vs. Beam Noise At Flare Altitude - No Wind

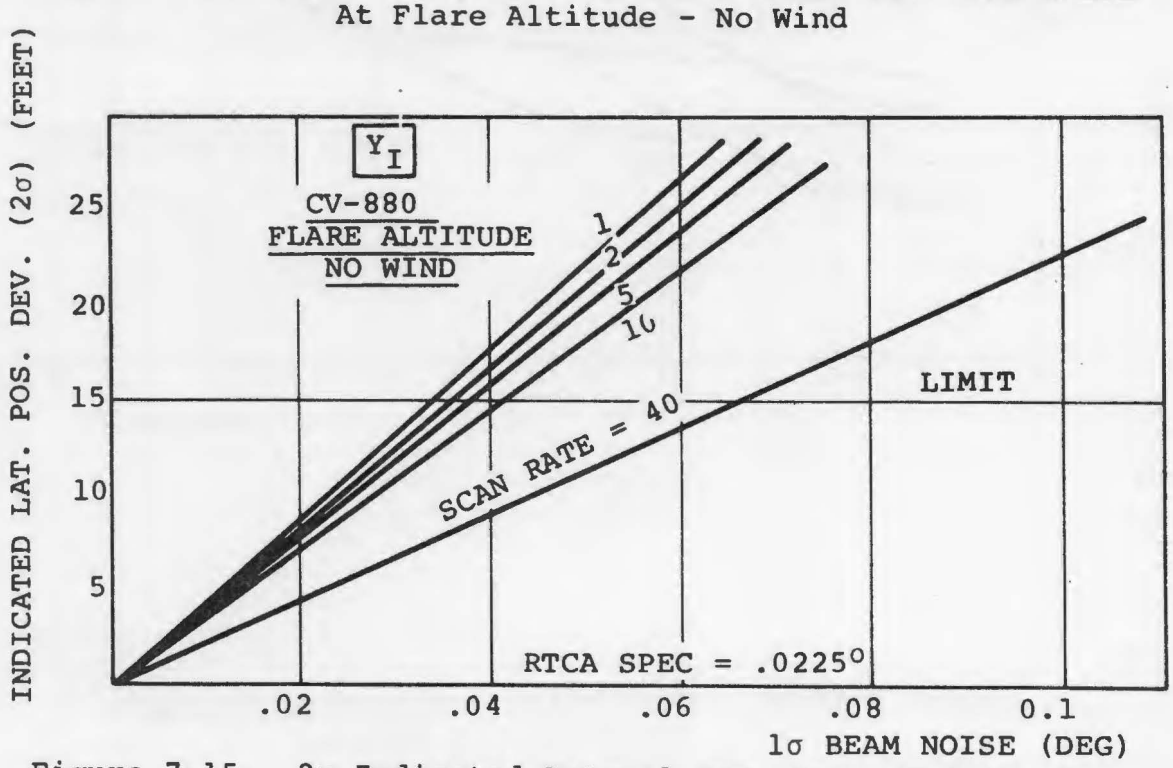

Figure 7-15. 2σ Indicated Lateral Pos. Dev. (Y_I) Vs. Beam Noise - Flare Altitude - No Wind

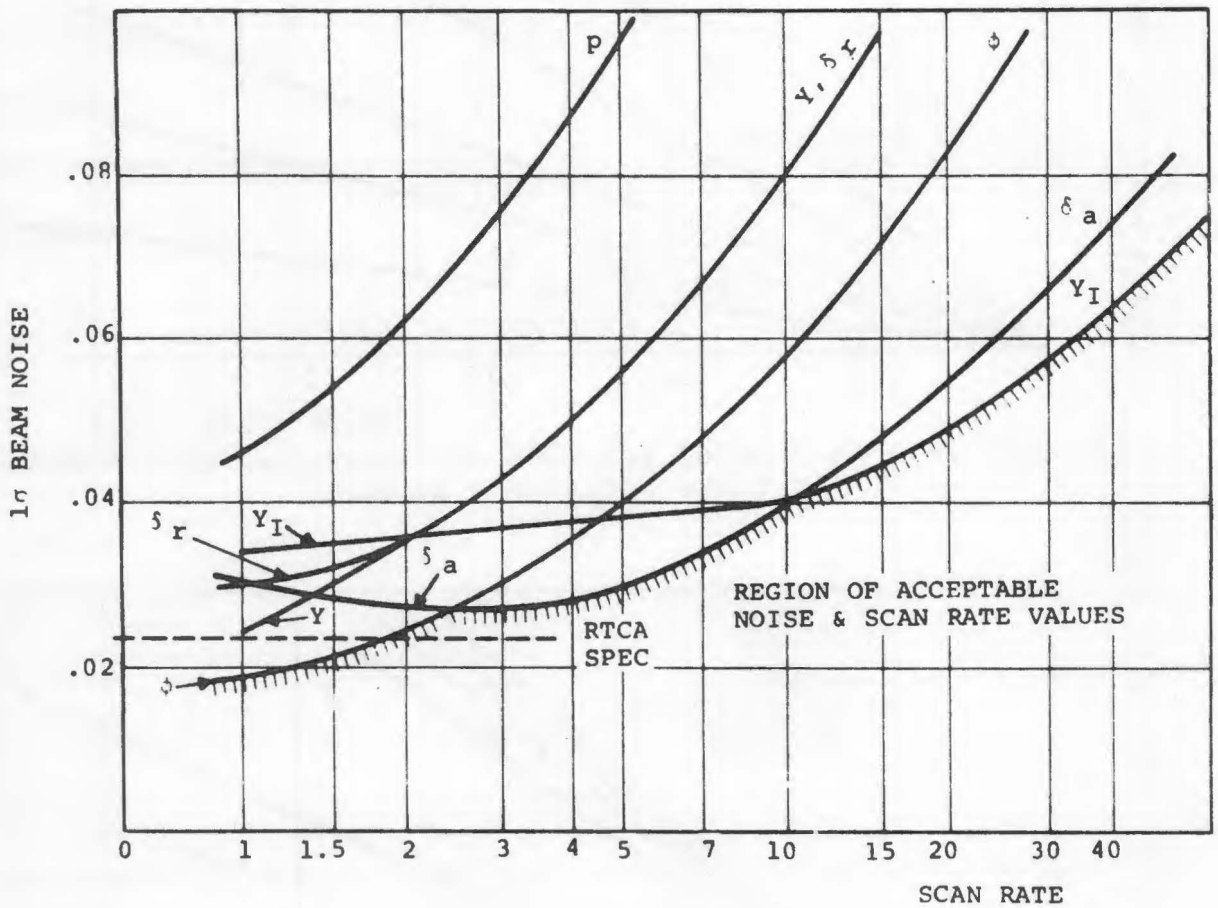

Figure 7-16(a). Beam Noise - Scan Rate Tradeoff
Pilot Acceptability Factors
CV-880 Lateral System
(Coupler Filter Time Constant = .025 Sec.)

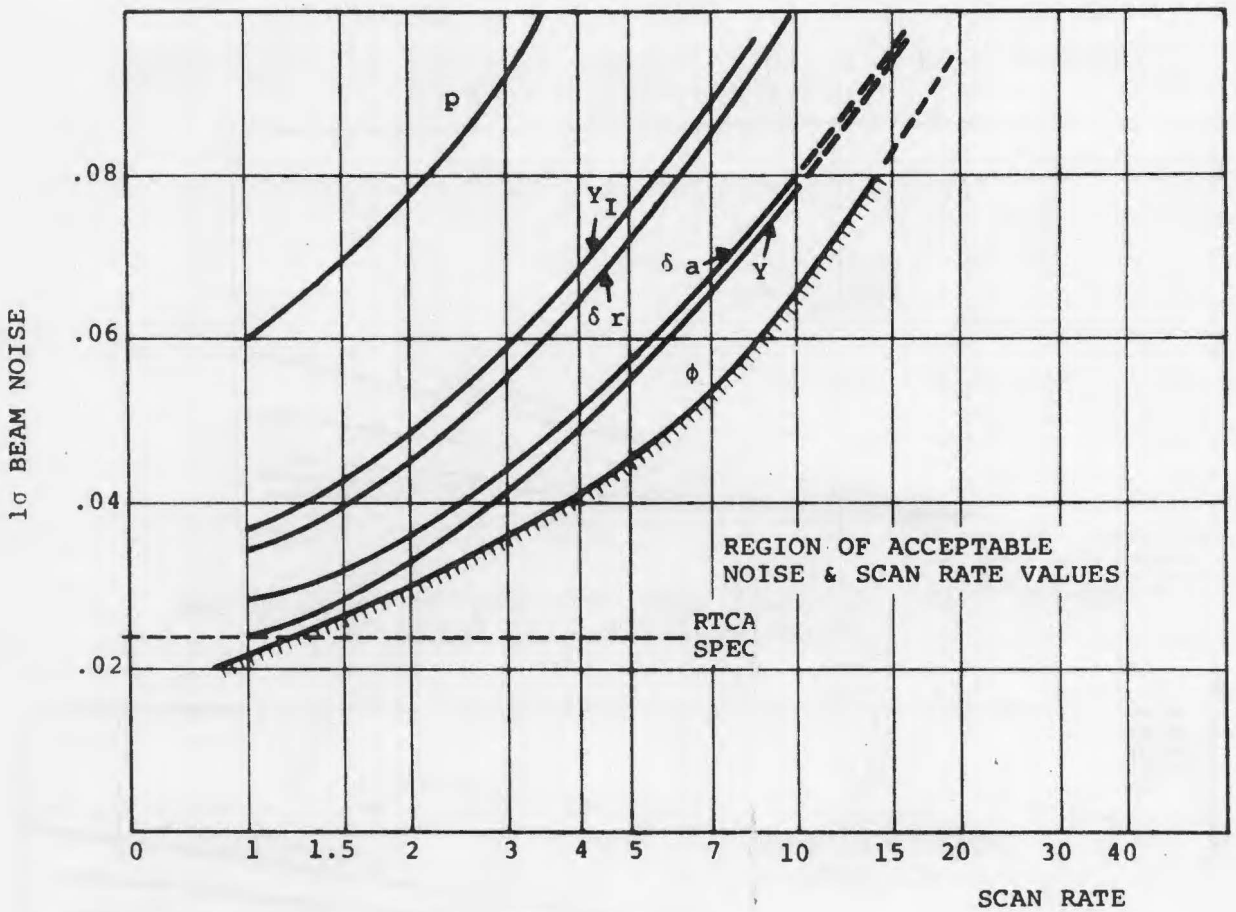

Figure 7-16(b). Beam Noise - Scan Rate Tradeoff
Pilot Acceptability Factors
CV-880 Lateral System
(Coupler Filter Time Constant = 0.5 Sec.)

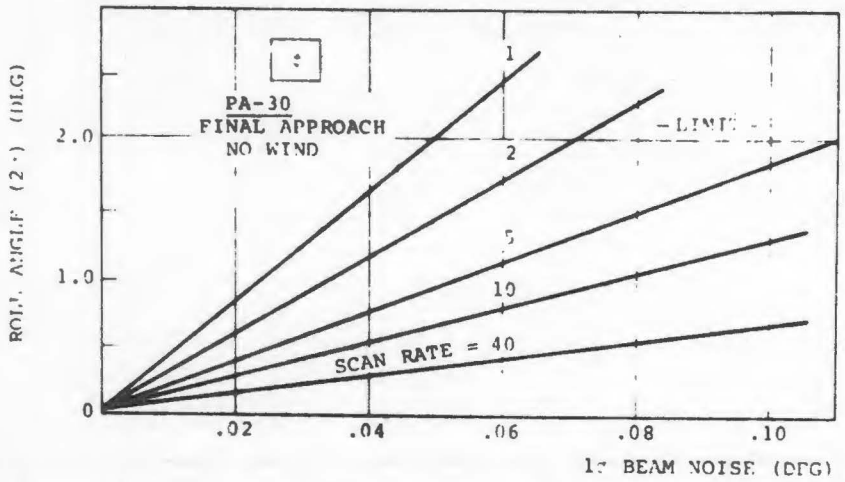

Figure 7-17. 2σ Roll Angular Activity Vs. Beam Noise
Final Approach - No Wind

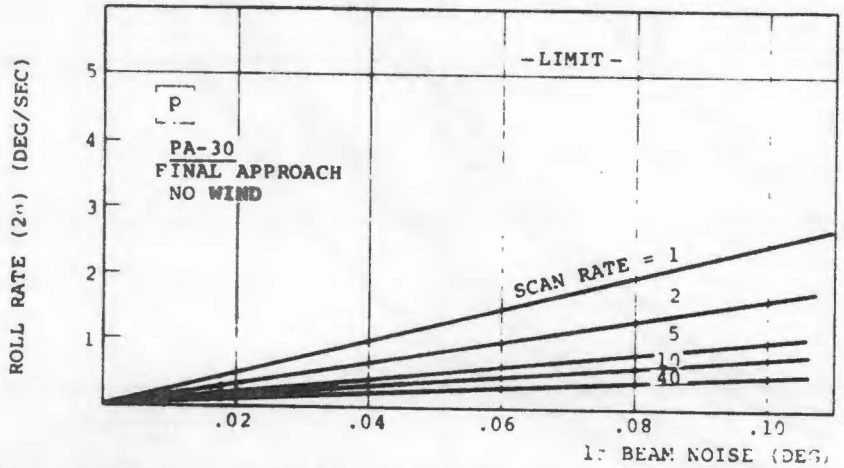

Figure 7-18. 2σ Roll Rate Activity Vs. Beam Noise
Final Approach - No Wind

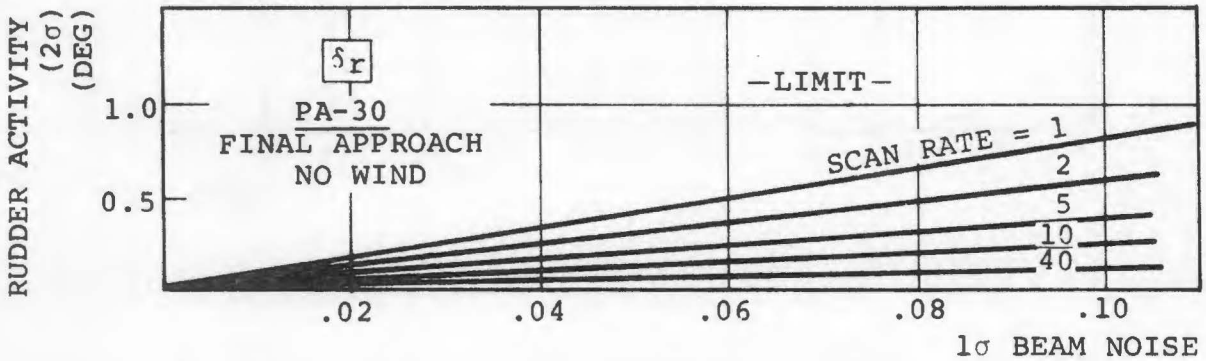

Figure 7-19. 2σ Rudder Activity Vs. Beam Noise
Final Approach - No Wind

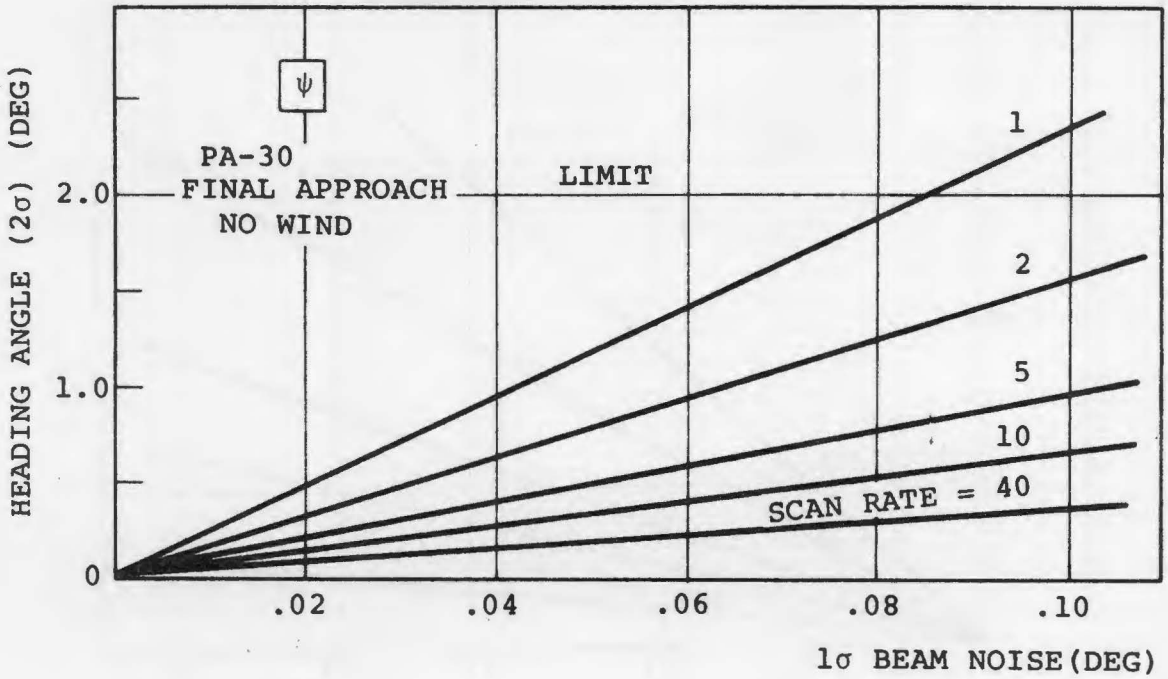

Figure 7-20. 2σ Heading Angular Activity Vs. Beam Noise

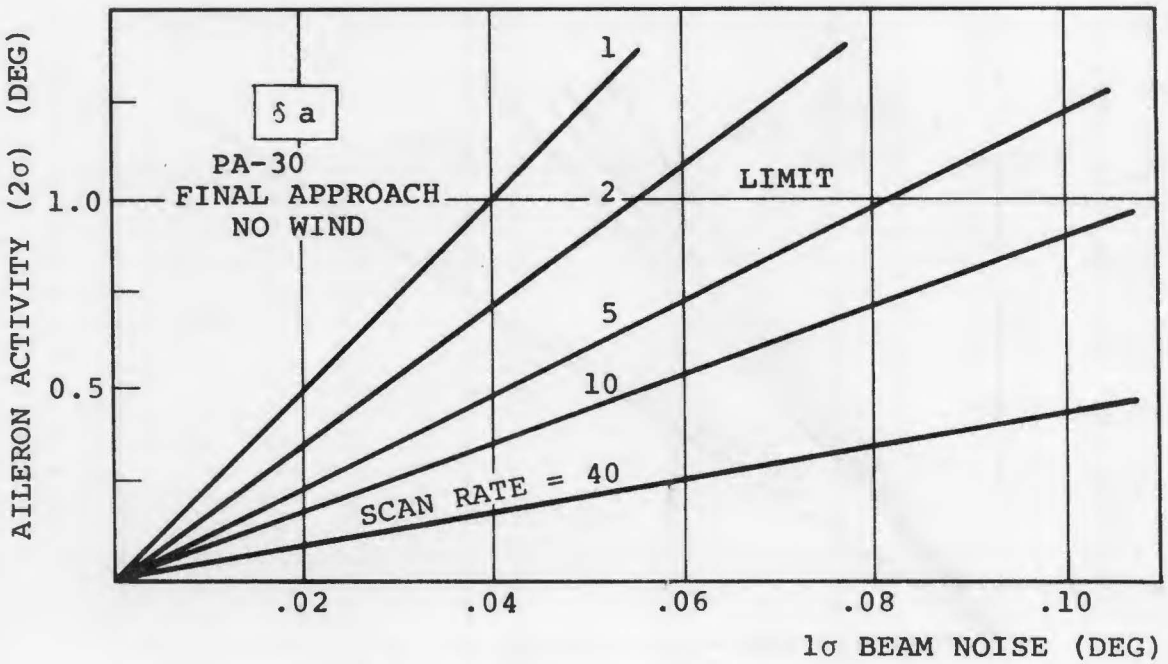

Figure 7-21. 2σ Aileron Activity Vs. Beam Noise

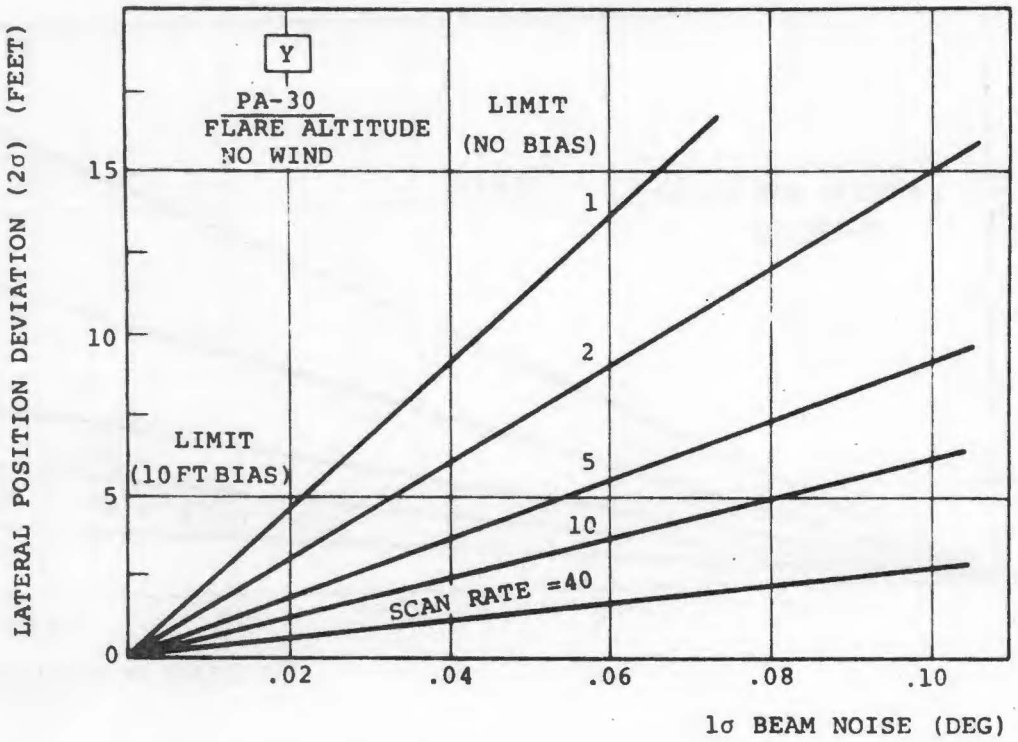

Figure 7-22. 2σ Lateral Position Deviation Vs. Beam Noise

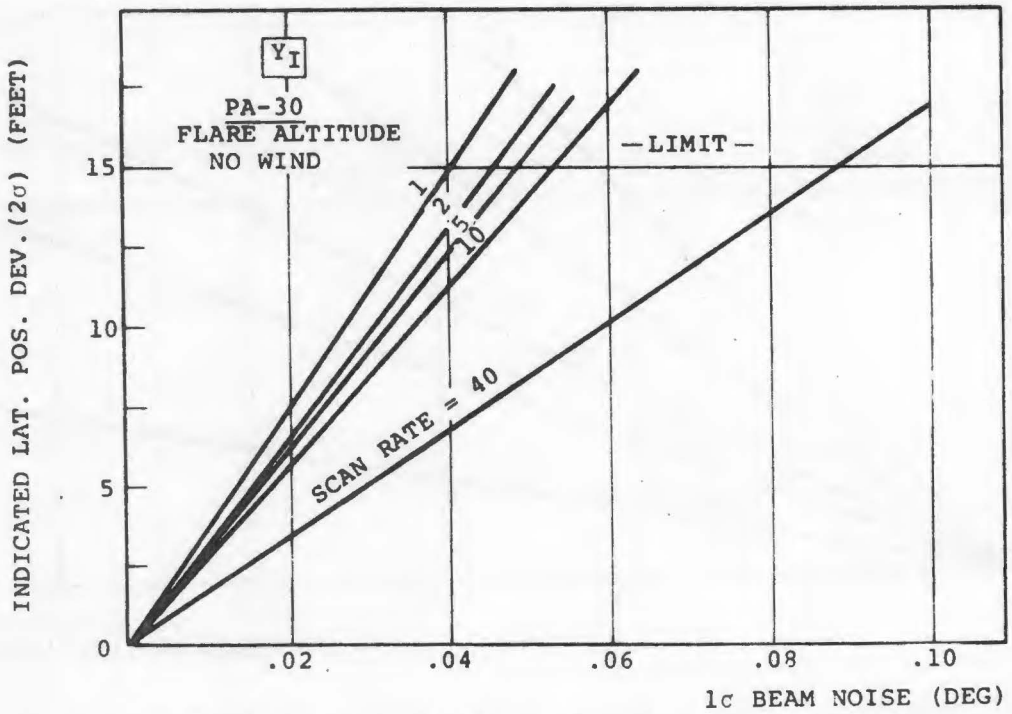

Figure 7-23. 2σ Indicated Lat. Pos. Dev. Vs. Beam Noise

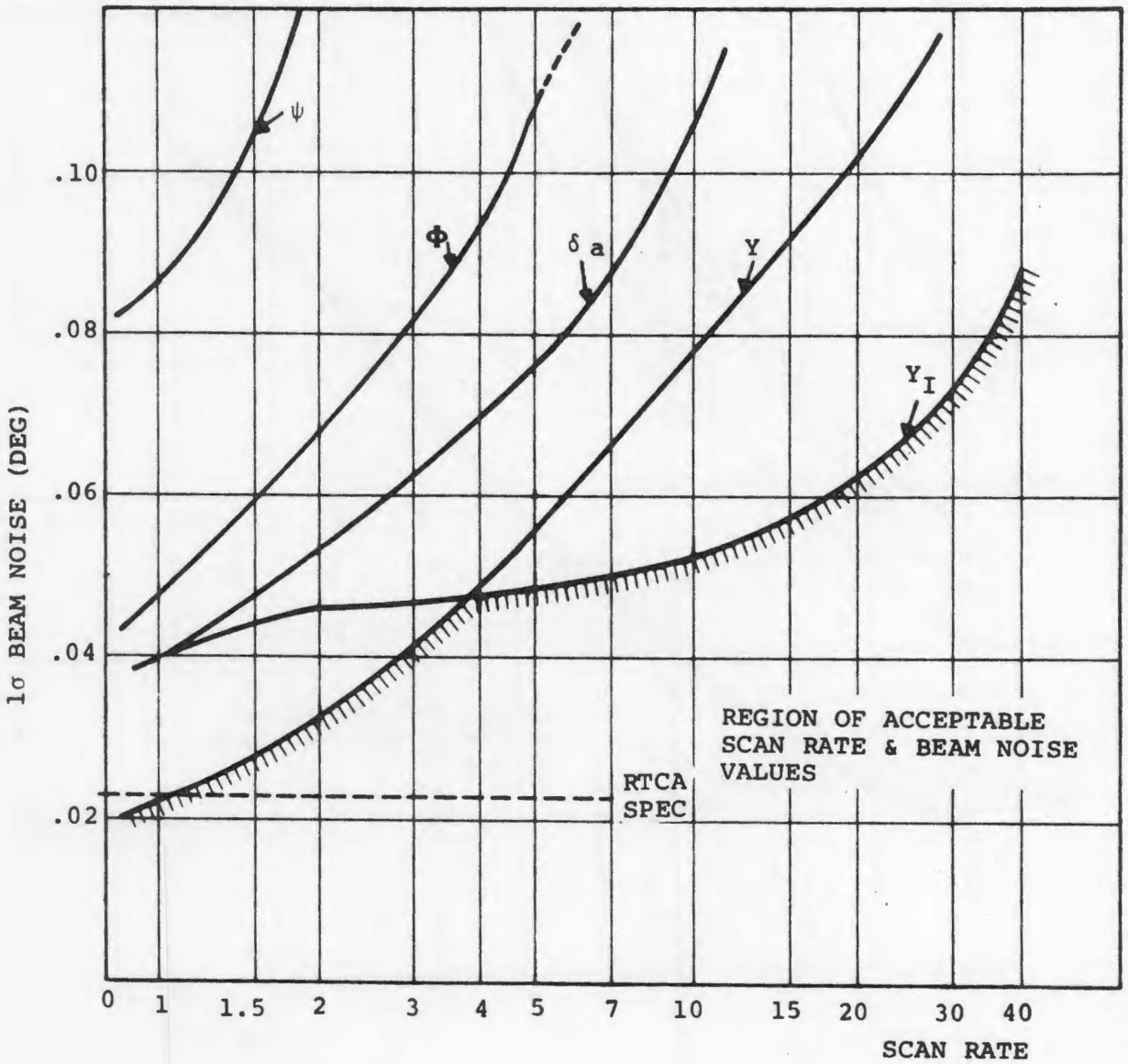

Figure 7-24(a). Beam Noise - Scan Rate Tradeoff
Pilot Acceptability Factors
PA-30 Lateral System
(Coupler Filter Time Constant = .025 Sec.)

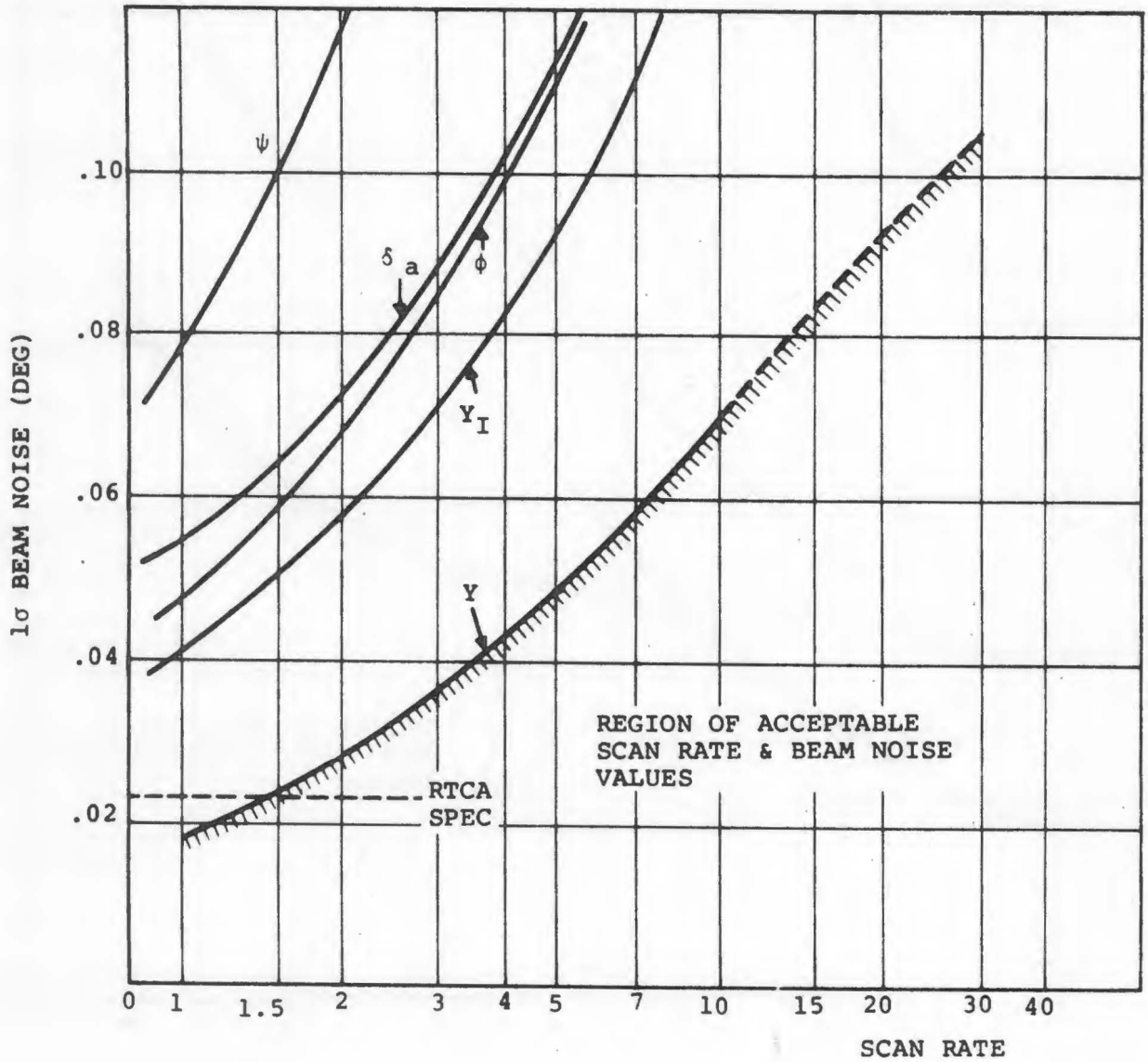

Figure 7-24(b). Beam Noise - Scan Rate Tradeoff
Pilot Acceptability Factors
PA-30 Lateral System
(Coupler Time Constant: 0.5 Sec.)

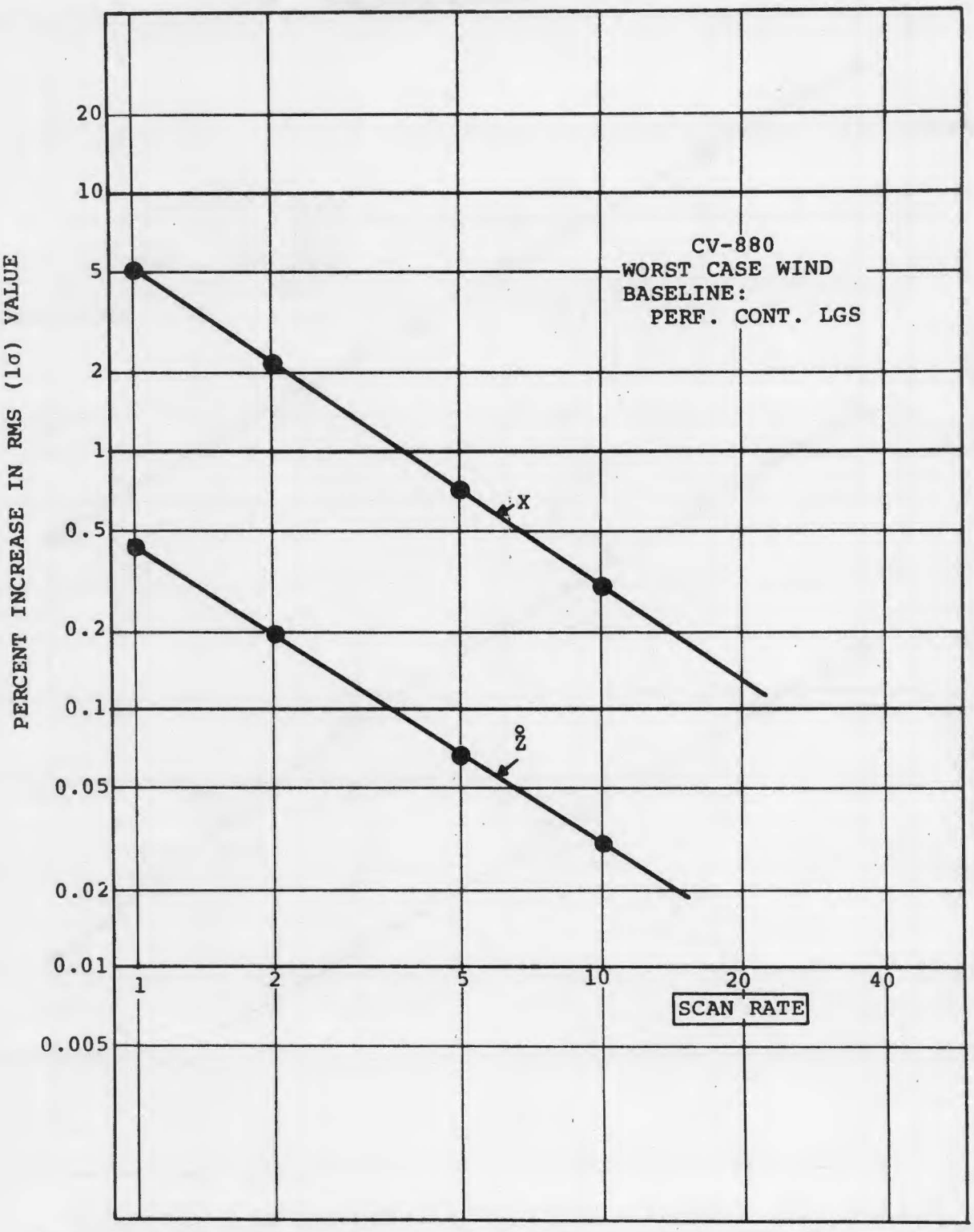

Figure 7-25. Relative Effects of Scan Rate on Longitudinal Touchdown Variables - Worst Case Wind - No Beam Noise

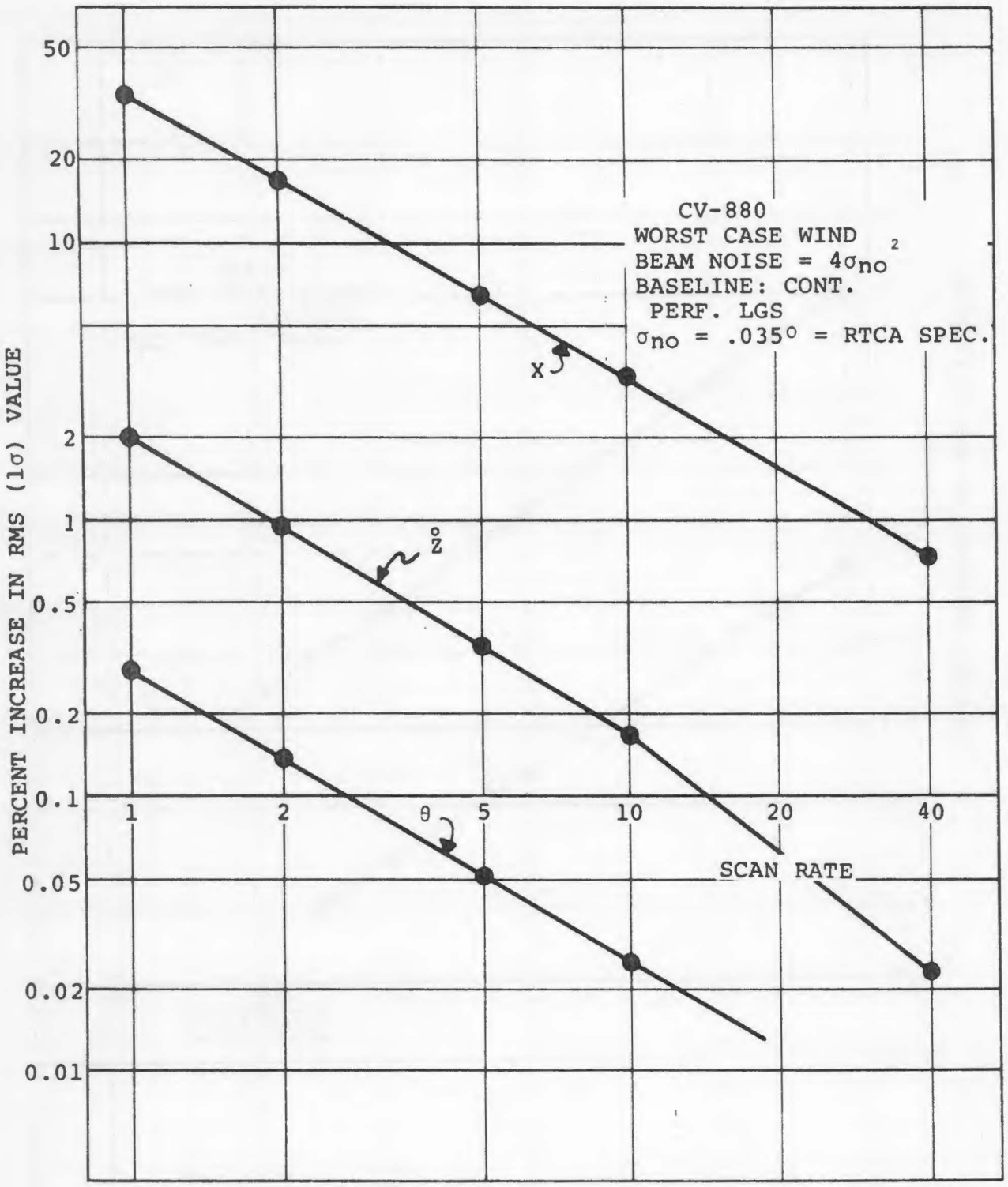

Figure 7-26. Relative Effects of Scan Rate on Longitudinal Touchdown Variables - Worst Case Wind & Beam Noise

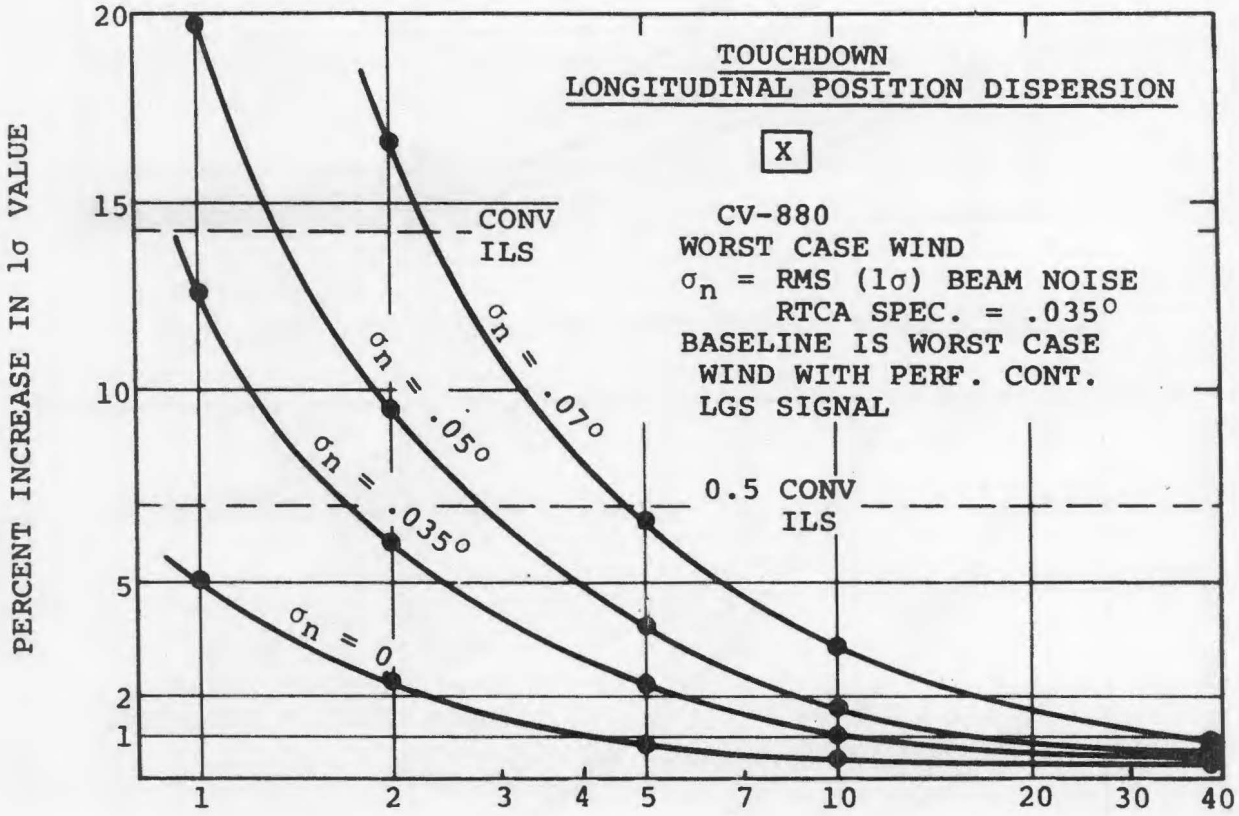

Figure 7-27(a). Longitudinal Position Dispersion Vs. Scan Rate

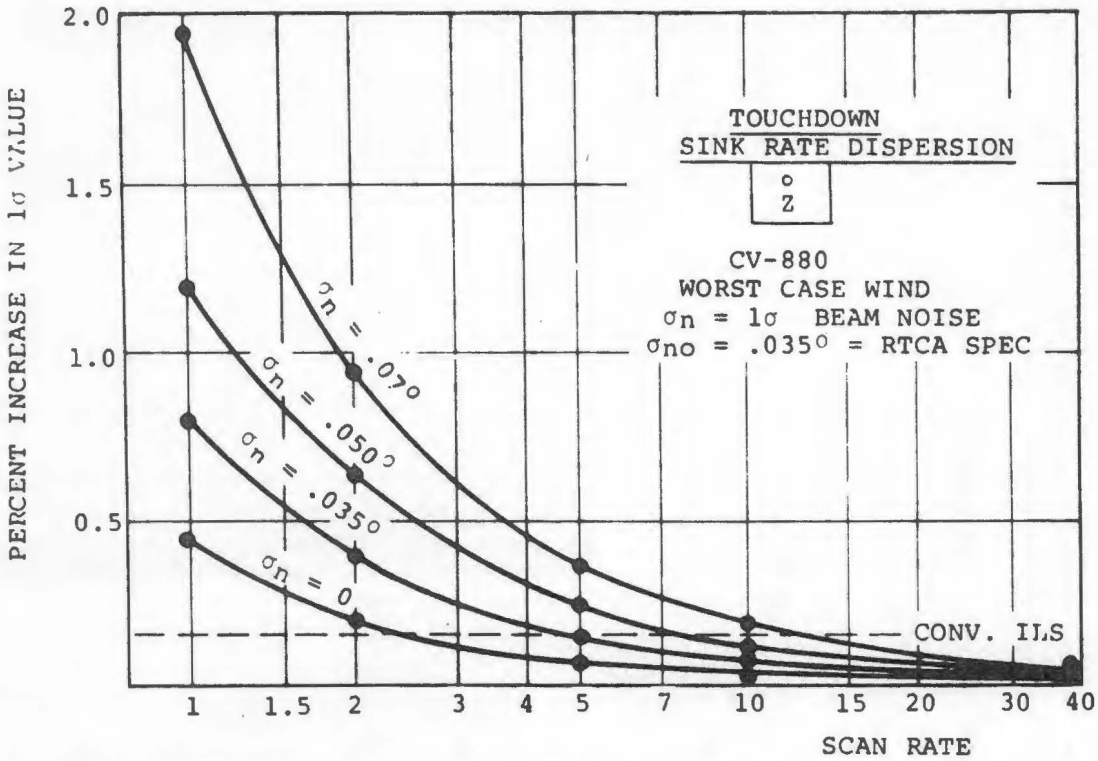

Figure 7-27(b). Sink Rate Dispersion Vs. Scan Rate

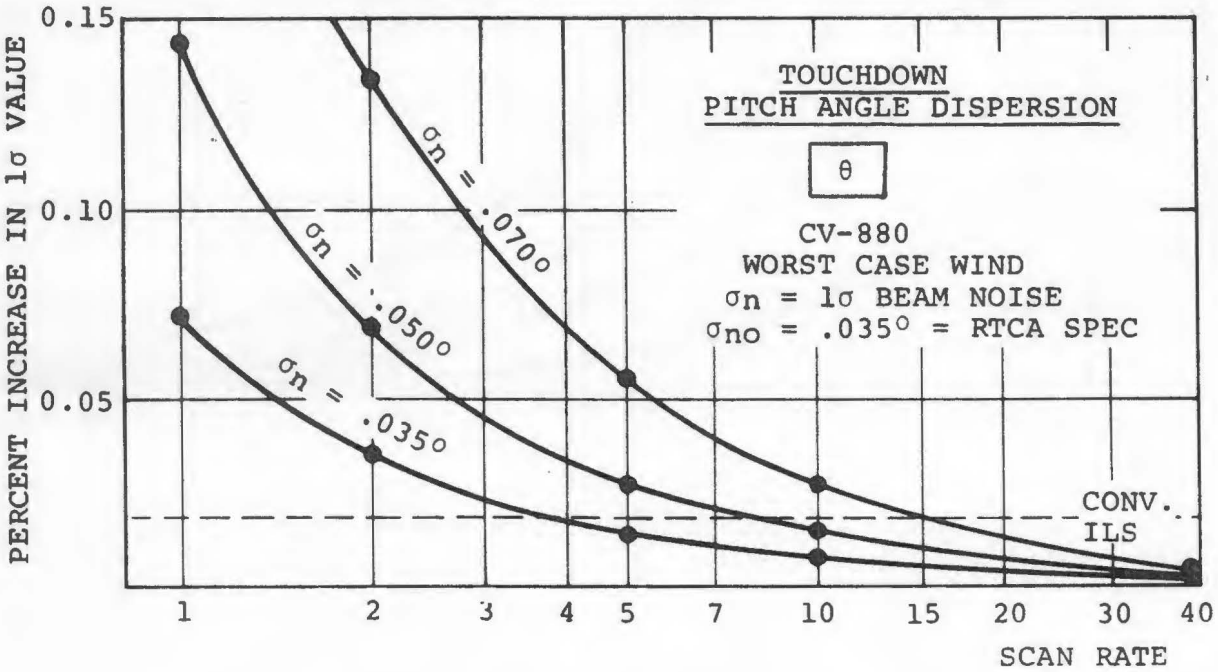

Figure 7-27(c). Pitch Angle Dispersion Vs. Scan Rate

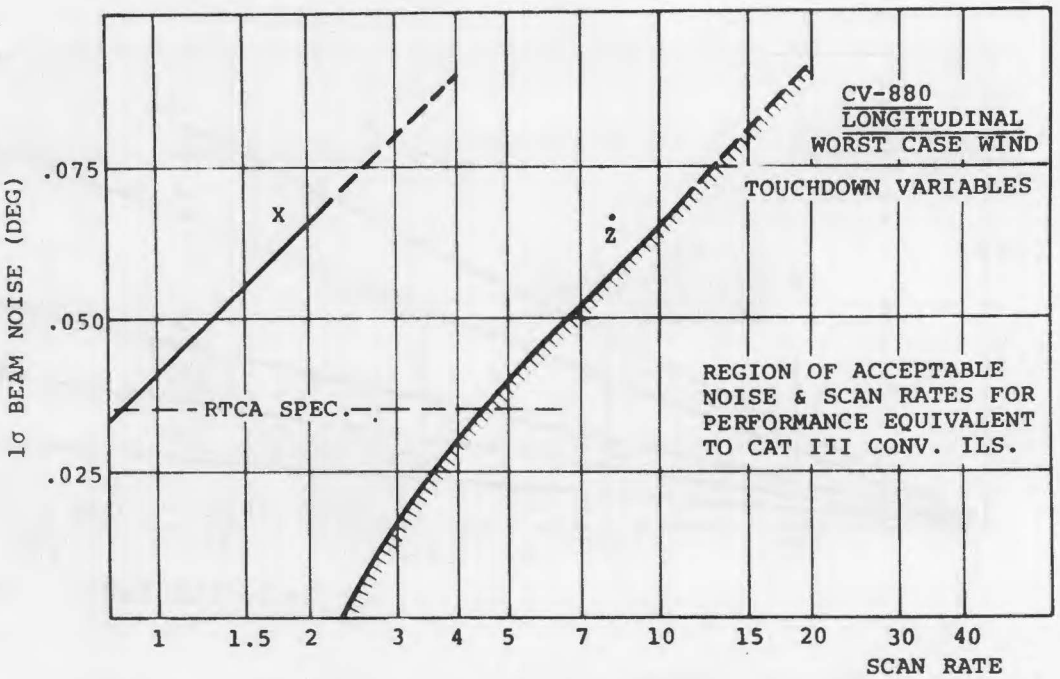

Figure 7-28(a). Scan Rate - Beam Noise Tradeoff For Performance Equivalent To Cat III Conv. ILS

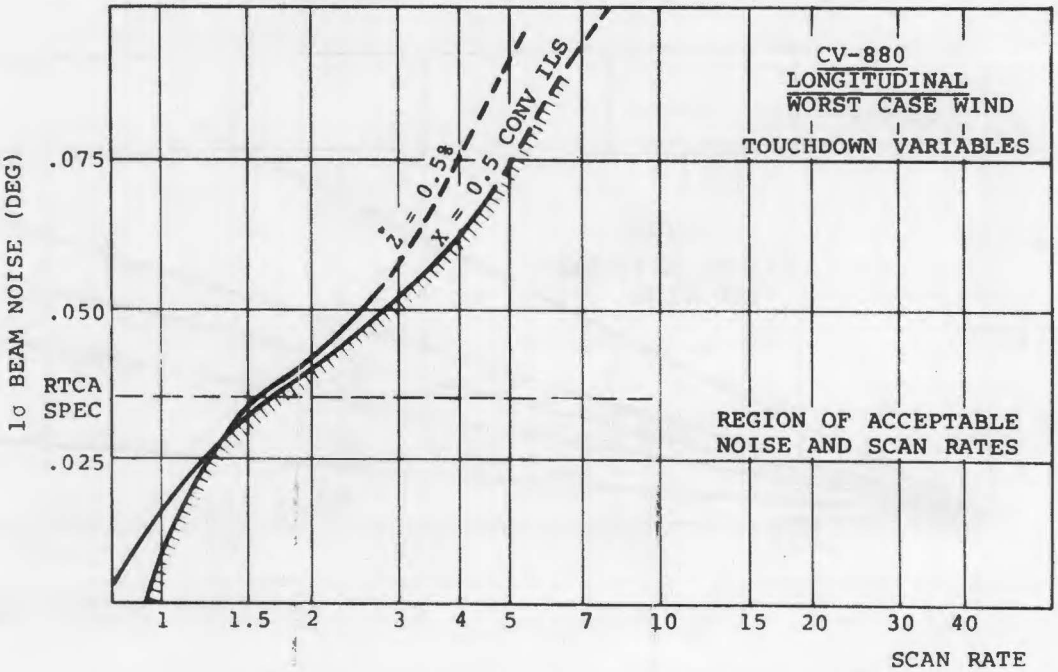

Figure 7-28(b). Scan Rate - Beam Noise Tradeoff For Long Pos. Dispersion Increase Half That With Conv. ILS and Sink Rate Disp. Increase 0.5%

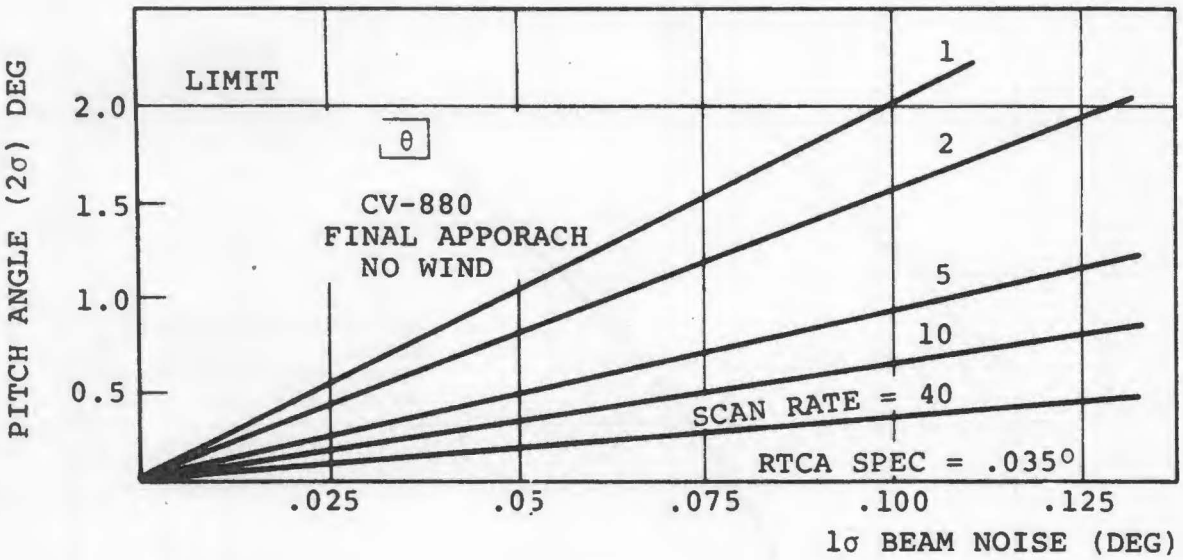

Figure 7-29. 2σ Pitch Angular Activity Vs. Beam Noise
Final Approach - No Wind

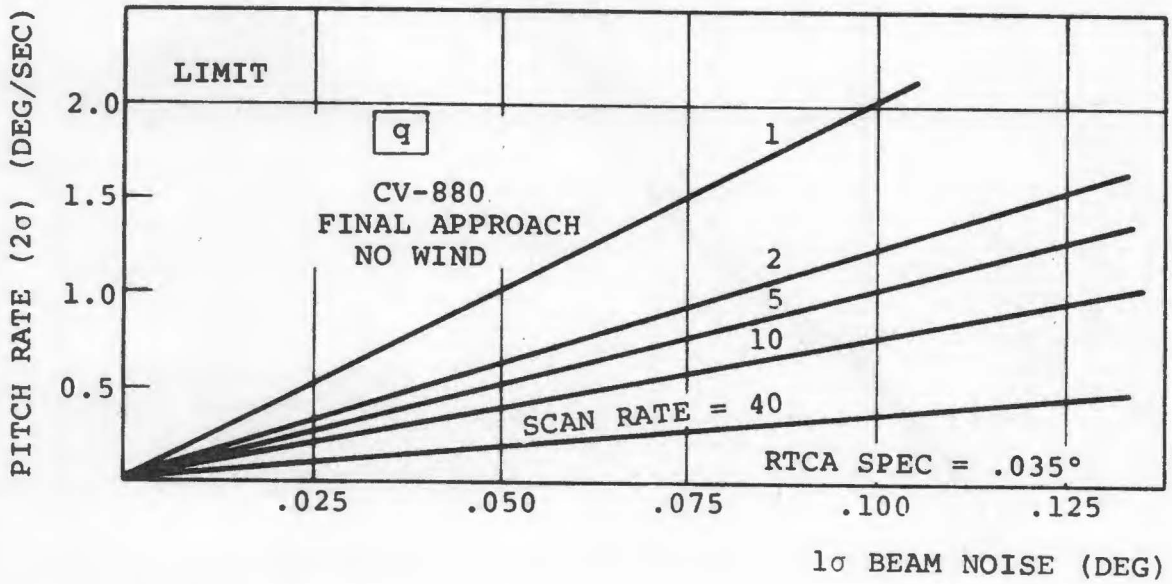

Figure 7-30. 2σ Pitch Rate Activity Vs. Beam Noise
Final Approach - No Wind

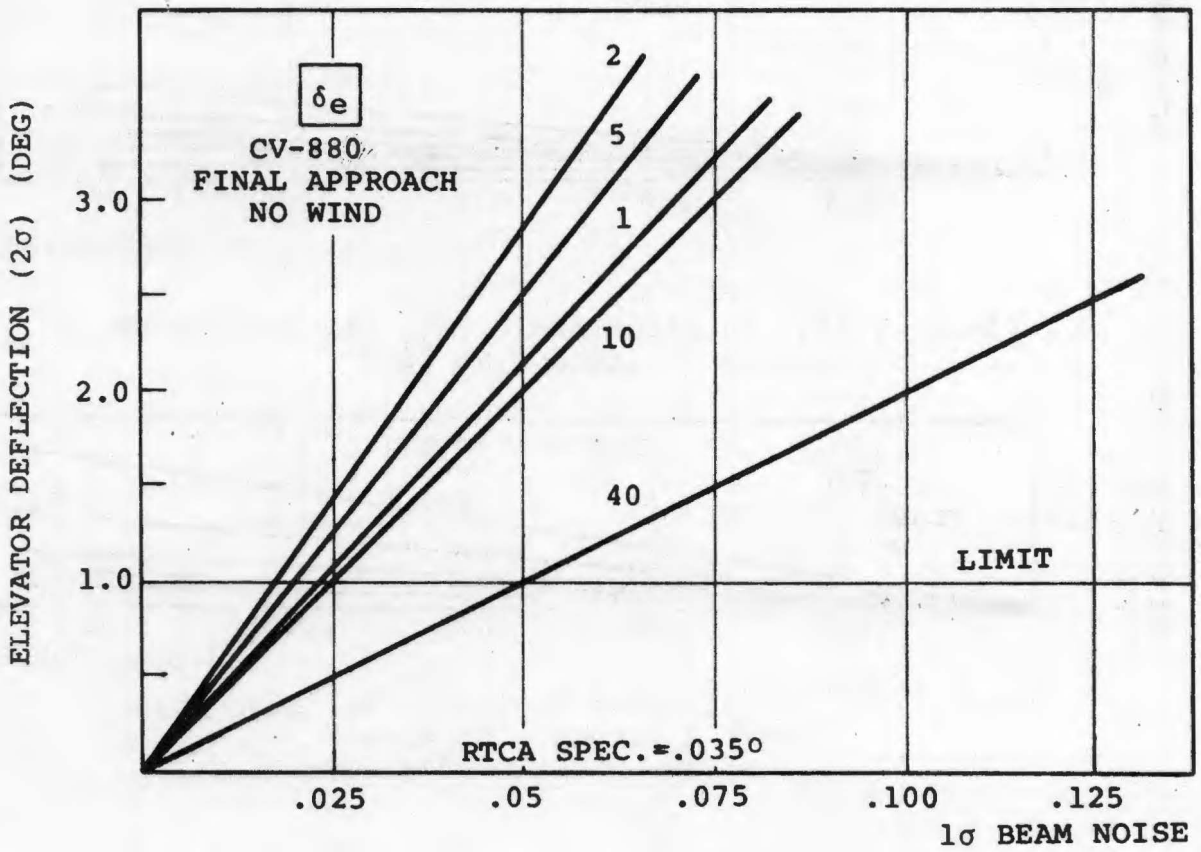

Figure 7-31. 2σ Elevator Activity (δ_a) Vs. Beam Noise
Final Approach - No Wind

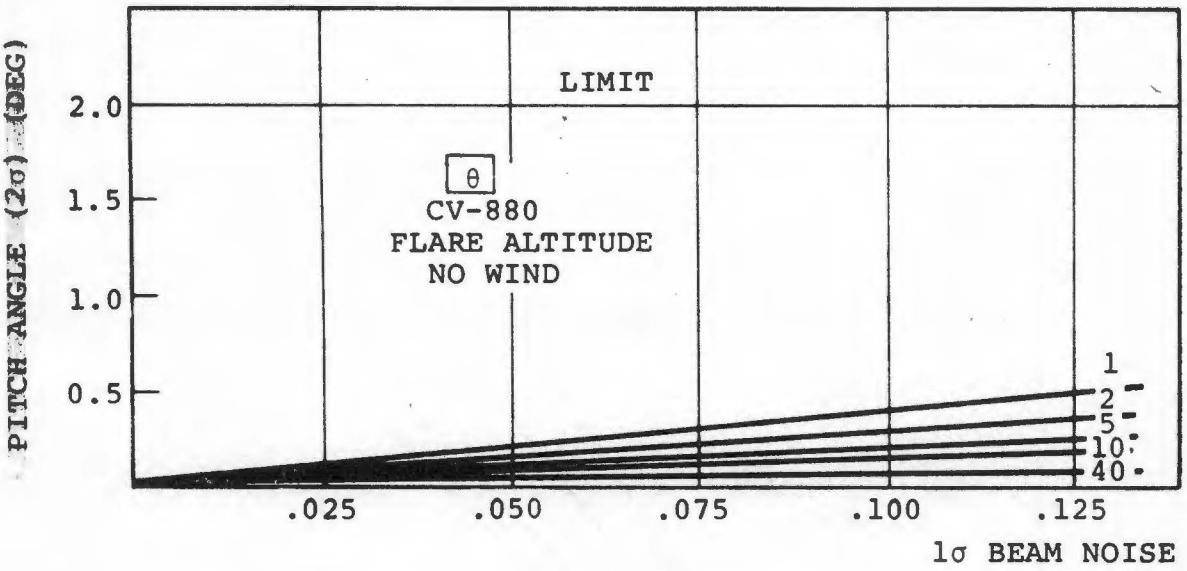

Figure 7-32. 2σ Pitch Angle Dev. Vs. Beam Noise
Flare Altitude - No Wind

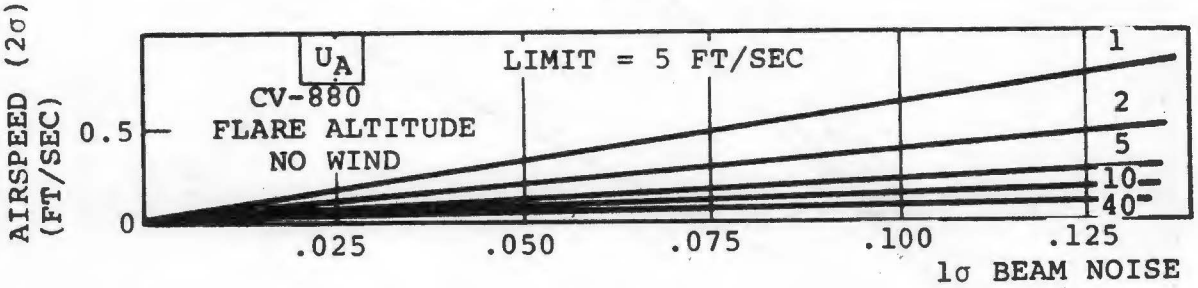

Figure 7-33. 2σ Airspeed Deviation Vs. Beam Noise
Flare Altitude - No Wind

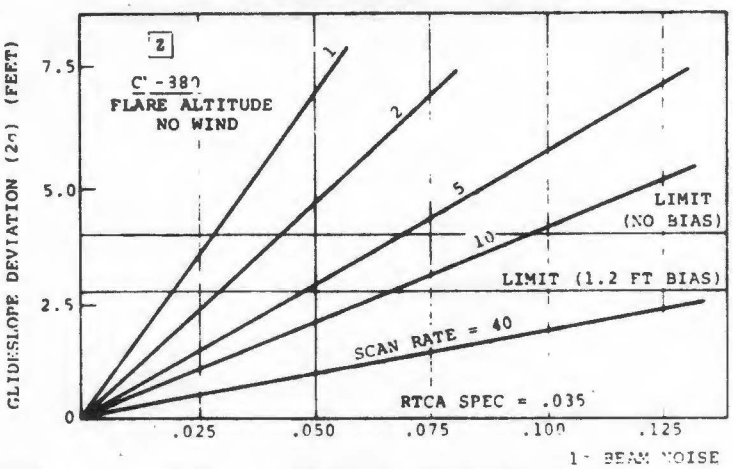

Figure 7-34. 2σ Glideslope Deviation (Z) Vs. Beam Noise
Flare Altitude - No Wind

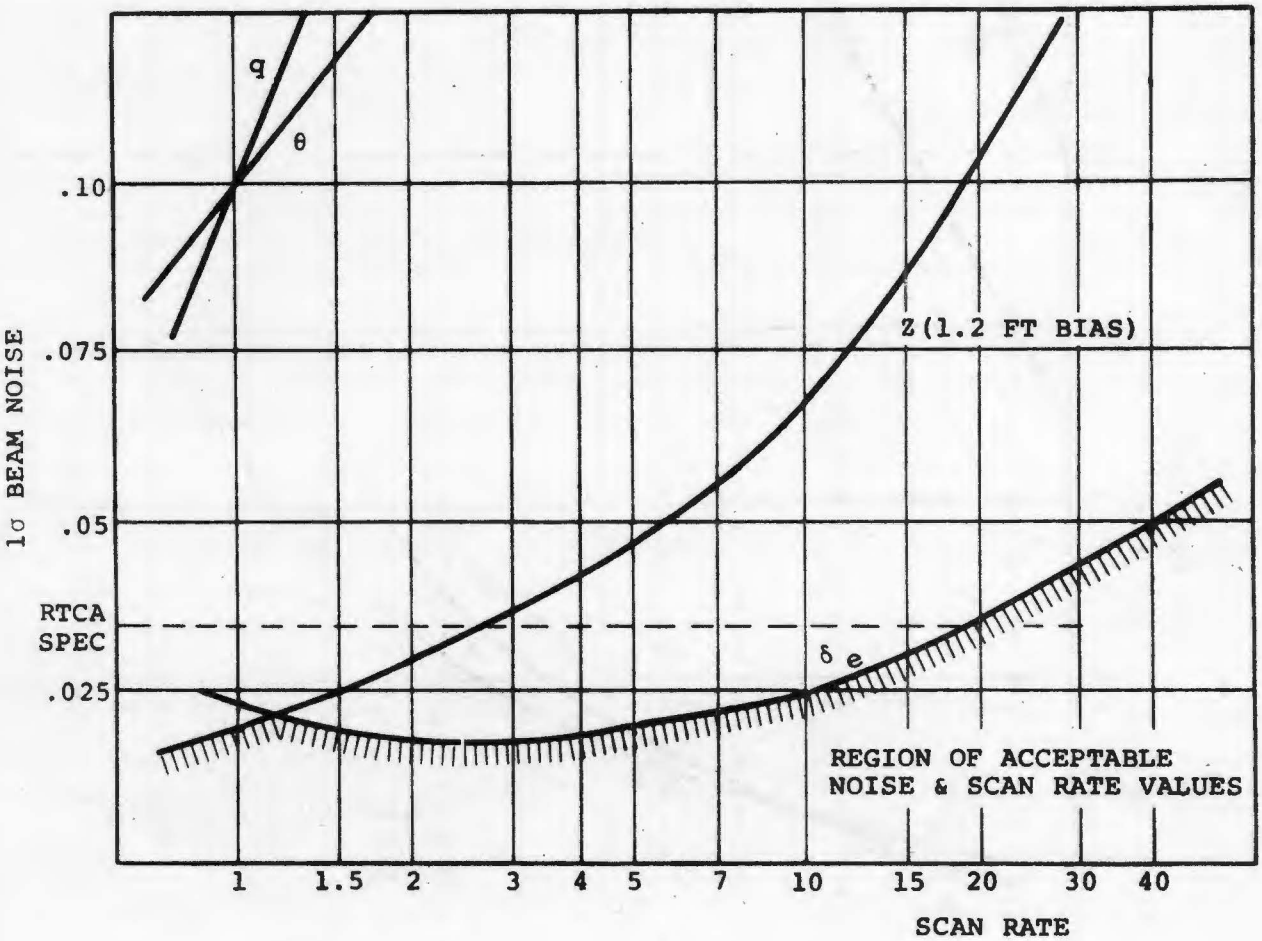

Figure 7-35(a). Beam Noise - Scan Rate Tradeoff
Pilot Acceptability Factors
CV-880 Longitudinal System
(Coupler Filter Time Constant: 0.025 Sec.)

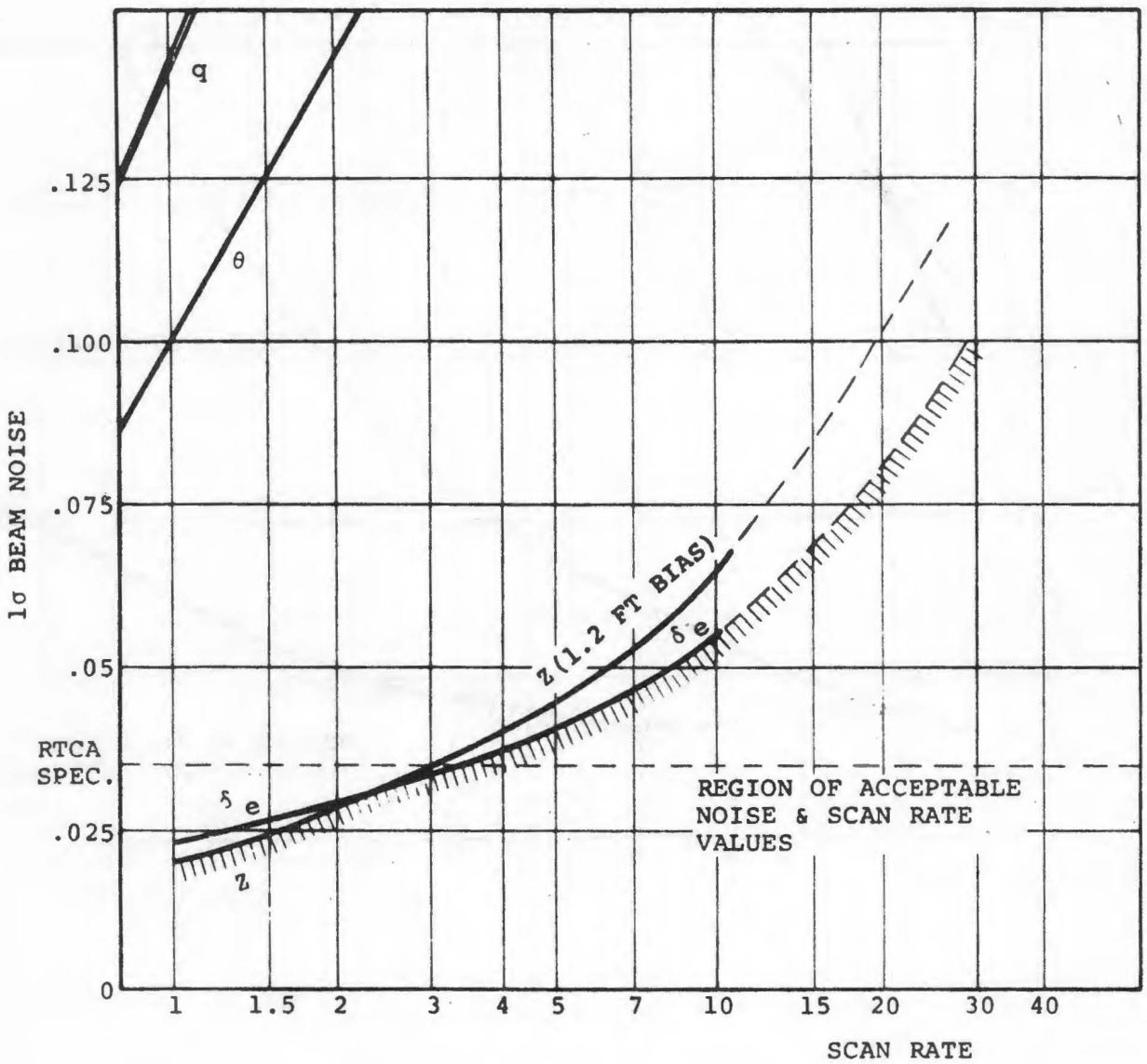

Figure 7-35(b). Beam Noise - Scan Rate Tradeoff
Pilot Acceptability Factors
CV-880 Longitudinal System
(Coupler Filter Time Constant: 0.5 Sec.)

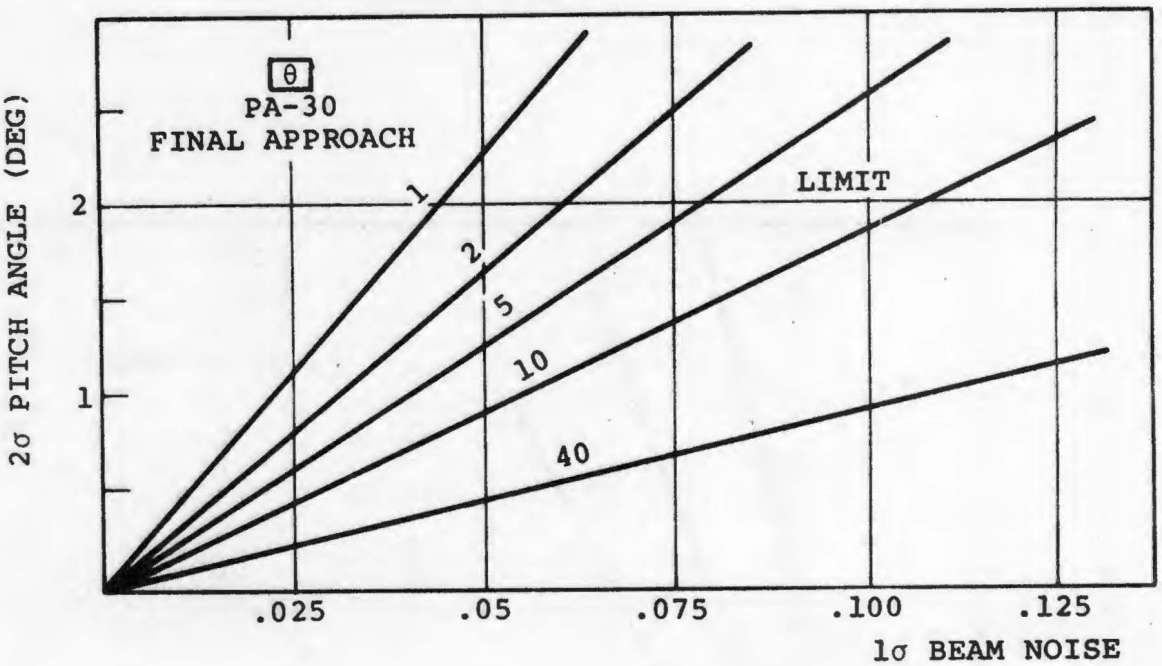

Figure 7-36. 2σ Pitch Angular Activity Vs. Beam Noise

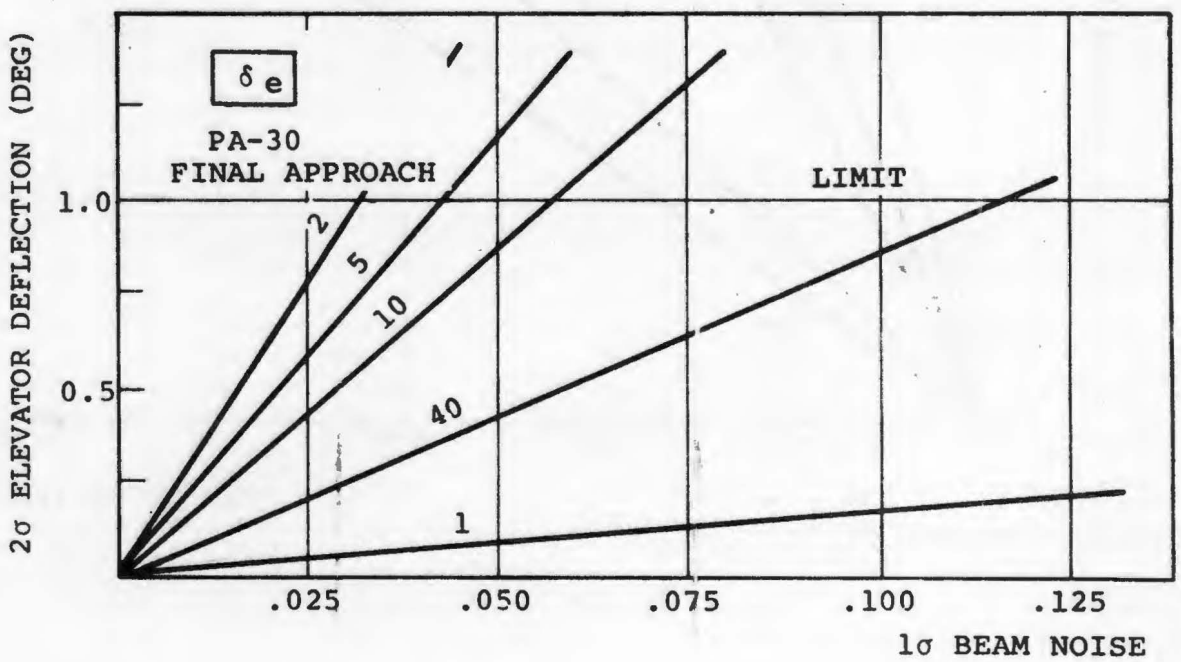

Figure 7-37. 2σ Elevator Activity Vs. Beam Noise

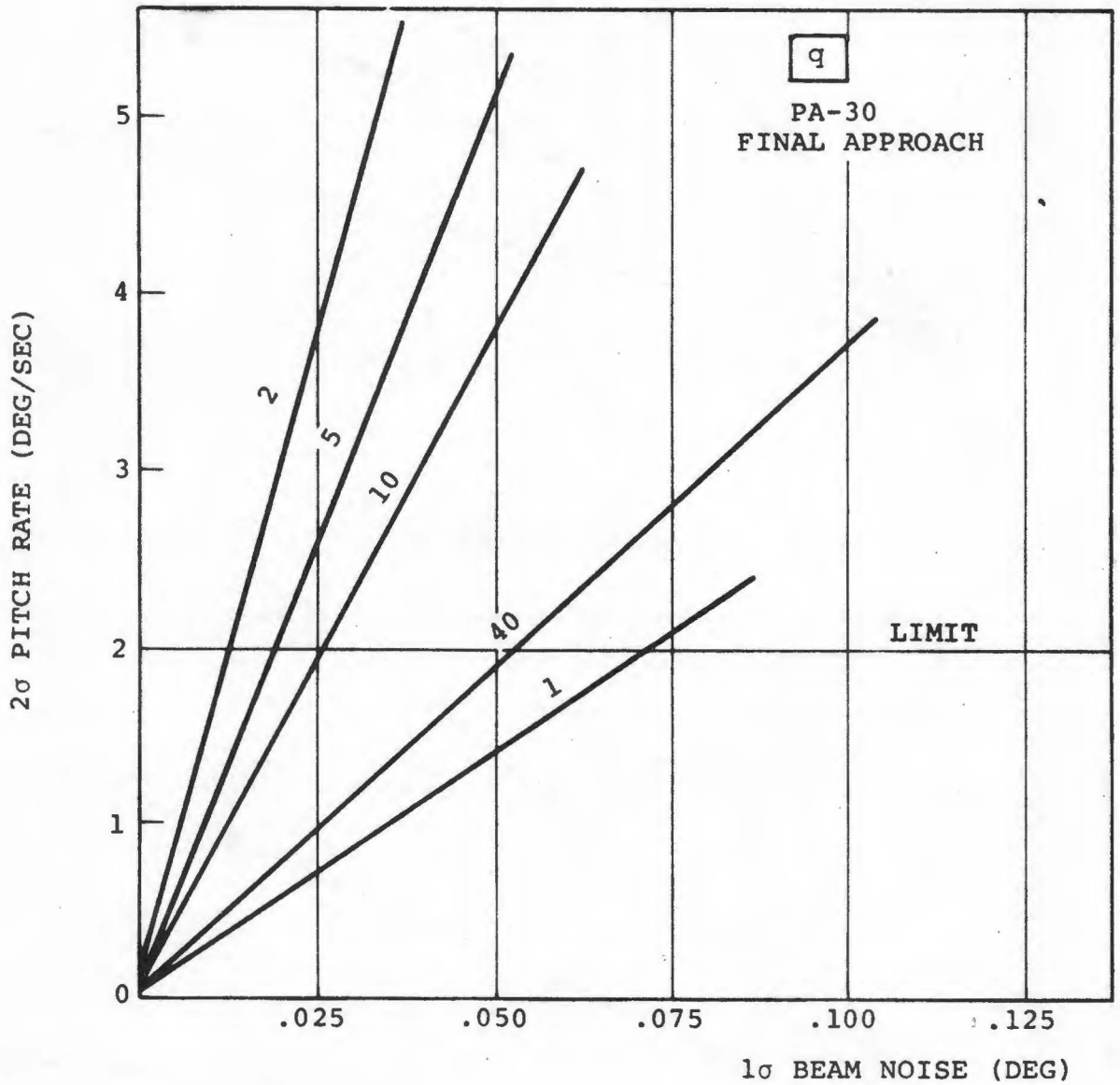

Figure 7-38. 2σ Pitch Rate Activity Vs. Beam Noise

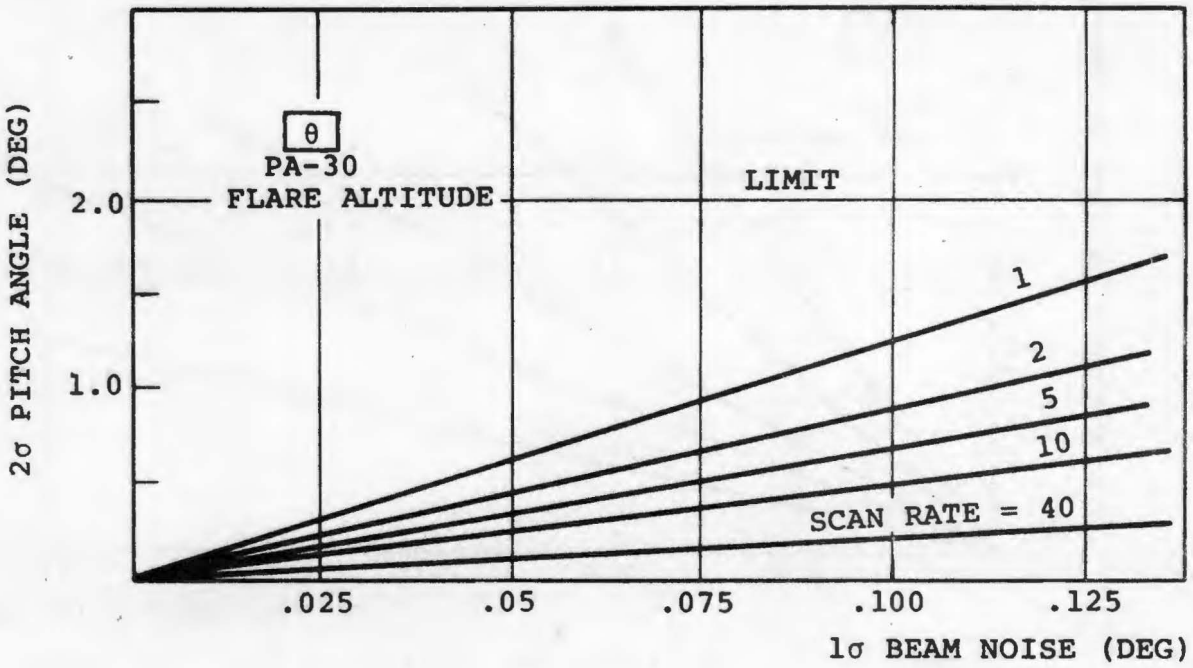

Figure 7-39. 2σ Pitch Angle Deviation Vs. Beam Noise

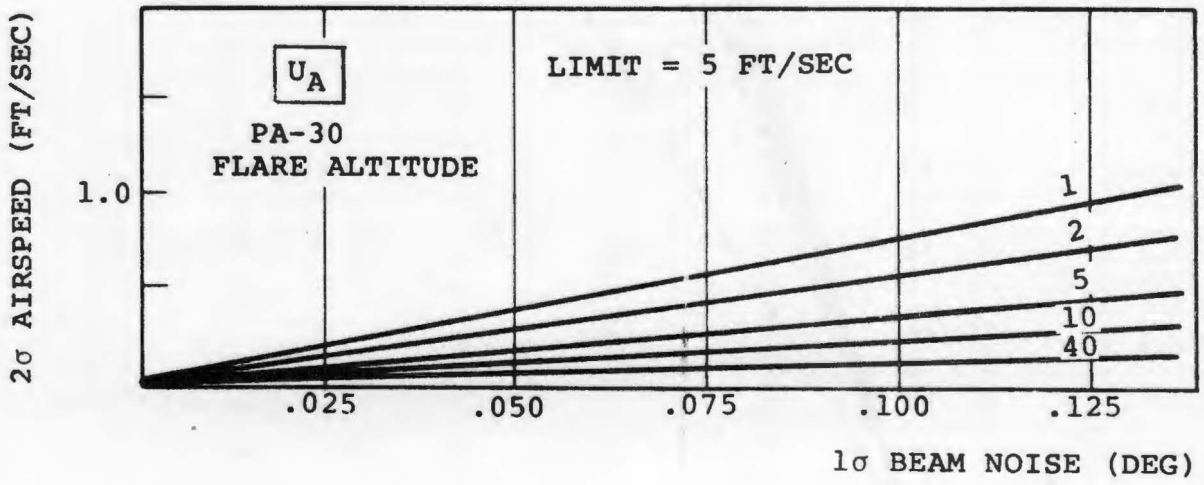

Figure 7-40. 2σ Airspeed Deviation Vs. Beam Noise

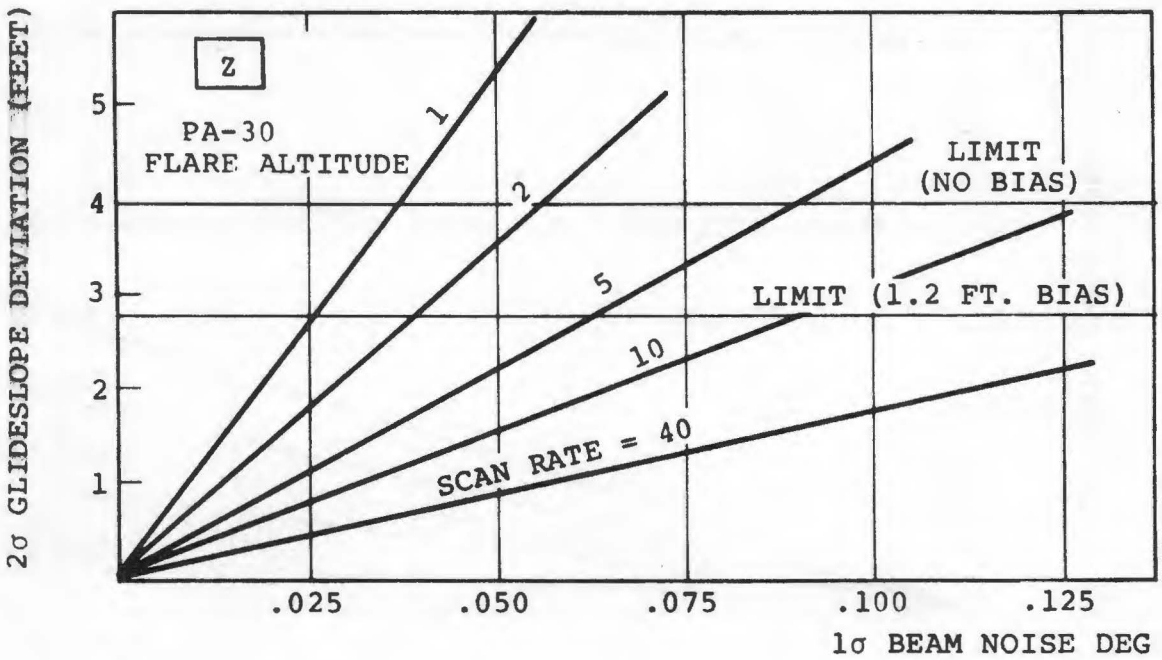

Figure 7-41. 2σ Glideslope Deviation Vs. Beam Noise

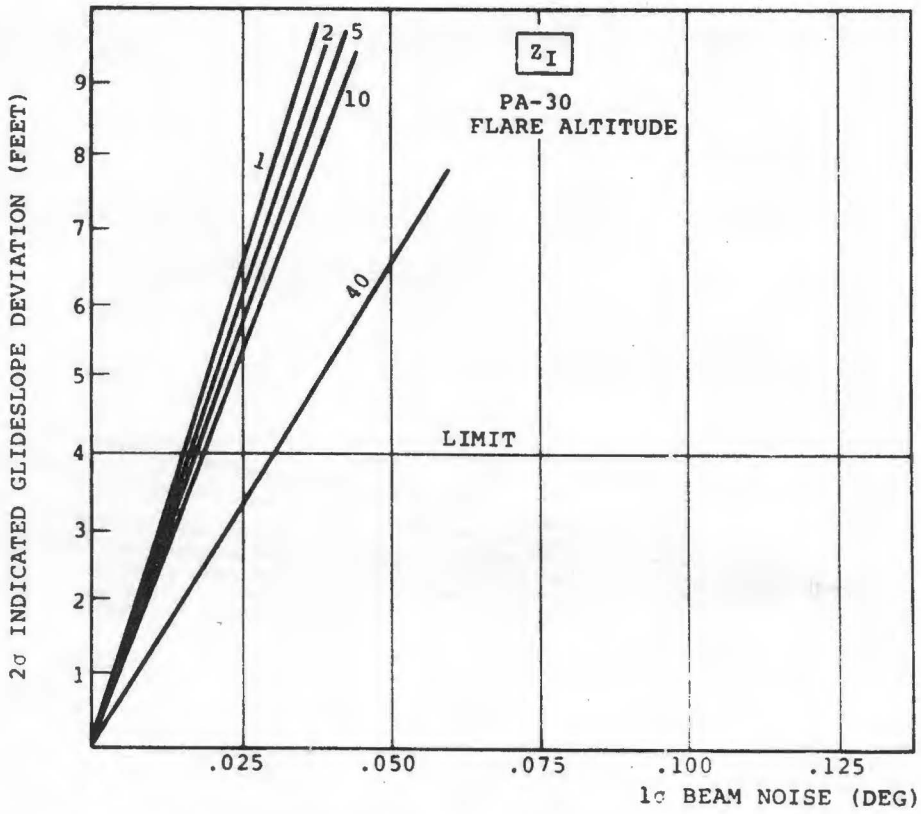

Figure 7-42. 2σ Indicated Glideslope Deviation Vs. Beam Noise

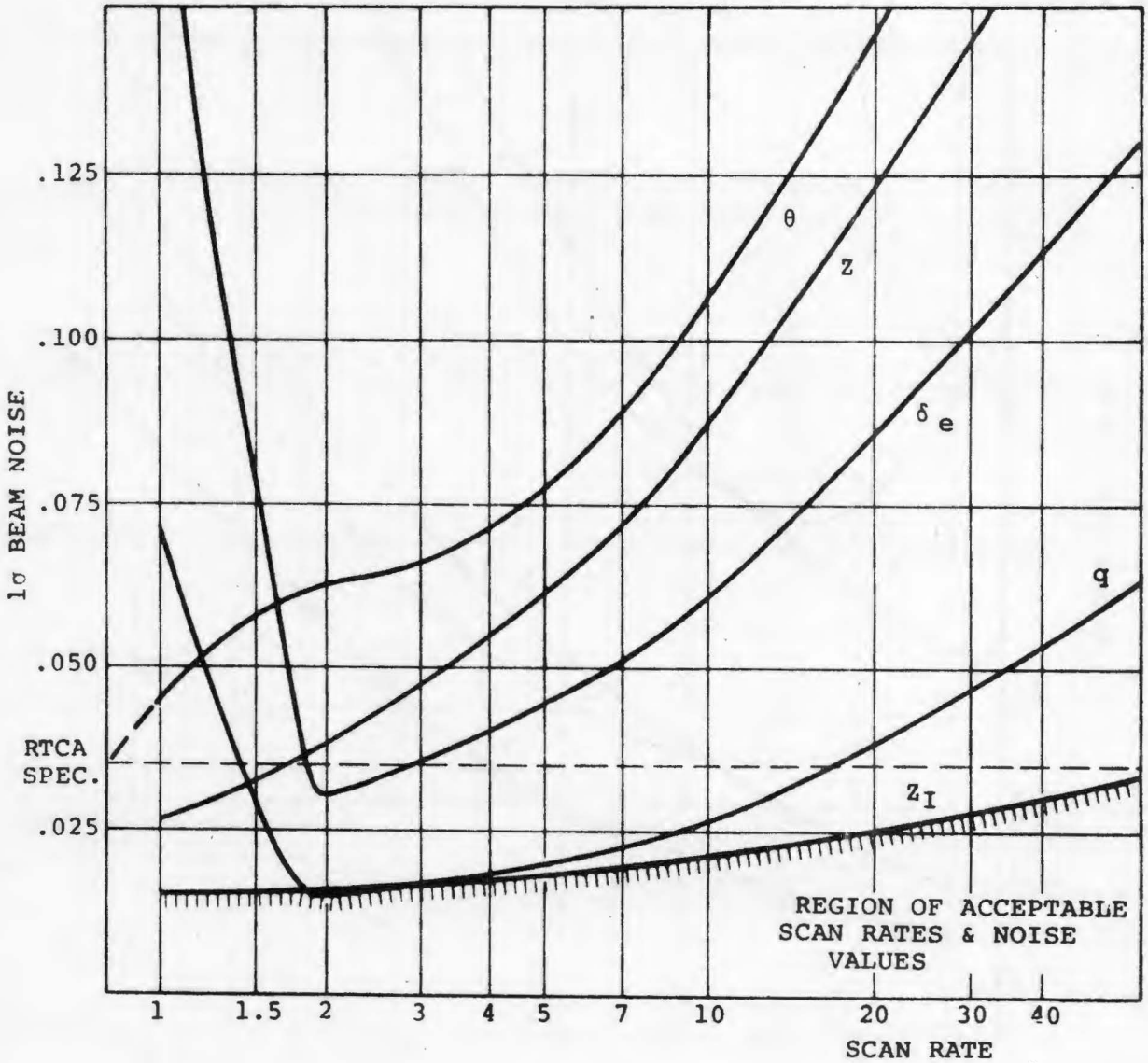

Figure 7-43(a). Beam Noise - Scan Rate Tradeoff
Pilot Acceptability Factors
PA-30 Longitudinal System
(Coupler Time Constant: 0.025 Sec.)

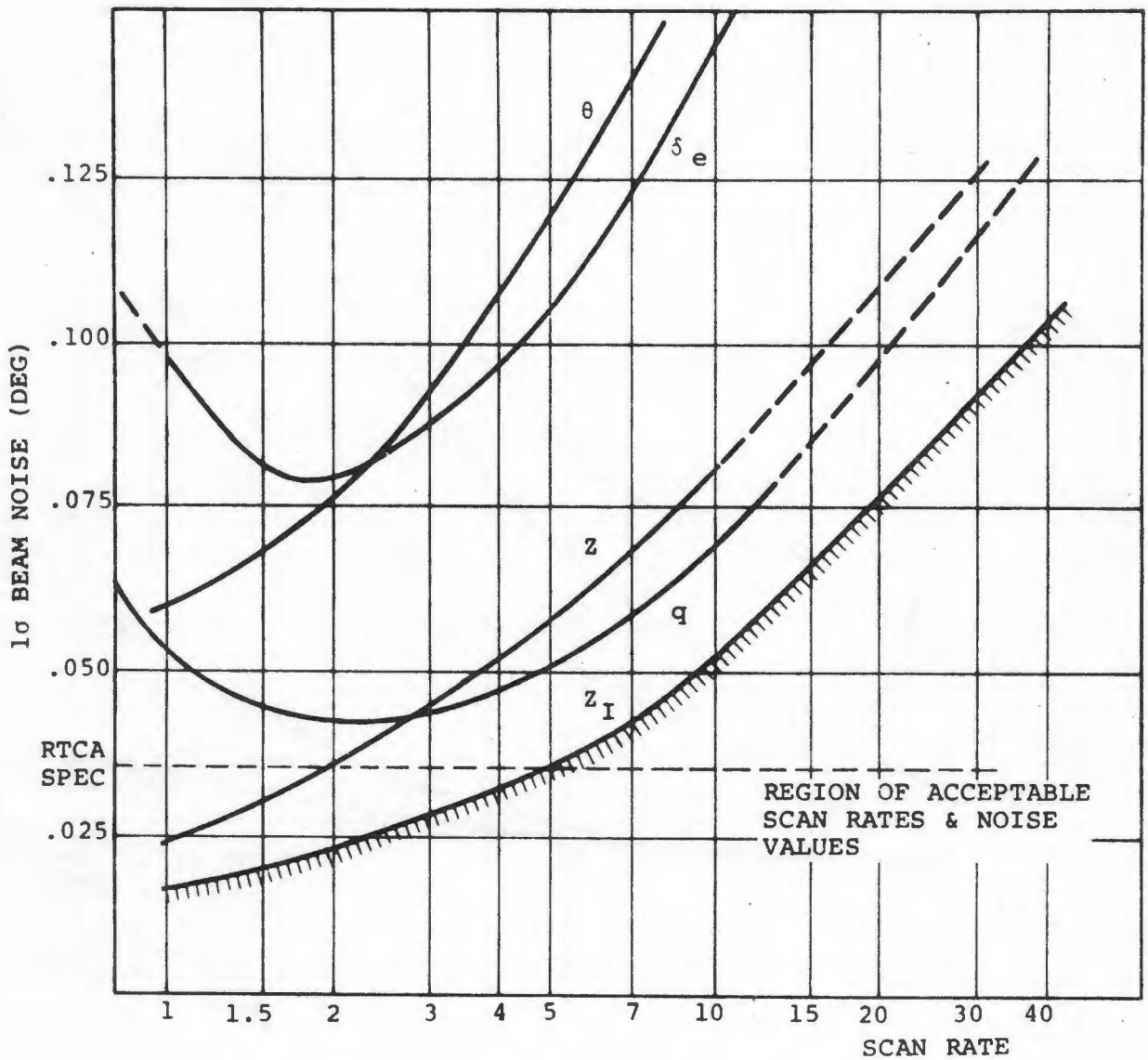

Figure 7-43(b). Beam Noise - Scan Rate Tradeoff
Pilot Acceptability Factors
PA-30 Longitudinal System
(Coupler Filter Time Constant: 0.5 Sec.)

8. CONCLUSIONS

8.1 GENERAL CONCLUSIONS

Figures 8-1 and 8-2 show in composite form the various important constraint curves for beam noise and scan rate for the azimuth and Elevation #1 signals, respectively.

From these figures and the data of Section 7, the following general conclusions can be drawn:

(1) Safety factors tend to set the absolute minimum scan rate requirement and are relatively insensitive to beam noise. The critical position variables at touchdown are at least an order of magnitude more sensitive to scan rate than are velocity or altitude variables.
(2) Pilot acceptability factors are slightly more sensitive to beam noise than scan rate and tend to limit maximum beam noise for scan rates above the absolute minimum. No particular generalization can be made concerning which acceptability factors are more critical than others.
(3) Processing-filtering techniques are extremely significant in determining constraints imposed by pilot acceptability factors.

8.2 CONCLUSIONS FOR THE AZIMUTH SIGNAL

Figure 8-1 shows that scan rates as low as two per second will provide satisfactory performance with the recommended value of beam noise. At the RTCA recommended scan rate of five per second, about twice the beam noise is tolerable.

It is therefore concluded that the range of acceptable beam noise and scan rates for both the PA-30 and CV-880 is sufficient to allow significant latitude in choosing azimuth signal parameters and performance of these aircraft should not seriously constrain the choice of these parameters.

8.3 CONCLUSIONS FOR THE ELEVATION #1 SIGNAL

It is apparent from Figure 8-2 that pilot acceptability factors significantly limit the range of acceptable scan rates and beam noise for the Elevation #1. At the recommended beam noise value, five scans per second (the RTCA recommended scan rate) is barely adequate to meet most of the constraints.

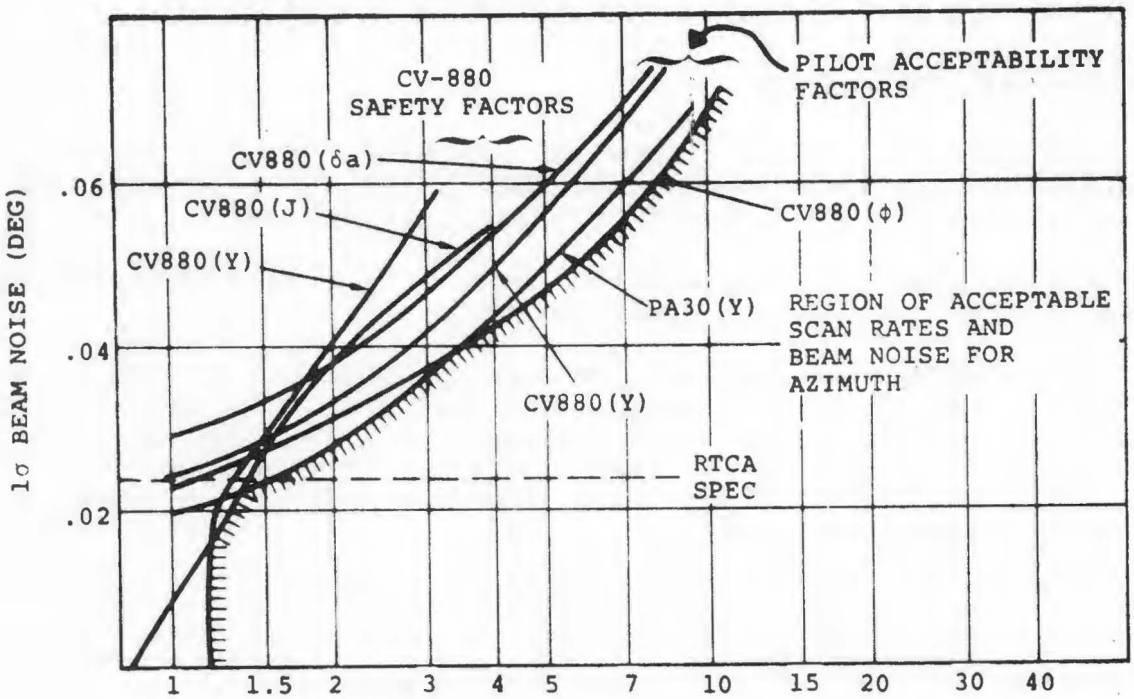

Figure 8-1. Scan Rate Beam Noise Tradeoff For Azimuth Signal

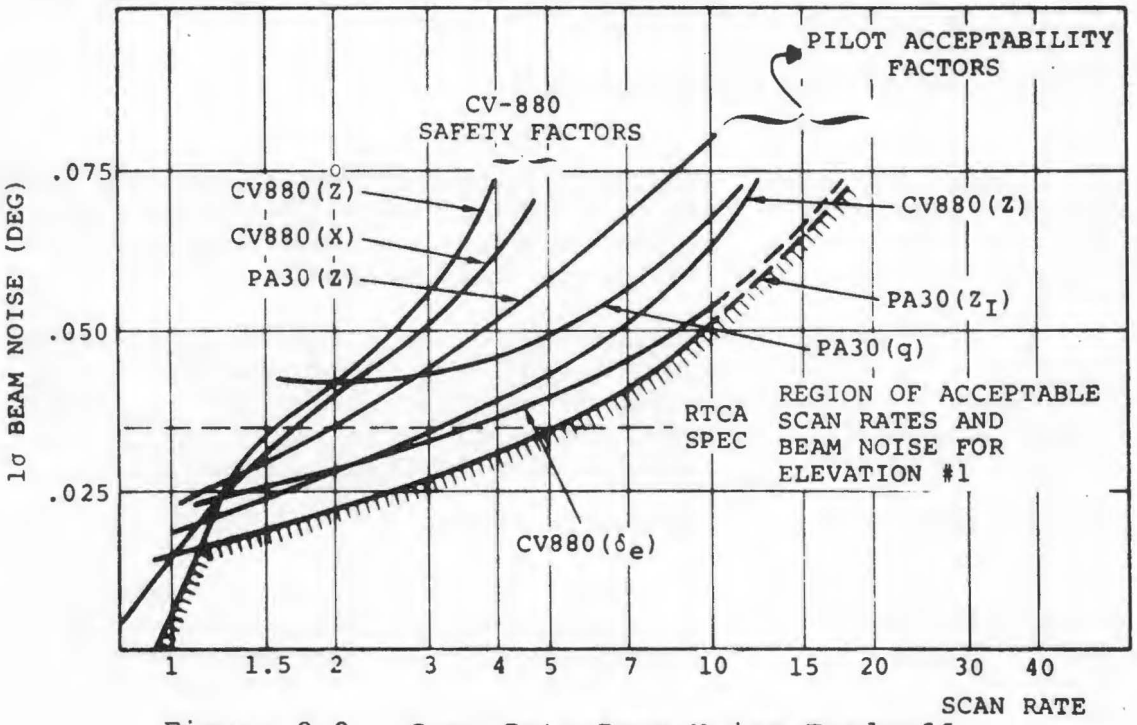

Figure 8-2. Scan Rate-Beam Noise Tradeoff For Elevation #1 Signal

It is therefore concluded that pilot acceptability factors for these aircraft may impose an eventual limitation on allowable beam noise and scan rates for elevation #1.

9. SUMMARY OF LIMITATIONS

9.1 GENERAL

Many of the limitations of this study are by now apparent; in the following sections the more important of these are summarized, including comments on further work required and possible effects on results.

9.2 COVARIANCE PROPAGATION METHOD

The covariance progagation method as now mechanized does not provide rigorously valid statistical results near touchdown. Two basic areas require significant work to eliminate this problem: (1) A linearization of the ground effect phenomenon so that results will more closely reflect very low altitude performance, and (2) A reformulation of the equations to include time dispersion and the effects of time dispersion implicitly. This may require some form of hybrid solution, i.e. a simultaneous integrated program including the full simulation and the linearized equations.

9.3 WIND MODELS

There is some evidence that turbulence does not produce the same magnitude of effects in real life as are indicated by simulation results. It is felt this may be due to the method of introducing turbulence noise into the simulation which is generally done ignoring high frequency effects and lags introduced by the airframe. Work is proceeding to include second order high frequency airframe effects to investigate their overall contribution to performance in turbulence.

9.4 LGS MODEL

As mentioned in Section 4, many possible significant error sources have not been considered in formulating the LGS scanning beam model. Perhaps the most important of these is the every-other-scan cyclic error which would result from a dual antenna configuration.

The filtering problem has been found to be extremely significant in defining beam noise and scan rate requirements. It should be possible to develope some general approach to simple filtering of the scanned signal, based on signal, beam noise, and sampling noise characteristics which will provide some better measure of protection against

the effects of noise than the first order filters used for this study. Work in this area is proceeding.

9.5 AIRCRAFT MODELS AND TOUCHDOWN CRITERIA

The portion of the approach and landing trajectory not considered to date is the rollout phase from the instant of touchdown. Touchdown criteria for safety may depend heavily on the dynamic and aerodynamic properties of the aircraft and autopilot during rollout, which are not as yet defined in terms of the simulation. In addition, the requirement for rollout guidance may affect azimuth and DME parameters.

Work is underway to model undercarriage and airframe dynamics in a form suitable for simulation.

9.6 PILOT ACCEPTABILITY CRITERIA

The results of Section 7 and Section 8 for pilot acceptability are based on definite but rather loosely defined criteria for acceptable performance in a zero wind environment. A change in some of the stated limits may produce a significant change in acceptable beam noise and scan rates. It is doubtful, however, that an absolute set of such criteria can ever be defined and every effort has been made in this study to remain on the conservative side.

9.7 STATISTICAL PROCEDURE–PROBABILITY OF SAFE LANDING

Assuming that the covaraince propagation equation can be made to generate statistically valid results at touchdown, the problem remains of converting variance and covariance data into data on the probability of a safe landing. One would like this data to be in the form of an average or mean probability of safe landing over all wind conditions.

This is an extremely complex problem analytically and must take into account the following:

(1) For highly correlated variables a joint probability function must be defined (e.g. all lateral system critical variables).
(2) Probability must be computed over the entire range of allowable winds.
(3) A probability density function for gust intensity must be defined in order to average the conditional probability of item (2) over all landings.

It should be possible as a method of simplification to eliminate certain variables as non-critical based on the relative relationship of all limits to variance.

The problem of averaging over all wind conditions is unlikely to be solved analytically for a general case and can probably be done only be numerical integration for specific cases.

9.8 DECISION WINDOW AND MISSED APPROACH

Another dimension to the problem of safe landing not considered here is the definition of decision height and decision variables which would lead to a missed approach under adverse conditions, thereby significantly affecting the probability of a safe landing.

It would be highly desirable to define decision variables and limits based on safe landing limits and the correlation between them. This is a largely impossible task to accomplish with any rigorous validity. The following comments apply however:

(1) The only variables which are likely to be significantly correlated from decision height to touchdown are those of position. A knowledge of position deviation at decision height can therefore serve as a direct indication of successful landing probability.
(2) Higher frequency variables (attitude, attitude rates, airspeed) at decision height are related to safe landing primarily indirectly, in that they serve as a measure of turbulence intensity and as such can be used to decide when turbulence levels have exceeded recommended or expected values.

9.9 SIGNAL REQUIREMENTS FOR TERMINAL AREA GUIDANCE

In addition to the problem of LGS signal requirements for safe and acceptable landings, signal requirements for coordination with other terminal area navigation aids, with terminal area air traffic control, and with desirable approach trajectories and flight interleaving must be considered.

Certain obvious tasks with respect to the above include:

(1) Signal requirements for curved approach and development of feed forward guidance techniques.
(2) Definition of minimum final trajectory acquisition points for various types of aircraft as a func-

tion of LGS parameters.

(3) Definition of dispersion in time to reach certain points in the trajectory, critical to close interleaving of flights, as a function of LGS parameters.

9.10 THE USE OF DME AND ELEVATION #2 INFORMATION

This report has not addressed the problem of DME and Elevation #2 signal requirements and uses due to the fact that this information is not used during approach by conventionally equipped aircraft.

DME will of course be required for curved approach guidance and can be used for precise gain scheduling during approach, for flare in combination with Elevation #2 information and for rollout guidance in combination with the azimuth function.

9.11 LGS SIGNAL REQUIREMENTS FOR ADVANCED AUTOPILOTS

Autopilot design will tend to take maximum advantage of whatever capabilities exist in the LGS. However, these are probably very definite tradeoffs which can be made between autopilot complexity and LGS integrity.

Work is currently underway to condition a previously designed advanced autopilot for the CV-880 to use scanning beam information. Such an autopilot must use derived beam rate data and may therefore impose more severe requirements on both scan rate and beam noise.

Appendix A

Notes on Digital Simulation and Covariance Propagation Methods and Mechanization

by Paul A. Madden and Mukund Desai

A.1.0 Introduction

A brief description of the MIT/DL digital simulation used to simulate automatic flight of the CV 880 and PA-30 in the approach and landing flight phases is contained in the following sections. A simplified block diagram of the digital simulation appears as Fig. (A-1).

A.1.1 Digital Simulation of an Automatic Landing System

The CV 880 and PA-30 aircraft and control systems were validated by digital computer simulation. Aerodynamic and LGS signal noise are simultaneously digitally simulated and input to the vehicle and control system equations.

The system of differential equations describing the vehicle, autopilot and automatic landing system were written in the form

$$\dot{x} = f(x, m, n) \tag{A-1}$$

where

- x is a vector describing the system and is not necessarily a state vector
- $\dot{x}$ is a vector of derivatives
- m is a set of control inputs
- n is a set of system and atmospheric noise inputs

The vectors x and $\dot{x}$ are subject to magnitude limits of the form

$$|x| < L_x \tag{A-2}$$

$$|\dot{x}| < L_{\dot{x}} \tag{A-3}$$

and a boundary condition

$$x(0) = a \tag{A-4}$$

A solution of (A-2) may be obtained by direct integration from the boundary value (A-4).

To generate the aerodynamic and system noise, a digital equivalent of random gaussian noise must be supplied to either differential or difference equations representing the noise spectra filters. In the current CV880 simulation difference equations are employed since this is an efficient means of computation. The resultant solution is numerically stable independent of the sampling interval, however, the output of the system will be realistic only if the sampling is done frequently enough to result in a stair-step waveform which is a good approximation to the original continuous input waveform.

The difference equations are written in the form

$$n(t + \Delta t) = \phi(t + \Delta t, t)\, n(t) + D(t + \Delta t, t)\,\omega(t) \tag{A-5}$$

where

- n is a vector of system and atmospheric noise sources
- ω is a vector of gaussian white noise inputs
- ϕ is the time-varying transition matrix associated with the spectral filters
- D is defined $\int_t^{t+\Delta t} \phi G\, dt$

A simplified block diagram of the simulation is shown in Fig. (A-1).

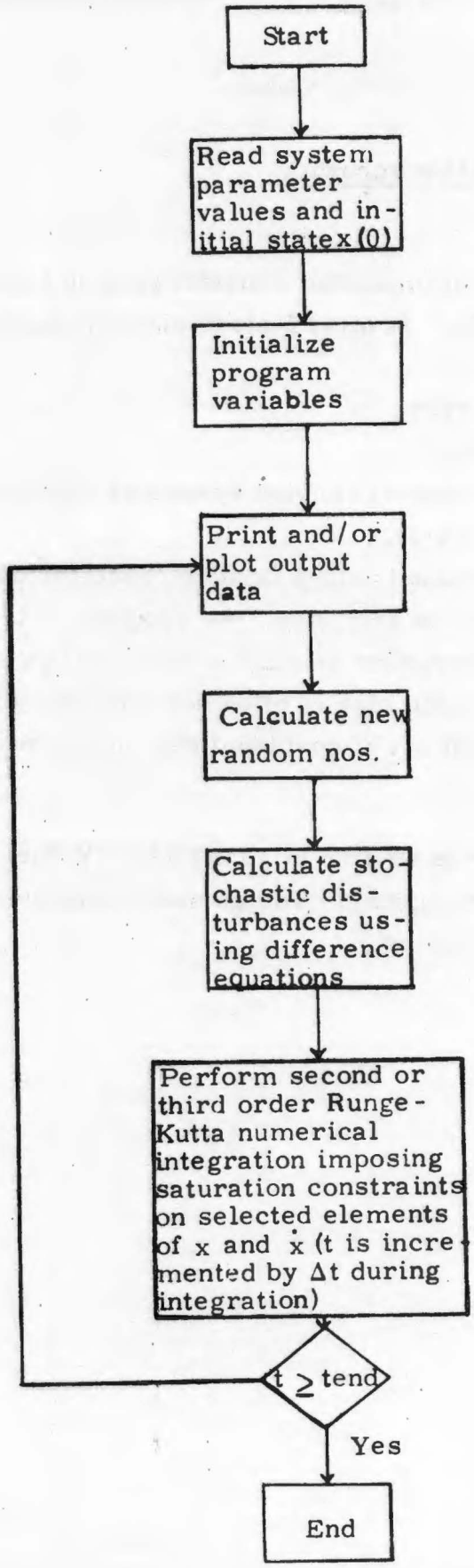

Figure A-1. Simplified block diagram of the digital simulation.

A.2.0 Factors affecting simulation accuracy

A.2.1 Integration step size

Integration step size is an important consideration in the construction of a digital simulation. Several factors play an important role in step size selection.

1. Solution accuracy
2. Integration law
3. Order of the largest coupled system of differential equations in (A-1).

Step size is normally reduced until a further reduction does not yield a significant improvement in accuracy. An integration law with improved convergence characteristics usually permits an increase in step size. An upper bound on step size is often determined by the order of the largest independent set of coupled differential equations.

A.3.0 Program and Computer

The simulation program is written in FORTRAN IV for ease of software development and debugging. The computations were performed using an XDS 9300 computer.

A. 4 Discrete Representation of a Flight Vehicle and its Control System

The following sections describe the development of a linear discrete model of flight path analysis for use in error or covariance propagation programs. A discrete model is required as a result of the sampled data character of the LGS information.

For the analysis of the statistics of the deviations of an aircraft from its nominal path in presence of noise, a state space approach (time domain) is to be favored over the frequency domain approach in view of the time discretization of the vehicle-control system can result in significant savings in computation time compared to numerical integration of the system differential equations.

A. 4. 1 Discrete Model for Flight Path Analysis

The deviations of an aircraft flight trajectory from its nominal approach path in a terminal area with microwave instrument landing guidance system (LGS) coverage subject to stochastic environmental disturbances and LGS measurement noise can be adequately represented by the following set of linear equations.

$$\frac{dx}{dt} = F_1 x + F_2^* x^* + G_1 u_1 + G_2^* u_2^* \qquad \text{(A-6)}$$

where x is an $n \times 1$ state vector; u_1 and u_2 are white guassian noise which include the effects of stochastic input components such as wind gusts and LGS measurement noise. The starred quantities represent the output of a sampler followed by a zero order hold filter as shown in the following figure.

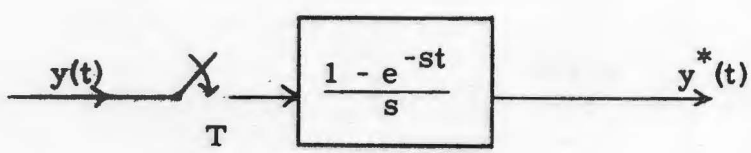

The statistics of the noise sources are

$$E[u_1(t)] = 0$$

$$E[u_1(t)u_1^T(\tau)] = Q_1(t)\delta(t-\tau) \qquad (\delta \text{ is a delta function})$$

$$E[u_2(t_i)] = 0$$

$$E[u_2(t_i)u_2^T(t_j)] = Q_2(t_i)\delta_{ij}$$

$$\delta_{ij} = 1 \text{ for } i = j$$

$$= 0 \text{ for } i \neq j$$

The system dynamics of (A-6) contains state and noise in continuous as well as discrete form, and consequently the format of the system dynamics as represented by (A-6) is unsuitable for analysis using linear system theory. This makes it necessary to develop a discrete state representation corresponding to the continuous state representation of equation (A-6). The next section outlines the development of a discrete model.

A.4.2 Development of Discrete Model

At $t_{i+1} = t_i + T$, we have

$$x_{i+1} = \Phi_1(t_{i+1}, t_i)x_i + \int_{t_i}^{t_{i+1}} \Phi_1(t_{i+1}, t)\,\{F_2x(t_i) + G_1u_1(t) + G_2u_2(t_i)\}\,dt$$

or $$x_{i+1} = \Phi(t_{i+1}, t_i)x_i + w(t_{i+1}, t_i) \qquad \text{(A-7)}$$

where T = sampling interval

$$\Phi(t_{i+1}, t_i) = \Phi_1(t_{i+1}, t_i) + \Phi_2(t_{i+1}, t_i)F_2 \qquad \text{(A-8)}$$

$\Phi(t, t_i)$ and $\Phi(t, t_i)$ and $\Phi_2(t, t_i)$ can be easily seen to obey

$$\frac{d\Phi_1}{dt} = F_1\Phi_1 \;;\quad \Phi_1(t_i, t_i) = I \qquad \text{(A-9)}$$

$$\frac{d\Phi_2}{dt} = F_1\Phi_2 + I \;;\quad \Phi_2(t_i, t_i) = 0 \qquad \text{(A-10)}$$

$$w(t_{i+1}, t_i) = w_1(t_{i+1}, t_i) + w_2(t_{i+1}, t_i) \tag{A-11}$$

$$w_1(t_{i+1}, t_i) = \int_{t_i}^{t_{i+1}} \Phi_1(t_{i+1}, t) G_1 u_1(t) dt \tag{A-12}$$

$$w_2(t_{i+1}, t_i) = \int_{t_i}^{t_{i+1}} \Phi_1(t_{i+1}, t) G_2 u_2(t_i) dt$$

$$= \Phi_2(t_{i+1}, t_i) G_2 u_2(t_i) \tag{A-13}$$

Equation (A-7) represents a linear discrete state system; and is an exact representation of (A-6), since no approximations have been made in the development of the discrete model.

A.4.3 Evaluation of Φ and Statistics of $w(t_{i+1}, t_i)$

Noise $w(t_{i+1}, t_i)$ may be viewed as a random sequence. It is easily seen that gaussian and white nature of the noise is preserved in $w(t_{i+1}, t_i)$. Also, it is apparent that $E[w(t_{i+1}, t_i)] = 0$. Let $W = E[w(t_{i+1}, t_i) w^T(t_{i+1}, t_i)]$ denote the covariance of w. W can be evaluated by evaluating its two components W_1 and W_2 separately, with

$$W_j = E[w_j(t_{i+1}, t_i) w_j^T(t_{i+1}, t_i)] \quad , \quad j = 1, 2$$

From (C.3.6), $w_1(t, t_i)$ is seen to obey

$$\frac{dw_1}{dt} = F_1 w_1 + G_1 u_1(t) \quad ; \quad w_1(t_i, t_i) = 0$$

Consequently, covariance $W_1(t, t_i)$ obeys

$$\frac{dW_1}{dt} = F_1 W_1 + W_1^T + G_1 Q_1 G_1^T \quad , \quad W_1(t_i, t_i) = 0 \tag{A-14}$$

Covariance $W_2(t_{i+1}, t_i)$ can be evaluated from the relation

$$W_2(t_{i+1}, t_i) = \Phi_3(t_{i+1}, t_i)G_2Q_2(t_i)G_2^T\Phi_3^T(t_{i+1}, t_i) \qquad \text{(A-15)}$$

The transition matrix Φ may be evaluated from (A-8) once Φ_1 and Φ_2 are evaluated from (A-9) and (A-10) or alternatively Φ may be evaluated by directly integrating the following equation

$$\frac{d\Phi}{dt}(t, t_i) = F_1(t)\Phi(t, t_i) + F_2(t_i) \quad ; \Phi(t_i, t_i) = I \qquad \text{(A-16)}$$

Transition matrix Φ, noise and its statistics has to be calculated at each sampling instant if (A-6) has time varying components. However, great simplification obtains if F_1 has time invariant elements and the only time varying components are those associated with starred (sampled) quantities.* In this case Φ_1 and Φ_3 need only be evaluated for one sampling interval, and Φ and the noise statistics can be evaluated from (A-8) and (A-9) at each sampling time.

A.4.4 Evaluation of Flight Path Statistics

Let $\bar{x} = E[x]$ and $X(t) = E[(x(t) - \bar{x}(t))(x(t) - \bar{x}(t))^T]$ represent the mean and covariance of $x(t)$. $\bar{x}(t)$ and $X(t)$ obey the following equations.

$$\bar{x}(t_{i+1}) = \Phi(t_{i+1}, t_i)\bar{x}(t_i) \qquad \text{(A-17)}$$

$$X(t_{i+1}) = \Phi(t_{i+1}, t_i)X(t_i)\Phi^T(t_{i+1}, t_i) + W(t_{i+1}, t_i) \qquad \text{(A-18)}$$

The above equations can be solved to give the history of the nominal path as well as of the statistics of deviations from this nominal path during the approach and landing.

*Such a case would usually obtain when aircraft is flying with autopilot in a particular control mode.

Appendix B

Simulation of Atmospheric Noise

By Paul A. Madden

B. 1 Statistical Considerations

Simulation of atmospheric noise implies the generation of time-varying functions whose statistics duplicate the spectrums of continuous atmospheric turbulence.

Exponentially correlated noise may be modeled by passing gaussian white noise through a suitable shaping filter whose dynamics adjoin the existing system providing a new system subject only to white noise input.

Let the continuous white noise autocorrelation function be given by

$$\phi(\tau) = Q\,\delta(\tau) \tag{B-1}$$

then its PSD function is

$$\Phi(\omega) = \frac{1}{2\pi} Q \tag{B-2}$$

If gaussian white noise is passed through a filter F, its output has the PSD given by

$$\Phi_n(\omega) = \left|F\right|^2_{s = i\omega} \Phi(\omega) \tag{B-3}$$

For $F = \frac{a}{s+a}$, the output is

$$\Phi_n(\omega) = \frac{Q}{2\pi} \frac{1}{1 + \left(\frac{\omega}{a}\right)^2} \tag{B-4}$$

Equivalence of (B-4) and the assumed empirical turbulence spectrum provides the values of correlation time and Q necessary to reproduce the spectrum. For the Dryden $\Phi_u(\omega)$ given by Table 3-1 (Chapter 3), this equivalence provides

$$\frac{1}{a} = \frac{L_u}{U_o}$$

$$Q = 4\sigma_u^2 \left(\frac{1}{a}\right) \tag{B-5}$$

The filter equation may then be written

$$\dot{n} = a(w-n)$$

where n is the correlated noise output and w the gaussian white noise input.

Evaluation of the constants involved in a second-order filter necessary to reproduce the spectrum, for example, given for $\Phi_{v,w}(\omega)$ follows in a directly analogous manner.

It is not possible to provide a continuous signal representing gaussian white noise in a digital simulation. The digital equivalent is a discrete series of uncorrelated random amplitude steps. For this step sequence, the autocorrelation function is

$$\phi(\tau) = \begin{cases} \sigma^2(1 - |\tau|/\Delta T) & |\tau| \leq \Delta T \\ 0 & |\tau| > \Delta T \end{cases} \tag{B-6}$$

where σ^2 is the mean-square value of the random step amplitudes and ΔT is the discrete time step. The associated PSD function, defined as

$$\Phi(\omega) = \frac{1}{2\pi}\int_{-\infty}^{\infty} \phi(\tau)e^{-j\omega\tau}d\tau \tag{B-7}$$

is given by

$$\Phi(\omega) = \frac{\sigma^2}{2\pi}\left[\frac{\sin(\omega\Delta t)}{\omega} + j\,(\sin(\omega\Delta T) - \omega\Delta T\cos(\omega\Delta t))\right] \qquad \text{(B-8)}$$

Considering only the long wavelengths ($\omega << \frac{2\pi}{\Delta t}$), a small angle approximation may be used to give

$$\Phi(\omega) = \frac{\sigma^2\Delta t}{2\pi} \qquad \omega << \frac{2\pi}{\Delta t} \qquad \text{(B-9)}$$

Equivalencing the above discrete-step approximation for the PSD of the white noise input with the previously given (B-2) continuous function provides

$$\sigma^2 = Q/\Delta T \qquad \text{(B-10)}$$

For the example that led to the result for Q expressed by (B-5), the root-mean-square value of the random-step amplitude would be

$$\sigma = \left[\frac{2\overline{w_g^2}\,\frac{1}{a}}{\Delta T}\right]^{1/2} \qquad \text{(B-11)}$$

A block diagram, Fig. B.-1, shows the operations which lead from a machine-generated random number sequence to a time history of gust velocity.

B.2 Effective Aerodynamic Noise Perturbations

The sequence of operations discussed in the last section and shown schematically in Fig. B-1 leads to a time history of the three uncorrelated gust-velocity components.

A vertical gust produces an angle-of-attack disturbance and, because of its varying intensity along the length of the aircraft, an effective pitch disturbance. Similarly, a lateral gust-velocity component produces a sideslip and effective yaw disturbance.

The pitch and yaw disturbances may be approximately represented by effective pitch and yaw rate perturbations, respectively, if the higher-frequency gust components are not admitted in evaluation of these effective rates. This is equivalent to the requirement that the gust component vary nearly linearly along the effective aerodynamic length of the aircraft. This requirement may be met with a lowpass unity-gain filter introduced in series. The break frequency of the filter is selected such that the shortest wavelength admitted is no less than about eight times the effective aerodynamic length of the aircraft. If ω_b is the break frequency, then

$$\omega_b = 2\pi\, U_0/\lambda_{min} \tag{B-12}$$

with λ_{min} equal to eight times the aircraft length.

In general, it has been observed that neglect of the short wavelengths has negligible effect upon rigid-aircraft response; the energy content of these spectral components is relatively small. Their inclusion, however, is of importance in the forcing of aircraft elastic modes.

It is recalled that the empirical PSD functions are functions of the longitudinal-axis coordinate only; spanwise variations in gust intensity are thereby neglected. It is not easily possible to simulate this variation with rigor. It may be approximately accounted for, however, by considering a span-averaged gust intensity. The factor K is defined

$$K = \left[1 - 0.3\,\frac{b}{2L}\left(1 + \frac{b}{2L}\right)\right] \quad b < L \tag{B-13}$$

where b is the wing span and L is the aircraft length. The factor K operates upon the mean-square gust intensity providing a span-averaged value. This is the gust intensity used when evaluating the vertical and longitudinal gust-velocity components. For the CV880M

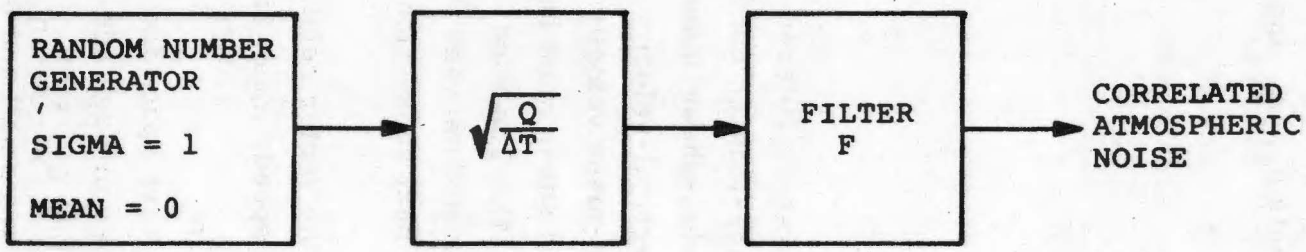

Fig. B-1 Discrete step sequence to generate time correlated atmospheric noise component.

aircraft, K = 0.968.

The aerodynamic noise perturbations may now be expressed as functions of the gust-velocity components u_1, u_2, and u_3.

$$
\begin{aligned}
u_n &= u_1 \\
\alpha_n &= u_3/U_0 \\
\dot{\alpha}_n &= \dot{u}_3/U_0 \\
\beta_n &= u_2/U_0 \\
q_n &= -(\dot{u}_3)_f/U_0 \\
r_n &= (\dot{u}_2)_f/U_0
\end{aligned}
\qquad \text{(B-14)}
$$

where the subscript f refers to the lowpass filtered component.

In addition to the above turbulence-induced components of aerodynamic noise, there exist also wind-shear-induced components. It is assumed that there is no mean vertical-velocity component to the air mass. The variations in mean air-mass velocity from the reference flight condition values due to wind shear must be added vectorially to the components u_n and β_n of (B-14). The wind-shear-induced components are evaluated as the difference between the current mean wind speed (w_{mean}), developed in the next subsection, and the initial flight condition value.

Figures B-2 and B-3 illustrate the vector relationships between noise, inertial, response, mean wind speed, mean airspeed and ground speed for two cases, u_n and β_n.

The components u_1, u_2, and u_3 are space fixed, and to be completely rigorous, should be resolved through actual instantaneous yaw, pitch and, roll angles in computing u_n, β_n, α_n, etc. It is assumed, however, that these angles are small and effects of ignoring the gust cross coupling negligible. In actual simulation therefore, u_1, u_2, and u_3 are generated with respect to aircraft axes.

U_o = nominal airspeed

U_{wo} = nominal headwind

$\dot{X}_{ao}$ = nominal groundspeed

u_n = instantaneous gust velocity

δU = $u + u_n$ = change in true airspeed

$\delta \dot{X}_A$ = u = change in true groundspeed

Auto throttle control operates to set

$\delta U = 0$ i.e. $u = -u_n$

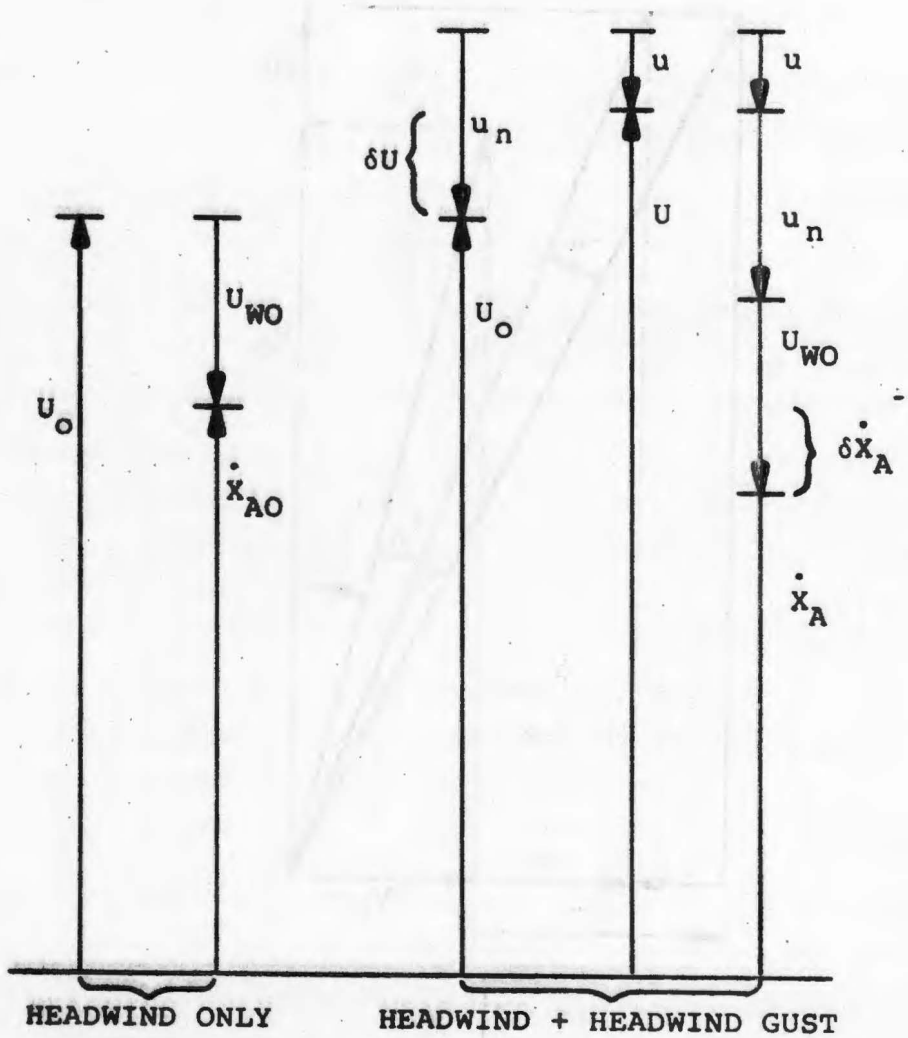

Figure B-2. Effects of Longitudinal Gust Noise on Air-Speed and Ground-Speed

U_o = nominal forward airspeed

$V_o = U_o \beta_o$ = nominal lateral airspeed

β_o = nominal sideslip angle

β_n $v_n/(U_o \delta U)$

= instantaneous gust induced sideslip

$v_n = u_2$ = instantaneous lateral gust

$\delta V = (U_o + \delta U_o)\beta$ = change in lateral ground speed.

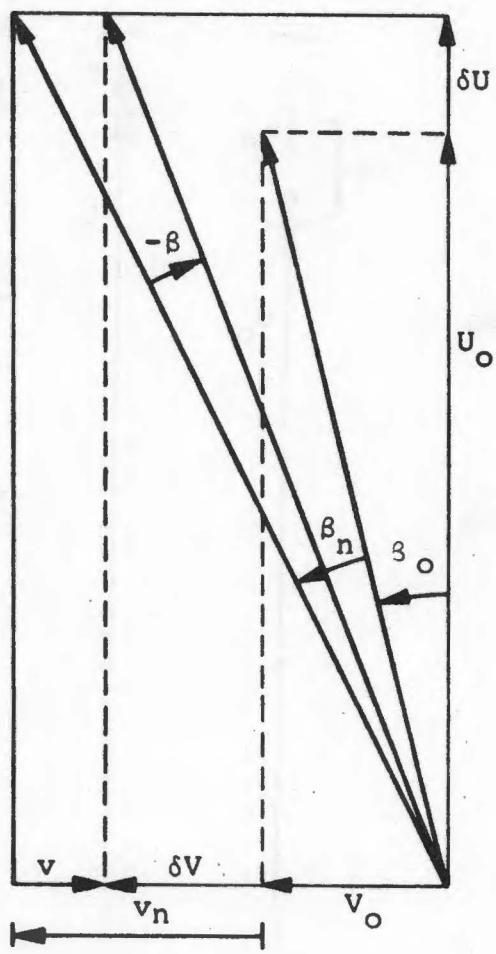

Figure B-3. Effects of Lateral Gust Noise on Sideslip Angle, Lateral Airspeed and Lateral Groundspeed

Appendix C

Granularity in Processed SBMILS Data

By Duncan MacKinnon

C.1 Introduction

The azimuth and elevation angle scanning beams of the Scanning Beam Microwave Instrument Landing System (MLS) indicate their angular position by information encoded on the transmitted signal. The encoded angular data changes as the beam sweeps through its specified angle as shown in Fig. C-1. The MLS airborne receiver measures the encoded data as the azimuth or elevation beam illuminates the aircraft. The receiver utilizes the observed measurements to estimate the actual angular relationship of the aircraft with respect to the azimuth or elevation antenna site.

Granularity (discrete changes) in the processed angular signal outputs may arise as a result of discrete quantization of the angle encoded on the modulation signal.

If quantization exists the signal measured by the receiver may be approximated by a sequence of values which are of the form

$$<\alpha> = <\alpha_1, \alpha_2, \alpha_3 \ldots\ldots \alpha_{N_b}> \qquad \text{(C-1)}$$

The number N_b of elements in the sequence is equal to the number of modulation quantizations during the period T_b when the MLS receiving antenna is illuminated by the scanning beam. The sequence is monotone

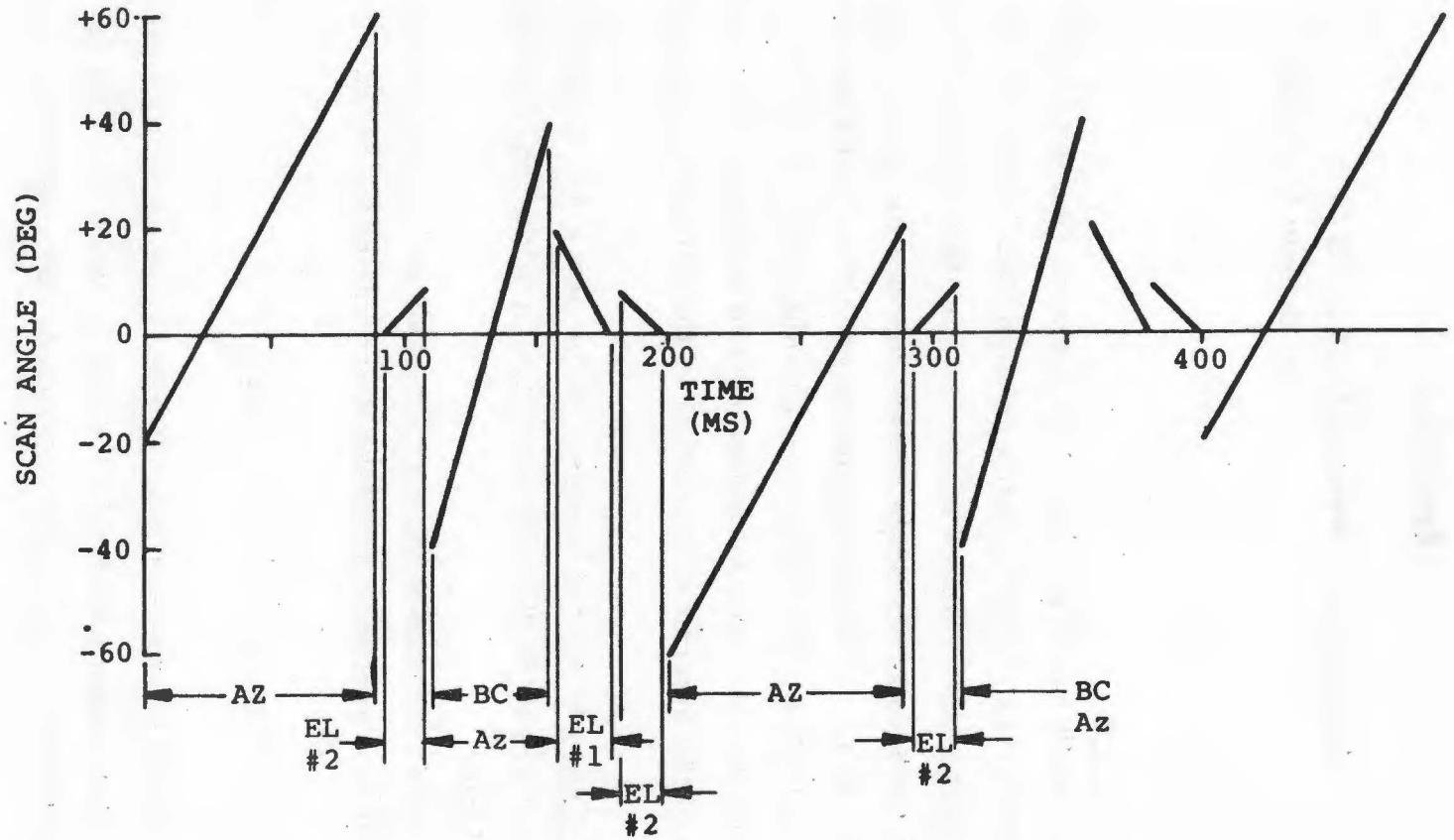

Figure C-1. Typical Scan Cycle for Mechanically Scanned Antennas

increasing or decreasing, depending on whether or not the angular modulation amplitude is increasing or decreasing with respect to time.

C.2 The Number of Samples in the Observed Sequence

The number of elements generated as a beam sweeps past the aircraft, depends primarily upon the beamwidth θ_b and the quantization level q of the encoded angular data

$$N_b \approx \frac{\theta_b}{q} \text{ samples} \qquad \text{(C-2)}$$

since the sequence elements are generated in a linear fashion as a function of angle. The quantization level q_r at the output of the MIL receiver depends upon the manner in which the sequence of measurement (C-1) is processed.

C.3 Digital Signal Processing

In order to estimate the value of the angle of interest the sequence of measurements (C-1) must be appropriately weighted. The weighting process can be analog* or digital in character. Digital filtering is a likely candidate as a result of small size, high accuracy and high reliability advantages. A digital output signal format is also extremely useful for interfacing with a general purpose navigation computer.

A simple digital filter to provide an estimate α_e of the measured angle α_m has the form

$$\alpha_e = \sum_{i=1}^{N_b} \beta_i \alpha_i \qquad \text{(C-3)}$$

where $\beta_1 \ldots \beta_{N_b}$ is a set of weighting coefficients. The characteristics of

---

* The problem is identical for the analog system if state variable techniques are exploited.

the filter are determined by the values associated with the ρ's.

C. 4 Granularity with Uniform Weighting

Suppose that the sample α_i is weighted uniformly by the processor. A suitable selection for ρ is

$$\rho_i = \frac{1}{N_b} \qquad i = 1, N_b \qquad \text{(C-4)}$$

in which case

$$\alpha_e = N_b^{-1} \sum_{i=1}^{N_i} \alpha_i \qquad \text{(C-5)}$$

the arithmetic mean of the samples. Granularity results when the angle measured at the aircraft passes a quantization level in the modulated signal. This results in a change d_u in the receiver output equal to

$$d_u = \frac{q}{N_b} = \frac{q^2}{\rho_b} \qquad \text{(C-6)}$$

The worst case occurs when N_b is equal to 1.

C. 5 Granularity with a Triangular Weighting

If a suitable nonuniform weighting sequence ρ is adopted, the effects of granularity may be significantly reduced. Suppose that ρ has the form shown in Fig. C-2 where

$$N_b = \text{odd number} \qquad \text{(C-7)}$$

and

$$\sum_{i=1}^{N_b} \rho_i = 1.0 \qquad \text{(C-8)}$$

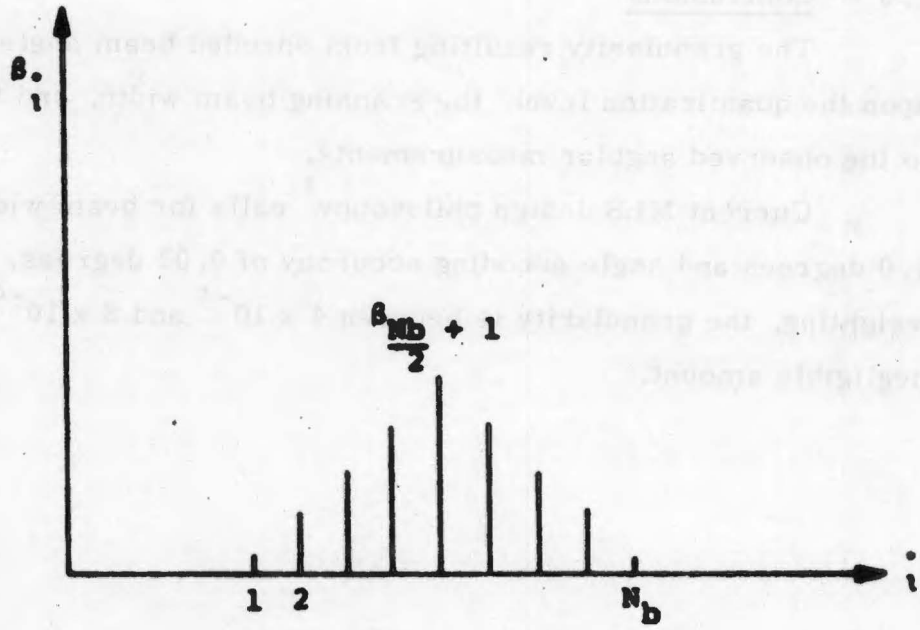

Figure C-2. Nonuniform Weighting Function

This weighting function places more confidence on measurements made near the beam center at a higher signal to noise ratio. The function is symmetrical with respect to the center value at $(N_b/2) + 1$. The quantization error in this case is equal to

$$d_u = q\beta_1 \qquad \text{(C-9)}$$

Note that β_1 can be much less than N_b^{-1} if $N_b > 2$.

C.6 Conclusions

The granularity resulting from encoded beam angle quantization depends upon the quantization level, the scanning beam width, and the weighting applied to the observed angular measurements.

Current MLS design philosophy[1] calls for beam widths between 0.5 and 1.0 degrees and angle encoding accuracy of 0.02 degrees. With a uniform weighting, the granularity is between 4×10^{-4} and 8×10^{-4} degrees, a negligible amount.

References

1. Signal Format Development Team Report to RTCA Special Committee 117, Radio Technical Commission for Aeronautics, Washington, D.C., September 1970.

Appendix D

Physical and Aerodynamic Characteristics of the CV880 and PA-30 Aircraft in the Approach and Landing Flight Configuration

by Paul A. Madden

D.1.0 Convair 880

D.1.1 Introduction

Physical and aerodynamic characteristics of the CV880 aircraft used as a basis for the SBMILS simulation studies are delineated in the following sections. Firstly, the aircraft approach speed is established for flight in the (defined) maximum wind condition; the nominal (no wind) flight condition (FC) is FC4 (See Reference (1).). Aerodynamic characteristics of the aircraft in the maximum wind condition follow from the derived approach speed and those characteristics given for FC4.

Derived Approach Speed

The approach speed is constructed following the empirical expression[2]

$$V_{app} = V_{ref} + \frac{1}{2} \text{ surface winds} + \text{reported gusts} \qquad \text{(D-1)}$$

where V_{ref} is the nominal (no wind) approach speed for FC4.

Physical and Aerodynamic Characteristics of the CV880

The following aerodynamic characteristics derive from the approach speed calculated using Eqn. (D-1) and aerodynamic characteristics given for FC4. The physical characteristics are identical with those of FC4.

D.1.2.0 Physical Characteristics

D.1.2.1 Aircraft

Gross weight = 126,000 lbs.

Flaps = 50 degrees (full down)

Undercarriage = down

C.G. position = .195% MAC

Speed brakes = 8 degrees

I_x = 1.51×10^6 slug-feet^2

I_y = 2.45×10^6 slug-feet^2

I_z = 4.07 slug-feet^2

D.1.2.2 Wing

Span = 118.3 feet

$\bar{c}$ = 18.94 feet

Area = 2000 feet^2

D.1.2.3 Elevator

Area = 88.28 feet^2

$\bar{c}$ = 2.44 feet

I = 33.6 slug-feet^2

D.1.2.4 Rudder

Area = 82.44 feet^2

$\bar{c}$ = 4.69 feet

I = 54.56 slug-feet^2

D.1.2.5 Aileron

Area = 2 x 27.37 feet^2

$\bar{c}$ = 2.96 feet

I = 2 x 19.11 slug-feet^2

D.1.3.0 Aerodynamic Characteristics

D.1.3.1 Trim Flight Condition

V_{app}	= 269 fps
Mach. No.	= .241
Dynamic Pressure	= 86.0 psf
Trim C_L	= .733
Trim C_D	= .13
Trim α	= 1.5 degrees
Zero-lift α	= -7.5 degrees

D.1.3.2 Longitudinal Stability Derivatives

	Out of ground effect	In ground effect
$C_{L,\alpha}$	4.66	5.56
$C_{D,\alpha}$	.317	.378
$C_{L,q}$	7.92	8.02
C_{L,δ_e}	.22	
$C_{L,\delta_{te}}$	.055	
$C_{m,\alpha}$	-.996	-.985
$C_{m,\dot{\alpha}}$	-4.17	
$C_{m,q}$	-12.22	-12.22
C_{m,δ_e}	-.657	
$C_{m,\dot{\delta}_e}$	-.0218	
$C_{m,\delta_{te}}$	-.164	

D. 1. 3. 3 Elevator Hinge Moment Coefficients

$C_{h,e,\alpha}$	-.043
C_{h,e,δ_e}	-.326
$C_{h,e,\dot{\delta}_e}$	-.023
$C_{h,e,\delta_{te}}$	-.287

D. 1. 3. 4 Lateral Stability Derivatives

$C_{l,\beta}$	-.2390
$C_{l,r}$	.3094
$C_{l,p}$	-.3950
C_{l,δ_r}	.0207
C_{l,δ_a}	-.0487
$C_{l,\delta_{ta}}$	-.00722
$C_{l,\delta_{tr}}$	.00208
C_{l,δ_s}	.0805
$C_{n,\beta}$	.1445
$C_{n,r}$	-.2178
$C_{n,p}$	-.0868
C_{n,δ_r}	-.0995
$C_{n,\delta_{tr}}$	-.02025
C_{n,δ_a}	.01862
C_{n,δ_s}	.0258

$C_{Y,\beta}$	-1.0150
C_{Y,δ_r}	.2230
$C_{Y,\delta_{tr}}$	.0493
C_{Y,δ_s}	-.0780
C_{Y,δ_a}	0.0
$C_{Y,r}$	0.388

D.1.3.5 <u>Aileron and Rudder Hinge Moment Coefficients</u>

C_{h,r,δ_r}	-.2140
$C_{h,r,\beta}$	.0733
$C_{h,r,\delta_{tr}}$	-.2550
$C_{h,r,\dot{\delta}_r}$	-.0468
$C_{h,r,r}$	-.0161
C_{h,a,δ_a}	-.6070
$C_{h,a,\delta_{ta}}$	-.2490
$C_{h,a,\dot{\delta}_a}$	-.0302
$C_{h,a,\beta}$	-.0149
$C_{h,a,p}$	-.0230

D.2.0 Piper PA-30

D.2.1 Introduction

Data for the PA-30 physical and aerodynamic flight characteristics in the flight condition chosen for LGS simulation studies is derived from the full-scale wind tunnel results for this aircraft reported upon in Ref. 3. The aircraft approach speed is established firstly, based upon the maximum wind condition chosen for the simulation studies.

Derived Approach Speed

The approach speed is constructed according to the empirical expression[2]

$$V_{app} = V_{ref} + \frac{1}{2} \text{ surface winds + reported gusts} \qquad \text{(D-2)}$$

where V_{ref} is $1.3V_s$ and V_s is the zero-flap stall speed.

D.2.2 Physical Characteristics

D.2.2.1 Aircraft

Gross weight	= 3600 lbs.
Flaps	= 0 degrees
Undercarriage	= down
C.G. position	= .1 MAC

Reference Body Axes Inertias

I_x = 2800. slug-feet^2

I_y = 1900. slug-feet^2

I_z = 4500. slug-feet^2

I_{xz} = 80. slug-feet^2

Stability Axes Inertias

I_x = 2801.7 slug-feet^2

I_y = 1900.0 slug-feet^2

I_z = 4513.7 slug-feet^2

I_{xz} = -7.9 slug-feet^2

D.2.2.2 Wing

Span = 35.98 feet

$\bar{c}$ = 5.00 feet

Area = 178.00 feet^2

D.2.3 Aerodynamic Characteristics

D.2.3.1 Trim Flight Condition

V_{app} = 176 fps

Mach No. = 0.158

Dynamic Pressure = 36.8 psf

Trim C_L = 0.55

Trim C_D = 0.034

Trim α = 2.95 degrees

Zero-lift α = -3.31 degrees

Trim δ_e = 0.4 degrees

D.2.3.2 Longitudinal Stability Derivatives

	Out of Ground Effect
$C_{D,\alpha}$	0.275
$C_{L,\alpha}$	5.04
$C_{L,q}$	9.12

$C_{L,\dot{\alpha}}$	5.30
C_{L,δ_e}	1.05
$C_{m,\alpha}$	-1.147
$C_{m,q}$	-25.0
$C_{m,\dot{\alpha}}$	-14.55
$C_{m,u}$	0.0
C_{m,δ_e}	-2.87

D.2.3.3 **Lateral Stability Derivatives**

$C_{l,\beta}$	-.086
$C_{l,r}$	0.11
$C_{l,p}$	-.5
C_{l,δ_r}	0.01147
C_{l,δ_a}	-.0803
$C_{n,\beta}$	0.0756
$C_{n,r}$	-.16
$C_{n,p}$	-.063
C_{n,δ_r}	-.0573

C_{n,δ_a}	0.00573
$C_{y,\beta}$	-.494
$C_{y,r}$	0.0
$C_{y,p}$	0.0
C_{y,δ_r}	0.143
C_{y,δ_a}	-.00916

D.3.0 References

1. CV880M Data, Lear Siegler Report ADR-595. Santa Monica, California.
2. Erwin, Ralph L., "Influence of Flight Dynamics on Terminal Sequencing and Approach Control," Report of the Department of Transportation Air Traffic Control Advisory Committee, Vol. 2, DOT, December, 1969.
3. Fink, Marvin P., Freeman, Delma C., Jr. "Full Scale Wind-Tunnel Investigation of Static Longitudinal and Lateral Characteristics of a Light Twin-Engine Airplane," NASA TN D-4983, Jan. 1969.

C_{n,δ_a}	0.00573
$C_{y,\beta}$	-.494
$C_{y,r}$	0.0
$C_{y,p}$	0.0
C_{y,δ_r}	0.143
C_{y,δ_a}	-.00016

D.3.0 References

1. CV880M Data, Lear Siegler Report ADM-395. Santa Monica, California.

2. Erwin, Ralph L. "Influence of Flight Dynamics on Terminal Sequencing and Approach Control." Report of the Department of Transportation Air Traffic Control Advisory Committee, Vol. 2, DOT, December, 1969.

3. Fink, Marvin P., Freeman, Delma C., Jr. "Full Scale Wind-Tunnel Investigation of Static Longitudinal and Lateral Characteristics of a Light Twin-Engine Airplane," NASA TN D-4983, Jan. 1969.

Appendix E

Nonlinear Vehicle Models for the Convair 880

by Paul Madden

E.1 Introduction

Initially, the nonlinear aircraft and trajectory equations are presented without derivation. A reference frame and axis system are then defined, followed by the development of a set of perturbation equations. The latter serve as the mathematical model for simulation of aircraft flight in a noisy atmosphere from an unaccelerated reference flight condition.

All assumptions and simplifications are discussed during development of the equations. The linear aerodynamic model is outlined, as is the manner in which ground effect and aerodynamic noise are incorporated. Tables listing all the equation coefficients and values for these coefficients pertinent to a specific approach-to-landing flight condition are presented.

The method of simulation of random aerodynamic noise, including wind shear, is presented and also the additional equations necessary to represent the elastic degrees of freedom of a flexible aircraft.

Finally, linearization of the non-linear equations is discussed with particular longitudinal and lateral models being delineated in a further appendix.

E.2 The Aircraft Nonlinear Equations of Motion

The general rigid-body nonlinear equations of motion have been derived often in the literature, and will not be rederived here. The equations are written with respect to an orthogonal set of axes fixed in the aircraft. The convention adopted for the axes, Euler angles, and rates is defined in Fig. F-1. The equations are

Lift

$$Z = - mg \cos \theta \cos \Phi + m (\dot{W} + PV - QU)$$

Drag

$$X = mg \sin \theta + m (\dot{U} + QW - RV)$$

Side Force

$$Y = - mg \cos \theta \sin \Phi + m (\dot{V} + RU - PW)$$

Pitch

$$M = B\dot{Q} + RP (A - C) + E (P^2 - R^2)$$

Roll

$$L = A\dot{P} - E\dot{R} + QR (C - B) - EPQ$$

Yaw

$$N = - E\dot{P} + C\dot{R} + PQ (B - A) + EQR \qquad (E-1)$$

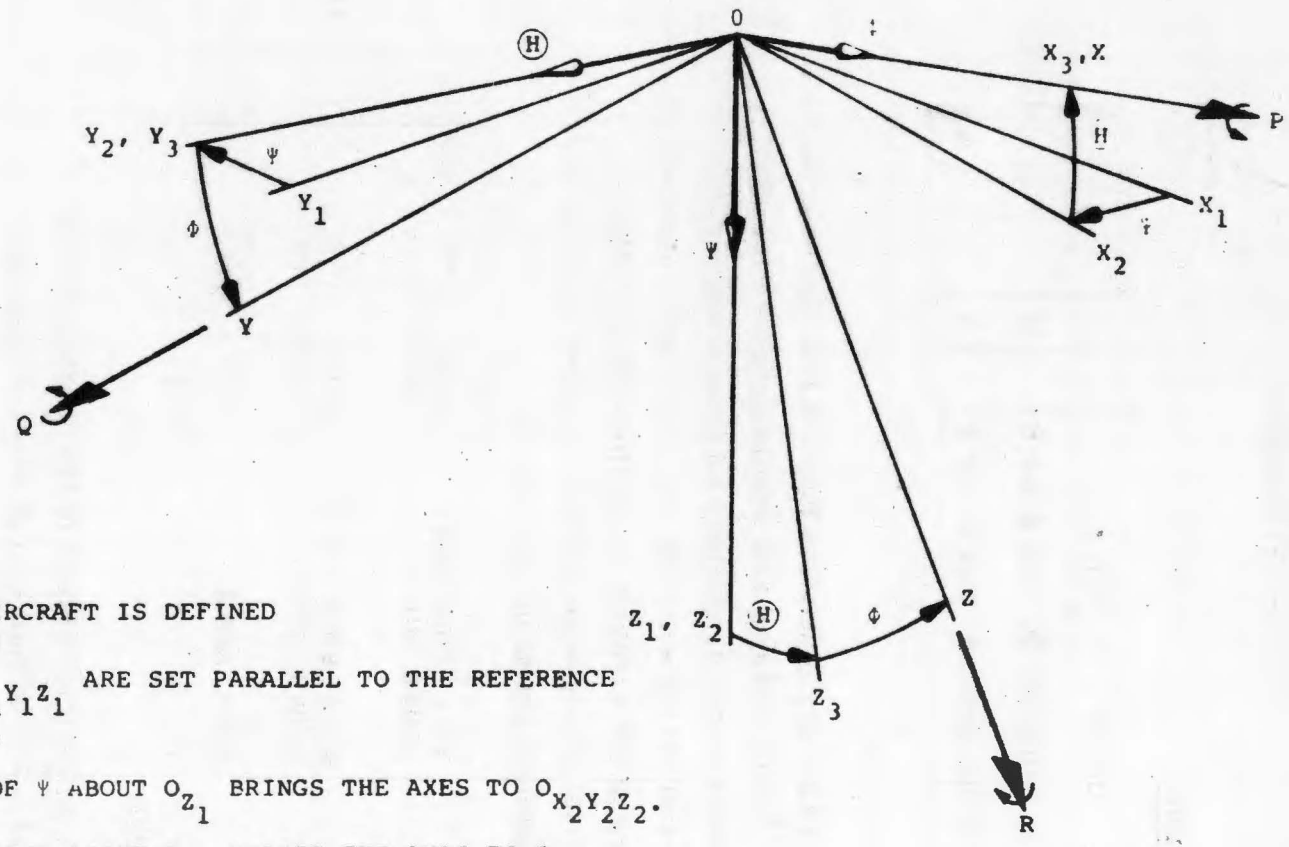

ORIENTATION OF THE AIRCRAFT IS DEFINED IN THE FOLLOWING WAY:

1) THE AXES $O_{X_1Y_1Z_1}$ ARE SET PARALLEL TO THE REFERENCE SET OF AXES.

2) A ROTATION OF ψ ABOUT O_{Z_1} BRINGS THE AXES TO $O_{X_2Y_2Z_2}$.

3) A ROTATION OF θ ABOUT O_{Y_2} BRINGS THE AXES TO $O_{X_3Y_3Z_3}$.

4) A ROTATION OF Φ ABOUT O_{X_3} BRINGS THE AXES TO THE FINAL POSITION, O_{xyz}.

Fig. E -1. Euler angle set.

Euler angle rate equations

$$\begin{bmatrix} \dot{\Phi} \\ \dot{\theta} \\ \dot{\psi} \end{bmatrix} = \begin{bmatrix} 0 & \cos\Phi & -\sin\Phi \\ 1 & \sin\Phi\tan\theta & \cos\Phi\tan\theta \\ 0 & \sin\Phi\sec\theta & \cos\Phi\sec\theta \end{bmatrix} \begin{bmatrix} P \\ Q \\ R \end{bmatrix} \qquad \text{(E-2)}$$

Trajectory equations

The aircraft trajectory equations require that the orientation of the aircraft be specifically defined and this is done in Fig. E-1. It should be remembered that the trajectory equations are written with respect to an inertial frame which is not necessarily earth-fixed. To obtain the trajectory of the aircraft in earth-fixed coordinates, the velocity of the inertial frame with respect to earth must be added vectorially to the following inertial velocities.

$$\begin{bmatrix} \dot{x}_i \\ \dot{y}_i \\ \dot{z}_i \end{bmatrix} = \begin{bmatrix} \cos\theta\ \cos\psi & \sin\phi\ \sin\theta\ \cos\psi - \cos\phi\ \sin\psi & \cos\phi\ \sin\theta\ \cos\psi + \sin\phi\ \sin\psi \\ \cos\theta\ \sin\psi & \sin\phi\ \sin\theta\ \sin\psi + \cos\phi\ \cos\psi & \cos\phi\ \sin\theta\ \sin\psi - \sin\phi\ \cos\psi \\ -\sin\theta & \sin\phi\ \cos\theta & \cos\phi\ \cos\theta \end{bmatrix} \begin{bmatrix} U \\ V \\ W \end{bmatrix} \qquad \text{(E-3)}$$

Choice of Inertial Frame

The only stipulation upon choice of the inertial frame is that it be unaccelerated. For simulation of quiet-atmosphere aircraft response, the simplest set of equations result when the inertial frame is chosen to be earth-fixed. However, for simulation involving a noisy atmosphere, the most convenient equations evolve when the inertial frame is fixed in the unaccelerated air mass associated with the reference steady-state flight condition.

Choice of Axes

The equations set down in the preceding sections are valid for any orthogonal axes fixed in the aircraft, with origin at the mass center, and known as body axes.

Any set of body axes may be chosen but it is most convenient to choose O_x such that it points in the direction of motion of the aircraft in a reference condition of steady symmetric flight. In this case, the reference values of V and W are zero, and the axes are termed stability axes. These are the axes adopted in the derivations of following sections owing to their resulting simplifications in the equations of motion and aerodynamic force expressions.

E.3 Perturbation Expansion of the Equations of Motion

Changes in the time-dependent variables from the reference steady-flight condition are now introduced in the manner,

$$U(t) = U_0 + u(t) \qquad \text{(E-4)}$$

similarly, the aerodynamic forces and moments (including thrust components),

$$X(t) = X_0 + \Delta X \qquad \text{(E-5)}$$

It is understood that an effective aerodynamic perturbation is the sum of a component due to inertial response of the aircraft and a component due to aerodynamic noise, viz.,

$$u(t) = u_i + u_n(t) \qquad \text{(E-6)}$$

Reference Flight Condition

The initial reference state is restricted to unaccelerated

flight in an unaccelerated atmosphere. The adoption of a stability axes set defines

$$V_0 = 0$$
$$W_0 = 0 \qquad \text{(E-7)}$$

Some additional assumptions have been made about the initial reference state. Although not essential, they considerably simplify the equations of motion with no important loss of generality. These further assumptions involve the initial values of aircraft pitch, roll, and yaw rates and aircraft roll attitude, all considered zero.

$$q_0, p_0, r_0 = 0$$
$$\phi_0 = 0 \qquad \text{(E-8)}$$

<u>The Perturbed Equations of Motion</u>

Substitution of the expressions for perturbed quantities, adoption of a stability axes set, and cognizance of the further assumptions (E-8) leads to the following equations

$$Z_0 + \Delta Z = -mg \cos\theta \cos\phi + m (\dot{w} + pv - qu - qU_0)$$
$$X_0 + \Delta X = mg \sin\theta + m (\dot{u} + qw - rv)$$
$$Y_0 + \Delta Y = -mg \cos\theta \sin\phi + m (\dot{v} + rU_0 + ru - pw)$$
$$M_0 + \Delta M = B\dot{q} + rp (A - C) + E (p^2 - r^2)$$
$$L_0 + \Delta L = A\dot{p} - E\dot{r} + qr (C - B) - pqE$$
$$N_0 + \Delta N = -E\dot{p} + C\dot{r} + pq (B - A) + qrE \qquad \text{(E-9)}$$

The reference flight condition is extracted by setting the perturbation quantities equal to zero

$$Z_0 + mg\cos\theta_0 = 0$$

$$X_0 - mg\sin\theta_0 = 0$$

$$Y_0 = 0$$

$$M_0 = 0$$

$$L_0 = 0$$

$$N_0 = 0 \qquad \text{(E-10)}$$

Substitution of (E-10) in (E-9) leads to the perturbation equations which may be written

$$\Delta Z = mg\cos\theta_0\,(1 - \sec\theta_0\cos\theta\cos\phi) + m\,(\dot{w} + pv - qU_0 - qu)$$

$$\Delta X = mg\cos\theta_0\,(\sec\theta_0\sin\theta - \tan\theta_0) + m\,(\dot{u} - rv + qw)$$

$$\Delta Y = -mg\cos\theta\sin\phi + m\,(\dot{v} + rU_0 + ru - pw)$$

$$\Delta M = B\dot{q} + rp\,(A-C) + E\,(p^2 - r^2)$$

$$\Delta L = A\dot{p} - E\dot{r} + qr\,(C-B) - pqE$$

$$\Delta N = -E\dot{p} + C\dot{r} + pq\,(B-A) + qrE \qquad \text{(E-11)}$$

It should be noted that, in view of (E-6) quantities like qu, pv, are not necessarily small (second-order). An approach to landing in a noisy atmosphere involves flight through turbulence and a wind gradient (shear), the sum of which constitutes terms like u_n. The response of the aircraft is such that the effective aerodynamic perturbation expressed as (E-6) is always small. Inasmuch as u_n is constituted of a fluctuating component (turbulence) superimposed upon what may be a large component due to wind shear, the inertial quantity u_i will be nearly equal in magnitude but opposite (in sign) to u_n. It is the inertial quantities that are

involved in the terms qu, pv referred to above.

E.4 The Aerodynamic Forces and Moments

A general force or moment change from the reference flight condition is represented by a Taylor series expansion

$$\Delta F \text{ (or } M) = g'x + \frac{1}{2}x' Ax + \text{higher-order terms.}$$

The first term of the expansion constitutes the quasi-steady (or linear) aerodynamic model where g is the vector of first-order derivatives (the stability derivatives) and x is the state vector.

All derivatives are evaluated at the reference flight condition; their nondimensional forms are usually referred to as the aircraft stability derivatives arising from their use in classical aircraft stability analysis. The stability derivatives together with trim aerodynamic quantities constitute the conventional characterization of the aircraft aerodynamics at a particular flight condition.

Ground Effect

An extraordinary aerodynamic perturbation occurs when the aircraft approches close to the ground.

In this situation the ground plane inhibits the normal downward-induced flow, increasing the lifting efficiency of the aircraft. Associated with this effect is usually a nose-down pitching moment which correction reduces to some extent the gain in lifting efficiency.

The nonlinear aerodynamic corrections are accomplished in the following way.

Changes in affected stability derivatives are approximated by

$$\Delta C = K(C_{ige} - C_{oge})$$

where

C_{ige} is the coefficient value in full ground effect

C_{oge} is the coefficient value out of ground effect

and K is given by a parabolic function typical of the aircraft type. For the subsonic jet transport class

$$K \approx -.498\Delta^3 + 1.758\Delta^2 - 2.126\Delta + .943$$

$$K = 0 \text{ for } \Delta \geq 1.6$$

where Δ is the aircraft altitude in semi-spans.

In addition to the derivative changes, there are net changes in the trim values of both lift and drag.

E.5 Equations of Motion as Mechanized in the Digital Simulation

Substitution of the aerodynamic force and moment changes into the perturbation equations (E-11) results in the following quiet-atmosphere aircraft equations of motion

Lift

$$\begin{aligned}\dot{\alpha} = \frac{1}{C}\Big[& C_\alpha \alpha + C_q q + C_u u \\ & + C_{\delta_e}\delta_e + C_{\delta_{te}}\delta_{te} + C_{\delta_s}\delta_s \\ & + C_{\beta p}\beta p + C_{qu} qu + C_{\Delta t}\Delta t \\ & + C_{L_0}(1 - \sec\theta_0 \cos\theta \cos\phi) \\ & + \langle \Delta C_L + \Delta C_{D\alpha} \rangle^* \Big]\end{aligned}$$

---

*<> terms are finite when aircraft is in ground-effect, zero otherwise.

Drag

$$\dot{u} = \frac{1}{C}\Big[C_u u + C_\alpha \alpha + C_{\delta_s}\delta_s + C_{r\beta} r\beta + C_{\Delta t}\Delta t + C_{L_0}(\sec\theta_0 \sin\theta - \tan\theta_0) + \langle \Delta C_D + \Delta C_L \alpha \rangle\Big]$$

Side Force

$$\dot{\beta} = \frac{1}{C}\Big[C_\beta \beta + C_r r + C_p p + C_{L_0}(\sec\theta_0 \cos\theta \sin\phi) + C_{\delta_s}\delta_s + C_{\delta_r}\delta_r + C_{\delta_a}\delta_a + C_{\delta_{tr}}\delta_{tr} + C_{ru} ru\Big]$$

Pitch

$$\dot{q} = \frac{1}{C}\Big[C_u u + C_{\dot{\alpha}}\dot{\alpha} + C_\alpha \alpha + C_q q + C_{\delta_e}\delta_e + C_{\dot{\delta}_e}\dot{\delta}_e + C_{\delta_{te}}\delta_{te} + C_{\delta_s}\delta_s + C_{\Delta t}\Delta t + \langle \Delta C_m \rangle\Big]$$

Roll

$$\dot{p} = \frac{1}{C}\Big[C_\beta \beta + C_p p + C_{\dot{r}}\dot{r} + C_r r + C_{\delta_a}\delta_a + C_{\delta_s}\delta_s + C_{\delta_r}\delta_r + C_{\delta_{ta}}\delta_{ta} + C_{\delta_{tr}}\delta_{tr}\Big]$$

Yaw

$$\dot{r} = \frac{1}{C}\Big[C_\beta \beta + C_p p + C_{\dot{p}} \dot{p} + C_r r + C_{\delta_a} \delta_a + C_{\delta_s} \delta_s + C_{\delta_r} \delta_r + C_{\delta_{ta}} \delta_{ta} + C_{\delta_{tr}} \delta_{tr}\Big] \quad \text{(E-12)}$$

Perturbations due to Aerodynamic Noise Input

$$\Delta\dot{\alpha} = \frac{1}{C}\Big[N_\alpha \alpha_n + N_q q_n + N_u u_n + N_{\dot{\alpha}} \dot{\alpha}_n\Big]$$

$$\Delta\dot{u} = \frac{1}{C}\Big[N_u u_n + N_\alpha \alpha_n\Big]$$

$$\Delta\dot{\beta} = \frac{1}{C}\Big[N_\beta \beta_n + N_r r_n + N_p p_n\Big]$$

$$\Delta\dot{q} = \frac{1}{C}\Big[N_u u_n + N_\alpha \alpha_n + N_{\dot{\alpha}} \dot{\alpha}_n + N_q q_n\Big]$$

$$\Delta\dot{p} = \frac{1}{C}\Big[N_\beta \beta_n + N_p p_n + N_r r_n\Big]$$

$$\Delta\dot{r} = \frac{1}{C}\Big[N_\beta \beta_n + N_p p_n + N_r r_n\Big] \quad \text{(E-13)}$$

Hinge Moment Equations

The dynamics of the aerodynamic effectors downstream of the control servos are represented by the hinge-moment equations.

The hinge-moment equations associated with the aerodynamic effectors and servo tabs of a conventional aircraft are

Elevator

$$\ddot{\delta}_e = HE_\alpha \alpha + HE_{\delta_e} \delta_e + HE_{\dot{\delta}_e} \dot{\delta}_e + HE_{\delta_{te}} \delta_{te} - \dot{q}$$

Aileron

$$\ddot{\delta}_a = HA_\beta \beta + HA_p p + HA_{\delta_a} \delta_a + HA_{\dot{\delta}_a} \dot{\delta}_a + HA_{\delta_{ta}} \delta_{ta}$$

Rudder

$$\ddot{\delta}_r = HR_\beta \beta + HR_r r + HR_{\delta_r} \delta_r + HR_{\dot{\delta}_r} \dot{\delta}_r + HR_{\delta_{tr}} \delta_{tr} - \dot{r} \qquad \text{(E-14)}$$

where

$$\delta_{te} = \delta_e - \delta_e^s$$

$$\delta_{ta} = - \delta_a^s$$

$$\delta_{tr} = \delta_r - \delta_r^s$$

and δ_e^s, δ_a^s, δ_r^s are the elevator, aileron, and rudder control-servo outputs respectively.

Control Surface Actuators

The aileron, elevator, and rudder control surface actuators are all modeled by a second-order system with $\omega_n = 2.86$ cps and damping ratio of 0.7. The transfer function of these servos is

$$\frac{\delta^s}{\delta^c} = \frac{324}{s^2 + 25.4s + 324}$$

The spoiler surface actuator is modeled by a first-order system with a time constant of 0.1 second.

Variables and Coefficients Defined

Define

$$\alpha = w/U_0$$

$$\beta = v/U_0$$

The variables α and β are referred to as angle-of-attack and sideslip angle respectively; a small-angle assumption is implied.

The equations of the previous section have been divided into longitudinal and lateral sets which for most aircraft are only weakly coupled for small rotational rates of motion.

Let μ, σ, and τ be defined by

	Longitudinal	Lateral
μ	$2m/\rho S\bar{c}$	$2m/\rho Sb$
σ	$\left(\frac{2}{\bar{c}}\right)^3 \Big/ \rho S$	$\left(\frac{2}{b}\right)^3 \Big/ \rho S$
τ	$\bar{c}/2U_0$	$b/2U_0$

Coefficients of the previous equations are defined in Tables F-1 and F-2 in terms of the aircraft geometry, inertia constants, reference flight condition, and stability derivatives.

E.6 Structural Flexibility

When separation in frequency between the elastic degrees of freedom and the rigid-body modes is not large, significant coupling can occur,

TABLE E-1. COEFFICIENTS DEFINED FOR THE LONGITUDINAL EQUATIONS

Equation / Coefficient	Lift	Drag	Pitch
C	$\tau[C_{z_{\dot{\alpha}}} - 2\mu]$	$-2\tau\mu/U_0$	$\sigma\tau^2 I_{yy}$
C_α	$-C_{z_\alpha}$	$-C_{x_\alpha}$	C_{m_α}
C_q	$-\tau[2\mu + C_{z_q}]$	---	τC_{m_q}
C_u	$[2C_{L_0} - C_{z_u}]/U_0$	$-[C_{x_u} + C_{L_0}\tan\theta_0]/U_0$	C_{m_u}/U_0
C_{δ_e}	$-C_{z_{\delta_e}}$	---	$C_{m_{\delta_e}}$
$C_{\delta_{te}}$	$-C_{z_{\delta_{te}}}$	---	$C_{m_{\delta_{te}}}$
C_{δ_s}	$-C_{z_{\delta_s}}$	$-C_{x_{\delta_s}}$	$C_{m_{\delta_s}}$
$C_{\beta p}$	$2\tau\mu$	---	---
C_{qu}	$-2\tau\mu/U_0$	---	---
$C_{\Delta t}$	$\sin\alpha_\varepsilon/(1/2)\rho U_0^2 S$	$-\cos\alpha_\varepsilon/(1/2)\rho U_0^2 S$	$z_\varepsilon/(1/2)\rho U_0^2 \bar{c} S$
$C_{r\beta}$	---	$-2\tau\mu$	---
$C_{\dot{\alpha}}$	---	---	$\tau C_{m_{\dot{\alpha}}}$
$C_{\dot{\delta}_e}$	---	---	$\tau C_{m_{\dot{\delta}_e}}$
N_α	$-C_{z_\alpha}$	$-C_{x_\alpha}$	C_{m_α}
N_q	$-\tau C_{z_q}$	---	τC_{m_q}
N_u	$[2C_{L_0} - C_{z_u}]/U_0$	$-[C_{xu} + 2C_{L_0}\tan\theta_0]/U_0$	C_{m_u}/U_0

TABLE E-1 (CONT). COEFFICIENTS DEFINED FOR THE LONGITUDINAL EQUATIONS

Equation Coefficient	Lift	Drag	Pitch
$N_{\dot{\alpha}}$	$-\tau C_{z_{\dot{\alpha}}}$	---	$\tau C_{m_{\dot{\alpha}}}$
C_{rp}	-	-	$\sigma\tau^2(I_{zz} - I_{xx})$
C_{p^2}	-	-	$-\sigma\tau^2 I_{xz}$
C_{r^2}	-	-	$\sigma\tau^2 I_{xz}$
$C_{q\alpha}$	-	$2\tau\mu$	-

TABLE E-2. COEFFICIENTS DEFINED FOR THE LATERAL EQUATIONS

Coefficient \ Equation	Side Force	Roll	Yaw
C	$2\tau\mu$	$\sigma\tau^2 I_{xx}$	$\sigma\tau^2 I_{zz}$
C_β	C_{y_β}	C_{ℓ_β}	C_{n_β}
C_r	$\tau[C_{y_r} - 2\mu]$	τC_{ℓ_r}	τC_{n_r}
C_p	τC_{y_p}	τC_{ℓ_p}	τC_{n_p}
C_{δ_a}	$C_{y_{\delta_a}}$	$C_{\ell_{\delta_a}}$	$C_{n_{\delta_a}}$
$C_{\delta_{ta}}$	---	$C_{\ell_{\delta_{ta}}}$	$C_{n_{\delta_{ta}}}$
C_{δ_r}	$C_{y_{\delta_r}}$	$C_{\ell_{\delta_r}}$	$C_{n_{\delta_r}}$
$C_{\delta_{tr}}$	$C_{y_{\delta_{tr}}}$	$C_{\ell_{\delta_{tr}}}$	$C_{n_{\delta_{tr}}}$
C_{δ_s}	$C_{y_{\delta_s}}$	$C_{\ell_{\delta_s}}$	$C_{n_{\delta_s}}$
C_{ru}	$-2\mu\tau/U_0$	---	---
$C_{\dot{r}}$	---	$\sigma\tau^2 I_{zx}$	---
$C_{\dot{p}}$	---	---	$\sigma\tau^2 I_{zx}$
N_β	C_{y_β}	C_{ℓ_β}	C_{n_β}
N_r	τC_{y_r}	τC_{ℓ_r}	τC_{n_r}
N_p	τC_{y_p}	τC_{ℓ_p}	τC_{n_p}

TABLE E-2 (CONT). COEFFICIENTS DEFINED FOR THE LATERAL EQUATIONS

Coefficient \ Equation	Side Force	Roll	Yaw
C_{qr}	-	$\sigma\tau^2(I_{yy} - I_{zz})$	$-\sigma\tau^2 I_{xz}$
C_{pq}	-	$\sigma\tau^2 I_{xz}$	$\sigma\tau^2(I_{xx} - I_{yy})$
$C_{p\alpha}$	$2\tau\mu$	-	-

TABLE E-2 (CONT). COEFFICIENTS DEFINED FOR THE LATERAL EQUATIONS

Equation Coefficient	Side Force	Roll	Yaw
C_{qr}	-	$qr^2(I_{YY} - I_{ZZ})$	$-qr^2 I_{XZ}$
C_{pq}	-	$qr^2 I_{XZ}$	$qr^2(I_{XX} - I_{YY})$
C_{pu}	$2ru$	-	-